Y 3. At 7:
36/ 8-4

POWER REACTOR TECHNOLOGY

A Quarterly Technical Progress Review

Prepared for DIVISION OF TECHNICAL INFORMATION, USAEC, by
ARGONNE NATIONAL LABORATORY

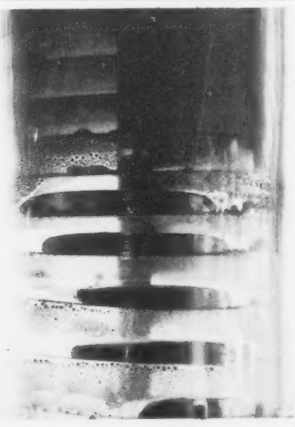

Trapping liquid-metal vapor ... see page 259

ILLINOIS STATE LIBRA
JUN 23 1966
U. S. Sup... of Docum...

Fall 1965

● VOLUME 8

● NUMBER 4

TECHNICAL PROGRESS REVIEWS

To meet the needs of industry for concise summaries of current atomic developments, the Atomic Energy Commission is publishing this series, Technical Progress Reviews. Issued quarterly, each of the reviews digests and evaluates the latest findings in a specific area of nuclear technology and science.

The five journals published in this series are:

Isotopes and Radiation Technology P. S. Baker, A. F. Rupp, and associates
Oak Ridge National Laboratory

Nuclear Safety Wm. B. Cottrell, W. H. Jordan, and associates
Oak Ridge National Laboratory

Power Reactor Technology
Argonne National Laboratory

Reactor Fuel Processing Stephen Lawroski and associates
Chemical Engineering Division, Argonne National Laboratory

Reactor Materials R. W. Dayton, E. M. Simons, and associates
Battelle Memorial Institute

See the back cover for availability information.

The views expressed in this publication do not necessarily represent those of the United States Atomic Energy Commission, its divisions or offices, or of any Commission advisory committee or contractor.

Availability of Reports Cited in This Review

Unclassified AEC reports are available for inspection at AEC depository libraries and are sold by the Clearinghouse for Federal Scientific and Technical Information, National Bureau of Standards, U. S. Department of Commerce, 5285 Port Royal Road, Springfield, Va., 22151. Some of the reports cited are not available owing to their preliminary nature; however, the information contained in them will eventually be made available in formal progress or topical reports.

Unclassified reports issued by other Government agencies or private organizations should be requested from the originator.

Unclassified British and Canadian reports may be inspected at AEC depository libraries. British reports are sold by the British Information Service, 45 Rockefeller Plaza, New York, N. Y.; Canadian reports (AECL series) are sold by the Scientific Document Distribution Office, Atomic Energy of Canada, Ltd., Chalk River, Ontario, Canada.

Classified U. S. and foreign reports identified in this journal as Classified may be purchased by properly cleared Access Permit Holders from the Division of Technical Information Extension, U. S. Atomic Energy Commission, P. O. Box 1001, Oak Ridge, Tenn., 37830. Such reports may be inspected at classified AEC depository libraries.

Y3.At7:
36/8-4

Contents

Power Reactor Technology

Vol. 8, No. 4

UNCONVENTIONAL APPROACHES	Liquid-Metal MHD Topping Cycles	199
PHYSICS	Evaluating Heavy-Atom Cross Sections for Plutonium-Recycle Calculations	210
	Critical and Exponential Experiments with Plutonium	211
	Use of Soluble Poisons in Critical Experiments	214
	Water-Reactor Data Generally Verify Theory	214
	Reactivity Changes with Long Irradiation	215
	Improvements in Resonance-Integral Theory	217
CONTROL and DYNAMICS	Reactor Control Experience	221
FLUID and THERMAL TECHNOLOGY	Heat-Transfer Conference Highlights	228
MATERIALS	Effect of Hydriding on Zircaloy Properties	245
FUEL ELEMENTS		
Letters to the Editor	Stainless-Steel Cladding in Boiling-Water Reactors	252
	Rebuttal	254
	Re-rebuttal	255
COMPONENTS	Vapor Traps Protect Liquid-Metal Systems	259
OPERATING EXPERIENCE	Operational Problems and Solutions	271
	Hallam Operation in Retrospect	279
SYSTEMS TECHNOLOGY	Advancements in Organic Coolants	290
INDEX	Volume 8	297

This issue of *Power Reactor Technology* is behind schedule because of problems attendant to the assumption of editorial and writing responsibility by Argonne National Laboratory and because of scheduling problems at the AEC production facility. It is expected that future issues will soon return to a proper seasonal schedule.

Issued quarterly by the U. S. Atomic Energy Commission. Use of funds for printing this publication approved by the Director of the Bureau of the Budget on October 14, 1963.

Statement by the New Editors

This quarterly review of developments in reactor technology has been prepared at the request of the Division of Technical Information of the U. S. Atomic Energy Commission. It is intended to help designers of power reactors stay abreast of significant progress and experience in their field. Thus its scope includes research and development in the various technical specialties in the field as well as design and construction practices, reactor concepts, applications, economics, and operating experience.

Although they are not meant to be comprehensive abstracts of all information published during the quarter, the articles in each issue will call to the reader's attention various publications that merit study. In addition, some articles will summarize and critically evaluate individual reports. Other articles will review a topic more broadly so that designers can interpret new developments and trends against the perspective of the state of the art. Because any appraisal involves the reviewer's opinion of the significance of the work reported, readers are urged to consult the references for additional information and the judgments of the original authors. If a reader has information that causes his evaluation to reinforce, modify, or contradict the opinions of our reviewers, he is encouraged to write to the Editor.

For reasonably timely coverage, articles often must be based on fragmentary information. Thus continuity will be maintained from one issue to another by use of the following subject headings whenever appropriate:

Economics, Evaluations, Programs
Specific Applications
Unconventional Approaches
Fuel Resources and Cycles
Physics
Control and Dynamics
Fluid and Thermal Technology
Containment, Radiation Control, Siting
Materials
Fuel Elements
Design and Construction Practice
Specific Reactor Types
Components
Operating Experience
Systems Technology

Because reactors are being developed and considered for power applications other than the generation of central-station electricity — and because of the similarity and transferability of the technology — the content of future issues will be broadened to include progress in reactor systems for process heat, desalting, undersea, space and other advanced applications.

This is the first issue prepared by Argonne National Laboratory. The new editors wish to express their appreciation to the previous editors, W. H. Zinn and J. R. Dietrich of Combustion Engineering, Inc., for earning *Power Reactor Technology* its respected stature in the field. Only from the experience of preparing an issue can their accomplishment be truly comprehended.

The Reactor Engineering Division (L. J. Koch, Director) has the principal responsibility for the preparation of *Power Reactor Technology*, with the regular assistance of the Reactor Physics Division (R. A. Avery, Director) and the occasional assistance of other Laboratory divisions (Metallurgy, Chemical Engineering, Chemistry, Reactor Operations, and Idaho). Thus, unless noted otherwise, the reviewers and authors of articles are Laboratory staff members. The editors will welcome interpretive review articles contributed by readers outside the Laboratory.

JAMES J. DUTTON, Editor; DAVID H. LENNOX, Technical Editor;
EDWARD J. CROKE and RAYMOND GOLD, Associate Editors
Argonne National Laboratory

Section

I

Power Reactor Technology

Unconventional Approaches

Liquid-Metal MHD Topping Cycles

By Michael Petrick

For all practical purposes, development of the steam cycle has reached a plateau. Further gains in efficiency by increasing steam pressure and temperature do not appear very profitable. Thermodynamically, steam is a poor working fluid because it absorbs too little heat at the maximum cycle temperature. However, no other single fluid is superior when all factors are considered. A logical improvement would be to use a binary system in which a second working fluid is used in a "topping" cycle.

A promising binary concept couples a liquid-metal topping cycle with a conventional steam bottoming cycle. In the topping cycle a liquid-metal magnetohydrodynamic (MHD) generator is tied directly to a liquid-metal-cooled reactor that heats the working fluid to 1500°F or possibly to as high as 2000°F.

Recent advances in magnetohydrodynamics show that an MHD device is a feasible way to convert heat into electricity. Although the plasma MHD cycle has a formidable obstacle to overcome—the attainment of adequate electrical conductivity within practical temperature limits—liquid metals have electrical conductivities five orders of magnitude higher than the electrical conductivity of plasma. The power density of an MHD generator is directly proportional to the fluid conductivity times the squares of fluid velocity and magnetic flux. Thus, even though the velocities that can be achieved in a liquid-metal generator are about a hundred times lower than with a plasma, liquid-metal MHD systems have a greater potential for compact or low-capital-cost generators than do plasma MHD systems.

The introduction of a topping cycle above 1000°F creates problems that must be resolved, e.g., high-temperature-material limitations affect component fabrication, cost, reliability, and, most important, longevity. The lifetimes of power equipment of various maximum operating temperatures are shown in Fig. I-1, which depicts typical experience with commercial rotating equipment, ducted gases, and reactors, as well as the goals of ambitious programs for space power using thermionics and alkali-metal cycles.[1] It appears that a turboelectric topping cycle would be limited to a range of 900 to 1400°F because of turbine reliability

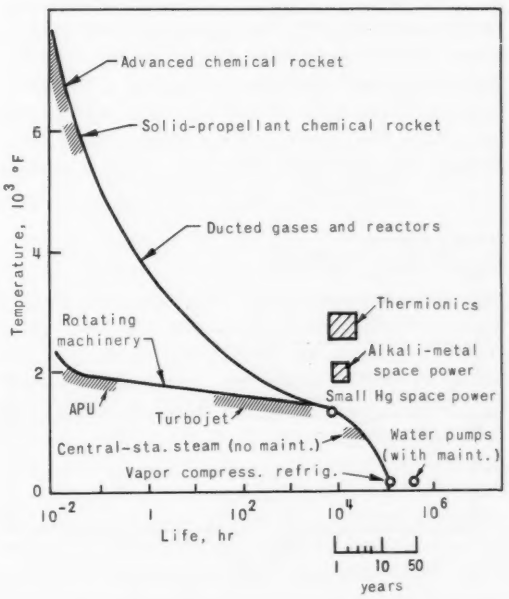

Fig. I-1 Operating temperature affects life of power equipment.[1]

problems. Unlike the conventional turboelectric generator, the MHD generator contains no moving parts that are subject to extreme temperature and dynamic stress and require close machine tolerances. As a result the MHD generator should be able to operate under conditions that conventional energy-conversion devices could not tolerate for prolonged times.

Liquid-Metal MHD Cycles

Five types of cycles have been proposed for liquid-metal MHD power systems. They are similar in that they are based on the conversion of thermal energy into kinetic energy, which then is converted into electric energy by an MHD generator. The cycles differ primarily in the way the thermal energy is converted to kinetic energy.

Two-Loop Two-Fluid Cycle. In the MHD cycle first proposed by Elliott[2] (of the Jet Propulsion Laboratory) as a space power cycle (Fig. I-2), one metal circulates in the vapor loop and another circulates in the liquid loop. The fluid circulating in the vapor loop leaves the condenser as condensate and is pumped (by an electromagnetic pump) to the mixer, where it vaporizes on contact with the liquid; the vapor expands with the liquid through a two-phase nozzle, separates from the liquid in the separator, and recondenses in the condenser. Cycle efficiency is raised by a heat exchanger that cools the vapor while it preheats the condensate. In the liquid loop the liquid is heated in the reactor heat source, is cooled as it vaporizes the condensate in the mixer, is accelerated by the vapor in the nozzle, separates from the vapor in the separator, decelerates by producing electricity in the MHD generator, and returns through the diffuser to the heat source.

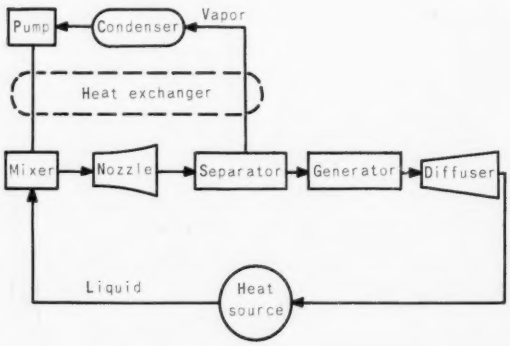

Fig. I-2 In the two-loop two-fluid MHD cycle proposed by Elliott,[2] one metal circulates in the vapor loop and another circulates in the liquid loop. Condensate from the vapor loop vaporizes when it mixes with hot liquid before both expand through a two-phase nozzle.

Two-Loop One- or Two-Fluid Cycle. The cycle proposed by Prem at Atomics International is also bicyclic.[3] It can be operated with either one or two fluids. The single-fluid version (Fig. I-3) is especially suited for large power stations. After the liquid metal in the first loop is partially vaporized by the heat source, the two-phase fluid expands by passing through a supersonic nozzle to transform the thermal energy to kinetic energy. Downstream of the nozzle, considerably cooler atomized liquid from the second loop is injected into the two-phase high-velocity stream. Momentum exchange accelerates the injected stream, and mass and heat transfer between the two streams condenses the vapor component of the two-phase fluid. The resulting high-velocity predominantly liquid stream enters the generator, where most of the fluid kinetic energy is transformed into electric energy. The second loop carries a portion of the liquid metal through a heat exchanger, where cycle waste heat is rejected.

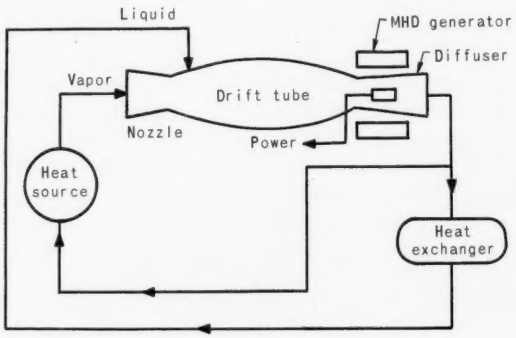

Fig. I-3 In the single-fluid version of the two-loop single- or two-fluid MHD cycle proposed by Prem,[3] hot partially vaporized fluid expands through a supersonic nozzle before cooler atomized liquid is injected to form mostly liquid stream.

One-Loop One-Fluid Cycle. A simplified single-fluid version (proposed by Petrick[4] at Ar-

gonne) of the two-fluid cycle is shown in Fig. I-4. After the velocity of a two-phase mixture or a saturated vapor from the reactor is increased by being passed through the nozzle, the two-phase fluid passes directly through the MHD generator to produce electric energy. When the fluid has been condensed, it goes through a diffuser and back through the reactor. This cycle has fewer parts and is more efficient than the two-fluid cycle of Fig. I-2 because of potentially lower friction losses and elimination of the vapor loop. Solubility and entrainment problems are also eliminated.

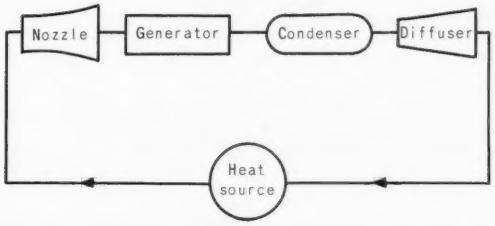

Fig. I-4 In a simpler single-loop single-fluid version (proposed by Petrick[4]) of the two-fluid MHD cycle, heat converts liquid metal to a two-phase mixture or a saturated vapor before velocity is raised in the nozzle. There is no separate vapor loop, mixer, or separator.

Two-Loop One-Fluid Condensing-Injector Cycle. The condensing-injector single-fluid MHD power cycle proposed by MIT's Jackson and Brown[5] (Fig. I-5) consists of a vapor loop (heating loop) and a liquid loop (heat-rejection loop). The vapor is generated in the reactor heat source and passes into the condensing injector, where it condenses in mixing with the liquid emerging from the waste heat exchanger to give a high-velocity liquid that passes through the MHD generator, where the kinetic energy is converted to electric energy. Then the liquid separates into two streams; one returns to the reactor, where it is vaporized, and the other stream goes to the liquid loop, where waste heat is rejected.

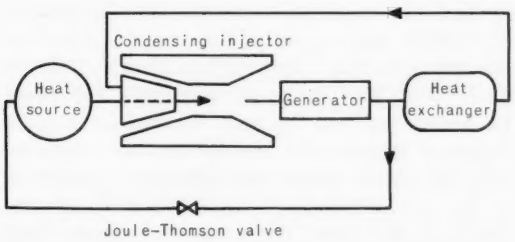

Fig. I-5 In the two-loop one-fluid condensing-injector MHD cycle proposed by Jackson and Brown,[5] vapor generated by heat condenses when it mixes with cooler liquid in the condensing injector before the fluid passes through the generator.

Slug-Generator Cycle. This cycle, proposed by Powell and coworkers at Brookhaven,[6] is similar in principle to a conventional steam-engine cycle. In this cycle (Fig. I-6) the vapor expands to accelerate liquid slugs through the generator.

The two modes of operation are either (1) to keep the intake valve open during the expansion stroke and irreversibly exhaust the high-pressure vapor through a Joule–Thomson isoenthalpic expansion to a condenser, or (2) to close the intake valve partway through the cycle and continue an adiabatic isentropic expansion to condenser conditions. The latter is more efficient and is used in conventional steam engines.

Potential Cycle Efficiencies

Calculated efficiencies for the various liquid-metal MHD cycles are reported in Refs. 6 to 9. Although the primary emphasis in this review is on the performance of the MHD cycle as a topping unit on a central-station power plant, the results of these studies also can be applied to compact power systems. Data are presented on the following working fluids: mercury, mercury–potassium alloy (40 mole % potassium), potassium, cesium, and lithium.

Two-Loop Two-Fluid Cycle. The efficiency of the Elliott cycle[9] employing cesium and lithium is shown in Fig. I-7. Assumptions made in the analysis are that: (1) the kinetic energy is converted to electric energy in the generator with 70% efficiency, including the effect of all fluid friction losses between the separator and the generator and between the generator and the diffuser; (2) diffuser efficiency is 85%; (3) the vapor-loop pump is 50% efficient; and (4) the pressure drops across the reactor, radiator, and mixer are each 10 psi.

Figure I-7 shows how cycle efficiency (defined as MHD generator output minus vapor-loop pump input divided by reactor thermal power) varies with sink temperature when the nozzle inlet is at 2000°F. Under the stated assumptions, cycle efficiency reaches a maxi-

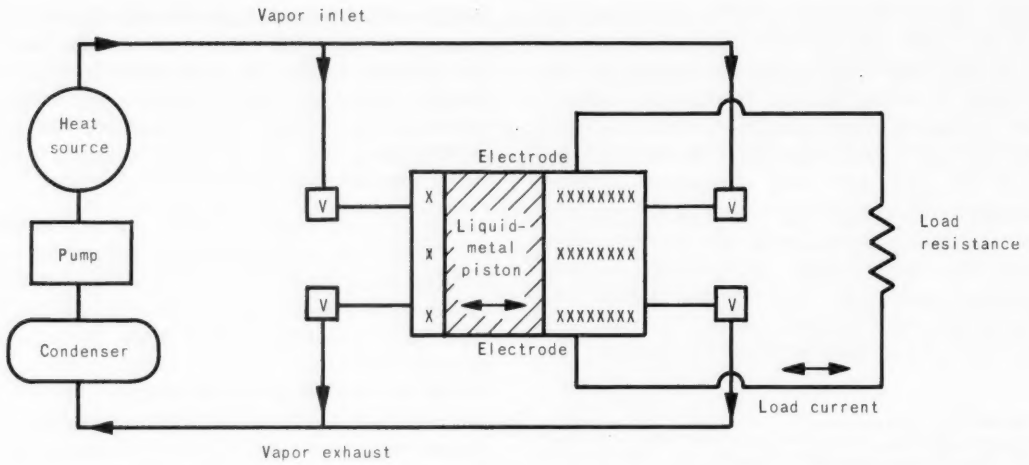

Fig. I-6 In the slug-generator MHD cycle proposed by Powell et al.,[6] liquid-metal vapor expansion pushes liquid slugs through the generator in a manner reminiscent of a conventional steam-engine cycle. V designates valves for liquid metals; X represents transverse magnetic field.

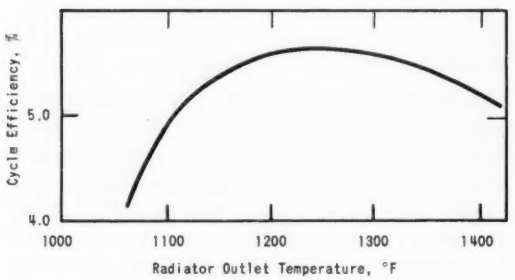

Fig. I-7 The efficiency of the two-loop cesium–lithium MHD cycle proposed by Elliott reaches a maximum of 5.7% when the sink is at approximately 1270°F (this curve is for 2000°F cesium–lithium at the nozzle inlet).[9]

mum of 5.7% when the sink is at approximately 1270°F. [At 30 kw(e) the flow rates are about 19 lb of cesium per second and 120 lb of lithium per second.] The efficiency decreases at higher sink temperatures because the Carnot efficiency decreases; it decreases at lower sink temperatures because the separator area increases and more lithium vapor enters the radiator.

Figure I-8 shows the cesium–lithium cycle efficiency as a function of the liquid and gas flow rates, exit nozzle pressure, and generator efficiency.[8]

It is apparent that this cycle has low efficiency. The maximum pressure of the system, and consequently the inlet pressure to the nozzle, is set by the working fluids used. For a cesium–lithium system, the temperature and pressure before the nozzle were set at 2010°F and 150 psia. Thus the maximum theoretical cycle efficiency is approximately 16% if the nozzle exit pressure is 0.25 psi and the generator is 100% efficient; but the maximum practical cycle efficiency is only approximately 7.5% with a more realistic exit nozzle pressure of 10 psi and an 80%-efficient generator.

Two-Loop One- or Two-Fluid Cycle. Efficiency analyses for both the single- and two-fluid versions of the Prem[7] cycle are shown in Fig. I-9; no attempt was made to optimize the cycle. Optimum cycle efficiency occurs at approximately 10% quality for a single-fluid system and supersonic nozzle inlet conditions of 2000°F and an outlet temperature equal to the vaporization temperature of the fluid at 14.7 psia. The upper three curves represent predicted efficiencies for the two-fluid cycle using an immiscible cesium–lithium mixture. The top curve shows how efficiency improves if the working fluid is expanded to 3 psia instead of 14.7 psia; the lower two curves (both of which are for 14.7-psia nozzle outlet pressures) show the importance of reducing average radiator temperature from 1050 to 780°F.

The predicted cycle efficiencies shown are based on assumed efficiencies of 70% for elec-

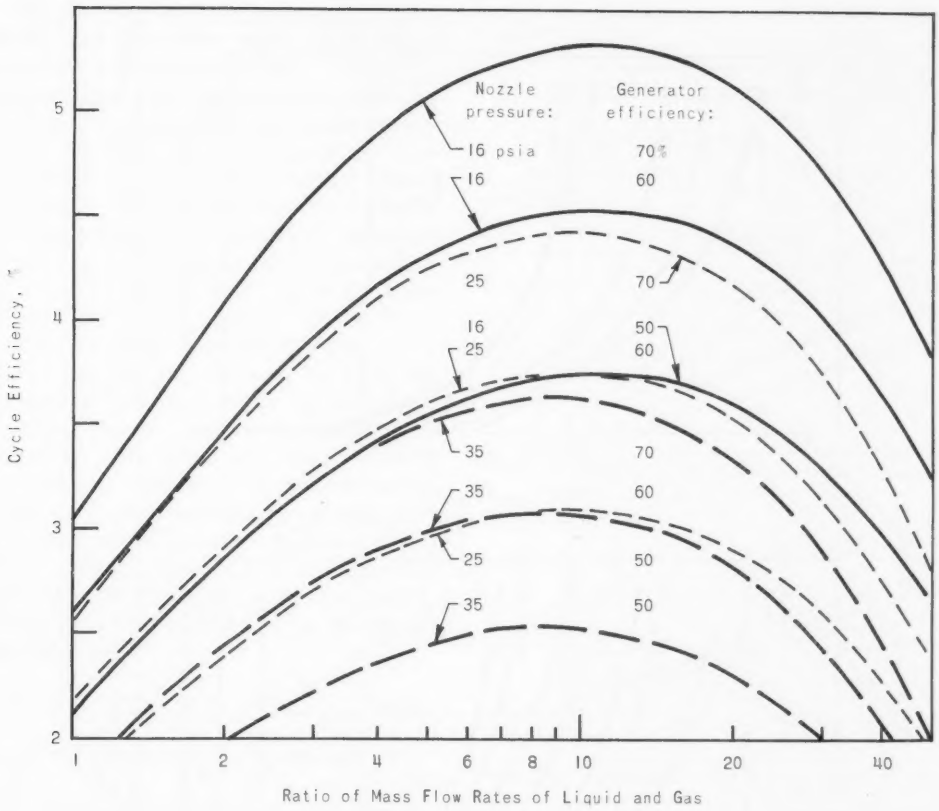

Fig. I-8 How efficiency of two-loop cesium–lithium MHD cycle varies with liquid and gas flow rates, exit nozzle pressure, and generator efficiency.[8]

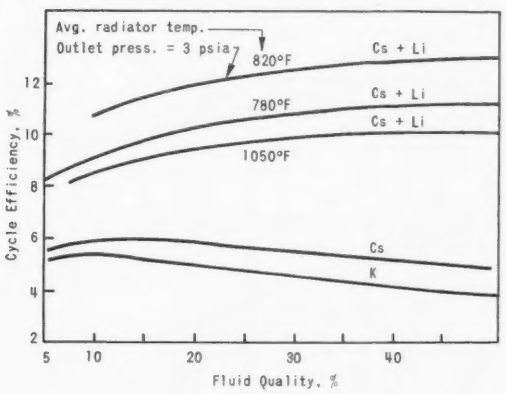

Fig. I-9 The efficiency of the two-loop MHD cycle of Prem with two fluids (upper three curves) is greater than with single fluids (lower two curves).[7] *Nozzle inlet is at 2000°F; outlet temperature is equal to the vaporization temperature at 14.7 psia, except for 3 psia for the top curve.*

trical conversions. The mechanical efficiency allows for losses in the nozzle plus frictional losses throughout the system; the electrical efficiency includes end losses in the generator and the magnetization current for producing the magnetic field.

One-Loop One-Fluid Cycle. Typical predicted cycle efficiencies for mercury, mercury–potassium, and potassium are shown in Figs. I-10 to I-12. The maximum efficiency in the cycle occurs with 100% vapor quality at the nozzle inlet.

Within the boundary conditions specified, mercury gives the highest efficiencies for the one-fluid cycle. The overall cycle efficiency is 22.5% with the source at 1540°F, the sink at 540°F, and the efficiencies of the MHD generator and the nozzle are 75 and 80%, respectively. For the potassium–mercury mixture,

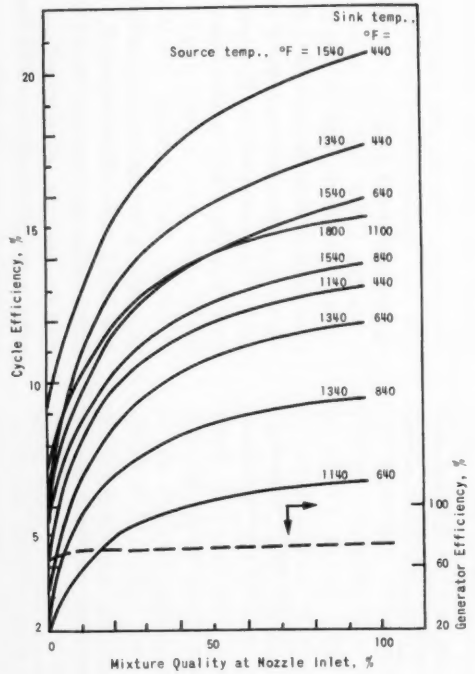

Fig. I-10 Cycle efficiency with mercury as the single fluid in the single-loop MHD cycle by Petrick.[8]

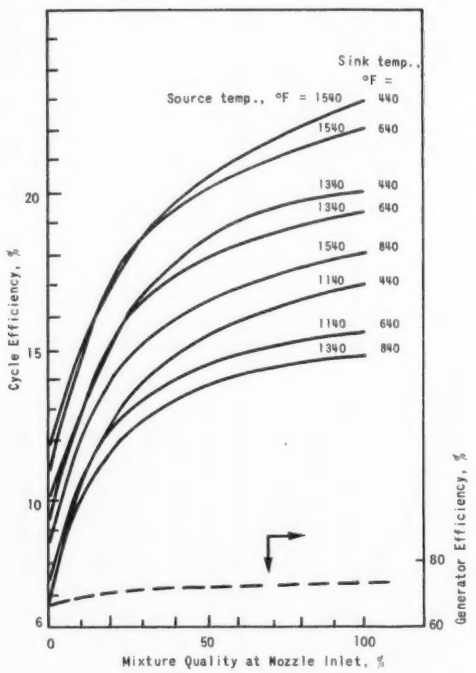

Fig. I-11 Cycle efficiency with a mercury–potassium alloy eutectic as the single fluid in the single-loop MHD cycle by Petrick.[8]

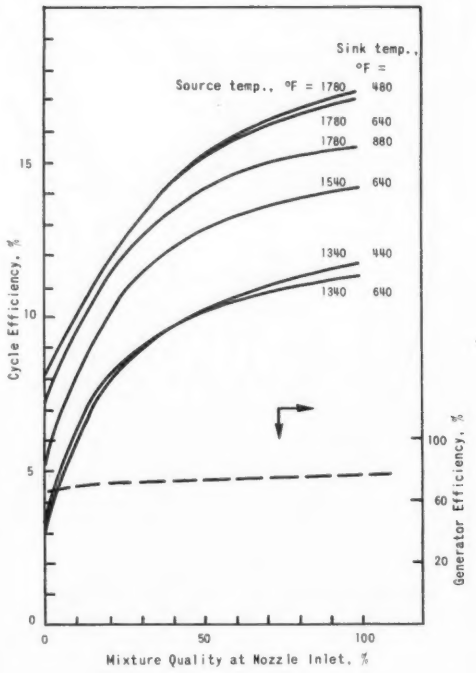

Fig. I-12 Cycle efficiency with potassium as the single fluid in the single-loop MHD cycle by Petrick.[8]

cycle efficiencies are approximately 10 to 25% lower and are much more sensitive to the source and sink temperatures.

In comparison with alkali metals, mercury and the mercury–potassium eutectic have lower boiling points, which permit operating temperatures nearer present technological limits. This advantage rapidly diminishes for the pure-mercury system because the vapor pressure of mercury increases rapidly with temperature; at 1540°F its pressure is 1762 psi. At the same temperature the vapor pressure of the mercury–potassium eutectic is only 198 psi.

Of the alkali metals, the best fluid for the one-component cycle apparently is potassium, whose calculated maximum cycle efficiency is approximately 20% over the range 2240 to 1160°F. Although cesium gives essentially the same efficiency as potassium, its lower electrical conductivity reduces its effectiveness in the MHD generator. The conductivity of sodium is higher than that of cesium or even potassium, but sodium as a working fluid yields the lowest cycle efficiencies.

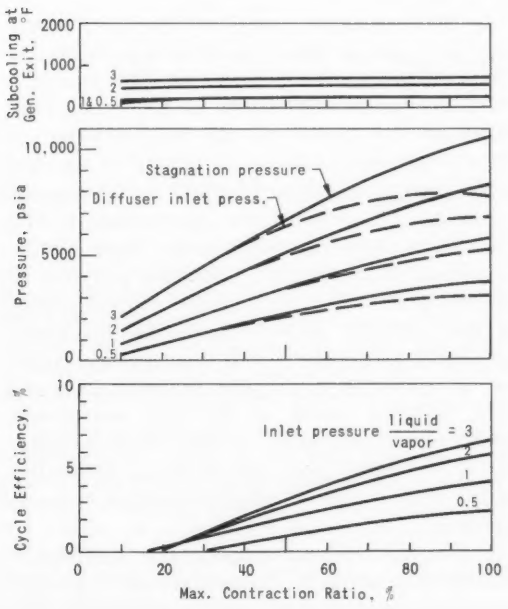

Fig. I-13 Efficiency with mercury in the condensing-injector MHD cycle when the source is at 1860°F, the sink is at 860°F, and the liquid-to-vapor mass flow ratio is 5. For inlet liquid-to-vapor pressure ratios of 0.5, 1, 2, and 3, maximum contraction ratios are 35, 49.2, 69.4, and 84.8, respectively.[8]

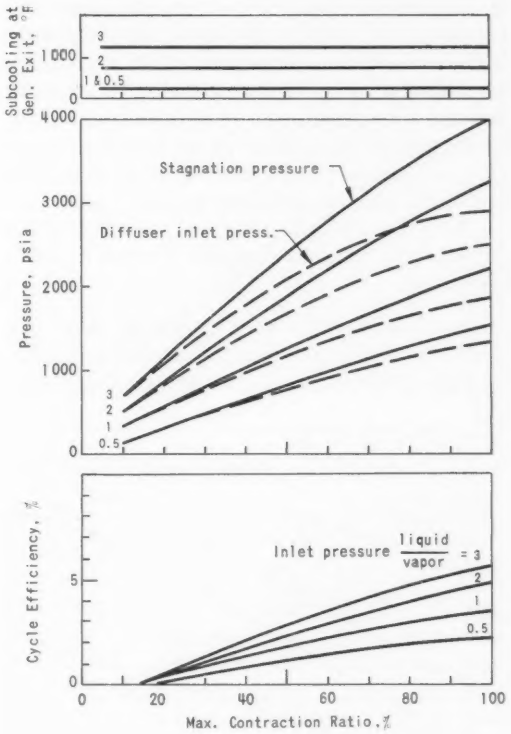

Fig. I-14 Efficiency with potassium in the condensing-injector MHD cycle when the source is at 2700°F, the sink is at 1060°F, and the liquid-to-vapor mass flow ratio is 3. For inlet liquid-to-vapor pressure ratios of 0.5, 1, 2, and 3, maximum contraction ratios are 23.2, 33.0, 46.7, and 57.2, respectively.[8]

Two-Loop One-Fluid Condensing-Injector Cycle. Figures I-13 and I-14 show typical estimated efficiencies of the condensing-injector cycle with mercury and potassium.[8] For these computations it was assumed that the MHD generator is 80% efficient and that the actual pressure rise in the condensing injector is 80% of theoretical. The cycle data show that mercury as a working fluid produces the highest cycle efficiency, 10%, and that it is followed closely by cesium at 8%. Sodium has the lowest performance potential. The ratio of the cycle efficiency to Carnot efficiency is in the range 0.17 to 0.25.

Some noteworthy trends derived from the cycle analysis are that: (1) cycle efficiency increases with injector contraction ratio and inlet stagnation pressure ratio but decreases with mass flow ratio (however, the variation of these parameters is limited by the second law

of thermodynamics); (2) cycle efficiency decreases with sink temperature and increases with heat-source temperature; (3) increasing the velocity from the condensing injector so that the total stagnation head is caused mostly by the kinetic head requires the injector geometry to give a contraction ratio greater than 50% of the maximum so that the MHD generator can be of the variable-area type, and thus it and the injector can be designed for much lower pressures.

Slug-Generator Cycle. Figure I-15 shows the calculated maximum ideal cycle efficiency for the slug-generator cycle,[6] assuming no generator losses, for adiabatic and isopressure expansions with potassium vapor. Note that isopressure expansion is about half as efficient as adiabatic expansion. As with all cycles, efficiency increases with vapor temperature.

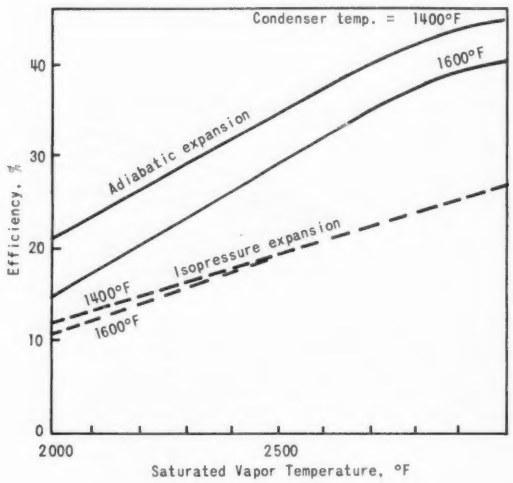

Fig. I-15 Ideal efficiencies for the slug-generator cycle with potassium vapor show that adiabatic expansion is nearly twice as efficient as isopressure expansion.[6]

Overall Plant Efficiency

The overall efficiency of a binary power system that has an MHD topping cycle and a normal steam cycle as the sink or bottoming cycle can be estimated by combining the efficiencies:

$$\epsilon_C = \epsilon_{MHD} + (100 - \epsilon_{MHD})\,\epsilon_{SC}$$

where ϵ_C is the binary cycle efficiency, ϵ_{MHD} applies to the topping cycle, and ϵ_{SC} is the efficiency of the steam bottoming cycle.

From this analysis the following conclusions are reached:

1. The potential overall efficiency of a central-station nuclear power system employing a liquid-metal MHD topping cycle appears to be excellent. (A fossil-fired boiler using a liquid-metal coolant also could be used as the heat source, in which case the boiler could operate at high cycle temperatures with the low vapor pressures possible with liquid metals.)

2. With an alkali metal as the working fluid, the maximum potential overall cycle efficiency appears to be 55% and results from either a potassium–steam or a cesium–steam binary cycle. The liquid-metal topping cycle operates between 2240 and 1100°F and produces 33% of the total power. The bottoming steam plant is the equivalent of a modern supercritical plant, such as the Eddystone unit, operating at 4000 psi and 1050°F; the efficiency of the steam plant is estimated to be approximately 45% and is based on upgrading the published Eddystone efficiency of 40.7% by eliminating boiler and stack losses.

3. The maximum potential efficiency of the mercury–steam binary cycle is approximately 53%, which is slightly lower than the cesium–steam or potassium–steam binary cycle. This efficiency is based on the source being at 1540°F and the condenser at 1100°F. If the sink temperature is dropped to 440°F, the overall cycle efficiency drops to approximately 47% even though the efficiency of the topping cycle increases substantially. Although mercury is thermodynamically the superior working fluid, it has several major drawbacks: (*a*) vapor pressure rises rapidly with temperature, (*b*) the use of additives to improve the wettability and heat transfer tends to increase operational problems considerably, (*c*) limited availability, and (*d*) relatively high cost. Thus the feasibility of the high-pressure mercury system is questionable.

4. For the medium-temperature range (1100 to 1600°F), mercury–potassium alloy and potassium appear to be the most promising working fluids for the liquid-metal cycle. Overall cycle efficiencies could be as high as 50%; the efficiency of the MHD topping cycle alone could be as high as 15% at a maximum working pressure below 75 psi.

Economics. Although no detailed economic studies have been reported, a preliminary study[8] indicates two major areas in which MHD topping cycles could save money: (1) the capacity of the steam bottoming plant could be reduced in proportion to the power generated in the MHD topping cycle, and (2) fuel costs would be lower because of the increased efficiency. The money saved in these two areas is available for converting the steam plant to the binary cycle and thus is a measure of the economic incentive for doing so.

For illustrative purposes, Fig. I-16 shows the total savings that would result from adding an MHD topping cycle to a base steam plant as a function of fuel cost and increase in plant efficiency. The values shown are for a 1000-Mw(e) plant operating with a 90% load factor, a cost of $30/kw(e) for the steam turbine-generator plant, and a 14.7% capitalization charge on the annual fuel savings (which transfers the annual fuel savings to an equivalent capital expenditure). As an example of the savings from a 20% increase in overall plant efficiency on a steam plant whose efficiency was 40%, the break-even point is approximately

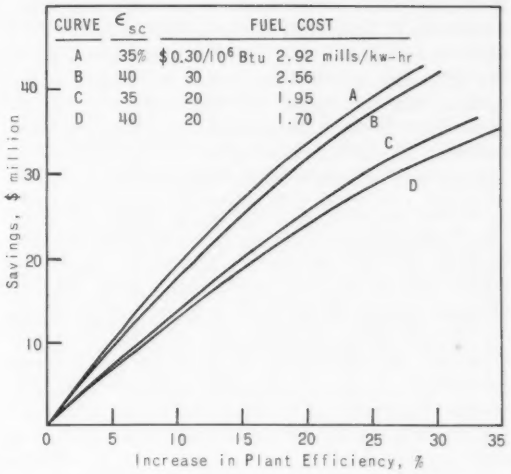

Fig. I-16 Savings from increasing plant efficiency by adding MHD topping cycle to a base steam plant.[8]

$25 million for a fuel cost of $0.20/$10^6$ Btu. The 20% increase in cycle efficiency can be achieved by an MHD topping cycle whose efficiency is 12.5%, which could be obtained with a maximum cycle temperature near 1600°F.

Liquid-Metal MHD: State of the Art

Active experimental programs are under way at Jet Propulsion Laboratory, Atomics International, Brookhaven National Laboratory, Massachusetts Institute of Technology, and Argonne National Laboratory to resolve uncertainties concerning the efficiencies of the various liquid-metal MHD cycles and components that have been proposed.

The Jet Propulsion Laboratory program to develop a space power source is the most comprehensive effort in liquid-metal MHD research that has been reported. In addition to tests on the MHD generator with NaK as the working fluid, the nozzle, separator, and diffuser have been tested with water and nitrogen. The nozzle has delivered 90% of isentropic exit velocity, the separator had about 1% liquid loss and 20% velocity loss, the diffuser was 75% efficient, and the generator operated at approximately 50% efficiency. Potential lifetime limitations due to erosion and to insulator loss were also investigated in water-flow and lithium-capsule tests; results indicated negligible material loss up to 1000 hr.[9,10]

The Atomics International development program is studying (1) the simultaneous mass heat-transfer and momentum-transfer process, which occurs in their "drift tube"; (2) the electrical resistivity of two-phase mixtures under various pressures, temperatures, void fractions, and impurities; and (3) generator types and performance. (Analyses and research toward the development of an MHD electric generator suitable for utility applications are being sponsored by the Edison Electric Institute.) The only results reported pertain to the acceleration and momentum-transfer process. Studies with sand and air indicate that the acceleration is accomplished very rapidly, reaching 60% of the air velocity at a distance of 30 to 40 cm from the injection point.[11] A potassium test-loop facility has been built to demonstrate the overall power-conversion process.

The Argonne National Laboratory program is studying the performance of liquid-metal generators and evaluating the condensing injector. The generator experiments will provide data on its efficiency with a dispersed two-phase entering fluid for various generator geometries, angles of incidence of the entering

fluid, and phase distributions. A second study, with a single-phase fluid, will confirm end losses in variable-area generators and establish maximum generator efficiencies, develop means to minimize end losses, and investigate the fluid mechanics of the generator. These investigations will provide data for defining the actual efficiencies of the condensing injector and two-phase single-fluid cycles.

At Massachusetts Institute of Technology, Jackson and Brown have concentrated on developing the condensing injector and the a-c generator. Brown has shown that a large pressure rise across the condensing injector is possible if a convergent mixing section is used. Jackson and coworkers[12,13] have developed the theory and outlined the performance limitations of the a-c induction generator. Experimental equipment is being fabricated to obtain extensive data on the performance characteristics of the a-c generator.

The Brookhaven National Laboratory program is oriented primarily toward investigating a slug generator.[6] Extensive studies of slug stability were made using high-speed movies of water, methanol, and mercury slugs accelerated through rectangular channels. Measurements of hydrodynamic and hydromagnetic wave growth rates agree approximately with theory. A mercury slug generator has reached an output of 100 watts, and, although its efficiency was only 10%, work is under way on an alkali-metal slug generator whose efficiency is expected to be 90% or greater. Also, work is being done on a reciprocating solid-piston MHD generator.

Others. Although programs are also being conducted at Allgemeine Elektrizitätsgesellschaft in Germany and at Space Technology Laboratories in the United States, they have not been reported in detail.

When these experiments have been completed, it should be possible to make a more thorough appraisal of the merits of the various liquid-metal MHD power cycles. Both efficiencies and needed materials development will be more clearly defined.

Comparison of Liquid-Metal and Plasma MHD Cycles

Because most of the work done in the field of magnetohydrodynamics has been on the plasma MHD cycle, the major problem areas and limitations of this concept have been pinpointed.

Efficiency and Temperature. Gunson et al.[14] have described a detailed study of a binary plasma MHD–steam power plant. Rosa and Kantrowitz[15] have calculated efficiencies for a closed-cycle plasma MHD–steam binary system, as well as for a purely MHD system; Fig. I-17 is based on their study. Both studies involved a helium cycle. Gunson reports a net efficiency of 47.1% for a plasma MHD–steam binary cycle operating with a top temperature of 3000°F.

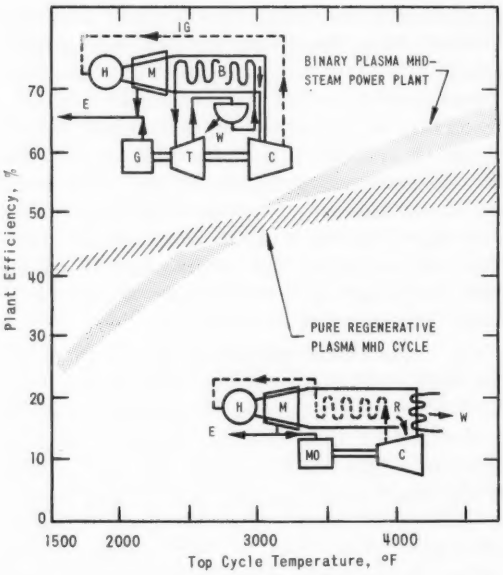

Fig. I-17 Plant efficiency with a closed-cycle plasma MHD–steam binary system exceeds that with a pure regenerative plasma MHD cycle when the top cycle temperature exceeds 2500 to 3500°F. Symbols: B, boiler; C, compressor; E, electrical output; G, generator; H, heat source; IG, inert gas; M, MHD generator; MO, motor; R, regenerator; T, turbine; and W, waste heat.[14]

For the same condition, Fig. I-17 indicates a value of approximately 51%. Thus, to better the efficiency of a modern steam plant, the temperature of a binary plasma MHD–steam plant must approach 3000°F. Temperatures must approach 4000°F to achieve overall cycle efficiencies of 55%. It also is interesting to note that the pure regenerative plasma MHD cycle (also shown in Fig. I-17) must approach 4000°F to achieve 50% efficiency. In studies of the open-cycle combustion-fired plasma MHD cycle, Way and Young[16] indicate that the overall efficiency of a binary system is 43 to 50% for a cycle top temperature of 4500°F; the highest efficiency would be achieved with a supercritical steam plant as the bottoming cycle. In comparison, liquid-metal MHD–steam binary system overall efficiencies of 50% appear possible at approximately 1600°F, and efficiencies of approximately 55% appear possible below 2200°F.

A major factor that tends to reduce the efficiency of the plasma MHD cycle is that it is essentially a Brayton cycle, and so a large fraction of the power generated is required for the compressors circulating the gas. For example, in the study made by Gunson et al., about 25% of the total electricity generated was used by the compressors. Seeding techniques and heat sources greater than 3200°F probably will be required to achieve an adequate

conductivity of the plasma in the plasma closed-cycle system. Although the development of a commercial reactor to operate at 3200°F appears possible, there are many unanswered questions about fuel performance and structural behavior.

Magnet Size and Cost. In addition to efficiency at reasonable temperatures, the liquid-metal MHD cycle offers other potential advantages. The power density achievable in a liquid-metal generator might be an order of magnitude higher than for a plasma generator; consequently smaller and less expensive magnets or coils (superconducting or normal) are feasible. Because the magnet or coil is a major cost item in an MHD plant, these potential savings are important.

Direct A-C Generation. Because d-c to a-c converters are expensive, the possibility of direct a-c generation is especially attractive. Jackson and Pierson[12] have shown that the feasibility of an MHD induction generator depends on a high magnetic Reynolds number, which is based on the wavelength of the field structure and the velocity difference between the wave and the fluid. Ionized gas flows in the conductivity range attainable now have very low magnetic Reynolds numbers, approximately 10^{-2}, and therefore direct a-c generation with such gases does not appear to be feasible. On the other hand, a characteristic magnetic Reynolds number of a liquid-metal generator would be approximately 10; thus the probability of producing a-c power directly is much more promising.

References

1. An Evaluation of Systems for Nuclear Auxiliary Power, USAEC Report TID-20079, January 1964.
2. D. G. Elliott, Two-Fluid Magnetohydrodynamic Cycle for Nuclear-Electric Power Conversion, *Am. Rocket Soc. J.* (June 1962).
3. L. L. Prem and W. E. Parkins, A New Method of MHD Power Conversion Employing a Fluid Metal, in *Proceedings of the International Symposium on MHD Electric Power Generation, Paris, France*, European Nuclear Energy Agency, Paper 63, July 1964.
4. M. Petrick and Kung-You Lee, Performance Characteristics of a Liquid Metal MHD Generator, USAEC Report ANL-6870, Argonne National Laboratory, July 1964.
5. W. D. Jackson and G. A. Brown, Liquid Metal Magnetohydrodynamic Power Generator Utilizing the Condensing Ejector, Patent Disclosure, Massachusetts Institute of Technology, October 1962.
6. J. R. Powell et al., Summary of Direct Conversion Work, USAEC Report BNL-8199, Brookhaven National Laboratory, March 1964.
7. L. L. Prem, Atomics International, private communication, September 1964.
8. M. Petrick and Kung-You Lee, Liquid Metal MHD Power Cycle Studies, USAEC Report ANL-6954, Argonne National Laboratory, June 1965.
9. D. G. Elliott, D. J. Cerini, et al., Liquid MHD Power Conversion, Vol. IV, JPL Space Programs Summary No. 37-27, Jet Propulsion Laboratory.
10. D. G. Elliott, D. J. Cerini, and E. Weinberg, Investigation of Liquid MHD Power Conversion, in *AIAA Third Biennial Aerospace Power Systems Conference, September 1–4, 1964*, Paper 64-760.
11. L. L. Prem, Fluid-Metal MHD/Steam Binary Cycle Developed, *Electrical World* (Oct. 19, 1964).
12. W. D. Jackson and E. S. Pierson, Operating Characteristics of the MPD Induction Generator, in *Proceedings of the IEE Magnetoplasmadynamic Electrical Power Generation Conference, New Castle upon Tyne, England, September 6–8, 1962*, Institution of Electrical Engineers Conference Report Series No. 4, pp. 38-42, 1963.
13. W. D. Jackson, E. S. Pierson, and R. P. Porter, Design Considerations of MHD Induction Generators, in *Proceedings of the International Symposium on MHD Electric Power Generation, Paris, France*, European Nuclear Energy Agency, Paper 61, July 1964.
14. W. E. Gunson et al., MHD Power Conversion, *Nucleonics*, 21(7): 43-47 (July 1963).
15. R. Rosa and A. Kantrowitz, MHD Power, *Intern. Sci. Tech.*, pp. 80-92 (September 1964).
16. S. Way and W. E. Young, The Feasibility of Large Scale MHD Power Generation, in *Proceedings of the International Symposium on MHD Electric Power Generation, Paris, France*, European Nuclear Energy Agency, Paper 98, July 1964.

Section

II

Power Reactor Technology

Physics

Evaluating Heavy-Atom Cross Sections for Plutonium-Recycle Calculations

By Edwin M. Pennington

Reactivity calculations were made[1] for Yankee critical experiments and for Hanford experiments that involved plutonium fuel. The calculational methods were standard. But significant is the fact that large reactivity differences were obtained by using different cross sections in the same computational model.

Experiments

The Yankee criticals studied consisted of four lattices with H_2O-to-UO_2 volume ratios varying roughly from 1 to 3.5. The UO_2 contained 2.73 at.% ^{235}U and was in 122-cm-high pins of 0.381-cm radius; the pins were clad with stainless steel 0.0407 cm thick.

Hanford criticals had PuO_2–UO_2 in 123-cm-high pins of 0.472-cm radius clad with zirconium 0.0685 cm thick; the isotopic enrichments were 1.366 at.% ^{239}Pu, 0.117 at.% ^{240}Pu, 0.011 at.% ^{241}Pu, 0.219 at.% ^{235}U, and 98.287 at.% ^{238}U. Four lattices were examined with H_2O-to-UO_2 volume ratios varying from 1 to 5.

Subcritical experiments at Hanford used 1.82 wt.% plutonium–aluminum fuel, with the plutonium consisting of 93.97 wt.% ^{239}Pu, 5.58 wt.% ^{240}Pu, and 0.44 wt.% ^{241}Pu. The pins were 111.3 cm high, of 0.635-cm radius, and were clad with zirconium 0.0762 cm thick. Five water-moderated lattices with hydrogen-to-plutonium atom ratios varying from 630 to 1418 were investigated.

Calculations

The calculational model of Ref. 1 involved three fast groups and a thermal group. Fast-group constants were obtained from the GAM-I code[2] using the original library,[3] except that versions of ^{240}Pu and ^{235}U having resonance parameters were used, and the Hanford RBU library[4] values were used for ^{238}U. When ^{239}Pu was involved, self-shielding factors calculated with the RIC code[5] were input to GAM-I. The RIC code computes resonance integrals in a manner similar to the Adler–Heinman–Nordheim method[6] used in GAM-I.

A preliminary SOFOCATE[7] problem using the actual isotopic densities as input provided thermal-group constants. The resulting cross sections were then used in a DSN[8] cell calculation with an extra scattering region to mock-up the isotropic return at the cell boundary. A final SOFOCATE problem using the DSN flux-weighted isotopic densities as input provided the thermal-group cross sections. Thermal-neutron cross sections for ^{235}U, ^{240}Pu, and ^{241}Pu for the SOFOCATE library were taken from Ref. 9. For ^{239}Pu, σ_f values from Ref. 9 were used with values of α^{49} adjusted as described in Ref. 1.

The four-group cross sections obtained as described above were used in one-dimensional diffusion theory (REX) calculations to obtain k_{eff} for the experimental radius. Values of k_{eff} were within approximately 1% of experimental values for all cases.

Comparisons

For the Yankee critical experiments, calculations were done both with the RBU library version of ^{238}U and the original GAM-I ^{238}U. Figure II-1 shows the calculations and provides a striking example of the reactivity differences

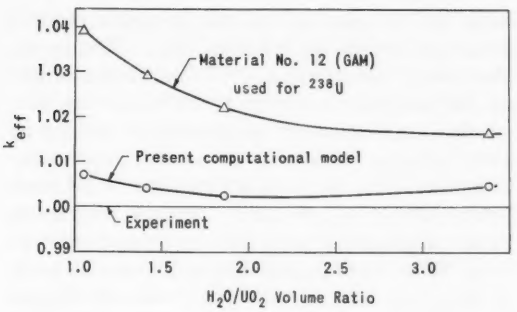

Fig. II-1 Comparison of computational model with Yankee critical experiments.[1]

that can result from using different cross sections in the same calculational model. Values of k_{eff} for the tightest lattice differ by over 3%, whereas it is desirable to calculate with an error of not more than about 1%. Even larger differences result[10] from using various cross sections in the same model for the highly undermoderated high-conversion critical experiments.[11–13]

For undermoderated light-water lattices, in which above-thermal processes are of considerable importance, uncertainties in cross sections are of more significance than errors produced by using approximate calculational methods. There is need for further work to determine basic cross-section data for use in reactor-physics computations.

Critical and Exponential Experiments with Plutonium

By Karl E. Plumlee

Plutonium produced by modern nuclear power plants significantly affects their economy. Various uses are made of recycled plutonium. Some has been used to enrich depleted uranium (as will be described). Plutonium also can be used for fuel spikes, driver regions, and full cores in reactors that require the larger number of neutrons produced per fission in plutonium than in uranium; in comparison with uranium, this characteristic tends to produce higher neutron fluxes without increasing the power level, which is an advantage for research and production reactors. On the other hand, if plutonium composition varies spatially, as it does during the operation of many cores, it poses a challenge to the physicist or engineer who is interested in determining the flux and power throughout such a core.

The Need for Data

Recent reports of critical and subcritical experiments indicate growing interest in plutonium-enriched cores and in the use of plutonium recovered from spent fuel.[14–24] Development of more durable fuel elements permits longer fuel exposures and greater plutonium utilization before the spent fuel must be reprocessed. Such highly exposed fuel contains plutonium having sizable concentrations of ^{240}Pu and ^{241}Pu (the ^{240}Pu is formed by nonfission capture of neutrons in ^{239}Pu, and the ^{241}Pu, by capture in ^{240}Pu). Because ^{240}Pu has a large capture resonance for 1-ev neutrons, its reaction rate varies nonlinearly with neutron-energy distribution as well as concentration (because of self-shielding). Thus differences in geometry, and operating variables, such as moderator temperature, affect the ^{240}Pu reaction rate. Designers must know the extent of these effects if plutonium is to be used economically.

Predictions of reactivity, power and temperature coefficients, burnup, and power and flux distributions are quite complicated for plutonium systems—particularly in the often-encountered situation in which both plutonium and uranium are in the core. Consequently experiments are needed to develop and check analytical approximations.

Experiments

Because there are several variables to be considered, measurement of the reactivity effects in plutonium cores requires carefully designed experiments and various fuel samples. But the elaborate procedures and equipment required with plutonium make fuel preparation and critical experimentation difficult. The extreme toxicity of plutonium limits permissible contamination to very low levels; the rapid accumulation of radioactive daughter elements severely limits the exposure time permitted during fuel handling.

In addition to showing the kinds of work being done, a review of the experiments being con-

ducted will indicate rates of progress and the problems encountered, even though some of the work is preliminary.

UO_2–PuO_2, Water Moderated. Critical and subcritical water-moderated experiments, fueled by rods of 1.5 wt.% PuO_2 blended with depleted UO_2 (0.22 wt.% ^{235}U in uranium), have been performed at Hanford.[14] Part of this fuel is being used in the Plutonium Recycle Program in the EBWR (Experimental Boiling Water Reactor), which will involve lengthy operation of the reactor to study reactivity trends, fuel burnup, and operational problems with a plutonium-fueled region. The 4-ft-high fuel rods are clad with Zircaloy-2 tubing 0.37 in. in diameter and 0.03 in. in wall thickness. The oxide-fuel content averages 827 g, of which approximately 86.7 wt.% is uranium and 1.3 wt.% is plutonium; the plutonium isotopic composition is 91.4 wt.% ^{239}Pu, 7.8 wt.% ^{240}Pu, and 0.73 wt.% ^{241}Pu.

The fuel rods were loaded in the subcritical experiment with hexagonal pitches of 0.55, 0.60, 0.71, 0.80, 0.90, and 0.93 in.; as much as 96% of the critical mass was accumulated so that inverse multiplication methods could be used to extrapolate the data to criticality. These extrapolated subcritical-experiment loadings indicated 2 to 5% smaller critical masses than predicted by calculations that were made using computer codes (GAM-I, HRG, TEMPEST, and THERMOS for cross sections, and HFN for criticality). Critical experimentation using the 0.7-in. fuel spacing indicated a somewhat larger critical loading (496 fuel rods) than did the subcritical experiment with the same spacing (484 rods). The change was mainly the result of component modifications, such as substitution of polycarbonate for Lucite plastic grids (or templates) to space the fuel rods.

Uranium and Plutonium Alloys, Graphite Moderated. A series of measurements was made at Winfrith in subcritical plutonium- and uranium-metal-fueled graphite-moderated assemblies that were representative of up to 4000 Mwd/metric ton fuel exposure.[15] The facilities, which were called Scorpio-I and Scorpio-II, were designed for buckling measurements and for fine flux and power-distribution measurements at 20 to 390°C; the experiments were planned to yield data for evaluating methods of calculating reactivity and temperature coefficients in power reactors. Plutonium compositions of ¼ and ½% of the uranium content were employed, with 2.5 to 3.2% ^{240}Pu in the plutonium; composition of ^{235}U was 0.42 to 0.44% in the uranium rods. In some cases the plutonium was present in plutonium–aluminum alloy strips, whereas in others plutonium–uranium rods were used; fuel-rod diameters were typically 1.1 to 1.2 in., and the length was 18 in. Volume ratios of moderator to fuel were from 17 to 108. Square lattice pitches were 7, 8, 9.9, and 11.3 in. Scorpio-I was the larger assembly with minimum dimensions of 84 by 84 by 84 in.; there were a few significantly larger arrays; the largest reported was 98 by 112 by 91 in. Details of the techniques used to measure power distribution in Scorpio-II have been described.[16]

Sample Measurements in Reactors. Related experiments were carried out by introducing a variety of 18-in.-long samples (similar to those described in Ref. 15) into an insulated cell in the uranium–graphite reactor Hector.[17] Because only samples are needed rather than complete uniform lattice loadings, this technique offers the advantage of savings in cost of fuel and in preparation.

Reactivity differences were measured over the range 20 to 450°C. Analysis of the results yielded values of k_∞ agreeing within 0.5% with the values obtained from uniformly loaded lattices. The report indicates that the effects of small perturbations in fuel composition (presence of small amounts of plutonium) can be compared without large corrections being applied in the analysis of results—provided the lattice spacing is large, typically 8.5 in. or larger. A comparison of the experimental results with the Tracer method of lattice calculation shows good agreement for room-temperature reactivities, but the calculation gave k_∞ values 1.5% lower than those measured at 400 to 450°C.

Experiments in France

A list of French CEA-operated critical facilities and typical experiments has been published.[18] Two graphite-moderated facilities are mentioned: Marius, which is operated at room temperature, and Cesar, which is operable at high temperatures. Aquilon is a D_2O facility, and both Alize and Azur are H_2O experiments. Alecto-I and Alecto-II are homogeneous-solution experiments.

Marius is a natural-uranium–graphite reactor that has been used for survey work, including variation of lattice pitch (19 to 38 cm), diameter of fuel channels (7 to 14 cm), and fuel-element geometry, including both annular and rod type fuel.[19] Tubular fuel elements were 3 to 10 cm in diameter, and fuel rods were 3 to 6 cm in diameter. The data have been used to develop improved methods of calculation, particularly in regard to large annular fuel elements. The development program requires measurements of relative fission rates in ^{239}Pu and ^{235}U and of their reactivities by oscillation and by substitution methods with plutonium–uranium fuel, irradiated fuel, and enriched and depleted samples. Experimental data and methods of analysis for obtaining reactivities, migration lengths, and related information have been reported.[19]

Marius and EDF-1. Measurements and analyses of flux fine structure and of indexes of neutron-energy spectrum, including some elevated-temperature experiments in the EDF-1 power reactor, as well as in Marius, have been reported.[20] The first part of the report details methods of fine-structure measurement and interpretation using ^{235}U, ^{239}Pu, and ^{115}In bare and cadmium-covered detectors, as well as comparison with calculated fuel and moderator flux ratios obtained by the Amouyal–Benoist–Hurwitz method. The second part concerns spectral index measurements (including ^{239}Pu, ^{235}U, indium, manganese, europium, and lutetium detectors), details of data treatment, and environmental conditions.

Marius and Minerve. Systematic experiments using oscillation techniques have been used to determine the reactivities as functions of sample composition of ^{235}U (enrichments up to 86%), ^{239}Pu, and boron (up to 12 ppm), for comparison with irradiated fuel samples.[21] The changes in effective cross sections of fuel as functions of neutron-energy spectrum and exposure will be studied by sample irradiation in the EL3 (D_2O) reactor, followed possibly by reactivity measurements in Minerve and by chemical and isotopic analysis. The precision of various techniques used to measure small reactivities, including sinusoidal- and square-wave input of reactivity or source, and also pulsed-source methods, has been studied.[22] Time requirements for equivalent accuracy are estimated for comparable methods. Limitations of the various methods are analyzed and reported, and sensitive areas are pointed out.

Aquilon-II. Bucklings and migration areas with depleted, natural, enriched, and plutonium-alloyed uranium lattices have been measured[23] in the D_2O reactor Aquilon-II. Progressive substitution measurements were made as the reference cores (natural-uranium lattices) were replaced by fuels containing 0.69, 0.71, 0.83, or 0.86% ^{235}U, and natural uranium plus 0.043% plutonium. Uranium pieces were 23.4 cm long and 2.9 cm in diameter; when assembled with aluminum containers, the rods were 240 cm long and 3.2 cm in diameter. The plutonium–uranium assemblies included double aluminum jackets and were also 240 cm long but 3.4 cm in diameter. Lattice pitches were 12, 13, 17, 19, and 21 cm. The analysis indicates consistent results by use of standard treatment. An interesting technique involves using the spontaneous neutron emission rate to measure the uniformity of the plutonium in the plutonium–uranium elements.

Homogeneous Experiments

Critical experiments have been conducted with H_2O solutions of 90% enriched uranyl nitrate and of plutonium nitrate.[24–28] The experiments provide data needed for safely handling fissionable material in solution. Typical geometries were cylinders and annuli. In addition to bare and H_2O-reflected systems, there were thick reflectors of wood and concrete and thin shells of cadmium. Experimental and calculated compositions of solutions involved plutonium in the range 19 to 104 g/liter. Experimental measurements are given for several geometries;[24] values of k_{eff} calculated by two- and four-group diffusion theory are also given for several cores; critical-height measurements are also compared with calculated values. Agreement was within 1% in most of the plain-geometry experiments. Further calculations were by the transport code TDC employing the S-4 approximation and four neutron-energy groups with RZ geometry. Monte Carlo calculations also are reported, and these indicate that 20 to 30 min of computer time is required to obtain a precision of approximately 1.2% in k_{eff} for complicated geometries involving plutonium solutions.

Homogeneous plutonium–hydrogen critical-mass measurements performed at Hanford over

the past few years have been summarized.[29] Data are reported for hydrogen-to-plutonium atomic ratios ranging from 15 to 870. The effect of nitrate was studied for concentrations as high as 460 g of NO_3 per liter. Assemblies were made with bare spherical geometry, with cadmium liners, and with reflectors of H_2O, paraffin, or concrete. A number of PuO_2–polystyrene plastic assemblies were reported, particularly for lower hydrogen-to-plutonium ratios. Information helpful in understanding the physics of the plutonium homogeneous systems was developed. Experimental techniques included standard critical-mass measurements, noise measurements, pulsed-source experiments, and spectral-index measurements with foils. Temperature variations also were studied.

Use of Soluble Poisons in Critical Experiments

By Karl E. Plumlee

Boric acid was used to poison the moderator of the Alize-II critical facility.[30] This was done to obtain measurements of temperature coefficients and excess reactivities at various temperatures; boric acid concentrations ranged from 20 to 300 ppm boron. Fuel was aluminum-clad enriched-uranium–aluminum alloy containing 12.8 g of ^{235}U per fuel plate. Plate size was 0.1 by 7.9 by 65 cm. Core composition was varied by assembling aluminum, boron–aluminum, and zirconium components, as well as fuel plates, into boxes. The boxes were inserted into grid positions to form cores. Different grids were available, providing a selection of box spacings. Numerous details are given of the steps taken to control the boron solutions. Measurements of boron deposition rates on aluminum, zirconium, and coated surfaces are reported for various conditions of temperature, concentration, etc. Residual amounts in the core were reported, as well as methods of analysis for less than 1-ppm boron concentration in rinse water. Degassing of the moderator to prevent bubble formation during temperature-coefficient measurements is also described.

Soluble-poison studies also have been conducted with cadmium sulfate solutions.[31] Cadmium solutions, which are alternatives to boron solutions as reactor poisons, were studied in detail to determine the circumstances under which irreversible deposition occurs on reactor components. Quantitative laboratory measurements were made with various surface finishes, both aluminum and zirconium components, and with variations of temperature, *p*H, etc., with 13-ppm cadmium solutions.

Water-Reactor Data Generally Verify Theory

By Charles N. Kelber

The growth of low-enrichment light-water-cooled and -moderated power-reactor technology has in large measure been predicated upon a massive amount of experimental and theoretical work in reactor physics. Although some discrepancies remain, a recent summary[32] demonstrates basic agreement between theory and experiment for these systems. Thus reactor theory can be used confidently as the major predictive tool in the design of these systems.

Material Buckling

Material-buckling measurements and calculations are compared and examined for systematic error. Two methods are in common use for measuring material buckling: "flux shape" and "variable loading." The flux-shape method, which uses a fit to activation traverses, has a major difficulty in that data from points near the lattice boundary must be rejected and, especially in small systems, the detector response depends on the system size. The variable-loading method involves measuring the axial flux distribution for each of many different-sized loadings of the lattice. A two-parameter least-squares fit to the axial buckling vs. lattice radius yields the reflector savings and material buckling. The basic assumption that leads to systematic error is the constancy of the radial-reflector savings. Theory predicts that this is not so, but to remove this assumption requires a three-parameter least-squares fit, with a loss of accuracy, in general.

Similarly, a number of systematic errors were found in theoretical analysis. Three chief sources were (1) use of incorrect thermal-neutron cross sections for ^{235}U, (2) neglect of the effect of cladding on the Dancoff correction,

and (3) overestimation of the fast effect. Buckling data were sorted for 96 lattices, and theory was compared with the experiment. For the 11 lattices with the smallest reported error in buckling, the predicted k_{eff} had an average value of 0.9992 ± 0.0016 instead of 1.0. For 55 lattices the average predicted k_{eff} is 0.9988 ± 0.0027. The greatest discrepancy, as expected, is in predicting the properties of closely packed lattices. The authors conclude that the "usual four-group theory" systematically underestimates the worth of the radial reflector.

Ratio of ^{238}U to ^{235}U Fissions

A quantity directly related to the fast effect is the ratio of fissions in ^{238}U to those in ^{235}U, δ^{28}. The determination of δ^{28} depends on knowledge of a function $P(t', t)$, the ratio of measured activity per fission in ^{235}U to that from ^{238}U; t' is the irradiation time, and t is the time between shutdown and measurement of the activity. Uncertainties in $P(t', t)$ contribute an error of 5% to δ^{28}. For specific fission products such as ^{140}La, the function $P(t',t)$ is a constant, but the relative yields are uncertain.

Fast-effect calculations are fundamentally homogeneous-mixture calculations, but heterogeneity calculations show that the rod advantage factor can yield as much as 1% in k_{eff} and 25% in δ^{28}. These effects can be treated accurately enough by a one-group treatment of neutrons above the fast-fission threshold in ^{238}U. Monte Carlo calculations using the MOCA-2 code[33] agree excellently with experiments. A simple relation can be obtained from a two-region representation of the lattice cell. The fast advantage factor (ratio of average flux in the fuel to that in the moderator) ξ^{28} can be represented by

$$\xi^{28} = 1 + V_1/V_0\beta\Sigma_1 l_0$$

where V_1 = moderator volume
V_0 = fuel volume
Σ_1 = removal plus absorption cross section of the moderator
l_0 = mean chord length of the fuel
β = a numerical factor that can be related to the chord-length distributions in fuel and moderator
$\beta = 0.67$ for a single rod and approximately 0.45 for typical light-water lattices

A second result is that δ^{28} (effects of leakage neglected) is given by

$$\delta^{28} = \delta^{28}_{\infty}\,\bar{l}/(\gamma + \bar{l})$$

where $\bar{l}$ is $l_0 + V_0/\Sigma_1 V_1$, γ is the mean free path in the fuel augmented by fast fission, and δ^{28}_{∞} is the fission ratio in an infinite block of fuel. This representation works best for closely spaced lattices.

Resonance Capture in ^{238}U

Measurement of this quantity or of the related ratio ρ^{28} (epicadmium to subcadmium capture ratio) is too inaccurate to evaluate the various theoretical methods available. Although some progress is being made, the authors feel that "... new and improved experimental methods are necessary to resolve the problems of resonance-neutron capture in light-water lattices."

Thermal-Neutron Distributions

Errors in measurement of thermal-neutron spatial and spectral distribution by means of foil activation stem in part from perturbations of the flux by the foil holder. Another source of error is reduced by careful selection and calibration of foils. Theoretical techniques in common use are the MARC-2B (Ref. 34) and THERMOS[35] codes and the Nelkin scattering kernel.[36] Predicted and measured spectra and distributions are in good agreement, but discrepancies of 1 to 5% in the disadvantage factors remain.

An important source of theoretical error is the treatment of the boundary, especially in closely packed lattices. Use of a condition of isotropic return eliminates most of this source of error.

Reactivity Changes with Long Irradiation

By Bernard I. Spinrad

As plant capital costs go down, reactor fueling costs become a larger fraction of power cost. Therefore the incentive to reduce fuel-cycle costs in reactors becomes greater, and

the impact of even small cost reductions becomes more significant. The ability to understand and predict the isotope and reactivity history of the reactor and its fuel is the major physics contribution to fuel economy.

Fuel-Management Methods

There are three general regimes of fuel management, and these depend on the specific power of the reactor. For reactors of low specific power and long fuel residence times (several years), reactivity changes are small over appreciable lengths of time; then, because the problem is to schedule fuel loading and unloading most advantageously, reactivity-change studies emphasize the achievement of criticality under steady-state fuel management. (The same situation holds for higher specific-power reactors if they have rapid fuel-change mechanisms, as do CANDU and the newer British gas-cooled reactors.)

For reactors of somewhat higher specific power, such as most of the higher power water reactors, refueling is not done frequently enough to be used as the major means of reactivity control. Because fuel residence times are from one year to a few years, reactivity changes appreciably during irradiation, requiring the use of control systems for major shimming. The change of flux shape and spectrum under irradiation, coupled with the fact that these changes also depend on the means of control adopted, become important. However, appreciable reactivity is also manageable by zoned or other forms of graded fuel loading, and some relocation of fuel elements at reloading times is possible.

At very high specific power, refueling time becomes a major economic factor; unless on-line fueling is adopted, fuel lifetime is limited by the excess reactivity loaded and the method of controlling this reactivity. One or two, or at most three, running periods exist between load and discharge of an element, and only very limited fuel management can be employed. The physics of control and of isotope—and flux—change as a function of position becomes the overriding problem.

A survey of papers presented at the Geneva Conference provides the opportunity of reviewing this important field. Future issues of this journal may then report further progress.

Prediction and Measurement

Four major papers were presented on this subject—one each from the United States, United Kingdom, Canada, and France.

Light-water reactor physics was emphasized in a bibliographic review of the status of U. S. technology.[37] Light-water power reactors tend to have rather high specific powers and long refueling times. Therefore the emphasis is on calculation of reactor changes over long irradiation, with fuel-management studies being less developed. References are given to the depletion and flux-evolution codes that have been used and are recommended. Because the detailed evaluation of a three-dimensional reactor, with control system, as a function of time is an expensive process even with modern computing machinery, there has been a recent trend toward reactivation of few-group diffusion theory and few-region flux synthesis, with very good results reported. These methods are all cited in the paper's bibliography. The authors conclude that calculational methods are, by and large, adequate and that the next improvement in predictive capability will come from isotopic analysis of irradiated fuel and its correlation with improved basic cross-section data.

Gas-cooled-reactor fuel management was studied in the United Kingdom.[38] Because these reactors are capable of virtually continuous refueling, the details of flux-shape evolution are unimportant, and the scheduling of regional fuel relocation is the major problem. No recommendations are made; the antagonistic aims of uniform power (maximum equilibrium reactivity on the reactor fringes) and maximum fuel residence time (maximum reactivity at the center) must be evaluated in detail for any set of reactor economic criteria.

Experimental burnup physics studies were described in a status report on the French program.[39] The report is of value, first, as a bibliography of pertinent French work (mostly CEA reports), and, second, as a good example of the sort of coordinated experimental program required to understand integral properties of irradiated fuels. To calibrate single-sample measurements on irradiated samples, the program features measurement of clean plutonium–uranium fuels as regional lattices in substitution experiments. The fuel enrichments are low, as would be employed in heavy-water reactors.

The D_2O reactors, particularly CANDU, benefit from comparisons of theoretical and experimental isotope—and reactivity—changes in D_2O reactors. The Canadian program, which is possibly the most integrated one of theory and measurement for a single reactor type, was described in detail.[40] The computational model used is the standard two-group four-factor formula with, however, each term rationalized for both logical correctness and experimental verifiability. As irradiation proceeds, effective cross sections and resonance integrals are varied to account for changes in neutron spectrum and isotopic concentrations. Fission-product cross sections have been measured and reported. The effect of radial nonuniformity of burnup in a rod has been investigated and found to be small owing to canceling effects of plutonium and fission products. The conclusion is that reactivity change in a D_2O reactor can be predicted closely—0.1% or so in reactivity, corresponding to ±10% of a 10,000 Mwd/metric ton lifetime.

Operating Experience

The measurement and prediction of reactivity changes in British gas-cooled reactors were described in some detail.[41] By frequent rod recalibration, both reactivity change and temperature coefficient of reactivity have been followed up to several hundred megawatt-days per metric ton. Reasonably good theoretical fit is obtained with a two-group reactor model, in which the neutron temperature is obtained by a thermal-spectrum calculation and self-shielding of plutonium resonances is computed in detail as a function of local plutonium concentration.

Reactivity experiments after irradiation of natural uranium, ^{235}U, and ^{233}U in the Materials Testing Reactor (MTR) were reported.[42] Although the irradiation spectrum in the MTR is not very characteristic of a power-reactor history, the results of the natural-uranium irradiations provide a valuable checkpoint for theoretical methods since they extend to 15,000 Mwd/metric ton. This work has been reported previously.[43] The experiments agree well with a standard depletion code. The ^{235}U and ^{233}U experiments serve as measures of the effective cross section of stable and long-life fission products (after the xenon transients, which they also measured, had decayed). An effective $1/v$ cross section of approximately 50 barns (for each fission caused by 2200 m/sec neutrons, *not* per fission product), in good agreement with theory, is found for several irradiations. A resonance integral between approximately 170 and 210 barns per fission is also reported, which is about 10% lower than theoretically estimated.

Burnup experience with the Novo-Voronezh reactor (WWER) was described without going into details of fuel or control management or of evaluation methods.[44] An initial fuel enrichment of 2% permits operation to a discharge burnup of 12,000 Mwd/metric ton.

Calculations

A method for calculating global flux changes during irradiation was reported without presentation.[45] The method uses two-group theory and a simplified method for solving the Helmholtz equations in a few-region system.

Local reactivity as calculated by standard depletion codes fits remarkably well to a quadratic in flux time.[46] With this simplifying assumption, analytic expressions for reactivity lifetime can be obtained for a variety of fuel-management schemes. Amusingly, this paper cites no Western references, even though the work is similar in spirit to Canadian and U. S. work reported at the 1955 Geneva Conference.

The use of soluble and burnable poison in water reactors was evaluated.[47] No reactivity experience is listed in the paper, which is to be considered rather as a bibliographic source. Soluble- and burnable-poison control-physics calculations are key problems in reactivity calculations for high-specific-power reactors because the errors in predicting control margin are comparable to the normal errors in reactivity-change prediction.

Improvements in Resonance-Integral Theory

By Paul F. Gast

During the slowing-down process, neutrons may be captured by the reactor materials

through the action of resonances. Because such captures in ^{238}U or thorium make important contributions to fissionable-material production, they have been studied extensively. Thus neutron-capture rates in ^{238}U and thorium can be computed satisfactorily for simple fuel shapes by semiempirical methods. However, captures in other materials or in more complicated fuel shapes require theoretical treatment, at least in the exploratory conceptual design stages. Work on resonance-integral theory began in the University of Chicago Metallurgical Laboratory days. Some recent developments are reported here.

It is now possible to calculate resonance integrals for isolated resonances to an accuracy limited only by a knowledge of the resonance parameters and by the time and effort appropriate for the case in hand. Monte Carlo methods have been available for some time; recently, numerical analytical techniques have been applied to these problems.

The collision densities and fluxes for homogeneous mixtures of uranium and carbon have been obtained for the 6.7-, 21.0-, and 36.8-ev resonances of ^{238}U by numerical solution of the integral equation.[48] A well-moderated case and one with very little moderation were considered. Although the results are unlikely to find direct application in reactor design, the paper has considerable didactic value because the six cases considered nicely illustrate most of the features of resonance absorption that are neglected in the usual approximations.

A similar solution for a uranium cylinder in a graphite lattice has been worked out for the 6.7-ev resonance only.[49] Details of the method have not been published, but isotropic scattering was assumed, and a polynomial approximation of the transport kernel was used.

In reactor design work such calculations are not usually feasible, so most theoretical attention has been directed toward less laborious methods that give accuracies appropriate for reactor work. The intermediate-resonance method[50] has been extended to the heterogeneous case[51] by the use of equivalence principles. A physical interpretation of the method[52] permits easy computation of the "width parameter" and extension to Doppler-broadened cases.

Equivalence principles rest on two approximations: (1) the assumption of a flat source in computing the escape probabilities from the absorber and (2) the use of a rational approximation to represent the resulting probabilities. The errors arising from the flat-source assumption have been examined.[51,53] The basic approach is the same in both papers, but the method of Ref. 53 has the advantage of not being limited to thin slabs. Table II-1 shows the results obtained by numerical integrations, which depend on the amount of resonance scattering and the slab thickness (in potential scattering mean free paths). Presumably, similar values would apply for other simple convex shapes with the same surface-to-volume ratio; appreciable errors occur when the resonance is a strongly scattering one.

Table II-1 PERCENT ERRORS FROM FLAT-SOURCE APPROXIMATION[53]

Slab thickness	Neutron width/resonance width, Γ_n/Γ			
	0.2	0.4	0.6	0.8
0.0	1.1	2.7	5.5	11.5
0.3	1.3	2.9	5.7	11.7
0.6	1.6	3.2	6.0	11.9

Improvements in the rational approximation are the subject of continuing investigation, and three recent efforts were described in the Summer 1965 issue of *Power Reactor Technology*.[54] An additional formulation has been reported,[55] and its extension to nonblack tubular absorbers has been developed.[56]

References

1. D. P. Moon, Consistent Heavy-Atom Cross-Section Evaluation for Plutonium Recycle Calculations, USAEC Report ANL-6972, Argonne National Laboratory, December 1964.
2. G. D. Joanou and J. S. Dudek, GAM-I: A Consistent P_1 Multigroup Code for the Calculation of Fast Neutron Spectra and Multigroup Constants, USAEC Report GA-1850, General Dynamics Corp., June 28, 1961.
3. G. D. Joanou et al., Nuclear Data for GAM-I Data Tape, USAEC Report GA-2451, Vols. I and II, General Dynamics Corp., Aug. 22, 1961.
4. R. C. Liikala, Updated RBU Basic Library, USAEC Report HW-75716, Vols. 1, 2, 3, Hanford Atomic Products Operation, 1963.
5. D. A. Klopp and W. E. Zagotta, Resonance Integral Determination, ARF Progress Report A-1918-8, Illinois Institute of Technology, Armour Research Foundation, March 1962.
6. F. T. Adler, G. W. Hinman, and L. W. Nordheim, The Quantitative Evaluation of Resonance Integrals, in *Proceedings of the Second United Na-*

tions International Conference on the Peaceful Uses of Atomic Energy, Geneva, 1958, Vol. 16, pp. 155-171, United Nations, New York, 1958.

7. H. Amster, The Calculation of Thermal Constants Averaged Over a Wigner-Wilkins Flux Spectrum: Description of the SOFOCATE Code, USAEC Report WAPD-TM-39, Westinghouse Electric Corp., Bettis Atomic Power Laboratory, January 1957.
8. B. Carlson, C. Lee, and J. Worlton, The DSN and TDC Neutron Transport Codes, USAEC Report LAMS-2346, Los Alamos Scientific Laboratory, February 1960.
9. D. J. Hughes, B. A. Magurno, and M. K. Brussel, Neutron Cross Sections, USAEC Report BNL-325 (2nd ed.) (Suppl. 1), Brookhaven National Laboratory, Jan. 1, 1960.
10. E. M. Pennington, Argonne National Laboratory, in preparation.
11. Q. L. Baird and A. R. Boynton, Bucklings, Disadvantage Factors, and δ^{28} Measurements in Some Undermoderated Slightly Enriched Cores, *Trans. Am. Nucl. Soc.*, 6(1): 258 (1963).
12. Q. L. Baird et al., Initial Conversion Ratio and ρ_c^{28} Measurements in Very Undermoderated Slightly Enriched Oxide Cores, *Trans. Am. Nucl. Soc.*, 7(1): 80 (June 1964).
13. A. R. Boynton, Experimental Thermal-Disadvantage Factors in Some Very Undermoderated, 3%-Enriched Water-Uranium Oxide Lattices, *Trans. Am. Nucl. Soc.*, 8(1): 249 (June 1965).
14. L. C. Schmidt, R. C. Liikala, W. P. Stinson, and J. R. Worden, Critical Masses and Bucklings of $PuO_2-UO_2-H_2O$ Systems, *Trans. Am. Nucl. Soc.*, 7(2): 216 (1964); USAEC Report HW-83187, Hanford Atomic Products Operation, July 1964; USAEC Report HW-84608, Hanford Atomic Products Operation, June 15, 1965.
15. D. H. Carter et al., Buckling and Reaction Rate Experiments in Plutonium/Uranium Metal Fueled, Graphite Moderated Lattices at Temperatures Up to 400°C, Part I. Experimental Techniques and Results, British Report AEEW-R-318, July 1964.
16. D. H. Carter, B. J. Puckett, and A. E. Richards, Measurements of Pu^{239}: U^{235} Fission Ratio Using Foils at Temperatures Up to 400°C, British Report AEEW-M-447, May 1964.
17. R. C. Bannerman, H. H. W. Pitcher, and R. Richmond, Analysis of the Results of Reactivity Change Measurements on Plutonium–Uranium Fuel Elements, British Report AEEW-M-441, July 1964.
18. D. Breton and P. LaFore, Experimental Methods in Thermal Reactor Physics, presented at the Third United Nations International Conference on the Peaceful Uses of Atomic Energy, Geneva, 1964, Paper A/Conf.28/P/102.
19. F. Congé, Mesures Globales de Reseau a Graphite dans l'Empilement Critique Marius, French Report CEA-R-2478, August 1964.
20. F. Cogné and J. Journet, Mesures Fines dans les Reseaux Graphite, French Report CEA-R-2479, 1964.
21. O. Tretiakoff et al., Mesure des Sections Efficaces Effectives d'Echantillons Fissiles par une Methode d'Oscillation dans les Assemblages Critiques, French Report CEA-R-2487, August 1964.
22. J. Valat and T. E. Stern, Analyse de la Precision de Certaines Methodes de Mesure des Tres Basses Reactitivities, French Report CEA-R-2229, August 1964.
23. R. Naudet et al., Experiences Critiques dans Aquilon Portant sur des Combustibles Legerement Enrichis en U^{235} et en Plutonium, French Report CEA-R-2477, August 1964.
24. M. F. Ithurralde et al., Interpretation des Experiences de Criticite sur des Solutions Homogenes de Plutonium et d'Uranium, French Report CEA-R-2488, August 1964.
25. D. Breton and C. Clouet d'Orval, Etudes de Criticite, presented at the Third United Nations International Conference on the Peaceful Uses of Atomic Energy, Geneva, 1964, Paper A/Conf.28/P/84.
26. J. G. Bruna et al., Alecto, Experiences de Criticalite sur une Solution de Plutonium. Resultats Experimentaux, Cuve No. 1, French Report CEA-2274, 1963.
27. J. G. Bruna et al., Alecto 1—Experience de Criticite sur une Solution de Plutonium et d'Uranium Enrichi a 90%. Resultats Experimentaux et Calculs Concernant la Cuve No. 2, French Report CEA-R-2453, June 1964.
28. E. Deilgat et al., Experiences de Criticite sur des Cylinders Annulaires Contenant des Solutions de Plutonium, French Report CEA-R-2495, June 1964.
29. E. D. Clayton, Progress in Plutonium Critical Mass Physics, USAEC Report HW-83603, Hanford Atomic Products Operation, October 1964.
30. J. Bailly et al., Etude des Reseaux a l'Eau Legere par la Methode d'Empoisonnement Homogene au Bore, French Report CEA-R-2489, August 1964.
31. O. Croix et al., Utilisation du Cadmium en Solution dans le Moderateur du Reacteur EL_4, Fixation Irreversible du Cadmium sur les Surfaces Metalliques, French Report CEA-R-2504, August 1964.
32. Glenn A. Price and R. L. Hellins, Lattice Studies in Light Water Moderated Systems, presented at the Third United Nations International Conference on the Peaceful Uses of Atomic Energy, Geneva, 1964, Paper A/Conf.28/P/264.
33. H. Rief, An IBM 704 Monte Carlo Code To Calculate the Fast Effects in Homogeneous and Heterogeneous Systems, USAEC Report BNL-647, Brookhaven National Laboratory, Jan. 1, 1961.
34. E. M. Gelbard, H. B. Ondis, and J. Spanier, MARC—A Multigroup Monte Carlo Program for the Calculation of Capture Probabilities, USAEC Report WAPD-TM-273, Westinghouse Electric Corp., Bettis Atomic Power Laboratory, May 1962.
35. H. C. Honeck, THERMOS. A Thermalization Transport Theory Code for Reactor Lattice Calculations, USAEC Report BNL-5826, Brookhaven National Laboratory, September 1961.
36. M. Nelkin, Scattering of Slow Neutrons by Water, *Phys. Rev.*, 119(2): 741-746 (July 15, 1960).
37. G. H. Minton and H. W. Graves, Jr., Calculation of Criticality, Power Distribution, and Fuel Burnup in Thermal Power Reactors, presented at the Third United Nations International Conference on the Peaceful Uses of Atomic Energy, Geneva, 1964, Paper A/Conf.28/P/266.
38. B. Cutts, A Study of Fuel Cycles and Fuel Cycle Problems for Advanced Gas Cooled Graphite

Moderated Reactors, presented at the Third United Nations International Conference on the Peaceful Uses of Atomic Energy, Geneva, 1964, Paper A/Conf.28/P/177.

39. O. Tretiakoff, Burn Up Physics, presented at the Third United Nations International Conference on the Peaceful Uses of Atomic Energy, Geneva, 1964, Paper A/Conf.28/P/77.
40. M. F. Duret et al., Fuel Burn-Up and Reactivity Changes, presented at the Third United Nations International Conference on the Peaceful Uses of Atomic Energy, Geneva, 1964, Paper A/Conf.28/P/26.
41. H. A. Hughes, D. A. L. Clinch, R. M. Horsley, D. J. Millard, and R. Razzell, Experimental Basis of Power Reactor Operation, presented at the Third United Nations International Conference on the Peaceful Uses of Atomic Energy, Geneva, 1964, Paper A/Conf.28/P/170.
42. R. G. Nisle, D. R. deBoisblanc, E. Fast, J. C. Connor, and S. B. Gunst, Fission-Product Build-up and Long-Term Reactivity Effects, presented at the Third United Nations International Conference on the Peaceful Uses of Atomic Energy, Geneva, 1964, Paper A/Conf.28/P/269.
43. S. B. Gunst, E. D. McGarry, and J. J. Scoville, The Reactivity of Natural UO_2 Irradiated to 6×10^{21} n/cm^2, *Nucl. Sci. Eng.*, 7: 407-418 (1960).
44. L. V. Kommisarov, G. L. Lunin, A. N. Novikov, V. A. Sidorenko, and V. P. Sidorenko, Physical Studies of Novo-Voronezh Atomic Power Station, presented at the Third United Nations International Conference on the Peaceful Uses of Atomic Energy, Geneva, 1964, Paper A/Conf.28/P/585.
45. F. Accinni, R. Bonalumi, C. Bruschi, F. Palazzi, S. Rubbia, and G. B. Zorzoli, The Physics of a Steam-Water Mixture-Cooled Heavy Water Power Reactor, presented at the Third United Nations International Conference on the Peaceful Uses of Atomic Energy, Geneva, 1964, Paper A/Conf.28/P/625.
46. V. Bartosek, M. Hron, V. Lelek, and M. Neprasove (Prague), On Some Physical Problems of Uranium Burnup in Heavy Water Reactors, presented at the Third United Nations International Conference on the Peaceful Uses of Atomic Energy, Geneva, 1964, Paper A/Conf.28/P/630.
47. A. Radkowsky and R. J. Creagan, Poison Control of Thermal Reactors, presented at the Third United Nations International Conference on the Peaceful Uses of Atomic Energy, Geneva, 1964, Paper A/Conf.28/P/274.
48. Hans-Jürgen Siegert, Das Neutronenspektrum in der Umgebung von Resonanzen, *Nukleonik*, 6(6): 307-310 (October 1964).
49. F. T. Adler and E. E. Lewis, Comparison of Exact and Approximate Treatments of Resonance Effects in Cylindrical Lattices, *Trans. Am. Nucl. Soc.*, 7(1): 29 (June 1964).
50. R. Goldstein and E. R. Cohen, *Nucl. Sci. Eng.*, 13(2): 132 (June 1962).
51. R. Goldstein and H. Brooks, Intermediate Resonance Absorption in Nonhomogeneous Systems, *Nucl. Sci. Eng.*, 20(3): 331-337 (November 1964).
52. Guido Forti, Evaluation of Resonance Integrals in Homogeneous and Heterogeneous Systems — An Intermediate Approximation, *Nucl. Sci. Eng.*, 19(4): 449-457 (August 1964).
53. J. Berg, The Flat Source Approximation in Resonance Integral Calculations, *Nukleonik*, 6(4): 202-209 (July 1964).
54. *Power Reactor Technol.*, 8(3): 159-160 (Summer 1965).
55. H. Neltrup, An Approximate Collision Probability Formula for Resonance Integrals, *J. Nucl. Energy, Pt. A & B*, 18: 704-708 (December 1964).
56. H. Aisu, Effective Surface of a Tubular Absorber in the Calculation of Resonance Integrals, *Nucl. Sci. Eng.*, 21(2): 250-255 (February 1965).

Section

III

Power Reactor Technology

Control and Dynamics

Reactor Control Experience

By Joseph M. Harrer

Control-system designers sometimes introduce plant features that, although good in principle or in laboratory tests, do not always work out according to plan when the plant is operated. Thus the experience with control equipment and the failure analyses that were aired at the Conference on Reactor Operating Experience (sponsored by the Reactor Operations Division of the American Nuclear Society) are significant for designers. One attendee's summary and interpretations are given here.

Reactor Accident Frequency

The general opinion exists that reactor accidents are unusual occurrences. Over a period of a little more than 20 years, all types of reactors and critical experiments have amassed a total of more than 1000 years of operating history. Despite the fact that many of these devices were of new or experimental configurations, no member of the general public has ever been overly exposed to radiation or suffered inconvenience from a reactor accident.[1] But during these 20 years there have been about 20 accidents or incidents that resulted in prompt criticality, crew fatalities, or massive damage to the plant. At least half of these accidents would not have occurred if the reactor safety systems had operated correctly.

Components Have Been Reliable. In an effort to prevent reactor excursions, reactors still are being built with equipment that automatically checks safety-system performance as frequently as once per second. The object of these tests is to detect safety-component failure before any reactor excursion occurs. But the actual record of one uncontrolled excursion per million operating hours shows that not one of them resulted from failure of a safety-system component.

The System Must Be Able. Some excursions occurred when the safety system lacked proper input information; several failures resulted from slow response by the safety system. In at least two cases, the safety system was paralyzed by the accident; in another case the accident was intensified by safety action—and in still another case the accident was caused by an attempt to scram the reactor. Thus, rather than being related to component failure or lack of reliability, these performance failures occurred because the safety systems were inherently unable to protect the reactors. Clearly, although it is impossible to anticipate or simulate the exact conditions under which the safety system must perform, much more must be done to make tests uncover more than just component failure. In this way designs and operating procedures can be corrected so as to prevent uncontrolled excursions.

Although the statistical experience of one uncontrolled excursion per million hours was acquired with all sorts of reactors and critical experiments—and thus is not really applicable to the situation in which we are operating proved and stably operated reactors—its importance can be appreciated from the facts that (1) most reactors today have higher powers and greater fission-product inventories and (2) direct extrapolation of these statistics would indicate (improperly, however) that, over a 25-year life, one out of four reactors would suffer an uncontrolled excursion that results in massive damage.

Perhaps a significant question is, "Have we been learning enough from experience?" Simple component testing is not the answer. Operators and designers must devolve tests and corrections that will prevent accidents more effectively.

Rod Problems

The primary safety device has always been control rods. Thus tests that detect impending trouble in control rods are important for preventing accidents. But how dependable is a test that simply assures the time for scram is less than a predetermined value? Not very dependable, according to experience with the UMRR (University of Missouri at Rolla, Reactor), a 10-kw swimming-pool reactor,[2] and with the 61-Mw Heavy Water Components Test Reactor (HWCTR) at Savannah River Laboratory.[3]

UMRR Rod Swelling. Each of the original shim-safety rods consisted of a type 304 stainless-steel shell lined with 30 mils of cadmium and filled with B_4C powder. Because such rods elsewhere have a history of failure, the UMRR rods were checked closely by measuring rod-drop times at six-month intervals. These tests were expected to yield information on the condition of the rods, particularly about swelling, as well as simultaneously checking the scram circuit.

But during one routine startup, control-panel instruments indicated that a control rod would not withdraw beyond 17 in. Inspection showed that the rod was hung at a partially withdrawn position. After the reactor was shut down, rod-drop times were measured and found to be normal for withdrawals of up to 16 in. After the core was dismantled and the suspect control rod was removed, measurement with a micrometer showed an 8.6% increase in rod thickness, which was enough to cause the rod to bind in its channel. Although similar measurements showed that the other two shim-safety rods had swelled 3.2 and 3.0%, rod-drop times gave no indication of this swelling.

A possible failure mechanism is that a shell leak allows water to accumulate in the rod, radiation decomposes the water, the gas pressure seals the hole by forcing damp B_4C powder into it, and subsequent water decomposition raises the pressure, which swells the shell.

The original rods in the UMRR have now been replaced by solid rods consisting of 18-18 stainless steel alloyed with 1.5% boron. As expected, these new rods have a measured worth 80% that of the original B_4C rods. This is more than adequate for the excess reactivity used in the UMRR. And, because of the greater reliability of the new rods, safer operation results.

The UMRR reactor staff concludes that, although rod-drop-time tests provide a good monitor on the total scram circuitry, they are not adequate for monitoring control-rod condition; for this, periodic direct inspection and measurement of rod dimensions are necessary.

HWCTR Rod-Guide-Tube Ruptures. The time measured in rod-drop tests is often judged as satisfactory if it is less than some standard value for a particular rod system. But experience at the HWCTR shows that a simple go–no-go test does not guarantee that failure is not in progress.[3] Safety-rod drop times were measured at HWCTR before each startup, analyzed for unusual results, and compared with previous results to indicate trends. When rod-drop time decreased, loss of snubbing action was the cause; the problem was traced to rupture of the Zircaloy-2 guide tubes for four of the six safety-rod assemblies. The rods had been in service for nearly three years.

The failures consisted of longitudinal splits starting at a transition in size of the guide tube. These tubes are 11.3 ft long, but the inside diameter of the bottom 3.4 ft is 1.310 in. (rather than 1.375 in. as in the upper section) to provide a $\frac{1}{4}$-in.-high transition piece for hydraulic snubbing action when the control rod drops. The splits were attributed to a combination of high residual stress in the necked-down area and cumulative tensile-stress pulses when the rods were snubbed.

The existence of residual stresses might have been expected. The upper and lower sections were of the same thickness, and the design called for absorbing the snubbing forces in tension in the lower section. This in itself leads to the second observation, that tension pulses contributed to the failure. It is well known that considerable tensile stress will develop under those conditions. The vertical tensile stress could have been eliminated by a bottom support for the guide tube, but the hoop stress that initiated the failures would remain. The correction involved lengthening the transition section from $\frac{1}{4}$ to 1 in. and changing the

specifications to assure less residual stress and higher ductility.

Further study of the tubes showed that D_2 content of the Zircaloy was 100 to 300 ppm, which is considered high; generally, the D_2 content at the transition piece was at the higher value. Other Zircaloy tubes that had endured the same reactor environment — but which were of low nickel content — did not display this high D_2 pickup and remained much more ductile when tested by completely collapsing the tubes. They did not crack even when fully collapsed. On the basis of these tests, an overall conclusion is that either Zircaloy-4 or low nickel Zircaloy-2 would be much better for use under the HWCTR conditions, which are 200 to 250°C, *p*D of 10 to 11 (at 25°C), chlorides less than 0.1 ppm, O_2 less than 0.1 cm^3 per kilogram of D_2O (0.14 ppm).

Gravity-Independent Rods

Gravity rod-insertion systems are as old as reactors themselves. But what if you do not have gravity acting in the proper direction at all times? A gravity-independent system with springs provided one answer.[4] The need arose because the Aerospace Shield Test Reactor (ASTR) had to be rotatable in two planes and positionable vertically for various shielding experiments. Thus, rather than heavy rods (on which gravity usually has a beneficial effect), a lighter rod had to be found for this reactor. Optimum performance was obtained by selecting a minimum thickness of silver–indium–cadmium by means of critical-experiment tests; in these tests a 0.200-in.-thick absorber was first tried in the critical assembly; then the silver–indium–cadmium was machined to 0.18, 0.15, 0.12, and finally to 0.100 in., at which thickness a sharp drop in effectiveness was observed. With the 0.125-in. thickness selected, each 24-in.-long rod weighs only 13 lb. Spring forces vary between 30 and 80 lb, with the higher force when the rod is fully withdrawn. Thus maximum and minimum forces are 6 and 2 *g*. Even if the reactor and rod are completely inverted so that gravity acts against the rod springs, the basic 1 *g* is always present to hold the rods in the shutdown position.

Springs Vs. Pneumatics. Gravity-independent rods are widely used on critical experiments, especially for fast reactors — where the assembly and the rods are operated horizontally (to make it easy to assemble fuel in trays), but in air rather than in water as is the ASTR. Many designers feel that air cylinders provide an adequate and neat stored-energy package and prefer them to springs. Assemblies of springs usually are much more bulky, and some mechanical designers do not consider them more reliable than a well-designed pneumatic system. But the big objection to pneumatic systems is that an oil explosion could suddenly wreck the entire system and rapidly remove the stored energy force. Although oil explosions in air storage systems can be prevented by using pumps that do not need an oil lubricant, self-lubricating pistons (for example, graphite rings) would also be needed in the scram cylinders. The pistons could be lubricated with high-flash-point oil, but this would not be an ideal solution.

The use of springs or pneumatic systems for stored energy in gravity-independent systems remains an open question. Designers and users are well-advised to keep abreast of pertinent experience and observe any failures realistically. It may well be that springs could be far superior when one considers the long-term maintenance problem and the fact that catastrophic failure of a spring is not likely if inspection is adequate.

Control of Critical Assemblies by Moderator Level

Usually the dumping of moderator from a critical assembly is considered a backup for control rods. But experience with moderator control at the Westinghouse Reactor Evaluation Center shows that variation of moderator level can be a useful primary control method.[5] The important principle is to vary the moderator level so that at the operating point the k_{eff} is approximately unity due to the upper reflector. Then the upper portion of the reflector is of decisive importance; lowering it will produce negative reactivity immediately even with the rods partially controlling the reactivity.

Use of the moderator as the basic control device is desirable when the cores being studied have nonhomogeneous fuel enrichments, dimensions, and cladding. Criticality is achieved first by movement of control rods and then by the exchange of reactivity in control rods and moderator until the rods are fully withdrawn.

Advantages. The achievement of uniform lattices requires complicated design and fabrication efforts if rods are used at all. Fueled followers (for control-rod slots) tend to produce core uniformity. But if any fuel protrudes into the lower reflector, nonuniformity is introduced. The coupling of control material to fuel represents a potential source of weakness in the rod structure, and, because a hazard is created, the absorber follower section could fall through the core. This type of problem calls for a meticulous design effort to assure safety. For a reduction in this time-consuming and costly work, and at the same time for an increase in the inherent safety, it is much better to rely on moderator-level control completely.

The most probable and most severe accidents considered in hazard analyses for critical facilities and reactors are presumed to come from rapid (step) movement of control material. Thus, in terms of positive insertion of reactivity, operation by moderator control is a significant step in the direction of safer operations because it eliminates a possible accident-creating component.

The ramp rate one obtains from moderator control is a single continuous variable, whereas the ramp rates of control rods vary with radial location; thus, for a given core, the operator does not have to be concerned with there being different ramps available at his fingertips. There is only one method of adding reactivity, and any mechanical failure in the moderator-fill system (leak, pipe failure, etc.) results in moderator loss and reactivity loss.

It has been argued that, with a high moderator level, the moderator reactivity differential effectiveness is low and then one has no rapid means of inserting negative reactivity. However, this argument tends to be countered by the fact that under such circumstances fast insertion of positive reactivity is not even possible.

The whole problem as discussed in Ref. 5 gives one side of one of the oldest arguments in critical-facility operation. Should one raise water with rods withdrawn ready to stop an uncontrolled reaction, or, knowing that the rods will prevent an uncontrolled reaction, should one leave the rods in place until the water moderator is fully in?

The usual method is a compromise. One or two rods are removed, then the water is raised, and later the other rods are raised to achieve a critical assembly. If moderator level alone is used, it is argued that first all rods should be raised and then the raising of the moderator should begin. However, in many assemblies this cannot be done without violating interlocks.

A strong case can be made for moderator-only control, but it is very difficult to prove that by itself it assures safety. If rods are present or even possible, it seems safer to use them in some way to limit the bulk moderator effect and then later achieve a uniform core by changing moderator level and exchanging moderator reactivity for rod reactivity as they are drawn out of the core.

Subcriticality Measurement

All reactor operators want a simple and sure way of measuring subcriticality during shutdown. Although this is one of the most difficult measurements to make in a power reactor, it can be done relatively well in "clean" critical assemblies and in low-power multiplication experiments. As always, the key factor is instrumentation—but, in theory, the measurement is always possible.

The measurement consists in comparing the neutron statistical variation at two or more frequencies. As the ratio of the low-to-high frequency amplitude increases, criticality is approached. But in a power reactor, the high gamma background makes this measurement difficult if not impossible. As a step toward circumvention of this problem, an experiment was performed in which a conventional 12 count/(sec)(nv) BF_3-filled detector was connected to a 20-Mc wide-band video amplifier by a 75-ohm-impedance transmission line.[6] A pulse width of about 100 $\mu\mu$sec was observed. Although neutron counting rates were higher, even with the wide-band electronics there was no significant improvement in gamma tolerance. This led to use of a lower-multiplication gas tube.

A boron-lined detector about 9 in. long by $\frac{1}{4}$ in. in diameter was selected. For greater sensitivity and efficiency, four prototype tubes were operated in parallel. One tube had a boron-coating thickness of 1 mg/cm^2 and was filled with argon–isobutane at a pressure of 250 mm Hg; the other three tubes were filled with argon–carbon dioxide to the same pressure, but their coating thicknesses were 0.8, 1, and 1.2 mg/cm^2. The detectors were checked

with a neutron source, and spent fuel elements served as a gamma source. The typical count-rate response for various pulse-height settings shown in Fig. III-1 indicates only slight desensitization of the detector in a gamma field of 19,000 r/hr. Thus the author concludes that extension of the wide-band techniques with miniature boron-lined detectors will permit measurement of the reactivity of shutdown power reactors by noise-analysis techniques.

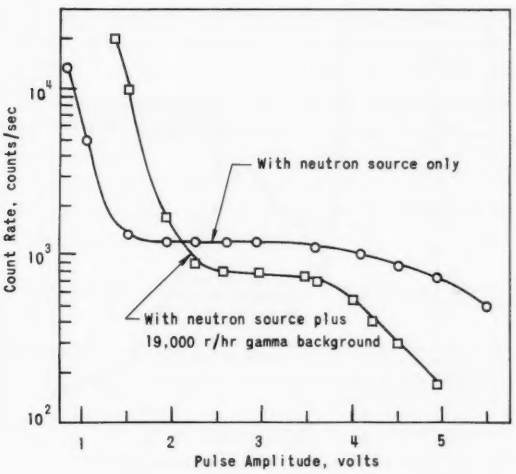

Fig. III-1 Count-rate response at various pulse-height settings for four miniature prototype boron-coated detectors operating in parallel shows that 19,000 r/hr gamma field desensitizes detector only slightly.[6]

Liquid-Poison Injection

Even with good instrumentation, fast safety circuits, and control rods to prevent and stop any uncontrolled excursion, reactor designers have always tried to install a backup system that could be used if the rods failed to control the reactor. A survey of the methods of backup protection used on reactors is given in *Nuclear Safety*, 7(1): 45-52. This backup often is in the form of a neutron-absorbing liquid poison, such as boric acid, that could be forced into the reactor coolant or moderator. But the design of such a system calls for a special approach. How fast should it operate? Should it be automatic or under procedural control? Is stored high-pressure gas a good force to inject poison into a pressurized reactor system? Experience with liquid-poison injection systems at Savannah River Laboratory can help answer such questions.

In the HWCTR[3] protection comes from injecting poison ($K_2B_4O_7-4H_2O$) into the coolant (D_2O) stream. The operator would actuate this system if the neutron flux fails to decrease after a scram signal. The solution has the same reactivity worth as the control rods, a minimum of 24% $\Delta k/k$. If uniformly distributed in the full 7000 gal of D_2O in the primary system, the poison would keep the reactor subcritical under all conditions.

The system was tested at least once a year during an outage by replacing the poison solution with D_2O and timing an injection; poison injection was never actually required during reactor operation.

As the system was originally designed and built, poison solution was delivered rapidly from a storage tank pressurized by helium from an external source. It was planned to adjust the helium pressure for the proper injection time, depending on whether the reactor was pressurized or unpressurized, and to determine the proper helium pressures experimentally during prestartup tests. These tests showed that this arrangement would not deliver the poison properly under certain combinations of reactor pressure and flow. On several occasions with the reactor unpressurized and when some D_2O was blown out of the tank, the main D_2O circulating pumps became gasbound by large volumes of helium.

These problems were avoided by the following changes: the pressure between the reactor gas space and the storage tank was equalized by connecting the reactor gas space to the poison storage tank, which was elevated about 50 ft above the reactor so that gravity would provide the driving force; an orifice was installed in the injection line to control the injection time. After these changes the remaining variable that affected the injection time was the coolant flow through the reactor. About half the system pressure drop is across the core—and thus between the reactor gas space and the moderator space where the poison is injected. Therefore the coolant flow in the reactor directly affects the driving force for injection.

Injection time must be quite a bit longer than the recirculation time of coolant to assure that enough poison is always in the reactor core. If too-rapid injection were allowed, each coolant-

flow cycle could sweep the poison completely out of the core and result in a power excursion. Table III-1 shows the amount of poison injected and compares its injection time to the D_2O circulation time for full flow and shutdown flow. This method was proved by test, and there was no gas binding in the pumps.

Table III-1 HWCTR POISON-INJECTION CHARACTERISTICS

	D_2O full flow	D_2O shutdown flow
D_2O circulation time, min	0.6	2.0
Poison total injection time, min	3.6	3.9
Total poison injected, gal	73	60

Actual injection of another neutron-absorber liquid was tested in a production reactor at Savannah River Laboratory.[7] This system injects $Gd(NO_3)_3$–D_2O solution directly into the D_2O moderator.

Important mechanical features of the system are that: (1) it operates on self-contained pneumatic power that is independent of other pneumatic or electrical networks, (2) injection is not automatic, but rather is initiated from the reactor control room in accordance with specified procedures, and (3) injection of $Gd(NO_3)_3$ starts not less than 5 sec after initiation of the signal but then is completed within 3 sec after injection is begun.

In a special test in a production reactor operating at power, reactor power began to decrease 3.5 sec after the system was actuated and had decreased to 50% after 6.5 sec. Reactor response to the poison injection is shown in Fig. III-2. (The poison was subsequently removed from the moderator by ion exchange.)

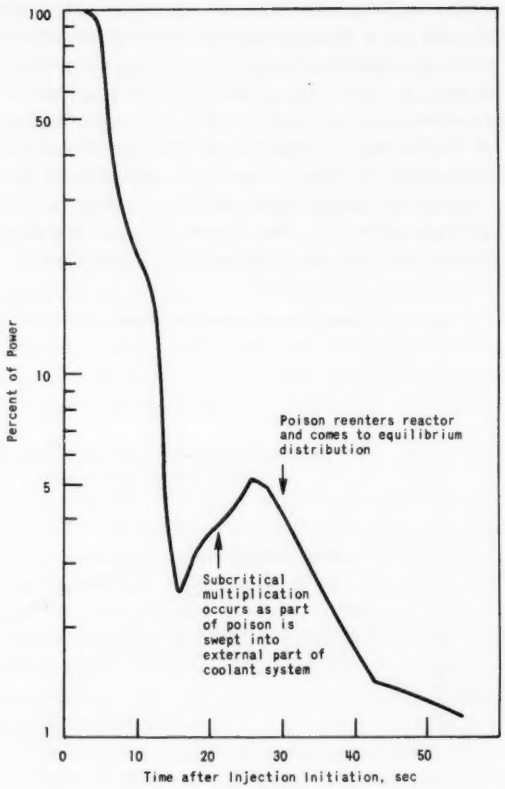

Fig. III-2 Rapid shutdown occurred when neutron-absorbent liquid was injected into reactor moderator.[7]

Computer Applications

The work of compiling a large amount of data accurately, quickly, and selectively is obviously the job for a computer. At Savannah River, the application of modern computer technology is helping ease operational problems.

An on-line digital computer[8] at the K production reactor there improves reactor safety and operating efficiency by providing more thorough surveillance and by compiling accurate operating information much faster than could be obtained otherwise. Signals from about 3200 thermocouples, flow and pressure meters, flux monitors, and other sensors provide information from all regions of the reactor.

Two types of data scans are provided: (1) a sequential scan of 2400 temperatures and flows in the 600 reactor-lattice positions, and (2) a random-access scan for nuclear instruments, in-core flux sensors, and miscellaneous sensors in the D_2O primary and H_2O secondary (river water) coolant systems.

Surveillance of reactor operating limits is an important function of the computer. Several types of fuel elements can be used in one reactor charge, and each may have distinct hydraulic characteristics and operating limits. Alarm programs compare reactor data with the appropriate limits for coolant flow, temperature, temperature rise, and bulk moderator (D_2O) temperature. An alarm is typed in red if an operating limit is exceeded. A periodic print-

out of the margin from the nearest limits is used by reactor operators to adjust reactor power level. Complicated limits, such as proximity to burnout heat flux, are calculated on demand with axial flux data from in-core sensors and fuel-coolant temperature data stored by the computer.

An analog system[9] was used to compute the safety margin from burnout in a special high-flux core [$> 4.3 \times 10^{15}$ neutrons/(cm^2)(sec)] in one of the D_2O-cooled and -moderated production reactors at the Savannah River Plant. The power density of greater than 130 kw per gram of ^{235}U was controlled with the aid of a direct-reading analog-computer circuit that displayed the safety factor against burnout of the fuel surface within an accuracy of 5%. The circuit compares the operating heat flux [$\sim 2.5 \times 10^6$ Btu/(hr)(sq ft)] to the heat flux at burnout as defined by the correlation

$$HF_B = 463{,}000(1 + 0.04V)[1 + 0.0167(T_s - T_b)]$$

where HF_B = heat flux at burnout in British thermal units per hour per square foot
V = coolant velocity in feet per second
T_s = coolant saturation temperature in degrees Fahrenheit
T_b = coolant bulk temperature in degrees Fahrenheit

For the burnout safety factor, the computer circuit solves the simplified equation

$$(BOSF)_x = \frac{(C_1 - C_2 x)\sum_{i=1}^{5} \Phi_i}{\Phi_x \Delta T} - \frac{C_3 \sum_{i=0}^{x-1} \Phi_i}{\Phi_x} - C_4$$

where Φ_x = relative power intensity measured by gamma-flux monitors at five vertical locations (x) equally spaced along the fuel surface
$\Phi_i = 0$ for convenience of notation
C_1 to C_5 = constants for fuel design, pressure, and velocity
ΔT = coolant temperature rise

For more information on control experience discussed at the same ANS meeting, see the article that begins on page 271.

References

1. E. P. Epler, Safety System Performance Failures, *Trans. Am. Nucl. Soc.*, 8(Suppl.): 49-50 (1965).
2. D. R. Edwards, Experience with Rod Drop Times at the UMRR, *Trans. Am. Nucl. Soc.*, 8(Suppl.): 53 (1965).
3. C. P. Ross, Performance of HWCTR Safety Systems, *Trans. Am. Nucl. Soc.*, 8(Suppl.): 50 (1965).
4. J. T. Pancoast, A Gravity Independent Reactor Control System, *Trans. Am. Nucl. Soc.*, 8(Suppl.): 51-53 (1965).
5. G. N. Hamilton, E. G. Taylor, and D. F. Hanlen, Design Considerations in Safety Analysis of Partial Moderator-Level Controlled Reactors, *Trans. Am. Nucl. Soc.*, 8(Suppl.): 49 (1965).
6. Irwin Bluestein, Neutron Measurements in High Gamma Backgrounds, *Trans. Am. Nucl. Soc.*, 8(Suppl.): 24 (1965).
7. L. A. Heinrich, Gadolinium Nitrate Injection as an Auxiliary Shutdown System for Savannah River Reactors, *Trans. Am. Nucl. Soc.*, 8(Suppl.): 58 (1965).
8. K. L. Gimmy and F. R. Field, On-line Computer Assists Reactor Operation at Savannah River Plant, *Trans. Am. Nucl. Soc.*, 8(Suppl.) 53-54 (1965).
9. E. S. Occhipinti, P. E. Mix, J. S. Stutheit, and F. R. Field, Analogue Computer Simplifies Operation of Savannah River High Flux Charge, *Trans. Am. Nucl. Soc.*, 8(Suppl.): 54-55 (1965).

Section

IV

Power Reactor Technology

Fluid and Thermal Technology

Highlights of the 8th National Heat Transfer Conference

By David Miller

Many papers of fundamental and applied interest for reactor technology were presented and discussed at the 8th National Heat Transfer Conference, Los Angeles, Aug. 9–11, 1965, which was jointly sponsored by the American Institute of Chemical Engineers and the American Society of Mechanical Engineers. Although many of the studies were sponsored by the U. S. Atomic Energy Commission (AEC) and have been published in project reports, most were being reported for the first time.

Topics discussed ranged from applications such as heat exchangers, packed beds, desalinization, and loss-of-coolant accidents in reactors to more fundamental studies of boiling and condensation, two-phase flow and pressure drop, and radiation and thermophysical properties.

Boiling and Two-Phase Flow

Boiling, two-phase flow, and stability received a major share of attention. In particular, studies of critical heat flux are of interest to reactor designers.[1–8]

Pertinent to the design of a greater than 600-psia forced-convection water-reactor system is a study in which the coolant entered cylindrical test sections of 0.1- and 0.2-in. inside diameters as a subcooled liquid and during certain tests left as superheated steam.[2] Emphasis was placed on the region with wall temperature higher than that corresponding to the critical heat flux where the surface temperature oscillations were not large; this region is often called the transition or partial film-boiling region. Experiments covered the pressure range 2420 to 3120 psia, mass flows of 0.5 to 2.5 $\times$ 10^6 lb/(hr)(sq ft), heat fluxes of 0.1 to 0.65 $\times$ 10^6 Btu/(hr)(sq ft), and exit qualities of 7 to 100%. These data were combined with other data[9] that extended down to 580 psi to obtain the equation

$$\left(\frac{hD}{k}\right)_f = 0.0193 \left(\frac{DG}{\mu}\right)_f^{0.80} \left(\frac{C_p\mu}{k}\right)_f^{1.23} \left(\frac{\rho_v}{\rho_b}\right)^{0.68} \left(\frac{\rho_v}{\rho_L}\right)^{0.068}$$

for flows of greater than or equal to 0.8 $\times$ 10^6 lb/(hr)(sq ft) over the range 580 to 3190 psia for steam qualities as high as 100%. This correlation has a 2σ probability limit of $\pm$19%. Density was calculated with a void-fraction-weighted sum of the gas and liquid densities; a homogeneous model was used to calculate the void fraction. This study showed that the two-phase entrance length and the length-to-diameter ratio have an important effect on heat transfer. Thermodynamic nonequilibrium found at low flows [0.5 $\times$ 10^6 lb/(hr)(sq ft)] was attributed to unevaporated water droplets passing through the test section; low-flow-rate data were not included in the correlation. The maximum heat-transfer coefficient after the critical heat flux occurred near or at 100% quality.

For a fog-cooled reactor concept, the "dry-out" heat flux (a term used to describe the critical or burnout heat flux at high steam qualities) was measured at mass velocities of 0.5 to 1.4 $\times$ 10^6 lb/(hr)(sq ft) and outlet qualities in the 38 to 78% range.[3] For two-phase inlet conditions, dry-out behavior of geometries simulating reactor fuels was investigated with: (1) angular misalignment of 0 to 60° between an unheated bundle upstream of the 19.25-in.-long heated bundle, (2) two bundle end geometries (CANDU-reactor type and flat-end), and (3) bundle-mounted stripping rings intended to

remove the parasitic water film from the unheated flow tube and redistribute it to the heated rods. All experiments were for a 19-rod bundle cooled by steam–water fog at 515 psia. Angular misalignment reduced the dry-out heat flux on some surfaces (usually inner elements) by as much as 20% but increased it on others (usually outer elements) by up to 70%. Stripping rings raised the dry-out heat flux by up to 100%.

The effects of upstream compressibility on subcooled critical heat flux were investigated.[4] Moderate upstream volumes of subcooled water were shown to have sufficient compressibility to promote oscillatory behavior, which greatly reduces the subcooled critical heat flux for a single channel. This oscillatory instability can be avoided only by operation to the right of the minimum in the overall pressure drop–flow curve characteristic of the heated section. Usually a flow restriction at the inlet of the heated section is needed to alter the overall characteristic so that stable critical heat fluxes can be obtained.

Although inlet-fitting losses make some systems inherently stable, it usually is necessary to provide another restriction at the heated-section inlet. The necessary throttling at the inlet can be estimated readily from

$$\frac{\partial(\Delta P)_{TS}}{\partial w} = 0$$

[where $(\Delta P)_{TS}$ is the pressure drop across the test section in pounds per square inch] if the heated-section hydraulic characteristics are known.

The influence of axially nonuniform heat fluxes on the departure from nucleate boiling (DNB) was studied.[7] Heat-flux distributions studied are shown in Fig. IV-1. For a limited range of parameters, the results are given in the form of a correction factor

$$F = \frac{C}{q''_{DNB,local} + 1 - \exp(-CL_{DNB})} \times \int_0^{L_{DNB}} q''(z) \exp\left[-C(L_{DNB} - z)_{dz}\right]$$

Here C is a coefficient defined as $h/\rho v s c_p$. Because the components of C are not known well enough to permit analytical evaluation, C was correlated by the equation

$$C = 0.44\,(1 - x_{DNB})^{7.9}/(10^{-6}\,G)^{1.72}\ \text{in.}^{-1}$$

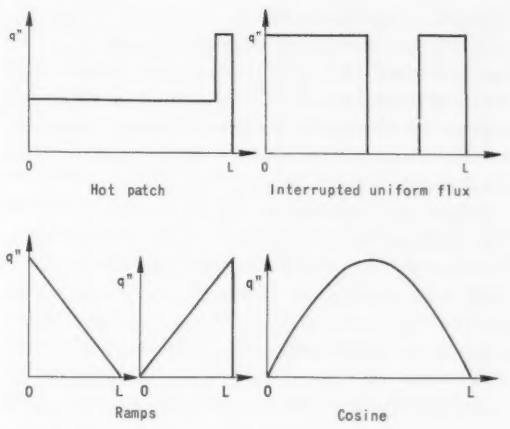

Fig. IV-1 Four shapes of heat-flux distributions were considered in studying how axially nonuniform heat fluxes influence the departure from nucleate boiling.[7]

Pool-boiling critical heat flux was studied by various investigators.[1,5,6,8] Saturated pool boiling on horizontal wire heaters of 0.0025 to 0.254-in. radii was measured[1] over a reduced-pressure (pressure divided by critical pressure) range of 0.0010 to 0.0197. The peak and minimum boiling heat fluxes were correlated with pressure and heater configuration (horizontal and vertical wires and flat horizontal plates) for five fluids: methanol, isopropanol, acetone, benzene, and water. All data can be represented by a single three-dimensional surface that is the product of a function of geometrical scale and a function of pressure. The function of pressure appears to be the same in any configuration. The effect of radius on critical heat flux for small wires at low pressures is significant and complex.

Experimental and analytical investigations of critical heat flux in pool boiling show that the addition of small amounts of calcium sulfate to distilled and deionized water allows increased boiling heat fluxes from stainless-steel heaters.[5] For a $\frac{1}{16}$-in. cylindrical stainless-steel heater coated with calcium sulfate, the critical heat flux was increased by 35%. Pool-boiling tests in water, with a porous graphite heater having air flow through its wall, decreased critical heat flux by 37% over the same heater with no air flow. If it is assumed that departure from nucleate to film boiling occurs when the heater surface becomes nonwetting at a temperature equal to the maximum

possible superheat for the liquid, it is possible to postulate a critical-heat-flux equation for the special case of a small-diameter heater. Significant variation in the critical heat flux with heater properties is predicted by this equation, which contains several coefficients that must be determined experimentally.

When the effects of thermal conduction on the critical heat flux and pool boiling were measured,[6] the critical heat flux of propanol that was boiling at atmospheric pressure on heater strips mounted horizontally in a saturated pool was seen to increase by a factor of 2 as the element conductance parameter, kt (which is the thermal conductivity times "effective" thickness of heater), increased in the range of 4.5 to 1680×10^{-4} watts/°C. A proposed analytical model qualitatively predicts these trends but does not agree quantitatively with the experimental data. The authors conclude that the prime reason that thin heat-transfer elements have lower critical heat fluxes is lower conductance and not lower heat capacity.

Designers concerned with space power units, fast reactor safety, and advanced reactor technology will be interested in studies of the critical heat flux for boiling liquid-metal systems.[8] Eighteen critical-heat-flux experimental data points were presented: two for sodium, eight for rubidium, and eight for water, all taken in the same apparatus. A correlation that represents 60 data points also includes data of other investigators for sodium and potassium; from it results the nondimensional equation

$$\left(\frac{q_c'' C_p \sigma}{\lambda^2 \rho_v k}\right) = 1.18 \times 10^{-8} \left(\frac{\rho_L}{\rho_v}\right)^{0.71}$$

where all values are at saturation conditions. This expression was modified by introducing the Prandtl number to the 0.71 power to include both metallic and nonmetallic data in a single dimensionless correlation

$$\left(\frac{q_c'' C_p \sigma}{\lambda^2 \rho_v k}\right) \mathrm{Pr}^{-0.71} = 1.02 \times 10^{-6} \left(\frac{\rho_L - \rho_v}{\rho_v}\right)^{0.65}$$

that is recommended for predicting the critical heat flux over a range of Prandtl numbers from 0.004 to 11; this correlation is shown in Fig. IV-2.

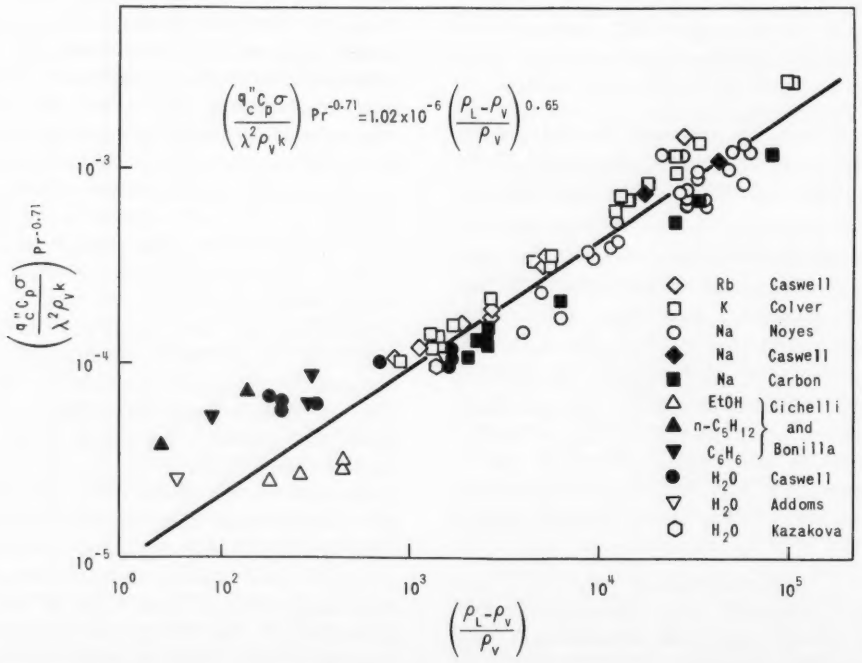

Fig. IV-2 Critical heat flux (q_c'') for various metallic and nonmetallic boiling fluids can be determined by means of a single dimensionless correlation.[8]

The boiling behavior of metallic liquids was also investigated.[10–12] How boiler surfaces ranging from highly polished mirror finishes to coarse, porous coatings affect nucleate pool boiling of sodium was studied.[12] Heat fluxes as high as 236,000 Btu/(hr)(sq ft) were attained at pressures below 1 atm with sodium at 1200 to 1500°F. The qualitative effects of roughness, aging, and hysteresis were determined. For reproducible data to be obtained, it was essential to employ uniform cleaning and filling procedures. Incipient nucleate-boiling heat flux vs. wall superheat were discussed, as were the effects of pressure and pool depth on the nucleate-boiling curve. The surface roughness and past history were found to affect significantly the incipient boiling, the nucleate-boiling wall superheat, and the slope of the boiling curve of sodium. The wall superheat required to initiate sodium nucleate boiling is significantly greater (at least a factor of 5) than that required to sustain it. Natural convection for a horizontal disk in pool boiling, particularly at low boiling heat fluxes, may appreciably influence sodium heat transfer. Clearly, nucleate-boiling heat-transfer data cannot be correlated without including the effect of surface conditions.

In a companion theoretical study of nucleate-boiling instability for alkali metals, a simplified theoretical model for bubble nucleation stability was proposed and an approximate stability criterion was developed.[10] This criterion contains both fluid and surface properties and predicts that nucleation for sodium should be unstable. Measurements of the effects of surface material and its chemical treatment, heat flux and cavity geometry on nucleation stability agreed with theoretical predictions. The stability criterion developed from an analysis of the bubble nucleation and dynamics is unique in that it includes the thermal properties of the surface, the cavity geometry, and the wetting behavior of the fluid. Inertial effects have been omitted. Only double reentrant type cavities appeared to be effective in maintaining nucleation stability of sodium. Thus an artificial nucleating site (such as a doubly reentrant type cavity, a patch of porous plate or porous weld, or a "hot finger") might be used to maintain stability in alkali-metal boilers.

A transient-quenching method of determining the critical heat flux and heat-transfer coefficients in film- and nucleate-boiling magnesium was presented.[11] A tungsten sphere, instrumented with thermocouples, was heated to 3100°R and then quenched in a boiling pool. As the sphere cools, its surface temperature and heat flux follow the boiling curve for the liquid metal being studied. Critical heat flux and heat-transfer coefficients in the transition- and nucleate-boiling regimes for subcooled (265°F) pool-boiling magnesium are included. Analytical predictions of the critical heat flux, however, were a factor of 5 to 10 higher. It was hypothesized that the low measured value of critical heat flux of magnesium was caused by the lack of wetting of the tungsten sphere by the magnesium during transition boiling.

Stability of Flow in Heated Channels

The interaction between hydrodynamics and heat transfer was studied analytically[13] and experimentally.[14] A very restrictive set of assumptions was applied in a theoretical calculation of the dynamic stability of flow oscillations in a heated channel.[13] The stability of this channel was investigated by applying the Hurwitz criterion after a perturbation solution of the usual equations. The resulting third-order characteristic equation shows that, under certain operating conditions, there exists both upper and lower stability bounds on the stability map. The analysis was applied to correlate experimental data of other investigators and to study the effects of various system parameters on system stability. The trends predicted agree with the limited range of experimental conditions (five points for two pressures by one investigator) for which the comparison was attempted.

Flow stability in multitube forced-convection vaporizers was investigated with a transparent closed test loop having Freon-113 as the test fluid.[14] Dimensionless simulation criteria were defined on the basis of the significant parameters determined from a literature survey. Conclusions and discussions are based on the measured data and high-speed photographs of two-phase flow in a five-tube boiler whose tubes had twisted-tape inserts. Stable flow was achieved by inserting an orifice at the entrance of each boiler tube to give pressure drops between 20 and 160% of the two-phase pressure drop. The importance of visual observations was stressed.

Theoretical Boiling Studies

Reactor designers will be interested in theoretical studies of boiling phenomena, including film boiling and bubble formation in nucleate boiling.

Film boiling was explored by several investigators.[15-18] The relation between bubble diameter and frequency of removal from a heated sphere during film boiling in saturated liquid nitrogen was studied,[15] as was the Leidenfrost phenomenon of film boiling of drops on a hot surface.[16-18] The vibrations and breakup of such a drop corresponded to those calculated from spherical-shell theory.[16] An analytical model for boiling heat transfer to waterdrops on a flat-plate-covered heat transfer to the waterdrop, heat transfer from the plate, and the heat-transfer coefficient for the special case where radiation can be neglected.[17] The effect of film boiling for large drops was measured experimentally and compared to theoretical analyses.[18] The maximum drop diameter and the minimum temperature difference for stable film boiling were predicted by stability considerations—similar methods have been suggested for nucleate boiling. These studies may be useful to estimate fuel-element cooling time after a reactor accident.

Bubble phenomena relevant to nucleate-boiling heat transfer were discussed.[19-21] The delay time, growth rate, contact diameter, and bubble size and shape at departure are interrelated.[19] A longer delay brings about faster growth, a larger contact diameter, and a bigger bubble at departure. Spherical bubbles have little or no delay time, slow growth, little contact area, and small size at departure; hemispherical bubbles have a long delay time, very fast growth, a large contact area, and a very large bubble volume at departure; oblate bubbles have intermediate values for all these factors.

Bubble shapes apparently can be explained in terms of inertial and surface-tension forces. For spherical bubbles, the surface-tension force is always greater than the inertial force, but for hemispherical bubbles the inertial force is dominant. For oblate bubbles, either can be dominant. Bubble departure diameters, departure velocities, and contact angles were measured by means of high-speed motion pictures of steady-state boiling.[20] A zirconium-ribbon heater insulated at its undersurface and edges was immersed in a pool of the liquid maintained at saturation temperature. Data for various liquids at subatmospheric pressure were represented by

$$D_d = 0.028\beta \left[\frac{g_c\sigma}{g(\rho_L - \rho_v)}\right]^{0.5} \left[1 + 0.0025\left(\frac{dD}{dt}\right)^{1.5}\right]$$

Mixtures are of interest for increasing boiling heat transfer and for determining the relative importance of thermal and diffusional resistances in the growth and formation of a bubble. Bubble growth rates were given for two mixtures.[21]

Condensation

Studies of condensation are of interest for the design of reactor equipment and, additionally, represent a phase change that is the inverse of boiling.

Laminar film condensation in two-phase channel flow was investigated in an analytical study that includes the interaction between the vapor and liquid interfaces and that proposes a dimensionless criterion for neglecting inertia and convection effects in the condensate film.[22] A relation was derived with the use of a universal velocity profile for predicting condensate-film heat-transfer coefficients for various surface-roughness heights.[23] Two regions were found—an upper limit corresponding to fully developed rough flow and a lower limit corresponding to hydraulically smooth flow. Some experimental data on the condensation of water gave results that fall between these two boundaries.

Film condensation of metal vapors has shown consistently lower heat-transfer coefficients than predicted from Nusselt's classical theory[24] or from more recent modifications of that theory. Kinetic-theory calculations to resolve this discrepancy between theory and experiment show that a significant thermal resistance can exist at the liquid–vapor interface of liquid metals.[25] This resistance increases with decreasing vapor pressure and depends on the value of an accommodation coefficient, named the "condensation coefficient." Experiments to verify this liquid–vapor interfacial-resistance hypothesis used mercury condensing on a vertical nickel surface at low pressures in the

absence of noncondensable gases. Because the condensation coefficient is a function of the state of the liquid surface, it is probably influenced by contamination in the experimental system and may vary with vapor pressure and temperature. Calculations for condensing metals at pressures significantly less than 1 atm should include the condensation coefficient. In practice, particular attention must also be paid to the presence of noncondensable gases in experiments and in operating equipment.

In certain cryogenic applications, heat exchange between condensing and boiling streams is limited by the condensing-side heat-transfer performance. This occurs primarily at high heat fluxes because condensing coefficients decrease with increasing heat flux. The Nusselt equation for film type condensation on a horizontal tube suggests that the coefficient increases in a multi-g acceleration field. More improvement would be expected if the resistance of the condensate layer to heat flow were reduced by a thin porous coating on the condensing surface. Results of condensation experiments in smooth and porous coated tubes under acceleration agree with the theory.[26] At the highest test acceleration of 325 g's, the condensing coefficient improved by a factor of at least 4.25 over that for 1 g with the same temperature driving force. At heat fluxes greater than 10,000 Btu/(hr)(sq ft), experimental coefficients were better than theory predicted; this was attributed to rippling of the condensate film with consequent enhancement of the heat-transfer coefficient. At 325 g's and with a heat flux of 20,000 Btu/(hr)(sq ft), condensation on a porous aluminum surface was 4.5 times better than on a smooth surface. Therefore the combined improvement over a smooth tube at 1 g was a factor of 19.1.

Experiments showed that radially grooved rotating disks reduced the condensing film resistance by some 65% but improved the rate of heat transfer through the disks by only 12 to 14%. In these experiments only a relatively small amount of the feed was evaporated, and thus most of the resistance to heat transfer was on the evaporating side.[27]

Dropwise condensation was discussed by Westwater in an invited lecture and in his papers,[28,29] which showed renewed interest in this method of improving condensing heat transfer. Dropwise condensation of water was shown to occur at active nucleation sites (and therefore should be termed nucleate condensation) whose number depends on the surface preparation and its subcooling.[28] The heat flux may be greater than, less than, or equal to that for filmwise condensation at the same temperature difference, depending on the active-site population. Exact calculation of the heat flux requires an involved iterative technique to account for the nucleation, growth, and coalescence of every drop. The functional relation between the temperature difference and active-site population is unknown for any surface. Oleic acid[29] promoted dropwise condensation of ethylene glycol on a copper condenser when the surface was cooler than 290°F. Correlation of data over a wide range of variables was achieved through modification of an Isachenko[30] equation to

$$\mathrm{Nu} = 1.46 \times 10^{-6} (\mathrm{Re}^*)^{-1.63} \Pi_k^{1.16} \mathrm{Pr}^{0.5}$$

where

$$\mathrm{Re}^* = k_L \Delta T / \mu_L \lambda \quad \Pi_k = 2 g_c \sigma (d\sigma/dT) T_s / J \lambda \mu_L^2$$

and

$$\mathrm{Pr} = (C_p \mu / k)_L$$

This study also indicates there may be as many as 7 million active nucleation sites per square inch during dropwise condensation. A drop may experience an estimated 400,000 coalescences in reaching its final size. Thus the liquid-film fracture theory of dropwise condensation is rejected.

Two-Phase Pressure Drop

Reactor thermal and safety analyses frequently involved predictions of the properties of two-phase fluids. That interest in this subject continues strong was evidenced by seven papers.[31-37] Two-phase frictional pressure drop was correlated on the basis of data for mercury–nitrogen, water–air, and three sets of data for steam.[37] The ratio of two-phase to all-liquid pressure-drop gradient was expressed as

$$\Phi_{L_0}^2 = \frac{(\Delta P/\Delta L)_{TP}}{(\Delta P/\Delta L)_{L_0}}$$

where the subscript 0 stands for total mass flow rate. The relation between this two-phase

multiplier and the Lockhart–Martinelli[38] correlation

$$\Phi_L^2 = \frac{(\Delta P/\Delta L)_{TP}}{(\Delta P/\Delta L)_L}$$

is given by

$$\Phi_{L_0}^2 = \Phi_L^2(1-x)^{1.8}$$

where x, the quality, is the ratio of gas (or vapor) mass flow rate to total flow rate, for both single- and two-component flow. The correlation consists in a plot of the two-phase multiplier as a function of the property index, $(\mu_L/\mu_g)^{0.2}/(\rho_L/\rho_g)$, with quality as a parameter for mass velocities from 0.25 to 3×10^6 lb/(hr)(sq ft). This correlation was based on 129 experimental points and the mass-flow-rate data of Sher and Green[39] for 2000-psia steam. The latter set of curves shows a rather unusual behavior and cannot be represented by any analytical expression.

Experimental pressure-drop and void-fraction data are compared with this correlation for water–air, kerosene–air, diesel oil–air, NaK–nitrogen, potassium (in a horizontal serpentine and an annulus with a helical tape), and steam. No effort was made to include the effect of changing flow patterns in the correlation. However, because the two-phase multiplier ratio may both increase and decrease at a given mass velocity and quality as the property index increases, this unusual aspect of the correlation may implicitly include the effects of flow-pattern changes. Application of the correlation to data on boiling potassium required the use of a previous correlation[40] to predict liquid fraction.

Bubbling mixtures in turbulent flow within a vertical plexiglass tube were used in an experiment that included analyses and separate measurements of frictional, hydrostatic, and momentum pressure drops.[35] Calculational procedures are suggested. The authors found the simplest correlation for bubbling-flow wall shear stress is obtained when a Reynolds number and friction factor are defined by use of the actual mixture velocity and density along with the liquid viscosity. The resulting friction factors are then approximately 10% above the Moody smooth-pipe friction factor. Momentum fluxes in bubbling flow were found to be not necessarily bounded by the homogeneous and separated flow models. The momentum fluxes were found to be better correlated by the separated model but would always be 5 to 25% larger than predicted by that model.

When the void fraction was less than 25%, bubbles formed at the wall diffused only slowly toward the center, giving rise to slip ratios less than 1. This behavior is characterized as "developing flow"; however, the length required for fully developed flow is not known. Photographs helped define a map of the boundary between bubbly flow and unsteady exit flow on the coordinates of superficial liquid velocity vs. superficial gas velocity. For large volumetric flow concentrations, the void fraction approaches the slug-flow limit.

The transition from the slug-annular to two-phase flow was studied with an electrical-conductivity probe.[34] The purpose of this study was to identify the flow pattern for correlations of pressure drop and heat transfer. Simultaneous void measurements indicate that the transition occurs when the void fraction is between 80 and 90%. For superficial liquid velocities greater than about 1 ft/sec, the mass quality at transition is a constant that depends only on pressure. For low superficial liquid velocities, transition occurs at a superficial gas velocity that depends on pipe diameter. When the liquid flow is small, transition is unaffected by a reduction in liquid surface tension or the effects of liquid impurities. The liquid viscosity does not significantly affect the transition line.

During the discussion of this paper, it was mentioned that substantial subcooling eliminates slug flow to give transition directly from bubbly to annular flow. As an alternate to the electrical-conductivity probe, a study of the power spectral density of pressure fluctuations at the wall was suggested for determining the flow regime.

Void fractions in a developing two-phase flow system with flowing and nonflowing liquid phases were investigated for steam–water mixtures flowing vertically in a large unheated duct over a wide range of flow conditions.[36] The scope of the experiment covered superficial liquid velocities of 0 to 20 ft/sec and pressures of 600 to 1500 psig. A gamma attenuation system was used to measure chordal void fractions, which were integrated to give an average. Also, a manometer technique was evaluated for giving the average void fraction.

Void distributions obtained with the variable-density model of Bankoff[41] (this reference was incorrectly cited in the paper) were compared with those from the film–exponential model. The latter model assumes a thin film of liquid at the wall. The average void fractions were compared with slip-ratio correlations of Marchaterre and Hoglund[42] and the kinematic-wave model of Zuber and Findlay.[43] In the discussion of this paper, the question of flow development was raised again. For an explanation of the slip ratios of less than 1, it is necessary to assume that the vapor was near the wall where velocity is least. Experimentally it was found, however, that there was liquid at the wall. It was also pointed out that equations for two-phase flow should include the dependence between velocity and void profiles. Fluctuations in velocity and density give rise to terms similar to the Reynolds stresses in turbulence theory.

The phase velocities in boiling flow systems are given by their relation for minimum voids in terms of phase densities and parameters related to the velocity distribution by use of a total energy balance.[31] The correlating interval (which is a function of the quality and the vapor- and liquid-phase viscosities and densities) was derived from diffusion theory. A simple relation was obtained between quality, vapor fraction, and power input per unit flow volume in the test section. Qualitative predictions of void variation with heat flux and hydraulic diameter were said to agree with data from the literature. In the discussion of this paper, it was pointed out that application of minimization principles without rigorous justification could lead to serious errors. Kinetic-energy distribution factors dependent on velocity distributions were introduced in this model; they varied from 0.5 to 1, and the variation depended on whether the flow was laminar or fully turbulent. If the flow pattern in each of the phases cannot be specified, these constants may only serve to curve-fit the data.

Sudden contraction in two-phase flow in round pipes caused pressure drops that were measured and reported as functions of system pressure, flowing-mixture quality, contraction-area ratio, and mass velocity.[32] No void measurements were made, and water at saturation pressures of 200 to 500 psia was the only fluid studied. Pressure drop caused by the contraction was correlated in terms of a contraction coefficient that was independent of mass velocity over the range of conditions studied. The homogeneous model gave the best correlation of the data, but it was about 20% high, supposedly because of a large amount of mixing in the reexpansion after the vena contracta.

Two-phase heat transfer was simulated by the bubbling of air through the wall of a porous heated tube into water and into ethylene glycol flowing upward at room temperature and atmospheric pressure.[33] A simplified superposition type model based on microconvection, vapor–liquid exchange, and "convection-area-reduction" mechanisms was found to predict the trends of the air bubbling rate on heat transfer. Heat transfer increases over that of pure forced convection at low and moderate bubbling rates compared favorably with those caused by pool nucleate boiling when convective heat-transfer rates were relatively low. Photographs of pool boiling and air bubbling from identical tubes in a tank of Freon-11 showed qualitatively that bubble diameters and flow formations were similar in both processes. The result of this theory suggests that the enhancement in heat transfer and boiling could be considered as hydrodynamic in nature, thus making latent-heat transport unimportant as a heat-transfer mechanism.

Heat Exchangers

A lively commercial and technical interest in heat-exchanger design and operation is indicated by the large number of relevant papers that were presented.

Experimental heat-transfer coefficients were presented[44] for in-line, turbulent flow of NaK along the surface of an unbaffled bundle of nineteen $\frac{1}{2}$-in.-diameter rods arranged on an equilateral triangular pattern with a pitch-to-diameter ratio of 1.75. The shell and all rods in the bundle were heated electrically to provide equal and uniform heat fluxes of 18,000 to 30,000 Btu/(hr)(sq ft) throughout the bundle. Tests covered conditions of fully established velocity and temperature profiles and also conditions where entrance effects were important. These results agreed with theoretical predictions and earlier similar experiments with mercury except at very low flow rates corresponding to Peclet numbers less than 500. It was hypothesized that the low heat-

transfer coefficient (~10% below theory) was caused by gas collection and incomplete wetting at the heated surface.

An analytical study of the wall and fluid temperature field in a counterflow heat exchanger includes the effects of longitudinal conduction in the wall and unbalanced flow.[45] In addition to the general solution, balanced flow and insulated boundary conditions are considered. Longitudinal conduction in the wall separating the fluids distorts the temperature-distribution curves for both streams and produces a larger temperature difference at the ends; the minimum difference is at some point between the ends. With these exact solutions and the temperature-distribution plots, it is possible to determine how thermal performance is affected at low flow rates.

The effectiveness (the ratio of the enthalpy actually transferred to the maximum possible) and temperature difference of the unmixed fluid in "split cross-flow" heat exchangers were determined analytically.[46] Of particular interest is the "split–mixed crisscrossed–unmixed" heat exchanger, which provides the most uniform exit temperature distribution of the unmixed fluid among the simple-configuration cross-flow heat exchangers (Fig. IV-3). Effectiveness and temperature distribution are compared with conventional cross-flow heat exchangers. Heat exchangers with one shell pass and n tube passes, where n is an even number, are often referred to as 1-n exchangers. A generalized equation[47] has been derived for the effectiveness, ϵ, of 1-n exchangers in terms of the capacity-rate ratio, R, and number of transfer units, NTU. Values of ϵ at small intervals of R and NTU are tabulated for the 1-2 exchanger together with correction factors to give ϵ for each 1-n exchanger through $n = 12$. Deviations from 1-2 exchanger effectiveness increase with n and NTU. Thus, in addition to the significant effect that these deviations have on thermal stability and control of exchangers, the correction factor is particularly important in the design and selection of large heat exchangers whose purpose is the economic recovery of heat from a fluid. Because economic evaluations of such exchangers often involve the difference between two large numbers, the accuracy of the deviations and correction factors is an essential factor. The use of analog and digital computers to design plate type

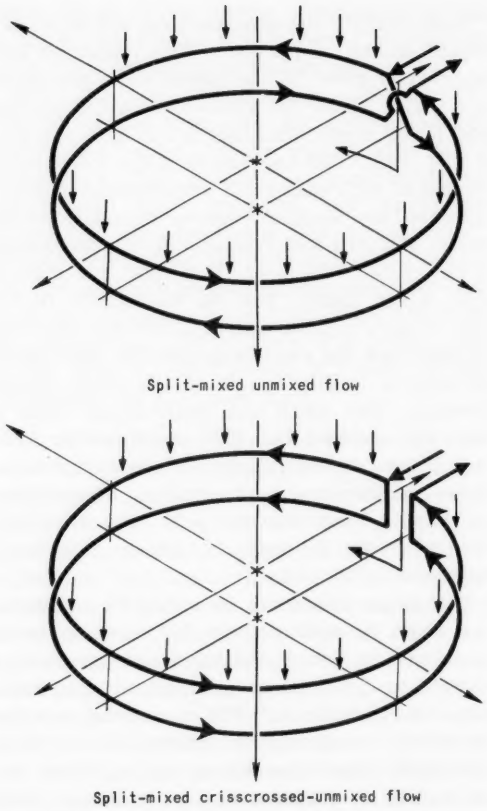

Fig. IV-3 Schematic of flows in split cross-flow heat exchangers within cylindrical envelopes.[46]

exchangers by the ϵ–NTU method was described.[48] The techniques were outlined in detail, and some results were given.

Finned tube heat-exchanger design data and procedures were given in seven papers.[49–55] Pressure drop of air flowing across triangular-pitch banks of finned tubes is correlated in the form of a friction factor as a function of a Reynolds number and a pitch-to-diameter ratio.[54] Measurements are reported of convective heat transfer and flow friction for nine pin–fin surfaces with square spacing of 2, 3, and 4 times the fin diameter and with plate spacing of 4, 8, and 12 times the diameter.[52] Vibration was found to be important, and intense noise occurred at certain flow velocities because of vortex shedding, which may have been coupled with a natural frequency in the heat exchanger. Vibrations increased the friction factor but did not significantly affect

the heat transfer. Natural frequencies of the heat exchangers may be either acoustical or mechanical. Free-convection heat transfer to a new type of extended surface covered with rows of finned pins was studied.[51] With an average temperature excess of 200°F at the roots of the pins, the rate of heat transfer from such an extended surface was 475% higher than that from the basic surface without the finned pins.

The problem of optimizing finned geometry to maximize free-convection heat transfer in air at atmospheric pressure, taking into account nonuniform fin temperatures, was investigated[49] by introducing the fin effectiveness into the Elenbaas[56] solution for uniform fin temperature. This yields an optimum fin spacing for the nonuniform case, together with optimum values for fin thickness and tube diameter for a tube with square fins. A theoretical analysis of optimization of parabolic-shaped fins considers the combined effect of conduction, radiation, and solar irradiation.[50] The governing differential equation is reduced to an equivalent double-integral equation that yields the relation between the finned geometry and weight parameters. The resulting geometry of least mass is plotted as a function of the dimensionless irradiation parameter and the structure-to-weight ratio (total weight to the weight of the fins).

A novel lightweight heat-rejection system for vapor was reported.[55] It uses cooling fins made of plastic film to condense the vapor coolant for a portable direct-conversion energy system. The plastic film can accommodate changes in heat input by changing shape or by partially collapsing. The durability and long-term performance of finned tubes under steady-state and thermal-cycling conditions were evaluated by means of tests on both extruded-fin tubes and tension-wound-fin tubes (in each specimen the fin and tube were of different metals).[53] Single-tube heat-transfer and strain-gauge tests were run both at the original contact pressures and at the isothermal tube-wall temperatures at which the fin-to-tube contact was lost.

A dynamic analysis was made of a concentric-tube heat exchanger with a time-varying flow as the forcing function.[57] The mathematical model agrees well with experiments for step, square wave, and sinusoidal changes in the tube flow rate. Errors introduced by linearization of the equations were investigated to determine the accuracy of the approximation.

Two novel heat-exchange devices were reported.[58,59] The Spiralator uses a rotating twisted tape to scrape the interior wall of tubes containing viscous or fouling liquids.[58] Small-diameter flexible-tube Teflon* heat exchangers offer high corrosion resistance, smooth slippery surface, tube flexibility, and inertness.[59] The favorable nucleation characteristics of Teflon for boiling and condensation and the fact that about 200 sq ft of surface area per cubic foot of shell volume can be built into a small tube exchanger stimulate interest in this new development. The higher thermal resistance of the Teflon wall can be offset by the lack of fouling for crystalline deposits and the versatility of its use.

Packed Beds

Relevant to some advanced reactor concepts are several papers on packed-bed heat transfer and pressure drop. Heat-transfer and pressure-loss characteristics of glass–ceramic matrices for regenerative heat exchangers were measured.[60] The steady-state axial temperature distributions in moving-bed fluid-to-particle heat exchange was determined analytically for a vertical duct of constant area in cocurrent and countercurrent flow.[61] If the regeneration principle is used, the distance over which the gas and solid temperatures are different and heat is transferred can be predicted. The small value of the effective length indicates that such a fluid-to-particle heat exchanger would be very compact. An analysis of unsteady-state heat transfer to a fluid flowing through porous heated solids provides solutions for both solid and fluid temperatures, some of which were verified experimentally.[62] Theory and experiments were reported for the heat-transfer and flow-friction characteristics of air-cooled matrices of high porosity that were heated by radiation which gives an exponential heat source.[63] A transient solution of simultaneous convection and radiation heat-transfer equations, when used with experimental data taken in the steady state, gave volumetric heat-transfer coefficients for convection only in the matrices. Correlations were obtained with

*Trademarked name for Du Pont fluorocarbon resin copolymer.

Reynolds numbers, based on a characteristic length obtained by equating pressure drop to the sum of viscous and inertial resistance terms. A related but more theoretical paper reported a study of the time-dependent temperature distribution for incompressible flow past a sphere.[64] A numerical solution of the diffusion equation showed that the temperature gradients at a spherical surface, as well as the time required to approach steady state, depend markedly on the value of the Peclet number.

Desalinization

The possibilities of the desalting of seawater as an auxiliary process while generating power in a dual-purpose nuclear plant have been receiving considerable attention from reactor designers. The interest in such technology is indicated by the six papers presented on this subject.[65-70] The thickness of a laminar liquid film draining from a vertical wall can be found analytically for the case of a constant evaporation rate from the surface of the film.[65] Transient as well as steady-state expressions are found that show the location where the film vanishes, the rate of evaporation, and the total mass evaporated.

The U. S. Department of the Interior's Plant No. 1 at Freeport, Tex., for desalting seawater by the falling-film distillation process was described thoroughly.[70] Reference 70 gives a description of the process, analysis of pilot-plant data and a report on evaporator performance. An alternate method of heat transfer in desalinization involves a multiphase exchanger that uses direct-contact heat transfer from a nonvolatile immiscible liquid to change the phase of a volatile fluid.[69] The initial diameter of pentane droplets evaporating within an immiscible water medium in a 3-phase (pentane, water, and pentane vapor) heat exchanger was found to affect the overall heat-transfer coefficients. The heat-transfer coefficient increased with a decrease in droplet size, and, apparently, surface tension and excess pressure from curvature are relevant parameters. Although scraped or wiped falling-film evaporators have been used industrially for some years, little has been published about their heat-transfer performance. An experimental study of evaporation at a scraped surface found that the Nusselt number was proportional to Reynolds number to the 0.25 power, to a rotary Reynolds number to the 0.43 power, to the Prandtl number to the 0.33 power, and to the number of the blades to the 0.33 power.[68]

Deposits formed beneath bubbles during nucleate boiling of radioactive calcium sulfate solution were found in detailed studies to be related to heat transfer and the problem of fouling of surfaces during evaporation of salt water.[66] Calcium sulfate is of interest because of its scale-forming ability. Studies of such deposits show that the bubble behavior is consistent with the microlayer vaporization hypothesis proposed by Moore and Mesler.[71] The relative distribution of the deposits revealed by autoradiographs indicates that there is more evaporation beneath the bubble (as was suggested by Moore and Mesler) than there is in evaporation at the triple interfaces (as was proposed by Partridge and White).[72] A second study of heat transfer and fouling rates during pool boiling of calcium sulfate solution shows the deposition rate is proportional to the square of the heat flux and nearly constant in time at constant heat flux.[67] It follows that the deposition rate is proportional to the concentration driving-potential squared, as proposed by Miyauchi.[73] Deposition of $CaSO_4$ on a surface in nucleate boiling creates additional nucleate-boiling sites, which raises the heat-transfer coefficient during part of the operating time—although the eventual result of fouling is to reduce heat transfer. Thin polyhydrocarbon coatings retarded scaling by an order of magnitude and increased the overall coefficient of heat transfer during calcium sulfate deposition. Polymerization fouling, which was also studied, produces a temperature–time behavior completely different from that of crystalline fouling and is not well understood. The heated surface temperature remained constant for a time that depended on the heat flux and polymer concentration. It then increased 350 to 400°F within 1 to 2 min and began oscillating with an amplitude of 40°F and a period of about 0.1 min.

Radiation

Interest in radiation heat transfer continues to grow because of the increase in design temperatures of reactor systems and because of the importance of this mechanism for heat sinks for space power plants.

A method was presented for calculation of radiative exchange in enclosures whose surface reflectance can be approximated by the sum of a diffused and a specular component.[74] Heat transfer by simultaneous internal conduction and surface radiation in plates with specular reflection was treated in terms of a nonlinear integro-differential equation that was converted to an integral equation and then solved numerically.[75] Solutions have been obtained for a wide range of conditions, including those for which diffuse reflection results are available. Reflection and transmission intensities from gray slabs were found by use of the powerful invariant embedding method that was developed for phenomena such as neutron transport.[76] Problems of simultaneous convection and radiation in a laminar boundary layer on a flat plate were formulated and solved.[77] In these solutions it was assumed that the plate surface is black and that the fluid medium is a perfect gas for which the mass absorption coefficient for radiation is independent of frequency and temperature. The iterative solution includes the effect of viscous dissipation, secondary emission and absorption, and incident external radiative fluxes.

Thermophysical Properties

A novel use of heat-transfer techniques enables the measurement of thermophysical properties at extremely high temperatures. The thermal conductivities of noble gases in the range 1500 to 5000°K were determined by measurement of heat-transfer rates from heated gases to the end wall from a reflected shock wave.[78] Consideration of density variation in the thermal boundary layer was found to be significant in evaluation of the data; some previous investigations had neglected this effect. The thermal conductivity of hydrogen from 2000 to 4700°F and 15 to 150 psia was determined from the measured effective conductivity of porous tungsten specimens filled with pressurized hydrogen;[79] thermal conductivity as determined by subtracting the solid conductivity contribution compares within a factor of 2 with existing experimental and theoretical work. Heat transfer through porous ceramics in a thermally degraded ablation material was measured and tested against different theories.[80] If the correct model is assumed, the apparent conductivity is the sum of the separate contributions of solid and gas conduction in radiation. The radiant portion of the conductance is proportional to the product of the mean temperature cubed times the average pore size.

Other Heat-Transfer Studies

Studies important to cryogenic heat transfer were described.[81,82] Heat transfer from laminar boundary layers was considered, with emphasis on large free-stream velocity gradients and highly cooled walls.[83] In experiments on how free convection affects laminar forced-flow heat transfer in a uniformly heated horizontal tube, the free-convection-flow component that caused secondary flow was observed as a decrease in the wall-to-bulk fluid temperature difference required to transfer heat as compared to the pure forced flow.[84] Local as well as average heat-transfer coefficients between an isothermal flat plate and impinging two-dimensional jets were measured for both single jets and arrays of jets.[85] Viscous and thermal boundary-layer behavior on the electrically insulating wall of a rectangular magnetohydrodynamic channel was analyzed theoretically by use of momentum and energy integral approximations.[86] Measurements of the way in which asymmetrical heating in a parallel-plate channel affects fully developed turbulent heat transfer show it to be qualitatively as predicted analytically.[87] An analysis of a thermal flowmeter includes the normally neglected effect of axial conduction along the tube.[88] Transient heat transfer between a thin circular tube and the incompressible fluid moving through it was analyzed for constant inlet fluid temperature;[89] both radial conduction in the wall and the heat loss at the outer surfaces of the cylinder were included. The effect of heat conduction on wall temperature was determined for a well casing passing vertically through a planar heat source of constant temperature.[90]

An approximate calculation was presented for natural-convection melting of an ice-water system.[91] Although an analytical study of transient heat transfer to a Bingham plastic (a material with a finite yield stress and linear stress–strain curve) in laminar flow in a circular tube with energy generated internally was given with a justification of its applicability to slurry reactors, experiments reported in the paper generally agree poorly with the theory, showing wall temperatures 30% lower to 100% higher

than predicted plus a different transient response.[92] Equations were given for the temperature of moving solid materials undergoing heating or cooling.[93,94] The determination of the surface heat flux from the measured-temperature history inside a heat-conducting solid is called the inverse heat-conduction problem; this problem becomes nonlinear if the thermal properties depend on temperature and was solved by a finite-difference method.[95] A stable, explicit numerical solution of the conduction equation for multidimensional nonhomogeneous media was presented.[96] This method, which may be called an alternating-direction explicit procedure, takes less computational time than the alternating-direction implicit procedure and appears to combine the computational ease of the explicit methods with the stability of the implicit methods.

Evaporation rates from hot vertical flat plates, which are relevant to reactor safety analyses, were analyzed.[97] It was concluded that a correction factor accounting for the effect of transverse mass flux must be incorporated in the correlation expression for pure heat transfer. Also of potential importance to reactor safety is an experimental study of transient heat transfer to liquids in cylindrical enclosures.[98]

The thermal-control techniques and the thermal-design calculations for the Nimbus satellite were reviewed.[99] Movable insulation panels provide active temperature control of exterior surfaces. The analytical methods described agree with thermal model tests and actual space-flight data.

Loss-of-Coolant Accidents

One facet of heat transfer directly related to reactor safety and containment was discussed by a panel. Most of the discussion concerned the LOFT (Loss-of-Fluid Test) program that is part of the reactor safety program of the AEC. For this program a 50-Mw(t) pressurized-water reactor and test facility are being built in Idaho to learn how a reactor is affected by a sudden loss of coolant and the extent of any resulting radioactivity release. Phillips Petroleum Company is responsible for building and testing the LOFT blowdown facility; Kaiser Engineers, a Division of Henry J. Kaiser Co., is designing the LOFT facility.

R. P. Rose (of Phillips) described the proposed five-phase test program: (1) containment pressure and leak tests, (2) coolant blowdown tests with a dummy core, (3) low-power physics tests and power operation, (4) loss-of-coolant test, and (5) facility cleanup and posttest examination. Rose pointed out that the many unknowns associated with the blowdown program have suggested the need for a scale model to mock up the LOFT geometry before the full-scale tests. He discussed the scaling down of the LOFT physical dimensions for the proposed blowdown test facility, which would preserve the relative dimensions of the piping, vessel, and core rather than the time scale. As a result the metastable fluid behavior during blowdown may be affected because linear three-dimensional scaling involves shortening of the time scale.

J. S. Busch, W. D. Harrington, and S. Fabic (of Kaiser) discussed analyses that gave the system boundary conditions for transient containment as well as for the primary-loop transients resulting from blowdown; generalized digital-computer programs and subsequent parametric analyses were used.

S. Esleak (of The Babcock & Wilcox Co.) discussed some of the more important problems pertaining to a loss-of-coolant accident: (1) two-phase critical flow, (2) two-phase pressure drop, (3) dynamic effect in the core, and (4) coolant expansion and degree of separation in the reactor vessel. The bases of his discussion are available in a recent state-of-the-art report.[100]

Specific phenomena pertaining to the loss-of-coolant accident were discussed by J. A. Redfield, P. J. Moody, and H. Fauske. Redfield (of Bettis Atomic Power Division, Westinghouse Electric Corp.) presented a simplified model for fuel-element heat transfer during a loss-of-coolant accident which has been applied to the Zircaloy-clad oxide-rod fuel elements for LOFT. He concluded that more data are needed for transient heat transfer under conditions of rapidly falling pressure, rapidly rising coolant quality, and highly unsteady flow conditions.[101]

Moody (of General Electric Company) discussed an idealized model for estimating critical flow rates and pressure drops for given vessel conditions and flow break geometry. Although this ideal-nozzle model agreed well with one previous test (for the Humboldt Bay nuclear power plant), it clearly overpredicted another test (for the Bodega Bay plant). An extension of the energy model to include fric-

tion losses yielded fair agreement with the recent data of Fauske.[102]

Fauske (of Argonne) evaluated existing models for calculating maximum escape rates of reactor coolant. On the basis of recent measurements of voids at critical flow conditions, he concluded that previously formulated models (Fauske,[102] Levy,[103] and Moody[104]) are physically incorrect and that their good predictions resulted from the high values of velocity ratios, which compensated for metastability effects. A new model was suggested, including both the effects of slip and metastability.

Nomenclature

A = area, sq ft
C_p = heat capacity, Btu/(lb)(°F)
D = test-section diameter, ft
D_d = diameter of bubble at departure
g = local acceleration, ft/sec^2
g_c = gravitational conversion factor, 32.16 lb_{mass}-ft/sec^2/lb_{force}
G = mass velocity, lb/(hr)(sq ft)
h = heat-transfer coefficient, Btu/(hr)(sq ft)(°F)
J = mechanical equivalent of heat = 778 ft-lb/Btu
k = thermal conductivity, Btu/(hr)(ft)(°F)
L = length, ft
NTU = number of transfer units = $AU_{av.}/(C_p w)_{min.}$
P = pressure, psi
q'' = heat flux, Btu/(hr)(sq ft)
q_c'' = critical heat flux, Btu/(hr)(sq ft)
R = capacity-rate ratio = $(C_p w)_{hot\ fluid}/(C_p w)_{cold\ fluid}$
s = liquid-layer thickness, ft
t = time, sec
t = effective thickness of heater, ft
T = temperature, °F
U = overall heat-transfer coefficient, Btu/(hr)(sq ft)(°F)
v = velocity, ft/sec
w = weight rate of flow, lb/hr
x = vapor weight fraction, lb vapor/lb fluid
z = distance from inception of local boiling, measured in the direction of flow, ft
β = contact angle, deg
ϵ = heat-exchanger effectiveness, heat transferred/maximum possible heat transfer
λ = latent heat, Btu/lb
μ = viscosity, lb/(ft)(hr)
ρ = density, lb/cu ft
σ = surface tension, Btu/sq ft = 778 × lb/ft
Φ = two-phase flow multiplier

Subscripts

$av.$ = average
b = bulk
c = critical
DNB = departure from nucleate boiling
f = film conditions
g = gas
L = liquid
S = saturation
TP = two-phase
v = vapor
max. = maximum
min. = minimum

References

Most of these papers were presented at the 8th National Heat Transfer Conference, Los Angeles, Calif., Aug. 9–11, 1965, sponsored jointly by the American Institute of Chemical Engineers and the American Society of Mechanical Engineers; they are marked with the initials of the appropriate society.

Individual papers are available from the two societies; some of the ASME papers will appear in the ASME Journal of Heat Transfer; but all the AIChE papers will appear in a volume in the Chemical Engineering Progress Symposium Series.

1. J. H. Leinhard and K. Watanabe, On Correlating the Peak and Minimum Boiling Heat Fluxes with Pressure and Heater Configuration. (ASME)
2. A. A. Bishop, R. O. Sandberg, and L. S. Tong, Forced Convection Heat Transfer at High Pressure After the Critical Heat Flux. (ASME)
3. E. O. Moeck, F. Stern, G. A. Wikhammer, and R. T. Dempster, Dryout in a 19-Rod Bundle Cooled by Steam/Water Fog at 515 psia. (ASME)
4. R. S. Daleas and A. E. Bergles, Effects of Upstream Compressibility on Subcooled Critical Heat Flux. (ASME)
5. W. J. Frea, G. S. Dzakowic, J. M. Hamelink, and W. S. Harjala, Some Experimental and Analytical Investigations on the Critical Heat Flux in Pool Boiling. (AIChE)
6. M. Carne and D. H. Charlesworth, Thermal Conduction Effects on the Critical Heat Flux in Pool Boiling. (AIChE)
7. L. S. Tong, H. B. Currin, P. S. Larsen, and O. G. Smith, Influence of Axially Non-Uniform Heat Flux on DNB. (AIChE)
8. B. F. Caswell and R. E. Balzhiser, The Critical Heat Flux for Boiling Liquid Metal Systems. (AIChE)
9. Z. L. Miropol'skii, Heat Transfer in Film Boiling of a Steam–Water Mixture in Steam-Generating Tubes, *Teploenerg.*, 10: 99 (1963) (in Russian). Also available as USAEC Report AEC-tr-6252.
10. P. J. Marto and W. M. Rohsenow, Nucleate Boiling Instability of Alkali Metals. (ASME)
11. J. M. Adams, An Investigation of Heat Transfer to Pool-Boiling Magnesium. (ASME)
12. P. J. Marto and W. M. Rohsenow, Effects of Surface Conditions on Nucleate Pool Boiling of Sodium. (ASME)
13. M. N. Ozisik and T. Cebeci, Dynamic Stability of Flow Oscillations in a Heated Channel. (ASME)
14. P. J. Berenson, An Experimental Investigation of Flow Stability in Multitube Forced-Convection Vaporizers. (ASME)
15. T. H. K. Frederking and D. J. Daniels, The Relation Between Bubble Diameter and Frequency of Removal from a Sphere During Film Boiling. (ASME)
16. G. J. Schoessow and K. J. Baumeister, Liquid Drop Model Vibrations and Simulated Fission. (AIChE)
17. K. J. Baumeister, T. D. Hamill, F. L. Schwartz, and G. J. Schoessow, Film Boiling Heat Transfer to Water Drops on a Flat Plate. (AIChE)
18. B. M. Patel and K. J. Bell, The Leidenfrost Phenomenon for Extended Liquid Masses. (AIChE)

19. M. A. Johnson, J. de la Peña, and R. B. Mesler, Bubble Shapes in Nucleate Boiling. (AIChE)
20. R. Cole and H. L. Shulman, Bubble Departure Diameters at Sub-Atmospheric Pressures. (AIChE)
21. J. M. Yatabe and J. W. Westwater, Bubble Growth Rates for Ethanol-Water and Ethanol-Isopropanol Mixtures. (AIChE)
22. G. J. Hordmann and Kwang-Tzu Yang, Laminar Film Condensation in Two-Phase Channel Flow. (ASME)
23. J. O. Medwell and A. A. Nicol, Surface Roughness Effects on Condensate Films. (ASME)
24. W. Nusselt, Die Oberflaschen Kondensation Des Wasserdampf, *Z. Ver. deut. Ing.*, 60: 541, 569 (1916).
25. S. P. Sukhatme and W. M. Rohsenow, Heat Transfer During Film Condensation of a Liquid Metal Vapor. (ASME)
26. D. W. Weiler, A. M. Czikk, and R. S. Paul, Condensation in Smooth and Porous Coated Tubes Under Multi-G Accelerations. (AIChE)
27. L. A. Bromley, R. F. Humphreys, and W. Murray, Condensation on and Evaporation from Radially Grooved Rotating Disks. (ASME)
28. J. L. McCormick and J. W. Westwater, Drop Dynamics and Heat Transfer During Dropwise Condensation of Water Vapor on a Horizontal Surface. (AIChE)
29. A. C. Peterson and J. W. Westwater, Dropwise Condensation of Ethylene Glycol. (AIChE)
30. V. P. Isachenko, Mechanism and Criteria Equations of Heat Transfer in the Condensation of Steam in Drops, *Teploenerg.*, 9: 81 (1962) (in Russian).
31. E. E. Polomik, Phase Velocities in Boiling Flow Systems by Total Energy and by Diffusion. (ASME)
32. G. E. Geiger and W. M. Rohrer, Sudden Contraction Losses in Two-Phase Flow. (ASME)
33. A. A. Kudirka, R. J. Grosh, and P. W. McFadden, Two Phase Heat Transfer in a Tube with Gas Injection from the Walls. (ASME)
34. R. E. Haberstroh and P. Griffith, The Slug-Annular Two-Phase Flow Regime Transition. (ASME)
35. S. C. Rose, Jr., and P. Griffith, Flow Properties of Bubbly Mixtures. (ASME)
36. K. F. Neusen, Void Fractions in a Developing Two-Phase Flow System with Flowing and Non-flowing Liquid Phase. (ASME)
37. C. J. Baroczy, A Systematic Correlation for Two-Phase Pressure Drop. (AIChE)
38. R. W. Lockhart and R. C. Martinelli, Proposed Correlation of Data for Isothermal Two-Phase, Two-Component Flow in Pipes, HART, *Chem. Eng. Progr.*, 45: 39 (1949).
39. N. C. Sher and S. J. Green, Boiling Pressure Drop in Thin Rectangular Channels, Chemical Engineering Progress Symposium Series, No. 23, p. 61, American Institute of Chemical Engineers, 1959.
40. C. J. Baroczy, Correlation of Liquid Fraction in Two-Phase Flow with Application to Liquid Metals, Chemical Engineering Progress Symposium Series, No. 57, p. 179, American Institute of Chemical Engineers, 1965.
41. S. Bankoff, A Variable Density Single-Fluid Model for Two-Phase Flow with Particular Reference to Steam Water Flow, *J. Heat Transfer*, 82: 265 (1960).
42. J. F. Marchaterre and B. M. Hoglund, Correlation for Two-Phase Flow, *Nucleonics*, 20(8): 142 (August 1962).
43. N. Zuber and J. A. Findlay, The Effects of Nonuniform Flow and Concentration Distributions and the Effect of the Local Relative Velocity on the Average Volumetric Concentration in Two-Phase Flow, USAEC Report GEAP-4592 (EURAEC-1096), General Electric Company, April 1964. [See also *J. Heat Transfer*, 87: 453 (1965).]
44. S. Kalish and O. E. Dwyer, Heat Transfer to NaK Flowing In-Line Through a Bundle of Circular Rods. (ASME)
45. C. L. Pan and N. E. Welch, Exact Analytical Wall and Fluid Temperature Field for a Counterflow Heat Exchanger with the Effect of Longitudinal Heat Conduction. (ASME)
46. H. Kamei, Effectiveness and Temperature Distribution of Split Cross Flow Heat Exchangers. (ASME)
47. A. D. Kraus and D. Q. Kern, The effectiveness of Heat Exchangers with One Shell Pass and Even Numbers of Tube Passes. (ASME)
48. B. W. Jackson and R. A. Troupe, Plate Heat Exchanger Design by ϵ-NTU Method. (AIChE)
49. D. R. Fairbanks and M. Mark, An Optimization Procedure for Finning in Free Convection. (ASME)
50. K. Kotan and O. A. Arnas, On the Optimization of the Design Parameters of Parabolic Radiating Fins. (ASME)
51. S. T. Hsu, B. C. Vatsaraj, and C. Hsieh, An Extended Surface with Finned Pins Under Free Convection Cooling. (ASME)
52. G. Theoclitus, Heat-Transfer and Flow-Friction Characteristics of Nine Pin-Fin Surfaces. (ASME)
53. E. C. Smith, S. P. Victory, and A. Y. Gunter, Evaluation of Fin Tube Performance Under Steady State and Thermal Cycling Conditions. (ASME)
54. K. K. Robinson and D. E. Briggs, Pressure Drop of Air Flowing Across Triangular Pitch Banks of Finned Tubes. (AIChE)
55. W. R. Martini, A Light Weight Vapor-Fin Heat Rejection System. (AIChE)
56. W. Elenbaas, Heat Dissipation of Parallel Plates by Free Convection, *Physica*, 9: 1 (1942).
57. W. J. Privott and J. K. Ferrell, Dynamic Analysis of a Flow-Forced, Concentric Tube Heat Exchanger. (AIChE)
58. W. R. Penney, The Spiralator — Initial Tests and Correlations. (AIChE)
59. R. E. Githens, W. R. Minor, and V. J. Tomsic, Small Diameter Flexible Tube Heat Exchangers. (AIChE)
60. F. J. Bayley and C. Rapley, Heat Transfer and Pressure Loss Characteristics of Matrices for Regenerative Heat Exchangers. (ASME)
61. L. E. Sissom and T. W. Jackson, Temperature Distribution of Solids and Fluid in Fluid-to-Particle Heat Exchange. (ASME)
62. F. T Hung and R. G. Nevins, Unsteady-State Heat Transfer with a Flowing Fluid Through Porous Solids. (ASME)
63. J. P. Chiou and M. M. El-Wakil, Heat Transfer

and Flow Characteristics of Porous Matrices with Radiation as a Heat Source. (ASME)
64. M. Bentwich, G. Szwarcbaum, and S. Sideman, Time Dependent Temperature Distribution in Flow Past a Sphere. (ASME)
65. J. R. O'Loughlin, Evaporation from a Draining Liquid Film. (ASME)
66. N. B. Hospeti and R. B. Mesler, Deposits Formed Beneath Bubbles During Nucleate Boiling of Radioactive Calcium Sulfate Solutions. (AIChE)
67. J. W. Palen and J. W. Westwater, Heat Transfer and Fouling Rates During Pool Boiling of Calcium Sulphate Solutions. (AIChE)
68. T. R. Bott and M. R. Sheikh, Evaporation at a Scraped Surface. (AIChE)
69. S. Sideman, G. Hirsch, and Y. Gat, Direct Contact Heat Transfer with Change of Phase: Effect of the Initial Drop Size in 3-Phase Heat Exchangers. (AIChE)
70. D. I. Dykstra, Desalination of Sea Water by the Falling-Film Distillation Process. (AIChE)
71. F. D. Moore and R. B. Mesler, The Measurement of Rapid Surface Temperature Fluctuations During Nucleate Boiling of Water, *A.I.Ch.E. J.*, 7: 620 (1961).
72. E. P. Partridge and A. H. White, Mechanism of Scale Formation of Calcium Sulfate Boiler Scale, *Ind. Eng. Chem.*, 21: 835 (1929).
73. T. Miyauchi and T. Moriyama, Rate of Anhydrous $CaSO_4$ Scale Formation in Seawater Evaporators, *Kagaku Kogaku*, 25: 531 (1961) (in Japanese).
74. A. F. Sarofim and H. C. Hottel, Radiative Exchange Among Non-Lambert Surfaces. (ASME)
75. R. G. Hering, Radiative Heat Exchange Between Conducting Plates with Specular Reflection. (ASME)
76. J. O. Mingle, Reflection and Transmission Intensities from Gray Slabs Utilizing Invariant Imbedding Methods. (AIChE)
77. C. C. Oliver and P. W. McFadden, The Interaction of Radiation and Convection in the Laminar Boundary Layer. (ASME)
78. D. J. Collins and W. A. Menard, Measurement of the Thermal Conductivity of Noble Gases in the Temperature Range 1500 to 5000 Deg Kelvin. (ASME)
79. S. L. Israel, T. D. Hawkins, R. T. Salter, and S. C. Hyman, Thermal Conductivity of Hydrogen from 2000 to 4700°F. (AIChE)
80. C. M. Pyron, Jr., and C. D. Pears, The Mechanisms of Heat Transfer Through Porous Materials at Elevated Temperatures. (ASME)
81. R. F. Barron and L. S. Han, Heat and Mass Transfer to a Cryosurface in Free Convection. (ASME)
82. J. C. Burke and A. H. Rawdon, An Experimental Study of Heat Transfer to Two-Phase Film-Boiling Nitrogen. (ASME)
83. L. H. Back and A. B. Witte, Prediction of Heat Transfer from Laminar Boundary Layers, with Emphasis on Large Free-Stream Velocity Gradients and Highly Cooled Walls. (ASME)
84. S. T. McComas and E. R. G. Eckert, Combined Free and Forced Convection in a Horizontal Circular Tube. (ASME)
85. R. Gardon and J. C. Akfirat, Heat Transfer Characteristics of Impinging Two-Dimensional Air Jets. (ASME)
86. W. C. Moffatt, Approximate Solutions for Skin Friction and Heat Transfer in MHD Channel Flows. (ASME)
87. E. M. Sparrow, J. R. Lloyd, and C. W. Hixon, Experiments on Turbulent Heat Transfer in an Asymmetrically Heated Rectangular Duct. (ASME)
88. G. E. Zinsmeister and J. R. Dixon. Thermal Flowmeters: The Effect of Axial Conduction. (ASME)
89. N. Hayasi and K. Inouye, Transient Heat Transfer Through a Thin Circular Pipe Due to Unsteady Flow in the Pipe. (ASME)
90. P. J. Closmann, Effect of a Heat-Conducting Well Wall on Temperature Distribution in an Observation Well. (ASME)
91. Chi Tien and Yin-Chao Yen, An Approximate Solution of a Melting Problem with Natural Convection. (AIChE)
92. C. D. Henning and W. J. Yang, Transient Heat Transfer to Laminar Bingham-Plastic Flow in a Circular Tube with Internal Energy Generation. (AIChE)
93. J. A. Clumpner, Equations for Calculating the Temperature of Moving Solid Plates and Cylinders Undergoing Heating or Cooling. (AIChE)
94. L. E. Erickson, L. T. Fan, and L. C. Cha, The Cooling of a Moving Continuous Flat Sheet. (AIChE)
95. J. V. Beck and H. Wolf, The Nonlinear Inverse Heat Conduction Problem. (ASME)
96. S. R. Allada and D. Quon, A Stable, Explicit Numerical Solution of the Conduction Equation for Multi-Dimensional Non-Homogeneous Media. (AIChE)
97. F. S. Li and W. H. Gauvin, Evaporation from Vertical Flat Plates in High-Temperature Surroundings. (AIChE)
98. L. B. Evans and N. E. Stefany, An Experimental Study of Transient Heat Transfer to Liquids in Cylindrical Enclosures. (AIChE)
99. A. London, Heat Transfer as Applied to the Thermal Design of the Nimbus Control System. (AIChE)
100. C. E. Parks, Blowdown Models Applicable to the Loss-of-Fluid Test Facilities (LOFT), USAEC Report BAW-1195-4, The Babcock & Wilcox Co., June 1965.
101. S. G. Margolis and J. A. Redfield, Heat Transfer Aspects of the Loss of Coolant Accident, USAEC Report WAPD-T-1811 (CONF-650920-1), Westinghouse Electric Corp., Bettis Atomic Power Laboratory, August 1965.
102. H. Fauske, The Discharge of Saturated Water Through Tubes, Chemical Engineering Progress Symposium Series, No. 59, p. 210, American Institute of Chemical Engineers, 1964.
103. S. Levy, Prediction of Two-Phase Critical Flow Rate, *J. Heat Transfer*, 87: 53 (1965).
104. F. J. Moody, Maximum Flow Rate of a Single Component, Two-Phase Mixture, *J. Heat Transfer*, 87: 134 (1965).
105. M. R. El-Saden, Theory of Nonequilibrium Thermodynamics with Application to the Transport Processes in a Solid. (ASME)
106. G. S. Springer and R. Ratonyi, Heat Conduction from Circular Cylinders in Rarefied Gases. (ASME)
107. V. P. Tyagi, Laminar Forced Convection of a Dissipative Fluid in a Channel. (ASME)

108. B. F. Elam, Heat Transfer in Honeycomb-Core Sandwich Panels. (ASME)
109. J. V. Beck and A. M. Dhanak, Simultaneous Determinations of Thermal Conductivity and Specific Heat. (ASME)
110. W. R. Stubstad, Thermal Contact Resistance Between Thin Plates in Vacuum. (ASME)
111. W. R. Wilcox and R. L. Duty, Macroscopic Interface Shape During Solidification. (ASME)
112. K. C. Cheng, Analog Solution of Laminar Heat Transfer in Noncircular Ducts by Moire Method and Point-Matching. (ASME)
113. T W. Jackson and K. R. Purdy, Resonant Pulsating Flow and Convective Heat Transfer. (ASME)
114. J. M. Davies, Input Power Determined from Temperatures in Simulated Skin Protected Against Thermal Radiation. (ASME)
115. B. Koh and J. E. A. John, The Effect of Interfacial Metallic Foils on Thermal Contact Resistance. (ASME)
116. D. H. Elliott, Thermal Conduction Across Aluminum Bolted Joints. (ASME)
117. J. R. Larson and R. J. Schoenhals, Turbulent Free Convection in Near Critical Water. (ASME)
118. H. A. Blum and G. J. Moore, Transient Phenomena in Heat Transfer Across Surfaces in Contact. (ASME)
119. J. H. Van Sant and M. B. Larson, Convection Heat Transfer for Turbulent Flow in Subsonic Diffusers. (ASME)
120. L. Hoogenboom, Electrical Analog Model of Two-Dimensional Transient Heat Conduction. (ASME)
121. E. Talmor, Film Cooling of Small Diameter Throat Tubes. (AIChE)
122. D. Gidaspow and B. S. Baker, Heat Transfer in a Fuel Cell Battery. (AIChE)
123. D. A. Willoughby and T. J. Dwyer, Heat and Mass Transfer with an Exothermic Chemical Reaction in a Tubular, Laminar Flow Reactor. (AIChE)

Section

V

Power Reactor Technology

Materials

Effect of Hydriding on Zircaloy Properties

By C. Roger Sutton

Zirconium-base alloys and austenitic stainless steels have been the preferred materials for the cladding of water-cooled power-reactor fuel elements. In choosing between them, reactor designers balance the lower cost and simpler fabrication of the stainless steels against the better neutronic efficiency of the zirconium alloys—thus the cladding for each reactor is selected on the basis of economic considerations. Today's economic conditions often favor the use of Zircaloy. With the transition to private ownership of fuel in the 1970's, there is expected to be a still clearer economic advantage for zirconium alloys. Zircaloy-2, the reference zirconium-base alloy for the fuel cladding of water-cooled reactors for many years, has very good corrosion resistance and usually adequate mechanical and physical properties. Nevertheless, anything that changes the properties of the cladding material can have a profound effect on the life and economics of the fuel.

Occurrence of Hydride

One factor affecting the life and properties of Zircaloy, and thus the economics of its use, is the formation of zirconium hydride. Investigations of failed Zircaloy-2 cladding on fuel rods has indicated that the presence of oriented zirconium hydride caused brittle failure.[1,2] When the hydrides are oriented perpendicularly to the stress axis, both ductility and strength are decreased appreciably.[3] Preferential orientation of the zirconium hydride platelets can be caused by strains during fabrication[4] or by the application of stresses greater than some threshold intensity while the hydrides are precipitating.[3,5]

Sources of Hydride

Zirconium-base alloys usually contain little hydrogen (10 to 25 ppm) of the melting and fabrication procedures as a result. When the alloys are exposed in oxidizing aqueous media, additional hydrogen is generated continuously by the reaction

$$Zr + 2H_2O \rightarrow ZrO_2 + 4H$$

In a system that is not degassed continuously, some of this hydrogen diffuses into the zirconium alloy. Because the solubility[6] of hydrogen in zirconium is very limited (see Fig. V-1), a second phase ($ZrH_{1.53}$) precipitates, usually in the form of platelets. The amount, size, distribution, and orientation of this precipitated

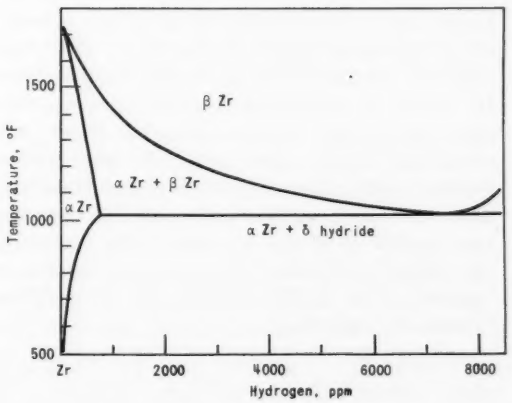

Fig. V-1 Zirconium–hydrogen phase diagram shows that solubility of hydrogen in zirconium increases with temperature up to about 1020°F, above which hydrides will not accumulate.[6]

phase may have a pronounced effect on the mechanical properties of the zirconium alloy.

Factors Affecting Hydrogen Uptake

Kirk[7] predicts that 30 to 50% of the available corrosion-product hydrogen will be absorbed by Zircaloy-2 and Zircaloy-4. Other data[8–10] indicate that 50% is probably the high side of the range and that absorption may be as low as 5%, depending on temperature, pressure, irradiation field, and other factors.

The dominant factors affecting the rate and amount of hydrogen uptake of available corrosion-product hydrogen are: zirconium-alloy composition, temperature, characteristics of the oxide film, radiation field, and coolant chemistry.

Alloy Composition. In discussing Zircaloy-2, nickel-free Zircaloy-2, and Zircaloy-4, Kass[11] states that hydrogen absorption is enhanced by the presence of nickel in the alloy. He reports that nickel-free Zircaloy-2 and Zircaloy-4 are superior to Zircaloy-2 in less than or equal to 680°F water because of their lower hydrogen pickup and decreased sensitivity to hydride failure but that above 750°F Zircaloy-2 has better oxidation resistance; beta quenching permits all three alloys to be used up to 850°F. Klepfer and Douglass[12] demonstrated that zirconium-base alloys containing copper and iron have less long-term hydrogen pickup than Zircaloy-2 (Table V-1). Greenberg and Youngdahl[9] report the combined effect of alloying and heat-treatment on hydrogen uptake (Table V-2); they conclude that hydrogen absorption in a particular alloy is primarily sensitive to exposure temperature and that a zirconium-base alloy containing 1.1% copper and 1.2% iron merits further study. Freer, Silvester, and Wanklyn[10] show the effect of 1% copper on hydrogen uptake at 932°F (Figs. V-2 and V-3). Weinstein and Holtz[13] determined the hydrogen pickup of various alloys in 680°F water and 750°F steam (Tables V-3 and V-4).

Temperature. Greenberg and Youngdahl[9] show (Table V-2) that hydrogen absorption by zirconium alloys after long exposure to steam is relatively insensitive to heat-treatment and composition of the alloys but very sensitive to temperature at least above about 1000°F. The percentage of corrosion-product hydrogen absorbed is much less at 1200°F than at 1000°F.

Table V-1 EFFECT OF TEMPERATURE ON LONG-TERM HYDRIDING OF THREE ZIRCONIUM ALLOYS*[12]

Alloy, at.%	Hydride rate, 10^{-2} mg/(dm^2)(day) At 750°F	At 930°F
Zircaloy-2	1.8	41.6
Zr–1 Nb–1 Cu–0.3 Fe	1.4	4.4
Zr–1.1 Cu–0.3 Fe	0.068	6.1

*In 1000-psi low-velocity flowing steam containing 20 ppm O_2 and 2.5 ppm H_2. Exposure time: rate data taken "posttransition," 1000 to 3000 hr. Specimens were fabricated from sponge by double consumable arc melting, forged and hot rolled at 1450°F, water quenched, 20% cold rolled, and alpha annealed 8 hr at 1050°F.

This result[6] is to be expected since zirconium hydride is unstable at temperatures above about 1020°F (see Fig. V-1).

Oxide Film. Gulbransen and Andrew[14] found that oxide films may inhibit the gaseous hydriding of zirconium by factors of 1000 or more. Smith[15] showed that the hydrogen pickup rate is inversely proportional to the ZrO_2 film thickness. Freer, Silvester, and Wanklyn[10] studied hydrogen uptake during initial stages of corrosion in superheated steam at 930°F. They suggest that reactions at the steam–oxide film interface, rather than bulk oxide films, control hydrogen entry into the alloy. Figure V-4 shows typical hydrogen uptakes[10] in steam at 932°F.

Irradiation. Exposure of zirconium alloys to irradiation conditions in a reactor can either increase or decrease hydrogen pickup. By contributing to a slow but steady buildup of oxide film on the surface of zirconium alloys (by means of radiolytically produced oxygen and activation of the surface), radiation can retard hydrogen pickup. MacDonald and Parry[16] found that the ZrO_2 film on alpha-annealed Zircaloy-2 fuel sheaths that had been irradiated 13,000 hr in less than or equal to 480°F pressurized water (the fuel was run at $\int_{T_1}^{T_2} k\,dT \leq 40$ watts/cm until a burnup of 10,000 Mwd per metric ton of uranium was attained) was 2 to 3 μm thicker than expected from out-of-reactor tests. This caused hydrogen pickup to be considerably less (3 to 20%) than the 50% pickup predicted by out-of-reactor tests.

In general agreement with MacDonald and Parry,[16] Burns and Maffei[17] state that a fast-neutron exposure of 0.3 to 8.2×10^{20} neutrons/cm^2 increases greatly the average corrosion

Table V-2 HOW COMPOSITION AND HEAT-TREATMENT OF ZIRCONIUM ALLOYS AND THE TIME AND TEMPERATURE OF THEIR EXPOSURE TO SUPERHEATED STEAM AFFECT THEIR ABSORPTION OF CORROSION-PRODUCT HYDROGEN[9]

Alloy, wt.% heat-treatment*	Exposure to 600-psi steam: Temperature, °F	Exposure to 600-psi steam: Time, days	Weight gain, mg/cm²	H_2 concentration, ppm	Hydrogen absorbed, %
Zr–3 Ni–0.5 Fe (initially contained 20 ppm H_2)					
As cast	1000	35	0.8	80	93
As cast	1000	97	1.8	119	56
Zr–3.1 Ni–0.6 Fe (initially contained 22 ppm H_2)					
As hot rolled	1000	1	1.1	166	45
As hot rolled	1000	7	1.9	203	41
H, Q, A	1000	108	5.30	666	55
H, Q, A	1200	88	9.38	348	14
H, Q	1200	88	9.19	330	14
H, C, Q, C	1000	108	6.88	1451	61
H, C, Q, C, A	1000	108	7.51	1320	53
Zr–2.1 Ni–0.6 Fe (initially contained 16 ppm H_2)					
As hot rolled	1000	117	8.63	1208	67
H, Q, A	1000	108	6.58	875	62
H, C	1000	117	9.69	1518	63
H, C, Q, C	1000	108	7.68	868	40
H, C, Q, C, A	1000	108	7.22	940	43
Zr–1.1 Cu–0.7 Fe (initially contained 22 ppm H_2)					
H, Q, A	1000	108	9.81	980	46
H, C, Q, C	1000	108	10.8	1175	41
Zr–0.5 Cu–1.0 Fe (initially contained 18 ppm H_2)					
H, Q, A	1000	108	6.21	641	47
H, C, Q, C	1000	108	4.80	356	25
H, C, Q, A	1000	108	7.25	1080	62
Zr–1.1 Cu–1.2 Fe (initially contained 21 ppm H_2)					
As hot rolled	1000	1	0.60	30	7
As hot rolled	1000	7	1.20	38	8
H, Q, A	1000	108	6.90	716	44
H, Q, A	1200	88	8.53	131	5.5
H, Q	1200	88	8.30	90	3.6
H, C, Q	1000	108	6.71	583	32
H, C, Q, A	1000	108	7.42	932	49

*H = hot rolled; Q = quenched from 1650°F; A = aged for 1 hr at 1290°F, then air cooled in capsule; C = cold rolled with <20% reduction.

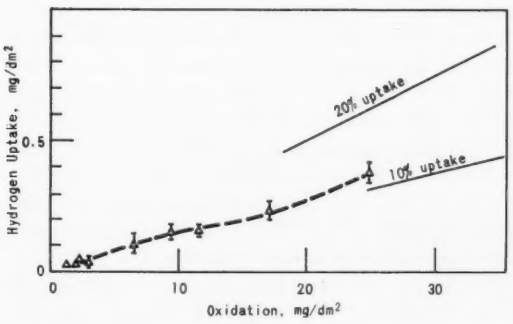

Fig. V-2 Hydrogen uptake of crystal-bar zirconium in 932°F steam of atmospheric pressure.[10]

rates of Zircaloy-2 in 540°F water having *p*H = 10, but that the fraction of corrosion–hydrogen pickup remains in the low part of the range normally found in the absence of radiation. They note that the corrosion proceeds at a nearly uniform rate above an as-yet-undetermined threshold flux rate.

On the other hand, under coolant flow and temperature conditions that erode the oxide film or encourage hydride pickup, the surface activation and hydrogen produced by irradiation can cause more total hydrogen to be picked up. Tobin[18] shows in Fig. V-5 that Zircaloy-2 at 540°F in a reactor loop picks up markedly more hydrogen than it does in an out-of-reactor loop at the same temperature; but he states that percentage uptake in the reactor is on the low side of the out-of-reactor results.

Water dissociates radiolytically. The amount and types of net steady-state dissociation products depend on at least two reactions: (1) a forward reaction that depends primarily on the intensity and type of radiation and (2) a back reaction that depends on temperature, the con-

centration of decomposition products, the type and intensity of radiation, the type and concentration of impurities in the water, and possibly on catalytic effects of materials in the immediate zone of dissociation.

In high-temperature pressurized-water reactors, the net dissociation is very low. It is probable that the only hydrogen available to react with the zirconium alloy is the small residual amount from reaction of equilibrium oxygen with metallic surfaces.

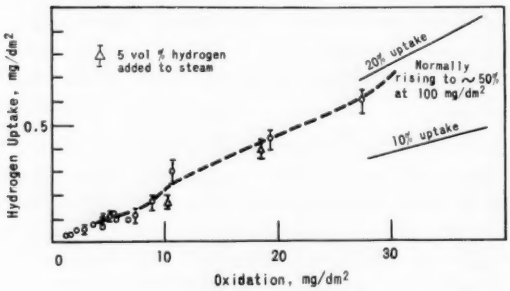

Fig. V-3 Hydrogen uptake of zirconium–1% copper alloy in 932°F steam of atmospheric pressure.[10]

Coolant Chemistry. Dalgaard[19] states that zirconium–2.5% niobium alloys, with or without 0.5% copper, are very sensitive to LiOH in water of pH = 10; he also reports that small concentrations of oxygen or oxidizing agents in water or steam may depress hydrogen uptake significantly.

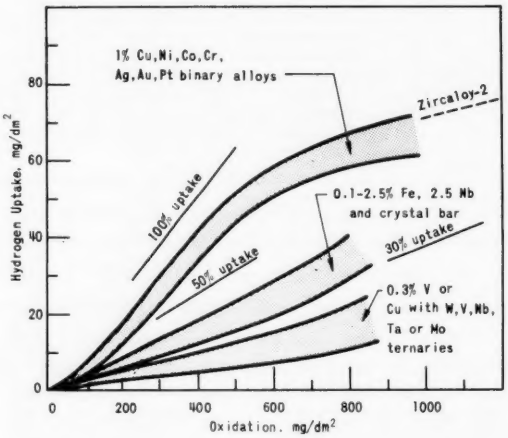

Fig. V-4 Hydrogen-uptake ranges of zirconium alloys in 932°F steam.[10]

Table V-3 HYDROGEN PICKUP AND TENSILE STRENGTH OF ZIRCONIUM ALLOYS IN 680°F WATER FOR 200 DAYS[13]

Composition, wt.%	Hydrogen pickup			Ultimate tensile strength (at 680°F), psi
	Weight gain, mg/dm²	Total H_2, ppm	Pickup, %	
Zircaloy-2	68.47	183	46	27,800
Zr–1 Cr–0.25 Te	35.79	54	15	32,800
Zr–1 Sb–0.5 Nb	68.59	63	12	
Zr–1 Sb–0.25 Te	49.66	62	17	30,300
Zr–1 Sb–0.25 Ge	52.85	38	8	32,700
Zr–0.5 Sn–0.25 Ge	36.98	51	18	25,100
Zr–0.5 Sn–0.25 Te	42.84	55	18	30,200
Zr–0.5 Nb–0.25 Te	46.88	65	22	30,700

Table V-4 HYDROGEN PICKUP AND TENSILE STRENGTH OF ZIRCONIUM ALLOYS IN 750°F STEAM FOR 125 DAYS[13]

Composition, wt.%	Hydrogen pickup			Ultimate tensile strength (at 750°F), psi
	Weight gain, mg/dm²	Total H_2, ppm	Pickup, %	
Zircaloy-2	87.96	256	50	26,500
Zr–1 Fe–0.25 Cr	51.81	126	55	24,800
Zr–1 Fe–0.25 Te	68.84	204	71	22,300
Zr–1 Fe–0.5 Nb	88.60	212	58	30,200
Zr–1 V–1 Fe	72.00	163	50	31,800
Zr–3 Cr–1 Fe	65.43	158	50	30,000
Zr–3 Cr–0.25 Te	67.03	141	43	32,700
Zr–0.5 Nb–0.25 Cr	97.47	79	13	27,900
Zr–0.5 Nb–0.25 Te	66.95	94	30	27,200

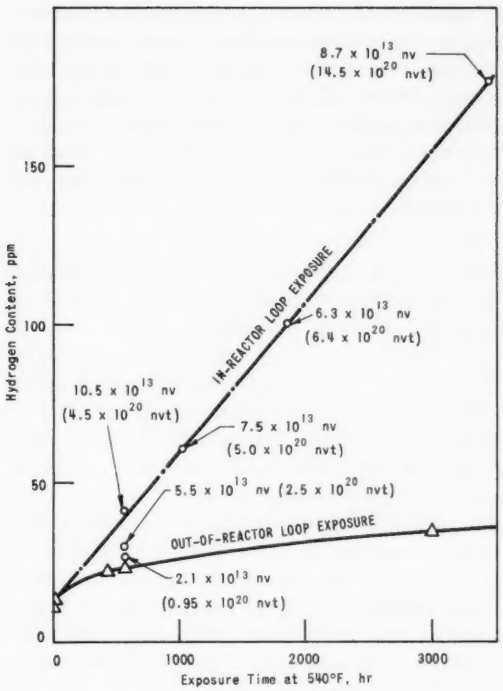

Fig. V-5 Much more total hydrogen is picked up by Zircaloy-2 in a reactor loop with 540°F water than in an out-of-reactor loop with same-temperature water.[18]

How Hydrides Affect Properties

The major effect of adversely oriented hydrides is to decrease ductility,[20] but tensile strength[20] and stress-rupture life[21] also might be reduced. From studies of the effect of irradiation on Zircaloy-2 containing 0 to 200 ppm H_2 and zirconium–2.5% niobium containing 0 to 300 ppm H_2, Sawatzky[22] concludes that hydrogen has little effect on tensile strength at 77 to 832°F. He also found that hydrogen decreased the ductility of both alloys, but the effect was less than that of irradiation to 10^{21} neutrons/cm^2 ($E > 500$ ev) at 536°F. Sawatzky also noted that deuterium and hydrogen have the same effect on the impact strength of Zircaloy-2 on an atom-for-atom basis.

By means of drop-weight tests on unirradiated pressurized tubes, Farrow and Watkins[23] found that 20%-cold-worked Zircaloy-2 containing less than 100 ppm H_2 does not support crack propagation at room temperature, but that tubes having 200 ppm H_2 exhibit crack propagation below 250°F. Standard drop-weight tests on the same material indicated a ductile–brittle transition temperature of 230°F; Zircaloy-2 with as much as 800 ppm H_2 has a ductile–brittle transition temperature less than 445°F, which is well below the operating temperatures of power reactors.

Babyak, Bourgeois, and Salvaggio[8] show that increased hydrogen content causes little loss of necking strain in Zircaloy-2 at 500°F. They also note that beta-quenched Zircaloy-2 with uniformly distributed hydrides shows greater necking strain than material to which no hydrogen has been added. At room temperature the necking strain of alpha-annealed Zircaloy-2 containing 500 ppm H_2 is about half the initial (low hydrogen) value, regardless of morphology, but beta-quenched material with uniformly distributed hydrides shows little effect. Samples containing 200 to 300 ppm H_2 in the form of grain-boundary hydrides show a decrease to only 1 to 2% strain.

Causes and Control of Orientation

Data presented by Burton[24] and by Mehan and Wiesinger[25] indicate (1) little if any effect of hydrogen content (up to at least 500 ppm) on the tensile strength of annealed Zircaloy-2 from room temperature to 600°F and (2) no effect on ductility above about 300°F. But if the hydride is situated in the grain boundaries or, particularly, if the hydride platelets are preferentially oriented in a direction perpendicular to the stress direction, brittleness develops.[5]

Marshall and Louthan[3] also report that, like the effect prior strain has on hydride orientation, stress applied during hydride precipitation causes the hydride platelets to orient preferentially—and, when the treatment produces hydrides oriented perpendicularly to the stress axis, both strength and ductility decrease significantly.

Marshall and Louthan[3] also observe that unfavorable orientation can be corrected by applying stress (in a direction perpendicular to the platelets) during hydride precipitation (precipitation occurs when the material is cooled below the hydrogen solubility temperature or during the longer times while the alloy is absorbing more than a soluble amount of hydrogen); the amount of stress needed depends on fabrication history. Although Louthan and Marshall[5] found that for highly susceptible material the minimum transverse stress to change hy-

dride orientation may be as low as 6000 psi, Wootton[20] shows that a stress of 16,000 psi appears to be somewhat below that required. But both investigators agreed that hydrides oriented parallel to the applied stress are unaffected by as much as 16,000 psi. Parry and Evans[4] found that the hydride precipitated parallel to the direction in which grains are deformed and that a minimum strain of 7% is required to produce directionality.

Significance

From the data described it can be concluded that reactor designers can avoid or alleviate the problems of hydride-induced brittleness and loss of strength in Zircaloy: (1) by selecting alloys and the surface films and water conditions that reduce hydrogen absorption, (2) by choosing operating temperatures that prevent hydride formation or accumulation, and (3) by designing components and specifying fabricating methods that cause any hydride platelets that do form to precipitate either in random orientation or parallel to the principal operational stress.

Slow Hydrogen Absorption. Much effort is being exerted to learn techniques to reduce the rate by which corrosion-induced hydrogen is absorbed by zirconium alloys. The fact that many reactor cores of pressurized- and boiling-water reactors have performed satisfactorily with Zircaloy-2 at about 600°F or less is prima facie evidence that either the reaction rate

$$Zr + 2H_2O \rightarrow ZrO_2 + 4H$$

is very slow below this temperature or that the diffusion rate of hydrogen through the existing oxide film is very low, or both. Above 600°F the amount of hydrides formed is, in many instances, sufficient to cause concern. The removal of nickel from Zircaloy-2 and other slight modifications has resulted in an alloy designated as Zircaloy-4. It is slightly less corrosion resistant than Zircaloy-2, but it is substantially less susceptible to hydriding. Although other alloys, notably zirconium–2.5% niobium, have been proposed, they have not yet been specified for a reactor core.

As noted by Burns and Maffei[17] and by MacDonald and Parry,[16] neutron irradiation lowers the percentage uptake of hydrogen, thus tending to offset any increased concentration of hydrogen in the coolant resulting from possible increased in-reactor oxidation rate of the zirconium alloy. Tobin[18] showed higher total hydrogen uptake under irradiation owing to increased corrosion rates but stated that the percentage uptake is on the low side of the out-of-reactor results.

Prevent Hydride Formation. Designers can select alloys and operating temperatures such that the solid solubility limit of hydrogen is not exceeded (so that zirconium hydride will not form and precipitate). In the intermediate-temperature range of interest for reactor application, moderate hydrogen pickup may not be deleterious because the solubility of hydrogen increases with temperature. For example, Fig. V-1 shows that, at 750°F, up to about 250 ppm H_2 can be accommodated without hydride formation; at 1000°F about 800 ppm can be tolerated. The designer can take advantage of this phenomenon if the operational conditions maintain the zirconium alloy above the temperature corresponding to the predicted hydrogen saturation level.

If the zirconium-alloy component operates at a temperature above that at which the zirconium hydride phase becomes unstable (~1020°F; see Fig. V-1), the hydride will accumulate slowly, if at all. This is supported by Greenberg and Youngdahl,[9] who report only a 5.5% uptake of corrosion-product hydrogen at 1200°F in out-of-reactor tests. However, the relief from hydride problems above about 1020°F is usually only of academic comfort because of oxygen embrittlement and loss of strength at such temperatures.

Random or Parallel Orientation. The orientation of the precipitated zirconium hydride phase in either a completely random fashion or in preferred orientations related to the operational stress is the factor that most readily lends itself to control by the designer. Although the presence of hydrogen, per se, in zirconium alloys has little effect on the metal properties, there is a pronounced deleterious effect if zirconium hydride precipitates as platelets either in the grain boundaries or preferentially oriented perpendicular to the principal stress. This behavior corresponds in many ways to the ductile–brittle transition in steel.

In fully alpha-annealed or beta-quenched zirconium alloys, the hydrides present at the

annealing or quenching temperature tend to precipitate randomly. However, slow cooling from these temperatures tends to cause the hydride platelets to accumulate in the grain boundaries, thus resulting in brittleness. If the metal is free of stress, corrosion-product hydrogen will form randomly oriented hydrides. However, when the metal is in a stressed condition, the hydrides precipitate preferentially in an orientation perpendicular to tensile stresses and parallel to compressive stresses; in fact, the preferential orientation can be changed by reversing the stress direction in service.[5] Hence it is important that the designer specify production and fabrication methods that yield optimum orientation of the hydride platelets. He also should design Zircaloy reactor internals in a manner that ensures platelet orientation parallel to the principal stress axis during operation.

References

1. A. S. Bain, G. M. Allison, L. M. Howe, and A. Ridal, Failure of Swaged UO_2 and Co-extruded U_3Si Specimens Irradiated in X-2 Loop (Test X-2-q), Canadian Report CRMet-904, Appendix III, 1959.
2. G. R. Caskey, Jr., G. R. Cole, and W. G. Holmes, Failures of UO_2 Fuel Tubes by Internal Hydriding of Zircaloy-2 Sheaths, in Proceedings of the Symposium on Powder Packed Uranium Dioxide Fuel Elements, Windsor, Conn., 1961, USAEC Report CEND-153, Vol. II, pp. 77-101.
3. R. P. Marshall and M. R. Louthan, Jr., Tensile Properties of Zircaloy with Oriented Hydrides, *Trans. Am. Soc. Metals*, 56: 693 (1963).
4. G. W. Parry and W. Evans, The Effect of Strain on the Directional Precipitation of Zirconium Hydride in Zircaloy-2, Canadian Report CRGM-1135 (AECL-1707), December 1962.
5. M. R. Louthan, Jr., and R. P. Marshall, Control of Hydride Orientation in Zircaloy, *J. Nucl. Mater.*, 9(2): 170-184 (1963).
6. D. H. Stone, Some High Temperature Mechanical Properties of Zircaloy-2, Type 304 Stainless Steel, and AM-350 Stainless Steel, USAEC Report NAA-SR-11047, Atomics International, June 15, 1965.
7. W. W. Kirk, Corrosion and Hydrogen Pickup of Zircaloy-2 and Zircaloy-4, in Zirconium Highlights, USAEC Report WAPD-ZH-21, pp. 8-14, Bettis Atomic Power Laboratory, Westinghouse Electric Corp., December 1959.
8. W. J. Babyak, W. F. Bourgeois, and G. J. Salvaggio, Effect of Hydride Morphology on the Tensile Properties of Zircaloy-2, in *Corrosion of Zirconium Alloys*, American Society for Testing and Materials, Special Technical Publication No. 368, pp. 76-100, 1964.
9. S. Greenberg and C. A. Youngdahl, Superheated Steam Corrosion of Zirconium Alloys Containing Small Amounts of Iron and Copper or Nickel, *Corrosion*, 21(4): 113-124 (April 1965).
10. D. W. Freer, D. R. Silvester, and J. N. Wanklyn, Hydrogen Uptake of Zirconium and Its Alloys During Early Stages of Corrosion in Steam, *Corrosion*, 21(4): 137-142 (April 1965).
11. Stanley Kass, The Development of the Zircaloys, in *Corrosion of Zirconium Alloys*, American Society for Testing and Materials, Special Technical Publication No. 368, pp. 3-27, 1964.
12. H. H. Klepfer and D. L. Douglass, The Factors Limiting the Utilization of Zirconium Alloys in Superheated Steam, in *Corrosion of Zirconium Alloys*, American Society for Testing and Materials, Special Technical Publication No. 368, pp. 118-142, 1964.
13. D. Weinstein and F. C. Holtz, Development of Improved Zirconium Alloys for Use in Superheated Water and Steam, USAEC Report GEAP-4089, Vol. 1, Paper 6, General Electric Company, Vallecitos Atomic Laboratory, Nov. 30, 1962.
14. E. A. Gulbransen and K. F. Andrew, Diffusion of Hydrogen and Deuterium in High Purity Zirconium, *J. Electrochem. Soc.*, 101: 560-566 (1954).
15. T. Smith, Hydrogen Permeation of Films on Zirconium, USAEC Report NAA-SR-6267, Atomics International, May 15, 1962.
16. R. D. MacDonald and G. W. Parry, Zircaloy-2 Clad UO_2 Fuel Elements Irradiated to a Burnup of 1000 MWd/Tonne U, Canadian Report CRFD-1178 (AECL-1952), January 1964.
17. W. A. Burns and H. P. Maffei, Neutron Irradiation and Cold Work Effects on Zircaloy-2 Corrosion and Hydrogen Pickup, in *Corrosion of Zirconium Alloys*, American Society for Testing and Materials, Special Technical Publication No. 368, pp. 101-117, 1964.
18. J. C. Tobin, Progress on the Irradiation Damage to Reactor Metals Program. A Summary of Hanford Laboratories Achievements in This Program under General Electric Company Management, 1962–1964, USAEC Report HW-83615, p. 28, Hanford Atomic Products Operation, Dec. 15, 1964.
19. S. B. Dalgaard, Factors Affecting Oxidation and Hydriding of Zirconium Alloys, *Trans. Am. Nucl. Soc.*, 6(2): 370 (November 1963).
20. G. C. Wootton, The Effect of Oriented Hydride on the Mechanical Properties of Zircaloy-2 Tubing, Canadian Report AECL-1989, March 1964.
21. R. C. Aungst, Stress Rupture Tests of Zircaloy-2 Pressure Tubes, USAEC Report BNWL-8, Battelle–Northwest, January 1965.
22. A. Sawatzky, The Effect of Neutron Irradiation on the Mechanical Properties of Hydrided Zirconium Alloys, Canadian Report AECL-1986, June 1964.
23. M. Farrow and B. Watkins, The Effect of Hydrogen on the Embrittlement of Zirconium-base Pressure Tubes, British Report TRG-Report-774, Apr. 23, 1964.
24. H. H. Burton, Hydrogen Effects of Zircaloy-2 Tensile Properties, USAEC Report HW-61077, Hanford Atomic Products Operation, July 10, 1959.
25. R. L. Mehan and F. W. Wiesinger, Mechanical Properties of Zircaloy-2, USAEC Report KAPL-2110, Knolls Atomic Power Laboratory, Feb. 1, 1961.

Section

VI

Power Reactor Technology

Fuel Elements

Letters to the Editor

Boiling-Water Environment Not Necessarily Detrimental to Stainless-Steel Cladding

In the letter by R. J. Allio in *Power Reactor Technology*, 8(2), the successful application of stainless-steel cladding in pressurized-water reactors (PWR) is contrasted with the experience with such cladding reported from the Vallecitos Boiling Water Reactor (VBWR).[1] It is the purpose of this communication to review the statements in the reference letter concerning the differences between PWR and BWR cladding behavior and, further, to examine in some detail why the VBWR data are *not* applicable to BWR's in general.

1. *System Pressure*

"Higher pressure prevents or delays development of tensile stress." The 12,000-psi compressive stress corresponds to an incremental strain of approximately 5×10^{-4} in./in., which with UO_2-fueled rods corresponds to an increase in allowable burnup of about 250 Mwd per metric ton of uranium. Since the PWR fuels cited exceeded the VBWR burnups by factors of 2 and 3, clearly the increased compression on the cladding due to the higher pressure cannot explain the difference in behavior.

"Crack propagation cannot normally occur in the absence of a tensile stress." Both tensile and compressive stresses lead to failure via cracking in *cold-worked* austenitic stainless steel even in oxygen- and chloride-free water.[2]

2. *System Chemistry*

"High oxygen concentrations have been shown in laboratory experiments to accelerate stress corrosion." This statement is erroneous unless qualified by the statement "in the liquid phase and in the presence of chloride ion."[3] The concentration of oxygen in the vapor phase in BWR's is immaterial to this discussion and, depending upon the residence time of the coolant in the core, reactor power density, system pressure, etc., can be an order of magnitude smaller than the 20 to 40 ppm cited. However, oxygen does not always act in a detrimental manner; some metals, including the austenitic stainless steels, form a highly impervious oxide film that provides resistance to further attack,[4] and oxygen has been employed to passivate steels in high-temperature water.[5]

3. *Corrosion-Product Deposition*

System chemistry and corrosion-product deposition are inseparable aspects of intermeshing phenomena and system design philosophy and criteria. Hence such an arbitrary separation is inappropriate to a technical discussion. The evidence indicates that corrosion-product deposition on stainless-steel claddings in both PWR's and BWR's has been negligible[6] and that only after relaxation of water purification specifications did the VBWR exceed negligible deposition.[7] Only in the Experimental Boiling Water Reactor (EBWR)[8] was scaling of fuel elements appreciable, and this was due to aluminum oxide formed in the core from the aluminum–nickel alloy dummy fuel elements.

One could argue that the dynamic action of nucleate-boiling bubble formation, at the fuel-element surface in BWR's, should "scour" the surface free of "crud"; therefore the "crud bursts" and short-term high-coolant impurity levels encountered in PWR's after thermal shocks should not occur in a BWR.

4. *Local Thermal Stresses*

The thermal fluctuations cited in the reference letter are based on measurements made under conditions (1) of atmospheric pool boiling, (2) of very low heat flux — to permit the study of individual bubble histories, and (3) of specially prepared poorly nucleating surfaces — again to study the life cycles of individual bubbles. The effect of pressure on boiling superheat (wall temperature minus saturation temperature) results in a decrease in required superheat, at equal heat fluxes, of factors of 3 for subcooled boiling,[9] and of 3.7 for bulk boiling;[10] thus the maximum magnitude of these fluctuations falls from the 30°F claimed to 8 to 10°F at 1000 psia. The effect of increasing heat flux at atmospheric pressure, according to the Eindhoven research,[11] is to decrease the amplitude and increase the frequency of thermal fluctuations; therefore higher heat fluxes cause damping even at low pressure where the driving force is large. Fuel-element surfaces are characteristically "rough" by laboratory standards, providing numerous, randomly spaced and random-sized nucleating sites (the "small surface crevices or pits" of the reference letter as well as grain boundaries, discontinuities in the oxide layer, etc.). With numerous nucleating sites scattered randomly over a surface, the surface temperature in a representative region will be the result of summing the thermal fluctuations from the surrounding bubble generating sites, each of which is randomly producing bubbles at various stages in their life cycles. Thus "real" surfaces tend to damp both the severity (amplitude) and frequency of thermal fluctuations.

In addition to these basic arguments, the measurements cited are inapplicable because they ignore the effect of coolant velocity on the bubbling layer adjacent to the heated surface. The large increase in frictional pressure drop with nucleate boiling is graphic evidence of increased shear in the bubble layer. A recent study[12] confirms that bubbles migrate on the heated surface under the influence of coolant velocity. Therefore, during the life cycle of a bubble, it may not remain at the nucleation site, and that site, therefore, cannot experience the full thermal fluctuation proposed in the reference letter.

VBWR Data Not Applicable to BWR's in General

We have discussed the points raised and have shown that the arguments against BWR's are questionable. It is appropriate, however, to examine why the VBWR fuel elements did fail and to show that the VBWR experience is atypical of BWR practice. The behavior of stainless steels in water-cooled nuclear reactor environments has been extensively studied. The results obtained to date may be conveniently summarized graphically[13] as shown in Fig. VI-1. Two regions may be defined: that below an exposure of approximately 10^{21} neutrons/cm^2 and that beyond this level. In the first region the effects of water chemistry (corrosiveness of coolant), degree of cold-work initially imposed on

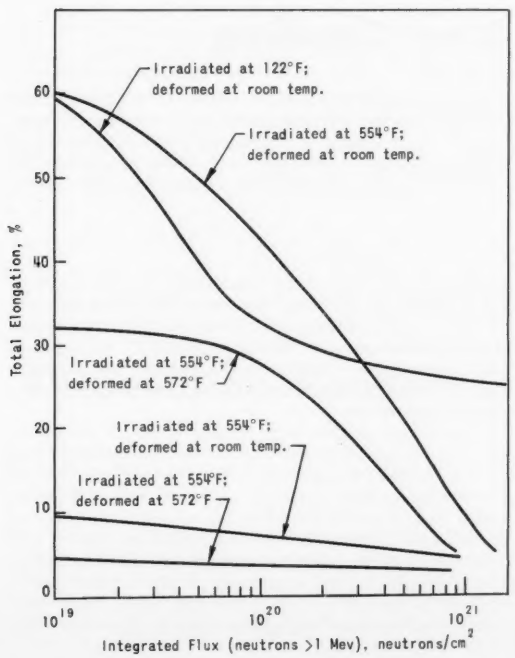

Fig. VI-1 Effects of radiation on ductility of type 348 stainless steel; upper three curves are for annealed samples; lower two curves are for 25% cold-worked samples.[13]

the metal, and stress imposed by the mechanical design all play an important role. This is the region in which all the VBWR failures lie. If a fuel-element design and the environment are both favorable, exposures in excess of 10^{21} neutrons/cm^2 (>1 Mev) may readily be attained, as shown by the PWR experience cited. The history of the J-10 loop (ETR) pressure tube[14] shows that thermal cycling and stress, of themselves, do not cause failure.

Despite the reported low level of chloride ion in the VBWR coolant,[15] coolant chemistry control must have been grossly inadequate, since chemical analysis of the crud deposited on some VBWR elements revealed up to 4000 ppm chloride ion.[16,17] This is not the whole story, however. Three classes of fuel cladding were irradiated in the VBWR: highly cold-worked, commercially annealed, and fully annealed. Although the VBWR personnel refer[18] to the commercially annealed cladding as annealed, they had measured the residual stress level in this tubing at 10,000 to 20,000 psi. Commercial annealing consists of a 10-min exposure to 1800°F; full annealing requires at least an hour at 1800°F for 300-series steels.[19] Both the cold-worked (residual stress of 10,000 to 40,000 psi) and commercially annealed tubing failed in the VBWR tests. However, a series of elements had been prepared by Nuclear Metals, Inc., by coextrusion of the UO_2 and type 304 stainless steel at temperature high enough (>1800°F) to assure full annealing of the cladding; these were irradiated under the same environmental conditions as the other elements, and, although the density of the UO_2 was higher (97 vs. 95% of theoretical) and these elements had no gap between the UO_2 and steel, none failed.[16,17] Thus we have evidence of the value of fully annealed cladding relative to the cold-worked varieties under irradiation, extending the out-of-pile experience previously reported.[20] In addition, the high chloride-ion content of the crud testifies to the hostile coolant environment in the VBWR. The inescapable conclusion is that the VBWR environment embrittled stainless-steel claddings causing intergranular and transgranular cracking.

To show that high-quality coolant ensures satisfactory BWR cladding performance, consider the experience in the Elk River reactor. Although the strength of the cladding has been compromised by incorporation of 600 ppm boron (as burnable poison), exposures have exceeded levels at which similar elements (0.003-in. diametral gap and 95% theoretical density UO_2) had failed in the VBWR without any failures.

Thus the assertion that the boiling-water environment is necessarily detrimental to stainless-steel cladding cannot be substantiated.

L. Bernath and B. W. Colston
Atomics International

Rebuttal: Boiling Water Is Detrimental to Stainless-Steel Cladding

I commend Messrs. Bernath and Colston for their attempts to provide additional insight into the behavior of stainless-steel-clad fuel elements in water-reactor environments. However, the validity of my original position, to wit, that a boiling-water environment is detrimental to stainless-steel cladding, has recently been affirmed by other knowledgeable investigators.[21,22] Nevertheless, the reader may appreciate our identification of several fallacies Bernath and Colston attempt to promulgate.

1. *System Pressure*

Both PWR and BWR stainless-steel-clad fuel elements are normally designed to have a 0.003 to 0.006-in. diametral fuel-cladding gap. In such fuel elements the primary source of stress is fission-gas accumulation. Thus a simple calculation of fission-gas release as a function of burnup shows that an increase in external pressure of 1000 psi may permit even a "factor of 2 and 3" increase in burnup, assuming exposure to be limited by the attainment of a specific tensile stress. The Bernath and Colston calculation of 250 Mwd per metric ton of uranium may refer to a fuel swelling phenomenon, which is not relevant to the fuel elements under discussion.

Crack propagation normally occurs only when the resulting decrease in elastic strain energy is greater than the energy required to create new surface. Bernath and Colston have misinterpreted their Ref. 2, which does not provide evidence for "crack propagation in the absence of a tensile stress." Nor does their Ref. 2 demonstrate that "compressive stresses lead to failure." Explicit interpretation of the experimental results of their Ref. 2 is not possible because of the failure of the authors to define the actual stress state at the surface. Stress state in the specimens tested will be determined by the sum of residual stresses introduced by the heat-treatment and cold-hardening process, local mechanical stress caused by the roller separating the specimens, and the gross bending load. Cracking kinetics will also be determined by strain energy of the specimen. Thus their Ref. 2 appears to demonstrate only that stainless steel can corrode intergranularly in high-temperature water under certain conditions.

2. *System Chemistry*

The presence of chloride was implicit in my observation that high oxygen concentration accelerates stress corrosion, as shown, for example, by the work of Williams and Eckel.[23] Moreover, the suggested qualification of "in the liquid phase" is unnecessary, as shown by the same research.

I cannot possibly disagree with the contention that "oxygen does not always act in a detrimental manner." Unfortunately the examples cited by Bernath and Colston deal with mass corrosion and are not germane to the matter of crack initiation and propagation.

3. *Corrosion-Product Deposition*

It is hardly sporting in a technical discussion to place heavy emphasis on evidence from privy sources, the validity of which cannot be verified by the reader (namely, Bernath and Colston Refs. 6, 15, and 18). Corrosion-product deposition is apparently adjudged to be "negligible"—by what standard, may I ask?

Bernath and Colston may choose to argue that nucleate-boiling bubble formation scours the surface. I prefer to accept the experimental evidence[24] that nucleate boiling in fact promotes crud formation.

4. *Local Thermal Stresses*

The thermal fluctuations measurements cited in my original letter were indeed performed at low heat flux and pressure. Although the magnitude of measured thermal fluctuations will diminish with increasing pressure, the finite mass and dimensions of the thermocouples result in a significant underestimate of the true thermal fluctuations at a point in the cladding surface. Furthermore, the implied generalization that increasing heat flux decreases the amplitude of thermal fluctuation is a gross simplification. In thermal transient phenomena the amplitude of thermal fluctuation is a complex function of not only heat flux but also thermal capacitance, thermal resistance, and source frequency.

The study of the effect of coolant velocities quoted in their Ref. 12 was limited to low pressure, low heat flux, and large bubbles; whereas bubble migration under these conditions cannot be extrapolated directly to behavior under PWR or BWR conditions. In any case, after the sudden growth of a bubble at a heat-transfer surface, liquid inertia will tend to pull the bubble away from the surface. The horizontal shear force associated with high coolant velocity will cut the bubble close to the surface, introducing cooler liquid. Collapse of the remaining bubble will still produce a large thermal fluctuation.

VBWR Data

The relevance of VBWR data to BWR's in general has been confirmed,[1,2] as noted previously.

Figure VI-1, showing decreases in total elongation of stainless steel with increasing neutron exposure (hardly a revelation), surely does not constitute a summary of the "behavior of stainless steels in water cooled nuclear reactor environments." For that matter, total elongation is not even a suitable measure of cladding ductility. I suggest that the relevance of the figure to the Bernath and Colston mechanism for failure is obscure at best.

The addition of boron to stainless steel does not compromise strength.[25] Fuel-element integrity in any event is not a unique function of cladding strength. Moreover, the exposure to date of Elk River fuel elements is insufficient to disprove the generalization that boiling-water environment is detrimental to stainless-steel cladding.

R. J. Allio, *Manager*
Materials and Processes Development
Westinghouse Atomic Power Division

Re-Rebuttal: Readers Can Decide Relevance

We are faced with the onerous task of affirming the factual and rejecting the extraneous and misleading from Allio's rebuttal. The difficulty arises from the fact that Allio's original letter was propaganda and, as such, was a melange of fact and "smoke-screen" against *all* BWR's.

Allio's rebuttal, Refs. 21 and 22, in fact, confirm our position by stressing the importance of the coolant environment. Allio has extracted, out of context, one statement to support his position, namely, "Contrary to initial expectations, Type-304 stainless steel clad fuels have proven unsatisfactory for boiling water reactor service above peak exposures of 15,000 Mwd/tonne." He fails to note, in the same sources, that "Type-304 stainless steel clad was found susceptible to intergranular cracking *in at least some water-reactor environments*," and he omits the table in Ref. 21, which shows that *four* BWR's have been operated to between 7500 and 17,000 Mwd/metric ton exposures

and that these are continuing to perform satisfactorily. Allio prefers to cite the VBWR experience as typical, to the possible embarrassment of the GE–San Jose people, who cannot fully defend themselves without admitting to a very cavalier treatment of the pertinent mechanical properties of the cladding as well as of coolant purity requirements. This may have been deliberate on the part of GE—at the initial of the VBWR tests, it was desired to show that no special care was required. It was precisely this situation that prompted us to cite the facts omitted by Allio and to present an objective assessment of the VBWR results.

1. *System Pressure*

Allio cites the existence of a 0.003- to 0.006-in. diametral gap between fuel and cladding to support his contention of the beneficial effects of increased system pressure. What he does not consider is that the cited gap exists only in the cold, as-fabricated condition; simple calculation of the differential expansions of UO_2 and stainless steel, at operating conditions, shows that at zero burnup this gap disappears and that as much as 0.1% strain may be imposed on the cladding. Thus fuel growth or swelling with increasing exposure is most pertinent to the discussion, refuting Allio's opinion that it is not relevant. In fact, Allio's coworkers agree (see page 320 of his Ref. 24) that dimensional stability of UO_2 (which determines the stress condition of the cladding with increasing burnup) is a function of such parameters as "burnup, heat rating, fuel density and grain size, and clad restraint."

As Allio points out, our original Ref. 2 was subject to interpretation. Obviously then, his statements that we have misinterpreted the reference are his opinion and are very much open to question. There is, however, significant merit to his further comments, namely, "Stress state in the specimens tested will be determined by the sum of residual stresses..." It was to summarize these effects, plus the effect of water chemistry and irradiation, that we included our figure of "obscure" relevancy.

2. *System Chemistry*

Allio's allegation that "the presence of chloride was implicit in my observation, etc." cannot be accepted, as repeated reading of his original letter fails to substantiate any appreciation of the effects of chloride ion. He glosses over his misconceptions relative to oxygen concentrations in BWR's and implies that vapor-phase stress corrosion is observed under high coolant purity conditions.

3. *Corrosion-Product Deposition*

Allio not only ignores the evidence we cited, but he also distorts the direct findings of his coworkers (his Ref. 24). The experimental evidence he cites is based on five out-of-pile tests at low bulk velocity and relatively low heat flux, in which ferrous hydroxide was injected to simulate in-reactor corrosion; the validity of this simulation is unsubstantiated. The results obtained are highly suspect since calculation of the density of the deposit (page 4.32 of Ref. 24) indicates a value of approximately 0.5 g/cm^3 rather than the customary one of approximately 3 g/cm^3, a factor of 6 that cannot be explained. The results show (page 4.42 of Ref. 24) that when vigorous boiling occurred (the 1000-psi test condition) the pressure drop across the test section decreased, confirming a significant removal of deposited material (scouring action?).

4. *Local Thermal Stresses*

Allio persists in his belief in the existence of large local thermal stresses in boiling. To buttress his case, he equates the "low heat flux and pressure" of the pool boiling data he cited [10,000 to 30,000 Btu/(hr)(sq ft) and atmospheric pressure] with our Ref. 12, channel flow data [~100,000 Btu/(hr)(sq ft) and 200 psi]; the ratio of liquid-to-vapor density in these two cases, which is a paramount factor in bubble dynamics, differs by more than an order of magnitude, 1600 in the former and 124 in the latter. Allio insists on "sudden growth of a bubble at a heat transfer surface" while ignoring the effects of high coolant velocity to keep bubbles small and to move them along the surface during their growth cycle. Collapse of the bubble, which can only occur in subcooled nucleate boiling, may produce a "thermal fluctuation," but such collapse occurs in the bulk of the fluid, not at the surface!

VBWR Data

The relevance of VBWR data to BWR's in general and of our figure showing the total elongation of stainless steel with increasing neutron exposure is discussed in the second paragraph.

We do wish to thank Mr. Allio for his one useful comment. We agree that the addition of boron to stainless steel does not compromise the strength. We inadvertently used the word "strength," instead of "ductility." The pertinence of our comment concerning the Elk River cladding is, however, substantiated in Allio's Ref. 25. It is shown in this reference that irradiated boron stainless steel shows large (70 to 90%) decreases in elongation after irradiation with the degree of deterioration increasing with thermal-neutron exposure and concentration of boron. We are sure that Mr. Allio is also aware of the recent work in this field.[26,27]

An argument such as this can only deteriorate — my father can lick your father — to the point where even the interpretation of the same results can be disputed with vehemence. We suggest, therefore, that only the individual readers of our comments can decide relevance and that each will utilize the discussion to delve into the referenced material to the extent of his immediate interest.

Again, we thank you for the opportunity, via publication of our letter, to present what we feel is a more objective interpretation of the VBWR results.

L. Bernath and B. W. Colston
Atomics International

Editors' Comment

Inasmuch as the objectives of *Power Reactor Technology* are to call its reactor-designer readers' attention to data of concern to them — and to venture interpretation and evaluation in the form of opinions as to the applicability of the data — we particularly welcome contributions from readers that either offer their original evaluations or interpretations that differ with those expressed in articles or letters in our issues. We believe the usefulness of our pages will be enhanced by expressions of differing opinions, which in turn will encourage our authors to venture and verify their interpretations more vigorously. As more data become available to substantiate or refute evaluations presented in our pages, we hope that readers will call them to our attention. In this light, we thank Messrs. Allio, Bernath, and Colston for their useful exchange and invite other readers to volunteer articles or communications on matters of mutual interest.

References

1. Stainless-Steel-Cladding Failures in VBWR, *Power Reactor Technol.*, 7(4): 354-355 (Fall 1964).
2. P. A. Akol'zin and L. V. Korneeva, Study of Corrosion Under Stress of 1Kh18N9T Steel Depending on the Composition of the Medium and State of the Metal, in Corrosion of Reactor Materials: A Collection of Articles, USAEC Report AEC-tr-5219, pp. 124-145, V. V. Gerasimov (Ed.), translated from a Russian publication of the State Publishing House of Literature in the Field of Atomic Science and Technology, Moscow, 1960.
3. D. J. DePaul (Ed.), Stress Corrosion, in Corrosion and Wear Handbook for Water Cooled Reactors, USAEC Report TID-7006, pp. 187-223, March 1957.
4. F. L. LaQue and H. R. Copson (Eds.), *Corrosion Resistance of Metals and Alloys*, 2nd ed., p. 378, Reinhold Publishing Corporation, New York, 1963.
5. Ya. M. Kolotyrkin, G. M. Florianovich, P. S. Petrov, N. K. Smirnova, and L. M. Vyazankin, Use of Oxygen for Protecting Steel from Corrosion in Water at High Temperatures, in Corrosion of Reactor Materials: A Collection of Articles, USAEC Report AEC-tr-5219, pp. 26-40, V. V. Gerasimov (Ed.), translated from a Russian publication of the State Publishing House of Literature in the Field of Atomic Science and Technology, Moscow, 1960.
6. T. J. Pashos, General Electric Company, Atomic Power Equipment Department, unpublished, September 1963.
7. F. J. Brutschy, H. W. Dreyer, and W. L. Pearl, Vallecitos Boiling Water Reactor, Coolant Technology, *Ind. Eng. Chem.*, 51: 1262-1264 (October 1959).
8. C. R. Breden et al., Water Chemistry and Fuel Element Scale in EBWR, USAEC Report ANL-6136, Argonne National Laboratory, November 1960.
9. W. H. Jens and P. A. Lottes, Analysis of Heat Transfer, Burnout, Pressure Drop and Density Data for High-Pressure Water, USAEC Report ANL-4627, Argonne National Laboratory, May 1, 1951.
10. W. M. Rohsenow, A Method of Correlating Heat Transfer Data for Surface Boiling of Liquids, *Trans. ASME*, 74: 969-976 (1952).
11. University of Eindhoven, Final Report on the Research Programme on Heat Transfer and Stability Studies in Boiling Water Reactors, USAEC–Euratom Report EURAEC-335, p. 22, February 1965.
12. G. J. Kirby et al., A Visual Study of Forced-Convection Boiling, Part I, British Report AEEW-R-281, March 1965.
13. J. E. Irvin et al., The Combined Effects of Temperatures and Irradiation on the Mechanical Properties of Austenitic Stainless Steel, in *Flow and Fracture of Metals and Alloys in Nuclear Environments*, pp. 236-250, American Society for Testing and Materials, Special Technical Publication No. 380, 1964.
14. William E. Murr, Frederic R. Shober, Robert Lieberman, and Ronald F. Dickerson, Effects of Large Neutron Doses and Elevated Temperature on Type 347 Stainless, USAEC Report BMI-1609, Battelle Memorial Institute, Jan. 21, 1963.
15. T. J. Pashos, GE–San Jose, personal communication, Dec. 16, 1963.
16. W. H. Arlt and S. R. Vandenberg, Fuel Failure Examinations and Analyses in the High Power Density Program, USAEC Report GEAP-4360,

General Electric Company, Vallecitos Atomic Laboratory, Sept. 16, 1963.
17. General Electric Company, Atomic Power Equipment Department, Nuclear Superheat Project. Nineteenth Quarterly Report, February–April 1964, USAEC Report GEAP-4619, May 1964.
18. T. J. Pashos, GE–San Jose, personal communication, Dec. 16, 1963.
19. V. V. Gerasimov, A. I. Gromova, and E. T. Shapovalov, Corrosion Cracking of 1Kh18N9T Steel, in Corrosion of Reactor Materials: A Collection of Articles, USAEC Report AEC-tr-5219, pp. 146-151, V. V. Gerasimov (Ed.), translated from a Russian publication of the State Publishing House of Literature in the Field of Atomic Science and Technology, Moscow, 1960.
20. A. V. Stanyukovich and E. E. Levin, Causes of Failure of Steam Superheater Pipes Made from 18 Cr/12 Ni/1 Ti steel, British Report TRG-Inf-Ser-191, 1963, translated from *Energomashinostroenie*, 10: 27-30 (1961).
21. T. J. Pashos, H. E. Williamson, and R. N. Duncan, Fuel Performance in Boiling Water Reactors, *Trans. Am. Nucl. Soc.*, 8(2): (1965).
22. T. J. Pashos (Comp.), Stainless Steel Failure Investigation Program. First Quarterly Progress Report, February 15–June 30, 1965, USAEC–Euratom Report GEAP-4915, General Electric Company, Atomic Power Equipment Department, Aug. 1, 1965.
23. W. Williams and J. Eckel, *J. Am. Soc. Naval Engrs.*, 68(93): (February 1965).
24. C. Roderick, Large Closed-Cycle Water Reactor Research and Development Program. Progress Report, April 1–June 30, 1964, USAEC Report WCAP-3269-3, Westinghouse Electric Corporation, Atomic Power Division, 1964.
25. W. K. Anderson and J. Theilacker, Neutron Absorber Materials for Reactor Control, *Naval Reactors, Division of Reactor Development*, Washington, 1962.
26. W. R. Martin and J. R. Weir, Effects of Elevated Temperature Irradiation on Hastelloy N. *Nucl. Appl.*, p. 160, April 1965.
27. R. S. Barnes, Embrittlement of Stainless Steels and Nickel Based Alloys at High Temperature Induced by Neutron Radiation, *Nature*, p. 1307, June 1965.

Section

VII

Power Reactor Technology

Components

Vapor Traps Protect Liquid-Metal Systems

By David H. Thompson

Instruments and equipment in liquid-metal systems are damaged if the liquid-metal vapor entrained in the inert cover gas condenses out on them. Vapor condensation also can plug gas supply, vent, or instrument lines. Traps that will prevent such damage or plugging are installed in the gas circuits of liquid-metal systems to remove the metal vapor.

We will consider here the principles of such traps, early versions, the variety of types and ways they are used in reactors and other dynamic systems, some recent developments, and conclusions and recommendations concerning their use and the need for improved technology for future reactors. Experience with traps for static systems also is discussed briefly in connection with fume traps for spent-reactor-fuel melt-refining furnaces.

Trapping Principles

Among the phenomena that have been studied for vapor traps are stagnation, impingement, condensation, adsorption, chemical reaction, and repulsion. Vapor traps now used in dynamic systems depend on condensation to remove liquid-metal vapor from the flowing inert gas; stagnation and impingement also are involved in trap operation. Table VII-1 summarizes the features of such traps.

Table VII-1 PRINCIPLES OF CONDENSING VAPOR TRAPS

Type (and temperature)
Configuration
Maintenance of operation
Examples
ACCUMULATING CONDENSER (outlet gas cooler than vapor freezing temperature)
Impingement–condensing type
Cylinder filled with mesh, shot, or liquid NaK; trap is cooled by natural or forced convection
Heated to remove accumulated Na when trap plugs — or replace trap internals
EBR-I, EBR-II, Fermi, SRE, Hallam, SCTI, FARET, SEFOR, SIG
Stagnation–condensing type
Lengths of relatively large diameter pipe
Heated to remove accumulated Na when trap plugs
STF, LAMPRE
CONTINUOUSLY REFLUXING CONDENSER (outlet gas slightly hotter than vapor freezing temperature)
Impingement–condensing type
Cylinder filled with mesh, shot, and/or baffles
After liquid metal agglomerates on trap surfaces, it runs off and is returned to system
FRCTF, Pratt & Whitney research, ANL research

In a condensing vapor trap, natural- or forced-convection cooling reduces the tempera-

ture of the inert gas passing through, which results in the metal vapor condensing on surfaces within the trap. The amount of metal vapor that passes through such a vapor trap is a function of the vapor pressure of the liquid metal at the trap outlet temperature—and is extremely small if gas temperatures are kept near the metal freezing point.

In impingement—condensing vapor traps, the extended surfaces formed by the mesh, shot, or baffles force the vapor-laden gas to follow a tortuous path, which promotes both heat transfer from the gas and condensation of the metal vapor.

In stagnation—condensing vapor traps, the relatively large-diameter lengths of pipe lack the extended-surface inner packing or fill of the impingement–condensing vapor traps. They operate most satisfactorily in systems that have slow flows of relatively cool gas.

Early Versions

In early work with sodium and NaK experimental facilities, it was postulated that the relatively large amount of sodium and NaK entrained in the gas was caused by the formation of a stable sodium or NaK aerosol that did not readily condense onto the surfaces over which it passed.[1] Another theory suggested that oxygen present with the inert gas reacted with the sodium vapor to form a stable aerosol of sodium oxide. The conditions required for aerosol production and the nature of the aerosol itself still are not fully understood. However, if aerosol is present in the cover gas of liquid-metal systems, it apparently is not present in concentrations large enough to influence vapor-trap effectiveness.

Some attempts at vapor trapping included experiments with a copper-coil condenser, an electrostatic precipitator, and a NaK bubbler.[1] Gas flow through these devices ranged from 130 to 1560 cu in./hr, and vapor was produced by passing purified argon over a 1500°F sodium pool. The room-temperature NaK bubbler operated effectively over the entire flow range (maximum velocity was ~1 ft/sec), but the condenser (a 16-turn 2-in.-diameter coil of ¼-in. copper tubing maintained at 235°F in an oil bath) allowed vapor to pass at high gas flows. The electrostatic precipitator was the least effective vapor trap for dynamic conditions, but it proved satisfactory under static conditions. In work predating the Sodium Reactor Experiment (SRE), it was shown that the stainless-steel wool- or mesh-filled trap could be very effective,[2] but these experiments showed that effectiveness depends on gas temperatures and flows.

Gas Systems, Trap Applications

Much of the developmental effort on vapor traps has been directed toward a particular system or systems for individual reactor projects. Thus most of the concepts, design details, and experience with them have not been reported in the literature. Because of the increasing need for dependable large fast reactor systems, it is worthwhile to describe in some detail the inert-gas blanket systems and vapor-trap installations at a number of liquid-metal-cooled facilities. In this discussion no attempt is made to distinguish between aerosol and vapor or to define the exact nature of the trapping action, whether it be technically termed a filter, trap, or condenser.

EBR-I, EBR-II, FERMI

These first-generation breeder reactors use metallic fuels and have reactor-coolant-outlet temperatures of less than 900°F. All three reactors have argon as the inert cover gas for the primary coolant system, and the gas-supply system of each was constructed with NaK-bubbler type purification units followed by a stainless-steel wool- or mesh-filled vapor trap. However, because the Experimental Breeder Reactor No. 2 (EBR-II) facility is supplied with relatively pure liquid argon, rather than bottled argon as originally proposed, the NaK-bubbler purifier has not been operated. At the Experimental Breeder Reactor No. 1 (EBR-I), the primary-system cover gas was continuously recirculated, whereas, at both EBR-II and the Enrico Fermi Fast Breeder Reactor, the cover-gas systems are operated on a demand type basis and provide for recovery and recirculation of the gas transferred from the primary vessel.

EBR-I. Because EBR-I used NaK, which is liquid at room temperature, as both the primary and secondary coolants, there was only a limited need for vapor traps. During operation a continuous downward flow of argon gas through the reactor top plate was maintained to retard

upward diffusion and condensation of NaK vapor on the surfaces near the top of the vessel. The NaK vapor was removed from the recirculating argon primary cover gas by a centrifugal separator and strainer near the inlet to the parallel centrifugal blowers.[3] The strainer tank, approximately 2 ft in diameter and 4 ft high, was fitted near the bottom with a perforated plate and was filled with steel wool. In operation the oxides and NaK liquid trapped in the strainer formed a semisolid mass that allowed little liquid to be withdrawn during draining attempts. When flow through the strainer became restricted, rapping the tank with a hammer was sufficient to restore free flow. This strainer fulfilled the EBR-I trapping requirements, without replacement, for the operation of all four cores. In addition to this strainer, a small-diameter stainless-steel-mesh-filled trap was installed ahead of the piston type positive-displacement depressurizing pump in the gas-transfer line.

Fermi. In addition to the purification-unit vapor trap, Fermi has (1) a Dowtherm-cooled vapor trap in the gas-recirculating system, (2) a vapor trap in the line to the fission-product detector, and (3) lengths or coils of pipe used as vapor traps in the gas lines having slow flows, such as instrument lines. The Dowtherm-cooled vapor trap and other components of the recirculating gas system are located in the Fermi inert-gas building; gas is conveyed from the reactor building to the inert-gas building through a resistance-heated gas line in an underground tunnel. In the gas building the gas flows into a 500-cu ft vacuum tank, then to the Dowtherm-cooled vapor trap, which protects the compressors from liquid-metal entrainment.

As shown in Fig. VII-1, this trap consists of a 26-in.-OD inner shell that is surrounded by a 41.5-in.-OD outer shell charged with Dowtherm A as coolant.[4] The contacting surface of the vapor trap is increased by a 6-ft section of stainless-steel wool enclosed between perforated baffle plates. Downstream from the vapor trap is a cyclone separator, followed by three gas compressors in parallel. Although the line downstream from the vapor trap is not equipped with a sampling means to check trap effectiveness, there has been no evidence of sodium reaching the compressor diaphragms, which are changed periodically.

The EBR-II primary-gas system, like that of Fermi, operates on a demand type basis, with

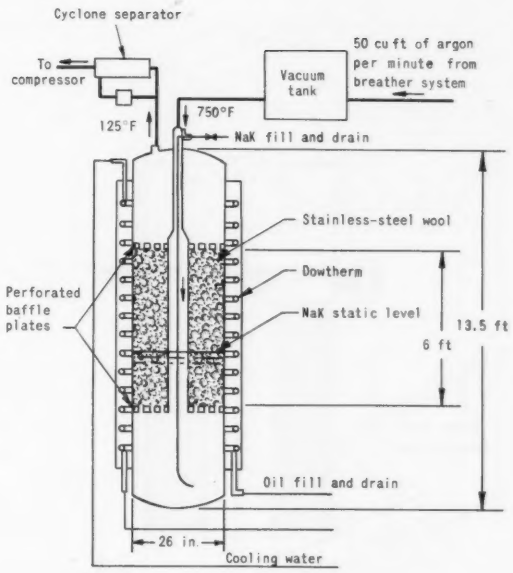

Fig. VII-1 Fermi vapor trap in gas recirculation system bubbles argon through NaK and passes it through stainless-steel wool; water-cooled Dowtherm in annulus cools trap and gas.[4]

the primary-tank argon pressure controlled by a floating-head tank. When gas volume changes because of temperature fluctuations, the floating head in the tank moves to maintain the cover-gas pressure constant.

Figure VII-2 shows the two stainless-steel-mesh-filled vapor or aerosol traps in the EBR-II argon cover-gas system.[5] These traps are not equipped with heaters, and therefore, if plugging occurs, the gas flow can be rerouted through a bypass line to keep the system operative while the traps or their mesh are replaced. Gas discharged from the primary tank passes up through a cleanout or access flange, then through the small vapor trap, through a silicone-oil-cooled heat exchanger that cools the argon to 150°F; then it passes through the large vapor trap and on to the floating-head tank. If the volume change exceeds the capacity of the floating-head tank, one of the two parallel blowers pumps gas into the argon receiver tank for future use (the second blower is a standby unit).

The traps see little flow except when the system is purged. When the primary tank was purged with the system still at approximately 700°F, the small vapor trap became plugged.

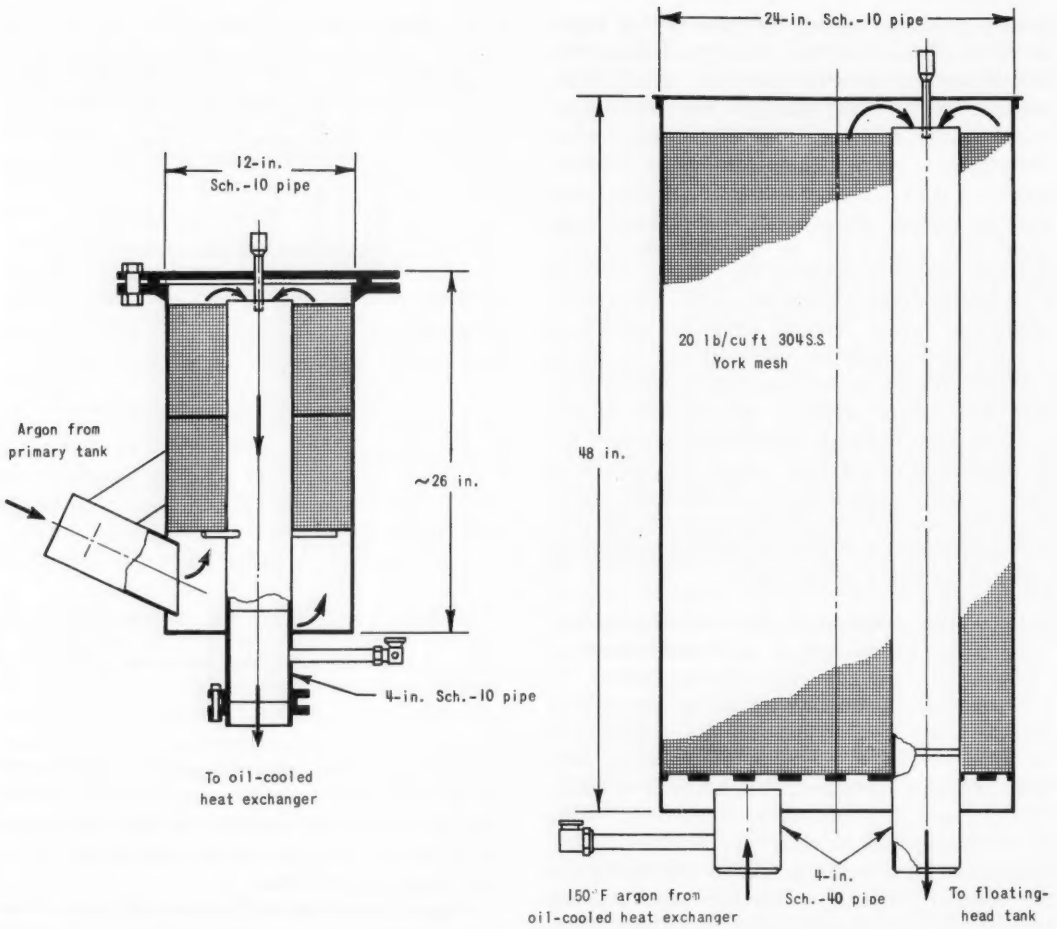

Fig. VII-2 EBR-II vapor or aerosol traps for primary-system argon are packed with stainless-steel mesh; heat exchanger in circuit between the traps cools the gas.[5]

When the operators removed the two-piece mesh packing through the flanged upper end of this vapor trap, they found that the lower section of mesh was plugged for approximately 1 in. from the mesh surface near the inlet nozzle, but the remainder of the mesh packing was relatively free of accumulated sodium. Although the operators removed the plugged-mesh piece and left only the upper piece of mesh in place, the trap has worked satisfactorily since.

The EBR-II fueling machine is cooled by an argon system, most of whose components are in an area depressed beneath the main operating floor. This argon system, which is separate from the reactor cover-gas system, includes two turbine type blowers, a multiple-tube natural-convection argon-to-air heat exchanger, a stainless-steel-mesh-filled vapor trap, and two molecular sieves in parallel. The vapor trap and molecular sieves, which are beds of crystalline sodium aluminosilicate pellets, remove vapor and fission-product gases from the argon drawn from the reactor vessel into the system piping during fuel-handling operations.

As shown in Fig. VII-3, mounted on the fueling-machine carriage are another lead-shielded vapor trap and molecular sieve, similar to the units in the argon system, for treating argon that is drawn directly into the fueling machine. Subassembly-heated argon (210 to 450°F) from the fueling machine passes through

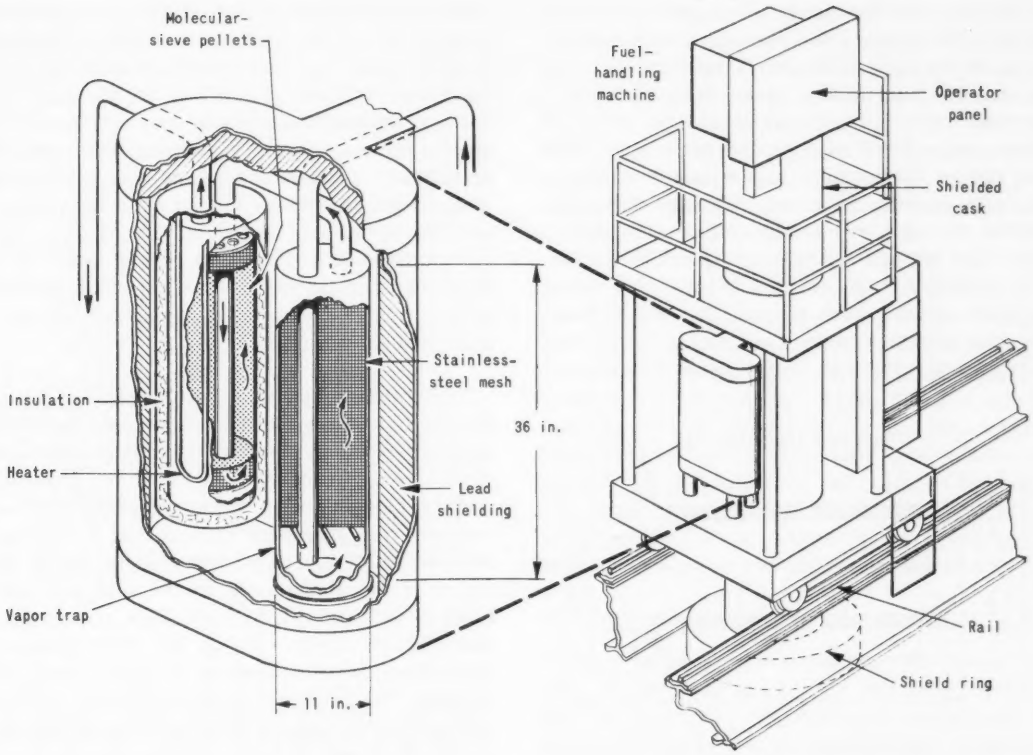

Fig. VII-3 EBR-II fueling machine has shielded vapor trap and molecular sieve to remove vapor and fission-product gases from argon drawn directly into machine.[5]

a 200-in.-long flexible hose to the heat exchanger, is cooled to approximately 100°F, and then enters the main turbine type blower (the smaller blower serves as a standby unit).

The vapor trap on the fueling machine has partially plugged once. Inspection revealed that the stainless-steel mesh had not plugged, but the lower opening of the gas-inlet tube had become blocked by sodium that had condensed onto the trap cold internal surfaces beneath the mesh.

The vapor trap in the depressed area also has plugged once. Operation was restored by removing the flanged outlet end of this horizontally installed trap and replacing the stainless-steel-mesh packing. When one of the turbine type blowers was disassembled recently to correct a manufacturing error, a fine white powder was seen in the piping and blower. This substance has not been analyzed, but its talcum-powder texture indicates that it is probably powder from the pellets in the molecular sieves and not sodium oxide.

Fission-Gas Monitor. When difficulty was experienced in obtaining vapor- and aerosol-free gas samples for the EBR-II fission-gas monitor that detects fuel-cladding failures, an 8-in.-diameter vapor trap containing a 4-in. thickness of stainless-steel mesh was installed in the gas line to the monitor and has operated satisfactorily. Argon enters this trap at 230°F and leaves at ambient temperature; gas flow is less than 200 cm^3/sec.

SRE, HALLAM, FARET, SCTI

These facilities can operate at temperatures up to 1200°F, where the vapor pressure is approximately 20 times greater than at 900°F. This is reflected in a wider use of vapor traps at these facilities than at EBR-I, EBR-II, or Fermi.

Hallam. Approximately 10 vapor traps are used in the primary and secondary sodium systems of the Hallam Nuclear Power Facility. As shown in Fig. VII-4, these traps are constructed with a 10-in.-diameter pipe within a 12-in. pipe fitted with pipe caps; vapor-laden gas enters the annular region and flows horizontally through the mesh, reverses direction, passes through the interior cylindrical volume, then exits through the outlet nozzle. These traps are equipped with heaters to melt the accumulated sodium when plugging occurs or when the rising pressure drop across the vapor trap indicates that the trap is becoming plugged.

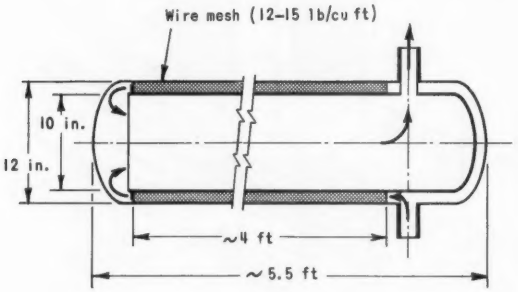

Fig. VII-4 Hallam vapor traps pass vapor horizontally through stainless-steel mesh in annular region, then through interior cylindrical volume; cooling is by natural convection. Heaters melt sodium when plugging occurs.[6,7]

The criterion for designing the Hallam vapor traps was to provide sufficient heat capacity and heat-transfer surface in the trap that the heat from the gas passing through the trap could be absorbed and dissipated rapidly enough to cool the gas below the melting point of sodium. Summary evaluation of the Hallam traps[6] indicates that "Operation of the vapor traps, installed in the system to prevent sodium vapor from entering and clogging the helium lines, has been satisfactory except at high reactor venting rates, such as when control-rod thimble leaks developed. Trap design and efficiency should provide many years of satisfactory maintenance-free service, but consideration should be given to the installation of more heaters."

The vapor trap in the reactor vent line plugged about four times during Hallam operation.[7] To unplug the trap, personnel entered the primary-system pipe gallery to insulate the plugged trap, which then was heated until sufficient sodium melted and drained to restore proper operation. The melted sodium drained directly into the liquid-metal system through the trap inlet nozzle. Although the plugging occurred during changes in reactor-operating conditions, no reactor shutdowns were caused specifically by the plugging of a vapor trap. If it had been necessary to shut down the reactor specifically to unplug the vent-line trap, an approximately 10-day waiting period would have been required for the radioactivity of the sodium in the primary pipes to decay enough for personnel to enter the gallery.

SRE. Atomic International's SRE at Santa Susana has mesh-filled vapor traps (one in the primary system, two in the secondary). Although SRE has operated without the trap becoming plugged, when the reactor vent line was removed for system modifications, it was discovered that approximately two-thirds of the cross-sectional area within the vent pipe was blocked with sodium. Nevertheless, the original mesh-filled vapor trap in the SRE primary system has been retained in modifications made recently to improve plant reliability and to permit reactor power to be increased from 20 to 30 Mw, with reactor-coolant temperature[8] raised from 960 to 1200°F.

SCTI. The vapor traps for the Sodium Components Test Installation (SCTI) at Atomic International's Santa Susana site differ from those at Hallam because of uncertainty concerning the flow rates through the SCTI gas system.[9] The cylindrical SCTI vapor traps are 6 in. in diameter and 3 to 4 ft high. Installed vertically, they are filled with $\frac{1}{8}$-in.-diameter steel shot to increase the heat capacity.

FARET. Vapor traps in the Argonne's Fast Reactor Test Facility will be of the annular design, similar to the Hallam traps, but the gas flow will be reversed so as to use the quiescent central volume of the trap as a refluxing condenser before the vapor-laden gas passes through the annular mesh. The design objective is to cool the outlet gas below 200°F regardless of whether the gas system has a slow flow of hot gas (to satisfy normal "breathing" requirements) or a fast flow of cool gas (such as during purging). As shown in Fig. VII-5, these traps will be installed with the longitudinal axis inclined 10° from the horizontal to facilitate

draining; they will be covered with 1-in.-thick insulation.

FARET vapor traps will be located in the argon supply and vent lines for the main secondary sodium system, auxiliary secondary sodium system, wet-fuel-storage tank, NaK drain tank, wet-fuel cooling system, and reactor-annulus drain tank—as well as on the argon supply line for the main primary sodium system and on the vent of the drain tank in the primary sodium system.

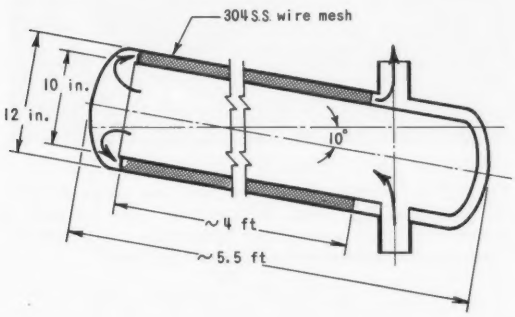

Fig. VII-5 FARET vapor traps, like those at Hallam, will be of annular design, but argon will flow first through quiescent central zone (which will serve as a refluxing condenser) before passing through mesh-filled annulus; 10° inclination will facilitate draining sodium.[10]

The coolant-gas-system equipment for the FARET fuel-handling machine, including the compressors, filters, vapor trap, heat exchangers, and argon supply tank, will be located in the transfer tunnel beneath the operating floor of the primary-containment cell and will be connected to the carriage of the fuel-handling machine by flexible metal hoses approximately 50 ft long.[10] For this system the functions of vapor trap and heat exchanger will be combined in a single unit that has an ammonia evaporative coil immersed in NaK maintained at 40°F; it is designed for gas flows of up to 60 cfm.

STF, LAMPRE, FRCTF

Los Alamos Scientific Laboratory has had notable success using stagnation type vapor traps on its 2-Mw Sodium Test Facility and the Los Alamos Molten Plutonium Reactor Experiment.[11] These facilities are relatively small, tight systems that do not require high gas flows and in which the gas is drawn from system locations where the sodium temperatures are relatively low. In general, the stagnation type vapor traps are pipes 4 to 5 ft long and greater than or equal to 3 in. in diameter that connect the liquid-metal system with smaller diameter gas piping. The traps are equipped with heaters to clear accumulated sodium when necessary.

The gas system of the Los Alamos Fast Reactor Core Test Facility is designed to recirculate the primary-system cover gas continuously. For this higher gas-flow system, it is planned to use continuously refluxing impingement type vapor traps.[12] Each of these reflux condensers will consist of a 1-in. pipe whose 30-in. length will be filled with $\frac{1}{8}$-in.-diameter stainless-steel balls. In the annulus between this 1-in. central pipe and an outer 2-in. pipe will be NaK that is cooled by air or water to maintain the outlet gas at approximately 300°F.

SEFOR

Vapor traps for the Southwest Experimental Fast Oxide Reactor, being designed by the General Electric Company for construction in Arkansas, will be 2- to 8-in.-diameter pipe sections that are packed with stainless-steel mesh for lengths[13] of approximately 18 in. These configurations, which were chosen as the result of General Electric experience with sodium loops and with the prototype power plant for the nuclear submarine *Seawolf*, are sized to maintain gas velocity less than 1 ft/sec. Although the larger traps will be equipped with heaters, sufficient heat is expected to be transferred through the short lengths of pipe between the vapor sources and the smaller vapor traps that heaters will not be required on these units.

LARGE TREAT SODIUM LOOP

The large sodium loop in the Transient Reactor Test Facility, located at the National Reactor Testing Station in Idaho, will be used to test unirradiated and preirradiated fast reactor fuels to failure under variable coolant temperature and flow conditions.

Possible contamination will be localized during fuel tests by operation of the loop on a once-through mode—sodium coolant will flow from a storage vessel through the test section and then to a dump vessel. A vapor-trapping

demister, molecular sieve, and liquid-nitrogen-cooled charcoal trap in the gas system remove gaseous fission products and entrained sodium or sodium vapor from the helium cover gas transferred between vessels during the once-through flow. The demister is constructed of a 12-in. length of 4-in.-diameter pipe fitted with knitted stainless-steel wire mesh having a bulk density of 20 lb/cu ft; the molecular sieve is a 9-in.-deep bed of $\frac{1}{8}$-in.-diameter sodium aluminosilicate (Linde 4A) pellets in an 8.5-in.-diameter container. Neither the demister nor the molecular sieve has heating or cooling provisions but are valved and flanged for replacement when necessary. Gas transfer through the system may reach 20 cfm at temperatures up to 900°F but will be sustained for a duration of only several minutes.

MELT-REFINING FURNACES

In conjunction with the development of the melt-refining process for purifying discharged EBR-II fuel, screening tests were conducted to determine the capability of various materials to trap alkali-metal vapors[14] as hot as 1470°F. Although the application was to statically trap sodium vapors and other condensible volatiles released by the melt-refining process, the materials were tested in a dynamic system. Argon gas was bubbled through a vaporizer containing a shallow pool of alkali metal and then through the bed material until breakthrough occurred; breakthrough was detected by white oxide fumes formed when the untrapped metal vapor reacted with oxygen at the end of the bed. The tests indicated that simple condensation alone is ineffective for retaining vaporized sodium but that nearly all surface-active materials, such as molecular sieves, activated carbon, and activated alumina, were effective.

Although molecular-sieve beds initially were used as fume traps for the EBR-II fuel melt-refining furnaces, their maintenance in a remotely operated plant would require additional handling equipment. Thus a simpler disposable fume trap was sought. Tests of an absorber type trap consisting of a molded, porous Fiberfrax (aluminum silicate ceramic fiber) cup showed it to retain sodium vapors quite effectively.[15,16] This trap works on the principle of absorption and chemical reaction of the sodium with the trap surface; the reacted layer can be seen in Fig. VII-6.

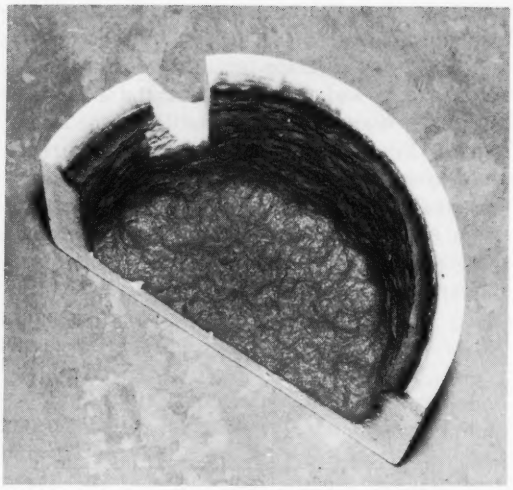

Fig. VII-6 Melt-refining-process development work for reprocessing spent EBR-II fuel showed that a porous Fiberfrax molded cup effectively traps sodium vapor by absorption and chemical reaction.[15]

Recent Developments

Recent research on vapor traps has been reported by Pratt & Whitney (CANEL) and by Argonne National Laboratory (ANL), with both efforts directed toward developing continuously refluxing vapor traps.

P&W. The lack of suitable design criteria can be seen in recent developmental work on vapor traps that was being conducted for the Lithium Cooled Reactor Experiment (LCRE).[17,18] Gas-system tolerances were to be defined as a result of long-term system testing, but, unfortunately, this work ceased when the LCRE project was terminated.

Four separate operating regimes had been defined for the LCRE vapor-trap tests: (1) 1000°F lithium vapor in 60 to 100 cu ft of helium per hour, (2) 120 to 1000°F lithium vapor in approximately static helium, (3) 700 to 1000°F NaK vapor in 30 to 50 cu ft of helium per hour, and (4) 100 to 300°F NaK vapor in approximately static helium. Air- or nitrogen-cooled traps were being developed to prevent more than an arbitrarily chosen 2-ppm (by weight) vapor carry-over; screening tests were made on a number of vapor-trap designs, including shell-and-tube heat exchanger, baffle, continuous-refluxing bubbler, mesh-packed, and helical-fin types. Most promising of these was

the continuous-helical-fin type vapor trap. Thus five helical-fin vapor traps were fabricated for tests to determine how helix pitch ($\frac{1}{4}$ to $\frac{3}{4}$ in.) and fin-surface slope affect trap performance; Fig. VII-7 describes their geometries. These lithium tests showed the trap with $\frac{1}{4}$-in. pitch to be the most efficient: approximately 80% for 1000°F lithium and approximately 99% for 1000°F NaK; Fig. VII-8 shows this trap. Figures VII-9 and VII-10 show the transparent housing for visually observing condensation in the helical-fin vapor traps and the tendency of the condensed liquid metal to agglomerate before draining back to the vapor source.

Stringent gas-purity requirements for the LCRE were to be met by the use of various settling, impingement, and filter devices downstream and in series with the $\frac{1}{4}$-in.-pitch helical-fin trap. Mesh-filled settling chambers were tested with the helical-fin traps for about 400 hr, but the LCRE termination prevented completing these evaluation tests.

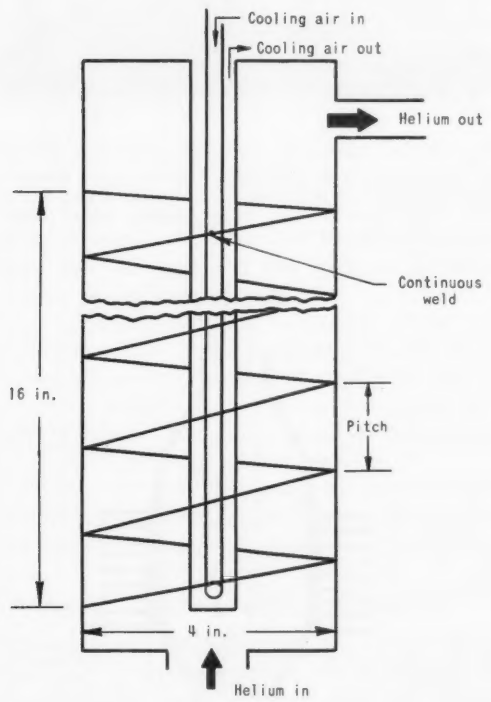

Fig. VII-7 When LCRE vapor-trap screening tests indicated that continuous-helical-fin type refluxing trap promises best efficiency, five such traps were built to test effect of helix pitch and fin slope. Fins of one trap were conical and on $\frac{1}{2}$-in. uniform pitch. Flat fins on each of other three were uniform $\frac{1}{4}$, $\frac{1}{2}$, and $\frac{3}{4}$ in.; Fig. VII-9 shows the fifth trap, whose flat fins had nonuniform pitch.[18]

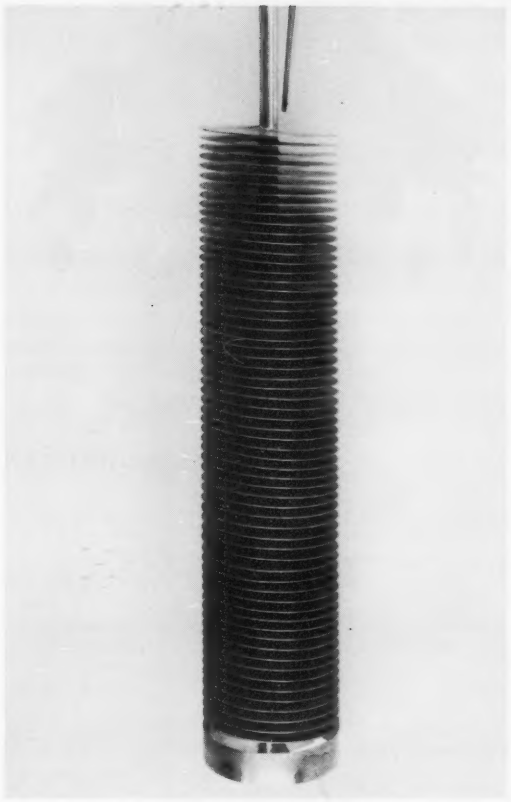

Fig. VII-8 Most efficient of the vapor traps tested by Pratt & Whitney for LCRE lithium vapor in helium was helical-flat-fin type trap having $\frac{1}{4}$-in. uniform pitch.[18]

ANL. Recent work on the development of a 1200°F sodium vapor trap at ANL has been reported.[19] Two experimental vapor traps were constructed. Figure VII-11 shows the second, mechanically improved vapor trap. It was tested with gas flows up to 40 cu ft/hr from a sodium tank maintained at 1200°F; vapor-removal efficiency was as high as 99.8%. Sodium condensation rates were determined by radiography of a calibrated U-tube beneath the vapor-trap inlet. At a gas flow of 20 cu ft/hr, the condensation rate was 13.6 cm^3/hr; it increased to 86 cm^3/hr when gas flow was 40 cu ft/hr.

These test results indicate that vapor-trap configuration and temperature can be adjusted

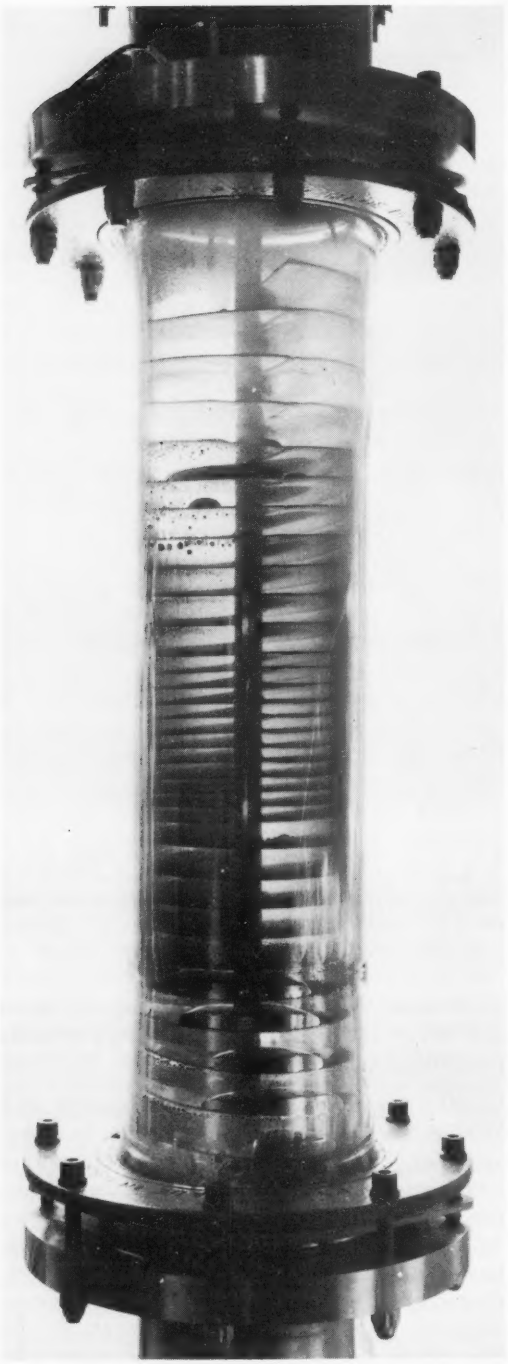

Fig. VII-9 Pyrex transparent shell permits observation of nonuniform pitch of this helical-flat-fin trap: 1/4 in. for middle 3 in. of helix, 1/2 in. for next 3.5 in. upper and lower, and 3/4 in. for top and bottom ends.[18]

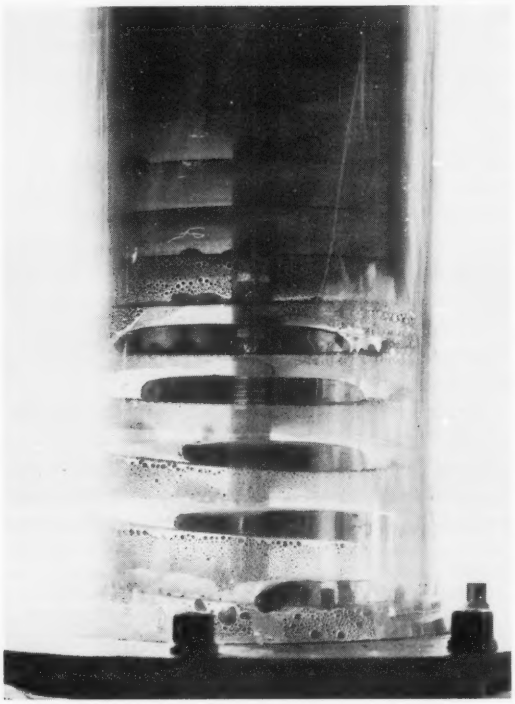

Fig. VII-10 Condensed liquid metal in helical-flat-fin trap tends to agglomerate on fins before draining back to vapor source, which in this case and in Fig. VII-9 was 1000°F NaK; photographs were taken[18] *after trap operated 5 hr.*

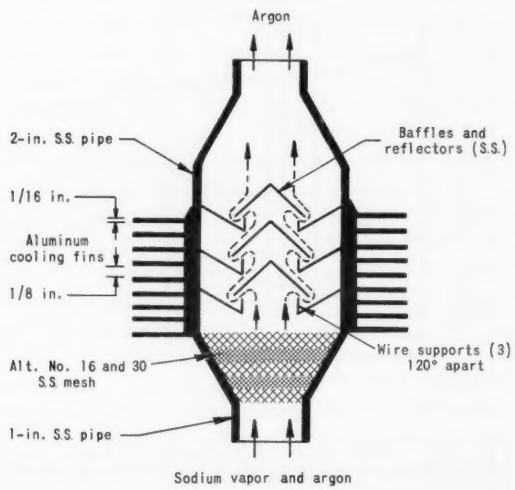

Fig. VII-11 Refluxing type impingement-condensing trap being developed at Argonne for 1200°F sodium vapor has cooling fins and internal baffles as well as mesh.[19]

to provide continuous refluxing of sodium vapor. In addition to avoiding trap plugging, this would permit reducing trap size and cost. But this trap would not operate satisfactorily if the gas contained an oxide aerosol because oxide accumulation on the limited condensing surface would plug the trap.

A larger trap with a 2-in. inlet is being tested now. It has operated for about 650 hr at 570°F and 800 hr at 1020°F. The major operating problem has not been with the vapor trap, but with maintenance of the tank heaters.

Recommendations for System Design

Vapor traps should be located near the vapor sources to minimize sodium plugging or obstruction of gas lines. However, because traps for handling appreciable gas volumes are rather bulky, and space within containment cells is often at a premium, traps cannot always be positioned next to sodium-containing vessels. Thus system designers must ensure that the gas piping has enough heat capacity to overcome liquid-metal accumulation and plugging and that the entrapped liquid metal can be drained from the piping.

Trap Design. Field experience with replaceable mesh-filled vapor traps indicates that plugging occurs in a small volume of the mesh near the gas inlet and that most of the mesh volume in a plugged trap remains relatively free of liquid-metal accumulation. This experience suggests that trapping capacity might be improved by the use of graduated-density or zoned-density packings. Another improvement on current practice might be to increase the frontal-area-to-volume ratio of the mesh packing, such as by arranging the mesh packing in a relatively thin annulus through which the gas would pass radially.

Conclusions: Development Needed

The mesh-filled vapor trap has found almost universal application in liquid-metal-reactor systems where large volumes of gas are transferred. The operation of these traps can be described as tolerable or even acceptable, but in few installations have they proven to be completely satisfactory.

There has not been a significant change in vapor-trap technology during the past decade. The early experimental work with vapor traps covered almost the entire spectrum of devices that are being used now. The first impingement type units were purposely oversized to compensate for lack of adequate design criteria and uncertainties surrounding the nature of the sodium vapor or aerosol, and this approach persists today. However, the vapor-trapping requirements of liquid-metal-cooled systems continue to rise as system size and operating temperatures increase. Thus a comprehensive developmental program is needed to provide vapor-trap and reactor-system designers adequate information upon which to base their designs.

References

1. A. J. Erickson, C. L. Gregory, and P. M. Lang, Vapor Traps for Handling Liquid Sodium, USAEC Report AECU-3200, MIT Engineering Practice School, Aug. 25, 1951.
2. J. C. Cochran (Ed.), Sodium Graphite Reactor Quarterly Progress Report, July–September 1955, Section B, USAEC Report NAA-SR-1513, Atomics International, Mar. 15, 1956.
3. R. O. Haroldsen, F. D. McGinnis, M. Novick, R. R. Smith, and F. W. Thalgott, Safety Analysis Report, EBR-I, Mark IV, USAEC Report ANL-6411, Argonne National Laboratory, February 1963.
4. Power Reactor Development Company, Enrico Fermi Atomic Power Plant Revised License Application, Part B, Technical Information and Hazards Summary Report, Report NP-10458, Vol. 1, pp. 107.7–107.12, July 1961.
5. L. J. Koch, W. B. Loewenstein, and H. O. Monson, Addendum to Hazard Summary Report Experimental Breeder Reactor-II (EBR-II), USAEC Report ANL-5719(Add.), Argonne National Laboratory, Jan. 7, 1964.
6. J. E. Price, Final Evaluation Report—Hallam Nuclear Power Facility, USAEC Report NAA-SR-9777, Atomics International, 1964.
7. G. L. Ballew, Hallam Nuclear Power Facility, personal communication, Aug. 31, 1965.
8. W. J. Freede and J. K. Roberts (Eds.), Sodium Reactor Experiment. Power Expansion Program—Heat Transfer Systems Modifications, USAEC Report NAA-SR-10379, Atomics International, Oct. 9, 1964.
9. R. Cygan, Atomics International, personal communication, Sept. 22, 1965.
10. W. R. Simmons et al., Argonne National Laboratory, unpublished, 1965.
11. L. A. Whinery, Los Alamos Scientific Laboratory, personal communication, Aug. 12, 1965.
12. B. J. Melton, Los Alamos Scientific Laboratory, personal communication, Sept. 22, 1965.
13. H. N. Bass, Atomic Power Equipment Department, General Electric Company, personal communication, Aug. 31, 1965.
14. J. Wolkoff and A. A. Chilenskas, The Melt Refining of Irradiated Uranium, Application to EBR-

II Fast Reactor Fuel. IX. Sorption and Retention of Sodium and Cesium Vapor on Stationary Beds at Elevated Temperature, *Nucl. Sci. Eng.*, 9(1): 71-77 (January 1961).
15. S. Lawroski, W. A. Rodger, R. C. Vogel, and V. H. Munnecke, in Chemical Engineering Division Summary Report for January, February, March 1960, USAEC Report ANL-6145, p. 32, Argonne National Laboratory, 1960.
16. J. C. Hesson, M. J. Feldman, and L. Burris, Description and Proposed Operation of the Fuel Cycle Facility for the Second Experimental Breeder Reactor (EBR-II), USAEC Report ANL-6605, Argonne National Laboratory, April 1963.
17. H. J. Banach, LCRE Auxiliary Systems Termination Report, USAEC Report PWAC-416, Pratt & Whitney Aircraft, Mar. 9, 1964.
18. E. H. Donnelly, Final Report on the Design and Development of Lithium and NaK Vapor Traps, Report PWAC-400, Pratt & Whitney Aircraft, Mar. 3, 1964. (Classified)
19. E. L. Kimont, Engineering Development of a Practical 1200°F Sodium-Vapor Trap, *Trans. Am. Nucl. Soc.*, 8(1): 147 (1965).

Section

VIII

Power Reactor Technology

Operating Experience

Operational Problems and Solutions

By Rolf C. Skaardal

Reactor designers should be interested to learn what reactor operators have found out about their products. Some reactor operational difficulties traced to design, fabrication, and inspection were reported at the Conference on Reactor Operating Experience sponsored by the Reactor Operations Division of the American Nuclear Society (ANS). Some of the "nuts-and-bolts" type problems are reported here. Most of these involved hydraulically induced vibrations, corrosion, leaks in components, and control-system peculiarities. Repair methods, control of oxygen in heavy water, and changes to research-reactor experimental facilities also are of interest to operators and designers and therefore are taken into account in this review.

Control Systems

Difficulties have occurred with neutron-absorber rods and control circuitry at various power reactors.

Control Rods. During a routine license test with the Indian Point reactor shut down, one control rod stuck when it was being inserted.[1] After borating the water, cooling the system, and removing the vessel head, the operators found that a tapered stainless-steel pin ($1\frac{3}{4}$ in. long by $\frac{5}{32}$ to $\frac{9}{32}$ in.) had wedged between the upper grid plate and a blade of the cruciform control rod. They removed the pin, of unknown origin, with a 19-ft-long slender wrench when the control rod was jacked from below.

Also at Indian Point, when it was time to remove the 12 boron–stainless-steel fixed shim rods that had been installed in the first core to limit reactivity during the early part of core life, several blades were found to be stuck.[1] The rods were freed by partially removing, as a unit, all four fuel elements around each rod. The sticking was caused by considerable buckling of the rods, which apparently occurred because of radiation-induced growth of the shim blades relative to their rigidly attached non-borated stainless-steel tips. These shim rods had been in the reactor for only 189 effective full-power days.

Specimens of Elk River reactor control rods of a similar material (2% boron–stainless steel) also suffered radiation damage, in this case, ductility loss.[2] About a year after the plant reached full power, the control rod was replaced because tests on a specimen of the rod material indicated that it might no longer meet the technical-specification requirement of 3.4% elongation. However, visual inspection of the removed rod showed no apparent mechanical damage. Studies are under way to determine (1) how much rod embrittlement is tolerable and (2) whether periodically changing the core location of the rods to expose all rods uniformly would be a more practical program than replacing each rod as it reaches its limiting ductility.

When the nickel plating on the silver–indium–cadmium control rods of the Yankee reactor failed to protect the silver from corrosion, radioactive silver corrosion products circulated and deposited throughout the primary system.[3] This caused maintenance problems, particularly during the first refueling. After the reactor pit was flooded (to provide shielding for the refueling crew) and the vessel lid was removed, the radioactive silver in the reactor water got into the pit water and plated out on the stainless-steel liner. To avoid the problem

thereafter, the operators replaced the original rods with hafnium rods. For two years they also have successfully used two experimental silver–indium–cadmium rods that are clad with Inconel and now have installed two new silver–indium–cadmium rods clad with stainless steel.

Chemical Shim. Yankee, like Indian Point, was designed to use boric acid solution in the coolant–moderator to reduce reactivity during cold shutdown. As an extension of this, during operation with the second core, the Yankee operators experimented with boric acid injection as a chemical shim method.[3] Although the experiments were successful, for some unexplained reason the boric acid in the operating reactor system was accompanied by higher crud concentrations and appeared to cause oxygen generation in the pressurizer. While the causes are being investigated, the solution at Yankee has been to arrange for degassing from the top of the pressurizer and recombination by reinjecting into the main coolant system with 25 cm^3 of hydrogen per liter in the coolant.

Temperature Sensor. The Elk River reactor experienced several spurious scrams caused by a malfunctioning temperature bulb and pressure switch.[2] After tests indicated this equipment was sensitive to radiation, it was replaced by a thermocouple system.

Level Control. When a water-level indicator in the Special Power Excursion Reactor Test No. 3 (SPERT-III) 2500-psi 650°F pressurizer reported that the water was more than 2 ft higher than it actually was, the electric heaters became partly uncovered and superheated the steam to 1000°F. This caused the pressurizer-vessel material to fail in creep and ruptured its seam weld.[4] The error illustrates the mutual dependence of instrumentation and mechanical-hardware designs. The signal from a differential-pressure cell was used to sense the water level. Compensation for the effect of density changes on the water-level indication was provided through a temperature signal received by the automatic controller from a single sensor near the top of the normal water level. Unfortunately this signal did not recognize the water-temperature stratification that occurred when certain operating conditions led to diminished internal circulation of the pressurizer water.

Reliable water-level control in the new pressurizer is to be obtained by (1) electric heaters staged to operate at different elevations so as to circulate the water by convection (heater response is delayed only slightly) and (2) taps for the differential-pressure cell located such that the normal operating water level is 25% of the differential range above the bottom tap. Although this increases the safety margin, temperature–density compensation is still necessary for water levels other than normal.

Electrical Circuit. Routine checks of the SPERT-III scram circuit five years after installation revealed abnormal operation and relay chatter.[5] After wiring checks did not find the cause, a complete evaluation of the system disclosed that electrical leakage to ground through faulty insulation could actuate relays that should be deenergized (such as the rod-withdrawal circuit). This failure by leakage to ground occurred on leg *a* of the "floating-ground" power-distribution system (Fig. VIII-1),

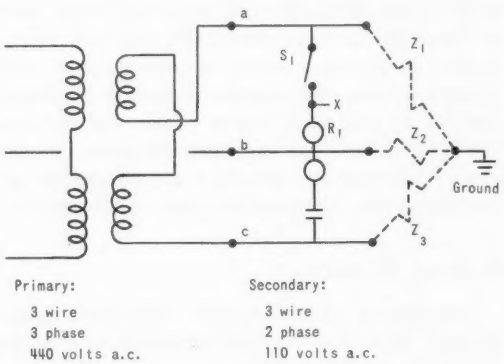

Fig. VIII-1 Original power-distribution scheme for SPERT-III proved "fail-unsafe" when the wire insulation deteriorated, permitting a short circuit in the wiring to override the control-rod switch by effectively shorting it closed.[5]

where the insulation on the wiring in the control-rod drives was particularly susceptible to deterioration because of exposure to vibration, heat, and moisture.

Because the leakage impedance Z on any of the three lines shown in Fig. VIII-1 was made up of both the resistance path through deteriorated insulation and the strong inherent capacitance built into the a-c control system by its long wiring runs to ground, an accident

could result (because the switch S_1 is effectively shorted by impedance Z_1, the relay R_1 cannot be deenergized) if a failure to ground occurs near point X in Fig. VIII-1. Although R_1 is a 110-volt relay, 60 volts will energize it, and it will remain energized down to 45 volts. Despite the intention to design a fail-safe system, the discovery that ground failures might not deenergize certain relays meant that the system was not, in fact, fail-safe.

Because of the hazard, the control-system power-distribution circuit was modified as shown in Fig. VIII-2 so that wiring deterioration can be detected before serious consequences result. The transformer neutral line

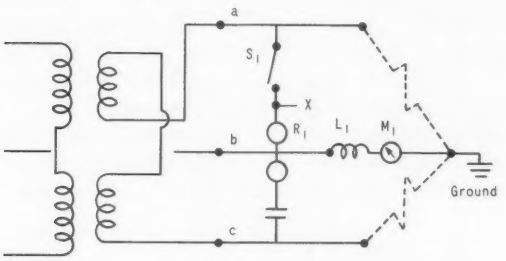

Fig. VIII-2 Modified circuit for SPERT-III alarms if deteriorated insulation permits leakage to ground. Thus insulation can be repaired before a short circuit occurs and overrides the switch.[5]

b was grounded through a current-limiting lamp L_1 in series with an ammeter M_1. Any leakage to ground from either of the high-voltage legs a or c then completes the circuit and causes current to flow through the lamp and meter. Although this system cannot prevent faults, it does keep the reactor operator informed as to the condition of the system and provides an alarm if an abnormality occurs.

This ground-loop problem at SPERT-III taught several lessons applicable to any electrical system. For instance, operators must bear in mind that the usual insulation checks are d-c measurements that will not detect capacitance paths, which are serious for a-c systems. Designers must consider the operating characteristics of components, such as relays, and the likelihood of large capacitance in their leads. Because of the impossibility of designing a completely failproof system and the chance of practical problems such as insulation deterioration, systems must be designed so that failures will not have serious consequences.

For more information on control experience discussed at the same ANS meeting, see page 221.

Flow Oscillations

The Elk River reactor[2] has exhibited flow pulsations ever since the initial power-escalation runs in 1963. The oscillations, which are well defined and repeatable, apparently are caused by surges in the feedwater flow at around 50% of rated power. These flow oscillations cause the reactor power to vary less than 2.5%. Although the conditions are adjudged to present no operational hazard to the reactor, studies are continuing to permit better understanding of the phenomenon.

Flow-Induced Vibrations

Flow of the coolant at high speeds through a reactor can buffet components and cause them to vibrate and wear. Failures resulting from this at the Big Rock Point, Yankee, General Electric Test Reactor (GETR), and SPERT-III reactors emphasize the need for designers to assess potential vibration sources, components that are susceptible to such damage, and ways to keep broken items out of the pumps and the core.

Excessive vibration loosened, and in some cases dislodged, bolts connecting fuel channels to channel support tubes in the high-power-density forced-circulation reactor in the Big Rock Point Nuclear Power Plant.[6] Investigations using accelerometers and strain gauges showed that the vibration was caused by inadequate distribution of the water coolant as it entered the reactor vessel. The manner in which the problem was solved by adding a baffle and by modifying the core support plate and 72 fuel channels will be described in an article on reactor-modification methods in the next issue of *Power Reactor Technology*. That article also will discuss modifications to the thermal-shield support in the Big Rock Point reactor.[7] These were required when several studs fractured by thread-root fatigue after fretting had enlarged clearances. The fretting occurred when small pressure fluctuations across the large surface of the thermal shield caused significant wear forces between line-contact sliding surfaces.

Hydraulically induced fretting corrosion was found when the Yankee power reactor was first refueled.[3] Zircaloy to stainless-steel joints on the fuel elements had corroded to a depth of more than 0.1 in. Later, stainless-steel tubes of the in-core instrumentation package were found to have been damaged by fretting corrosion to a depth of 0.040 in. Evidence also has been found that the Yankee control rods had fluttered, causing notches to be worn into the stainless-steel rubbing straps.

Steps to prevent such hydraulic problems at Yankee have included substitution of stainless steel for Zircaloy in parts that might rub, replacement of the 24 guide tubes, and installation of impact sleeves to act as cushions or vibration absorbers, and at the same time to give larger (100-fold in some cases) surfaces for dissipating impact.

The problem caused by hydraulic flow at Yankee has been the failure of 10 holders for irradiation coupons. Four were recovered in 1963, but the other six holders and basket parts remained lodged in uncertain positions in the reactor vessel until they were recovered during the 1965 refueling.

In the GETR,[8] hydraulically induced vibrations of control-rod guide tubes caused excessive wear of aluminum core-component spacer pads (see Fig. VIII-3). The pads provide lateral support for the upper ends of the fuel elements and beryllium filler pieces; there is no upper grid plate. The ½-in. 8-cps vibration of the guide tubes affected the reactor log-*N* period instrument, causing large-period recorder oscillations as the spacer pads ablated. When the reactor was operating at a steady 30 Mw, the recorder showed periods as short as ±30 sec, which caused repeated alarms.

Reactor modifications to stop the vibration consisted in bolting the free upper ends of the control-rod guide tubes to the coolant-flow distributor, replacing the guide-tube aluminum spacer pads with stainless-steel bands (fitted into slots milled circumferentially around each aluminum guide tube in the pad region), and installing complete stainless-steel top ends on the beryllium pieces.

No significant log-*N* period oscillations have been observed since; at a steady 30 Mw, recorder oscillations indicate periods of ±400 sec (for reference, the period indication is ±1000 sec with the reactor shut down). No pad wear could be detected after operation for one year.

In the SPERT-III reactor primary system, vibrations broke loose a thermowell.[5] Fortunately this failure occurred downstream of the pumps, and the 8-in.-long piece of ½-in. pipe was caught below the core. This occurrence, together with earlier fatigue failures of in-core instrumentation (due to vibration of small parts exposed to the turbulent coolant stream), caused concern about the 17 remaining thermowells in the primary system. Investigation revealed that none of these conformed with vendor's drawings. Strain-gauge tests showed that 9- and 6-in. wells were excited at their natural fre-

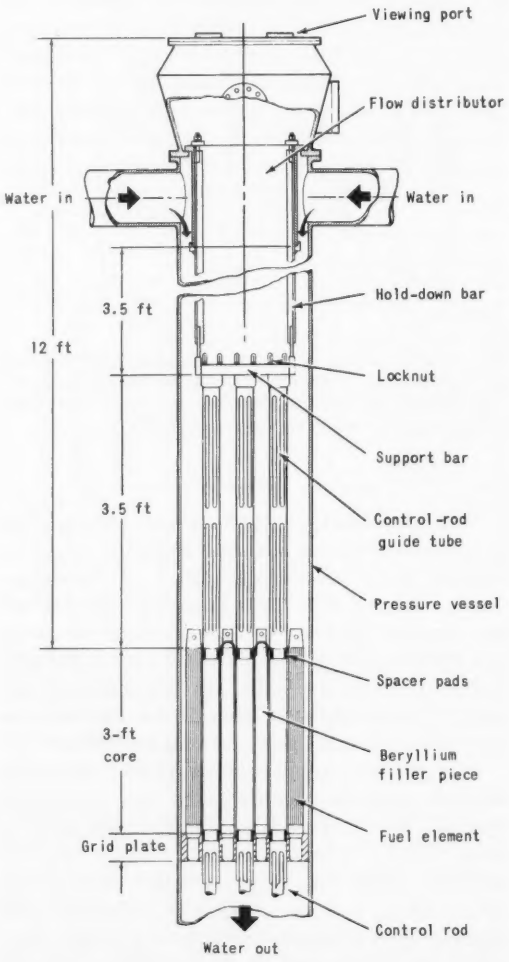

Fig. VIII-3 The GETR, which does not have an upper grid plate, employed aluminum spacer pads for lateral support of the upper ends of the core components.[8]

quencies, but 5-in. wells showed essentially no excitation. Thus 5-in. wells have been installed, and no further thermowell problems have been encountered.

Corrosion Problems

A mysterious form of corrosion of Inconel has been discovered at the Ågesta Nuclear Power Plant in Sweden.[9] The Ågesta reactor, a pressurized D_2O-cooled and -moderated reactor, has a flat hollow lid that is filled with light water for cooling the lid and for radiation shielding. This lid is penetrated by 188 Inconel pipes for heavy water; 11 of these pipes, used for charging irradiation specimens, are located at the periphery and barely pass through the inside of the lid (Fig. VIII-4). Leakage of heavy water into the lid was discovered and found to be caused by corrosion of three of these peripheral tubes.

Examination revealed intercrystalline stress-corrosion cracking on the tube surface, originating from the light-water side. The lid-water chemistry had been harmless—*p*H was maintained between 9.5 and 10.5 by addition of LiOH. Chloride-ion concentration was ≤0.5 ppm, and stresses were less than 20% of yield stress. Thus this stress-corrosion phenomenon is not fully understood; the damaged tubes are being examined metallurgically. In this reviewer's opinion the cause for this "abnormal" stress corrosion might be traced to the Inconel-tube manufacturing process itself.

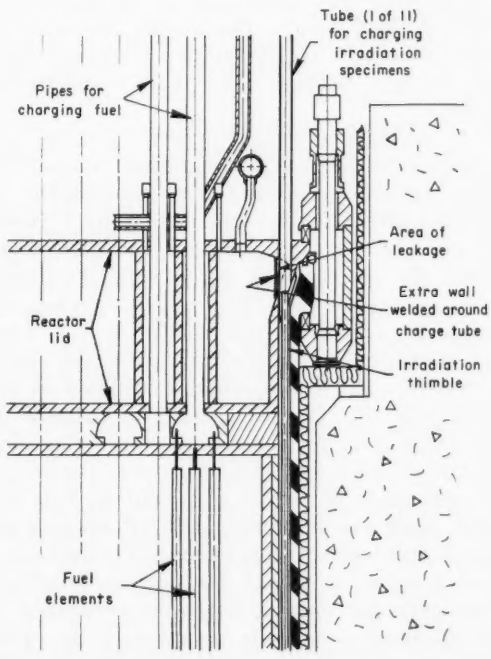

Fig. VIII-4 Extra wall section was welded around each of 11 Inconel specimen-charging tubes in the shield lid of the Ågesta reactor after three tubes cracked due to stress corrosion.[9]

Leaks in Mechanical Components

The Yankee and SPERT-III pressurized-water-reactor systems have experienced a variety of difficulties with leaks in mechanical components and resulting troubles.

At Yankee, early problems were encountered with leaks from canned-motor-pump flanges and from stem-leakoff type valves.[3] The flange leakage, which was caused by differential thermal expansion, is prevented by the use of the thermal expansion itself for final tightening of the closure; the operators do not pressurize the primary system when fluid temperature is low. For any cold hydraulic test of the system, the operators must adjust the pump flange by tightening the bolts. When the inner packing on the leakoff type valves could not control the leakage to desirable levels, it was necessary to remodel the valves to provide deeper inner packings. Leakage from the refueling water cavity and the ion-exchange pit at Yankee presented vexing problems. Also, one 2-in. stainless-steel pipe in the charging line failed by cracking due to suspected vibration and fatigue, and eight socket welds and seal welds have leaked. As the plant has become "broken in," such problems have tapered off—Yankee has now logged two complete one-year cycles without a primary-system cooldown or depressurization.

The SPERT-III reactor has experienced leaks from valves, gaskets, and piping.[5] The desirability of waterproofing all control-system electrical connections was demonstrated by the failure of a single tube fitting in the primary-coolant system. Extensive damage from short circuits resulted from the complete drenching of control-system wiring.

An unusual kind of leakage was experienced with one of the four canned-motor pumps in the SPERT-III primary system. During a plant cooldown in November 1964, a pump circuit breaker dropped out. Inspection showed that

water had leaked through the seals of the stator-winding terminal posts and short-circuited the windings. The rotor can, stator liner, and stator were damaged, and the motor section had to be completely rebuilt. Although no cause for the leak has been ascertained, it is believed that the pump had operated for some time with a damaged rotor can. Thus the initial damage might have been caused either by a foreign particle entering the motor from the primary system or by a piece corroded from the nitrided surface of the thrust disk. This latter is considered more likely because some corrosion has been observed on the thrust disks of all four pumps. The operators are considering replacing the nitrided 17-4 PH material on the thrust-bearing disks by Stellite 19, which better resists pitting corrosion.

All gaskets in the SPERT-III system, except the heat-exchanger head gaskets (which are solid stainless steel), are of the spiral-wound asbestos-filled stainless-steel type (Flexitallic); diameters range from 1 to 53 in. Although experience with this type of gasket has been generally satisfactory, some flanged connections leak slightly during the cooldown portion of about the first three cycles after gasket installation. Thus retightening during each cycle is necessary until the gasket firmly seats. Also, if this type of gasket is installed without an inside-diameter retaining surface, water flow tends to unwind the gasket and pieces break off. This adds tramp metal to the system as well as weakening the gasketed joints.

The SPERT-III experience with metal gaskets has not been satisfactory. The heat-exchanger stainless-steel gaskets leak slightly and erratically at operating temperature. Although the primary control valves originally were fitted with solid-metal gaskets and welded canopy seals, frequent leaks and repair difficulties have prompted their replacement by Flexitallic type gaskets.

Stem galling and leakage through valve seats also occurred at SPERT-III. The motor-operated temperature-control valves were furnished with chrome-plated type 304 stainless-steel valve stems and Stellite 6 bonnet bushings and lantern rings. After about a year of service, a valve stem seized and the motor force, in addition to the 2500-psi internal pressure, broke the packing-gland bolts, necessitating an emergency shutdown. After the valve stems were overlaid with Colmonoy 6 and new bushings of bearing bronze were fitted with greater clearance, there were no further troubles of this kind.

Repair Procedures

At Indian Point, two maintenance jobs involved welding in high-radiation areas.[1] One job was the modification of the nuclear boilers secondary-side blowdown piping (the original design did not provide for differential thermal expansion relative to the boiler shell). To protect the welder from the 1.5 to 3 r/hr radiation field, a special lead shield on four wheels was made of 3- by 3-ft 0.25-in.-thick lead plates stacked as many as eight thick; the shield was just high enough for the welder to position himself under it and "turtle" along while doing the work, which required two to three weeks to complete. The other task involved rewelding of an inspection cover on a control-rod guide tube in the upper grid-plate assembly. This plate is located 4 ft below the reactor-vessel flange. The radiation field was 10 r/hr with the water level lowered to just below the plate. A 3- by 4- by 4-ft lead box, with its top open and a small round hole in the bottom was made from 0.25-in. lead sheets. The welder did his work through this hole. He spent an uninterrupted 30 min and received only a very low radiation dose.

At the Ågesta Nuclear Power Plant, an unusual repair job was accomplished in connection with the peculiar stress-corrosion cracking of Inconel-600 tubes in the shield lid.[9] These tubes, which are part of the D_2O circuit, penetrate the periphery of the H_2O-filled lid over the reactor vessel; they serve as charging pipes for irradiation specimens. Only 3 of the 11 peripheral tubes were cracked by the intercrystalline corrosion, which originated on the H_2O side, but it was decided to protect all 11 tubes from further attack by enclosing each within an extra wall section that would be welded to the inside of the lid (Fig. VIII-4). This repair work was extremely difficult because the work area was severely restricted by the heavy-water piping on the lid. Further, the lid structure permitted holes of only approximately 6 in. in diameter to be made for access to the welding area. Thus it was necessary to use mirrors and bent electrodes. The repairs took four months, including demonstration of an efficient repair method and recommissioning of the lid.

The radiation levels in the work area were moderate, 1 to 5 mr/hr, and were chiefly from crud deposits in the heavy-water piping atop the lid. The fuel contributed to the background only slightly and, therefore, was not discharged from the core during the repair. No worker received more than 0.7 rem.

Control of Oxygen in D_2O

Operators of the Plutonium Recycle Test Reactor (PRTR) reported difficulties in reducing the oxygen content of the helium-blanketed heavy-water systems.[10] The oxygen came from radiolysis of the D_2O and air leaks. The excess oxygen quickly disperses through all the D_2O systems because of the common surge tank, for the helium, which is the pressurizing medium for the reactor coolant, provides an inert atmosphere over the moderator and reflector, as well as serving as blanket gas between the calandria and shields.

The usual method for reducing the excess oxygen involved recombination by adding "shots" of hydrogen gas directly into the D_2O coolant. Although chromatographic analyses of the helium showed that these injections partially reduced the oxygen, they also unexplainably decreased the indicated content of hydrogen in the gas. Investigations employing mass-spectrometric analyses showed that the chromatograph was inaccurate (at equilibrium before H_2 was injected, no H_2 was present and only 12 to 17% as much D_2 as the chromatograph had indicated total H_2 plus D_2) and that the oxygen in the gas preferred to combine with the H_2 injected into the water rather than with the D_2 already present in the gas.

When it became clear that injecting hydrogen gas into the coolant still did not sufficiently reduce the oxygen content of the D_2O, tests were made to learn the effectiveness of a uniform concentration of excess hydrogen in the helium supply. Although calculations indicated that an initial concentration of 0.3% H_2 would be enough to combine with the oxygen from radiolytic dissociation and air inleakage, it only very slowly reduced the O_2 concentration in the D_2O. Increasing the H_2 concentration to 0.6% produced faster results, but only after reactor systems reached equilibrium temperature after startup. Since a 1% H_2 concentration in the helium was selected for routine operation, there has been very little problem with excess oxygen.

Research-Reactor Modifications

Designers of reactor experiments will be interested in considering the modifications made to irradiation facilities at two pool type research reactors to increase their usefulness for certain types of experiments.

Rabbit Facility. An interesting pneumatic irradiation system has been operated in the thermal column of the Industrial Reactor Laboratories (IRL) 5-Mw pool type research reactor.[11] It permits samples to be inserted and removed from the 10^{11} neutrons/(cm^2)(sec) flux in the column during full-power operation. The unique feature of this rabbit facility is that the track and 1- by $\frac{1}{2}$-in. vent line were machined from graphite and assembled to form two 4- by 4- by 51-in. standard graphite pieces (Fig. VIII-5) which, when connected end-to-end, fully penetrate the thermal column. The $1\frac{3}{8}$-in.-diameter track has an S shape to prevent radiation streaming. The low-friction graphite track is ideal for rabbit travel; no liner is needed that might perturb the flux or cause contamination problems in the column.

A maximum rabbit-surface contamination of 0.05 μc/cm^2, due mainly to the 12.9-hr ^{64}Cu and 2.58-hr ^{56}Mn from impurities in the AGOT graphite, has presented no serious handling problems.

Figure VIII-6 shows the pneumatic system used in inserting and returning the rabbit.

D_2O Reflector. A vented rectangular aluminum tank[12] containing 45 gal of heavy water has been installed along one full face of the core of the University of Michigan reactor (Fig. VIII-7). When the core size was reduced, installation of the tank converted two radial beam ports into tangential ports, increased the thermal-neutron flux at the beam-port source planes by 80%, and improved the signal-to-background ratio by factors of 2.8 and 4.7. Figure VIII-8 shows how the installation of the heavy-water reflector influenced the ionization-chamber readings.

When tests showed that the D_2O-filled-tank reactivity worth (compared to H_2O) was only half the +0.04 $\Delta k/k$ prediction calculated, the operators increased the core operating mass by 12% so as to provide enough excess reactivity for routine operation at 2 Mw.

The maximum credible accident is postulated to involve the release into the reactor pool of tritium produced in the D_2O tank. Thus the

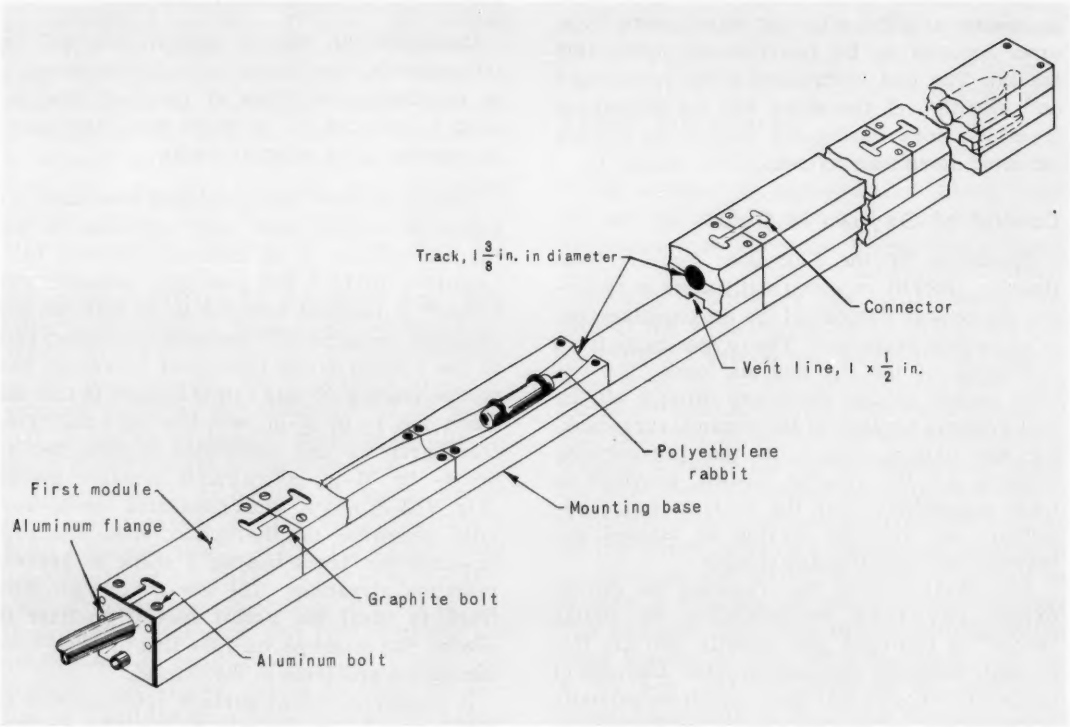

Fig. VIII-5 Assembly of graphite modules for rabbit-travel guide in IRL reactor thermal column. Graphite modules, each 12 3/4 in. long, are mounted on two 1- by 4- by 51-in. graphite pieces placed end-to-end.[11]

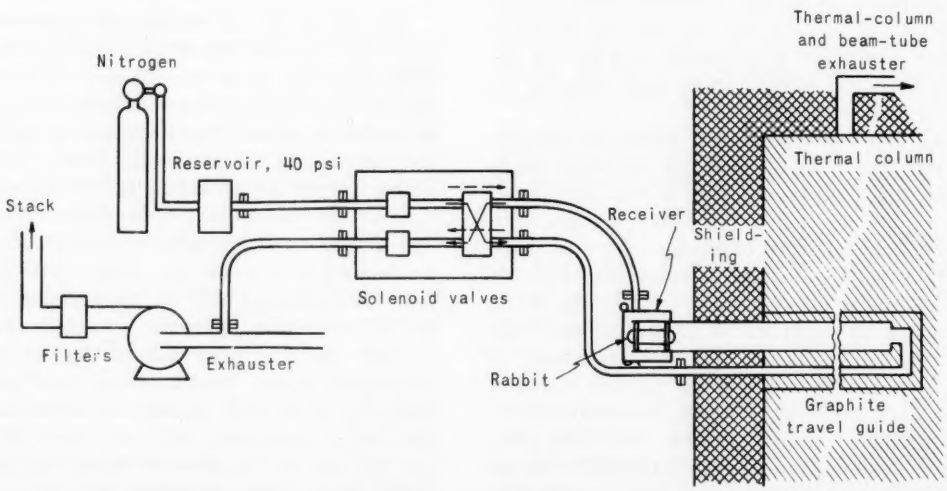

Fig. VIII-6 Pneumatic system controlled by solenoid valves supplies 40-psi nitrogen pulse for insertion and return of rabbit.[11]

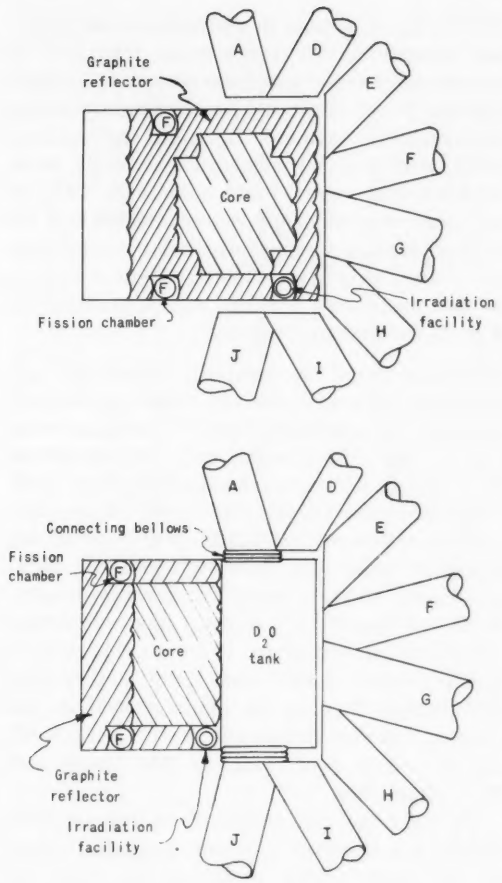

Fig. VIII-7 Arrangement of core, graphite reflector, and beam tubes of the University of Michigan reactor was modified from standard configuration (top) by adding D_2O reflector next to north face of core (bottom).[12]

tritium content in the tank will be checked every 800 Mw-hr to ensure that it does not exceed 50 curies; production-rate measurements predict that the D_2O will not need reprocessing or replacement until the reactor has operated 15,800 Mw-hr. Calculations had predicted a neutron-flux peak in the tank of twice the core flux, but preliminary measurements in the tank show that no peak occurs. No evidence of D_2O radiolysis has been detected.

Hallam Operation in Retrospect

By Fred A. Smith

The future operation of the Hallam Nuclear Power Facility has been under serious consideration since the reactor was shut down in September 1964, after failure of seven moderator elements,[13,14] and August 1965, when the U. S. Atomic Energy Commission announced termination of its operating contract with the Consumers Public Power District of Nebraska. Nevertheless, the operating experience gained in starting up and operating the 250-Mw(t) sodium-cooled graphite-moderated reactor is well worth reviewing because of its applicability to other reactors, particularly those cooled by sodium.[15–22]

On the basis of a review of the information on Hallam testing, startup, operation, problems encountered, corrective steps, and recommendations for improving plant performance and reliability, I have summarized highlights and

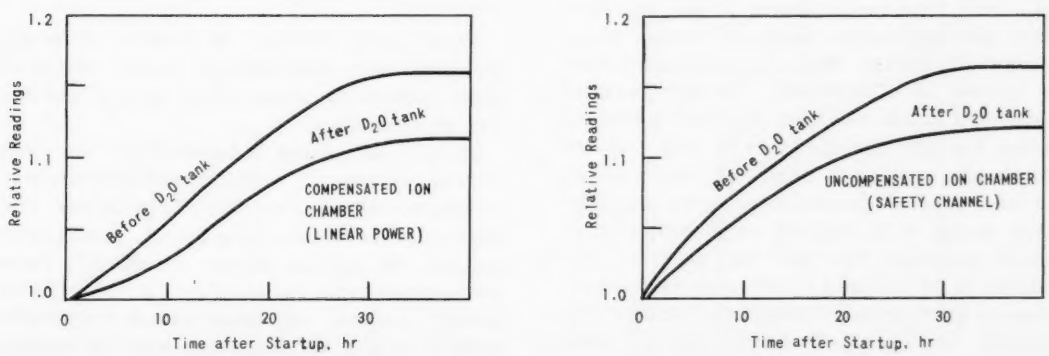

Fig. VIII-8 Effect of D_2O reflector on reactor ionization-chamber readings (average data from 10 runs before and after tank installation).[12]

have attempted to evaluate the significance of this experience. For convenience, I have considered the experience in three categories: normal operation, difficult component problems, and unresolved problems.

Summary

In general, the 80-Mw(e) plant performed well until the moderator elements failed.[14,23–25] Figure VIII-9 summarizes the plant operating history. The measured core-physics parameters agreed well with predictions. Although the sodium-heated steam generators operated safely, they were not in service long enough to appraise realistically their operating and maintenance costs. The numerous difficulties encountered in operating with sodium components, and some caused by sodium chemistry, emphasize the need for progress in these technologies.

Normal Operating Experience

As with the startup and early operation of most power plants, many Hallam activities and components gave no trouble, and others caused minor difficulties that required modifications involving only modest cost and time to make.

Plant Preoperational Tests. These tests, which involved 57 systems or functions,[20] began after "beneficial occupancy" of the facility in August 1961. Dry criticality was achieved in January 1962. Then seven months of system checkout were required before wet criticality was attained on Aug. 25, 1962. Rise-to-power tests followed; electricity was generated May 29, 1963, and full power was reached in July 1963. Thus the total time to take this plant from postconstruction occupancy to full power spanned 23 months. This accomplishment must be classed as a successful, normal operating experience much like that which should be expected for any nuclear plant of this size and complexity. Although some of the systems tested contained components whose operation later proved to be difficult or presented unresolved problems, the plant test program represents a successful joint venture between Atomics International, Consumers Public Power District, and the U. S. Atomic Energy Commission.

Initial Sodium Fill. The primary and secondary systems were initially filled with 741,500 lb of sodium in a problem-free operation similar to the large-scale transfers of sodium at Fermi and Experimental Breeder Reactor No. 2 (EBR-II). An electrically heated oil-circulation system liquified the sodium, which was pumped electromagnetically from railroad tank cars. Plant cold traps reduced the oxide content of the sodium enough that the sodium plugging temperature was brought below 250°F after only approximately 24-hr operation in the secondary system and approximately 36 hr in the primary system.

Nuclear Tests. In general, calculated and measured nuclear reactivity values agreed excellently. In criticality tests[26,27] sodium worth at 350°F in a 53-element core was measured as $-6.1\%\ \Delta k/k$; the value calculated was $-5.5\%\ \Delta k/k$. For the 140-element cold, clean core, k_{eff} was measured as 1.109 ($9.8\%\ \Delta k/k$); the predicted value was 1.069 ($6.5\%\ \Delta k/k$). Measurements of zero-power temperature coefficients of reactivity[28] showed the isothermal coefficient of reactivity to be +0.123 cent/°F at 400°F and +0.088 cent/°F at 500°F. With 20% sodium flow in the primary system, the "prompt" power coefficient is −0.4 cent/Mw(t) and is −0.05 cent/Mw(t) at 240 Mw(t) with 96% sodium flow.

The peak of ^{135}Xe buildup[29] occurs approximately 4.5 hr after a scram from full power and is worth −263 cents of reactivity. Samarium-149 has a peak buildup of 160 full-power days and an equilibrium worth of −122 cents.

For power operation, investigations of control-rod patterns[30] indicate that the axial power distribution has a range of peak-to-average ratios of 1.40 to 2.62.

Plant Control System. A number of minor problems were experienced. These related to faulty components, fabrication errors, and design shortcomings.

Of 13 interrelated subsystems of the plant control system, 7 demonstrated satisfactory operation without any corrective action. The satisfactory systems were the (1) plant power control, (2) nuclear power control, (3) fuel-temperature and coolant-flow ("convection power") control, (4) outlet steam ("attemperator") control, (5) steam-generator pressure-relief control, (6) primary block-valve control, and (7) secondary-flow control. Minor modifications were required to the division-of-load

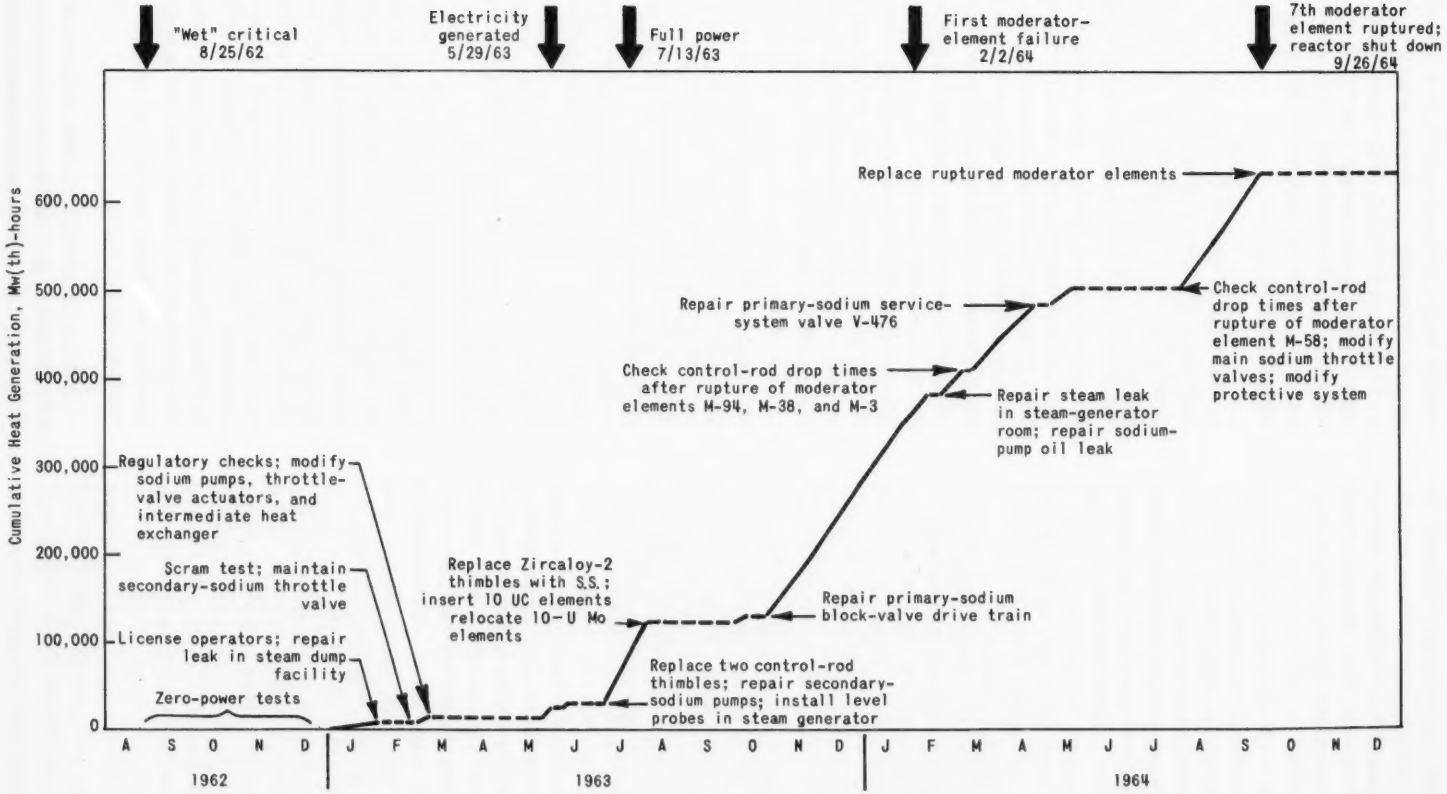
"Wet" critical 8/25/62
Electricity generated 5/29/63
Full power 7/13/63
First moderator-element failure 2/2/64
7th moderator element ruptured; reactor shut down 9/26/64
Cumulative Heat Generation, Mw(th)-hours
600,000
500,000
400,000
300,000
200,000
100,000
0
Replace ruptured moderator elements
Repair primary-sodium service-system valve V-476
Check control-rod drop times after rupture of moderator element M-58; modify main sodium throttle valves; modify protective system
Check control-rod drop times after rupture of moderator elements M-94, M-38, and M-3
Repair steam leak in steam-generator room; repair sodium-pump oil leak
Regulatory checks; modify sodium pumps, throttle-valve actuators, and intermediate heat exchanger
Scram test; maintain secondary-sodium throttle valve
License operators; repair leak in steam dump facility
Zero-power tests
Replace Zircaloy-2 thimbles with S.S.; insert 10 UC elements relocate 10-U Mo elements
Repair primary-sodium block-valve drive train
Replace two control-rod thimbles; repair secondary-sodium pumps; install level probes in steam generator
A S O N D J F M A M J J A S O N D J F M A M J J A S O N D
1962
1963
1964

Fig. VIII-9 Summary of Hallam reactor operating performance shows cumulative thermal power generated vs. time and reasons for various outages. Before the last shutdown, moderator-element failures during 1964 seriously affected operations; a 1668-hr outage followed failure of moderator element M-58. Two other 1964 outages lasted 230 and 253 hr; 12 others lasted less than 100 hr each.[59]

computer, moderator–coolant control, and steam-dump control systems. Although the primary-sodium flow control system has operated satisfactorily, the need for the existing recorder–controllers for this system should be evaluated more completely for actual plant load-following conditions.

The neutron-flux control system encountered difficulties because of below-average reliability of components. However, after more reliable plug-in components were installed, the neutron-flux control system operated uninterruptedly longer and was easier to maintain. Feedwater-level control posed a difficult problem; because level control was limited by the lack of vertical head in the horizontal steam generator, it was really a problem of steam-generator design rather than of instrument control.

In general, the overall control system has responded excellently to intentional transients.[31] On one occasion the operator manually overrode the instruments, which resulted in a reactor scram. Subsequent investigation revealed that the automatic control-rod response had been legitimate.

On another occasion, when both the conventional and nuclear plants were operating simultaneously and the conventional boiler suddenly dropped off the line, nuclear response was immediate. As designed, the reactor picked up the full turbine load faster than approximately 20%/min.

Control-Rod Operation. The control-rod design speeds were verified by preoperational tests in air.[32] No change in drive speed and no malfunctions were found when the control rods were tested again during the plant rise to power.[33] There were small differences in design-vs.-actual rod drop times for the 9-ft free fall and full drop-to-snubber closure, but they were well within specifications.

Faulty magnets, shorted coils, and improper limit switches caused spurious scrams of the control rods. After the causes of these problems were corrected, the control rods worked perfectly. Although the difficulties with the rod drives involved normal installation adjustments, the original control-rod-drive thimbles, which were to keep the control rods in a dry helium atmosphere, failed; they are discussed further under the subsection Unresolved Problems.

Reactor Heat-Transfer Systems. Overall performance of the heat-transfer system has been equal to or better than design. Total heat losses were independent of load and remained at approximately 1.5 Mw(t), which is less than a 1% loss at full load. High-temperature, high-flow, and low-pressure operation has been effected satisfactorily for prolonged periods. Reactor operation as a load-following plant has been very successful.

Sodium Mechanical Pumps. Both during preoperational testing and after plant power operations, the six vertically mounted overhung mechanical type pumps had to be removed for maintenance.[19] Subsequently, these centrifugal and free-surface pumps (the primary and secondary systems each have three) were modified to: (1) loosen the diametral running clearances of the impeller upper and lower wear rings, (2) make more uniform the temperature distribution of the exterior casings of the pumps so as to prevent impeller binding, (3) provide greater area for sodium flow from the bearings to the pump suction, and (4) install sintered metallic filters to prevent foreign material (beads from the welding rods that had been used in fabricating the steam generators) from entering the secondary-system pumps. Since the corrections, overall performance of the pumps has been satisfactory. Fortunately, like the EBR-II and Fermi mechanical pumps, the Hallam pumps were designed so that that the impeller and shaft can be removed relatively easily from the volute casing, making field maintenance possible.[19] It is easier to remove, maintain, and replace a sodium pump than a deep-well pump, a boiler feedwater pump, or a similar major pump.[34]

Leakage Through Sodium Valve Seats. For plant safety the sodium in the reactor drain and fill lines must be kept molten by heating the lines. However, seepage of radioactive sodium across the drain-line valves limited personnel access to the sodium service cell (where the cold and hot traps are located) during reactor operation. To avoid the problem, a bypass line has been installed in the primary-sodium service system to connect each main coolant loop to the drain tanks without passing through the sodium service cells.

Bellows-Seal Valves. The bellows in about 11% of the 2-in. (or less) sodium valves in the cold-trap and drain circuits have failed. Most of the leaks occurred on valves that were

partially open for throttling service—none of the bellows valves that normally are either fully open or closed failed. The bellows-seal valves that have not leaked were operated subsequently as stop valves. The failed valves have been replaced with freeze-seal valves or fixed orifices, both of which are recommended for future installations. It also has been recommended[35] that the number of throttle valves should be minimized in future sodium plants and that any bellows-seal valves be tested thoroughly at various openings and with sodium turbulence to be certain that any bellows will not oscillate.

Plugging Meters. These units, which indicate the oxide concentration in sodium, have operated well in each of the primary and secondary systems. However, to eliminate poor flushing of the plugged area when the oxide saturation temperature approaches the bulk sodium temperature, a minor modification would be desirable—a heater should be added to raise the temperature of the sodium flowing through the meter above the bulk sodium temperature.[36]

Handling of Core Components. These handling operations have involved the movement of fuel elements and control-rod thimbles and, more recently, the removal of moderator elements. Facilities for cleaning and inspecting core components have operated as designed.[37,38] The fuel-handling machine and its gantry and trolley assembly were tested with a core mockup vessel before delivery to the site.[39] Thus the system has operated well with only minor changes required since installation. This success indicates the desirability of pretesting full-size components. Hallam experience with handling damaged core components points up the desirability of handling-equipment designers giving thought to being able to dislodge and remove damaged core components expeditiously.

Difficult Component Problems

The operation of some components and systems revealed considerable or sustained difficulties that involved substantial cost and time to correct.

Nuclear Instruments. Electrical noise interference, high instrument temperatures, and difficulty in achieving rapid response have been problems. Power-range instruments required only minor modifications. But the intermediate-range log-N instruments encountered difficulties caused by poor design and poor quality control. Because the average signal-to-noise ratio was only 5 : 1, the startup-range channels initially provided readings with fluctuations of far greater magnitude than normally associated with nuclear statistics.

These instrument problems were greater than should be expected. An evaluation[40] report recommends more stringent performance specifications for future plants to eliminate extensive testing, repair, and modification of nuclear instrumentation.

Plant Protective Instruments. The main functions of this system,[41] which is separate from the plant regular control systems, are to prevent inadvertent hazardous operation and to detect off-normal conditions and then act automatically to prevent damage to the reactor system or heat-transfer-system components.

Tests and use of the plant protective system[42] led to numerous improvements that eliminated (1) noise caused by poorly regulated a-c power, (2) noise caused by the grounding pattern, (3) drift related to insufficient cooling, (4) short lifetime of mechanical "choppers" in the amplifier, and (5) interaction between protective-system components. With these modifications the system proved to offer adequate protection against potentially hazardous conditions. For future designs of such systems, it has been recommended that electric power be regulated at the point of end use rather than at the source with a common regulator.[43] Future designs also should be studied closely for clear definitions of the purpose and function of protective-system components.

Control-Rod Thimbles. The control-rod thimbles were intended to isolate the rods from the reactor sodium by containing them in a pressurized helium atmosphere.[41] The reason for the selection of a dry control-rod system was the state of development of mechanisms in sodium at the time the design was fixed. However, the Zircaloy-2 walls of 3 of the 19 thimbles cracked early in the prestartup tests of the primary sodium system. Study indicated[44] that a possible cause of the failure was hydrogen embrittlement due to the diffusion into the Zircaloy-2 of hydrogen from the titanium hydride used as a shielding material in the control-rod-drive housing. (For more informa-

tion on hydrogen embrittlement of Zircaloy, see page 245.) It is interesting to note that earlier engineering proof tests of the control-rod-drive mechanism and thimbles in sodium were conducted without the titanium hydride shielding installed. The problem was solved when all 19 Zircaloy-2 thimbles in the reactor were replaced with thimbles of type 304 stainless steel.

Throttle Valves. The Hallam primary-system throttle valves are freeze-seal ball valves actuated by a double jackscrew driven by an air motor.[45] Difficulties were encountered with the valve actuator, shafts, torque limiter, and jackscrews. Although the various modifications eventually resulted in satisfactory operation, the problems were bothersome and both they and the corrective measures involved an extended period of time.

Intermediate Heat Exchangers. Vibration caused a tube to fail in one of the three intermediate heat exchangers—which convey heat from the radioactive primary-system sodium to the nonradioactive sodium in the secondary system—in November 1962, which was before the reactor was used to produce power. Analysis indicated that failure was caused by flow-induced vibration in the shell (secondary) side near the sodium inlet baffles.[46] The natural frequency of vibration was changed when shims were installed between tube rows in the 12 to 15 ft/sec sodium inlet area. Subsequent tests and operations indicate that the vibration ceased. Nevertheless this internal modification was difficult to make.

More favorable was the fact that the heat transferred by the intermediate exchangers was within 12% of the value predicted,[26] and it did not vary significantly over the plant history. Pressure drops were greater than predicted—6 vs. 1.2 psi on the primary side and 14 vs. 6.8 psi on the secondary side. These greater than predicted drops are of little concern because the pump head is sufficient to achieve the flows required.

Steam Generators. These units, of which there are three, are described in Refs. 19, 20, 41, 47, and 48. When plant auxiliary steam was used to preheat the steam generators to 300°F before they were filled initially with sodium, the steam did not distribute the heat evenly over the entire steam generator. This relatively minor problem was corrected by maintaining a partial vacuum on the steam generator while admitting the preheat steam; this procedure distributed the heat so that temperatures were within ±25°F.

A more difficult problem arose during the tests for the initial rise to power. The three steam generators had 0.60 to 0.70% liquid water in the steam leaving the separator, which exceeded the maximum acceptable moisture carry-over of 0.25%. After numerous tests,[49,50] it was found that the water level was dropping enough that some of the horizontal sodium-heated tubes did not have water over them. Water level was varying as much as 5 in. at full power. Thus carry-over was limited by the installation of more precise control equipment to hold the water level in the evaporator section within ±0.7 in. at full power. With these conditions the steam separators have little capacity above their steam rated capacities of 251,000 lb/hr.

Although it is significant that the overall heat-transfer coefficients for steam generation have remained essentially constant (which means no fouling has occurred) and that the steam generators have not leaked sodium to air or to water (which testifies to the safety of the design bases and the fabrication quality control), the need for the numerous tests and modifications to solve the moisture carry-over problem makes it necessary to consider the experience with Hallam steam generators as having been difficult.

Gas Entrainment in Sodium Expansion Tank. Originally, all sodium in the three secondary-system parallel loops flowed through an expansion tank in each loop. During preoperational tests, it was discovered that helium cover gas in the expansion tanks became entrained by the sodium and circulated through the system. Although this problem was eliminated by modifications that caused 96% of the sodium flow to bypass the expansion tanks,[51] this type of design deficiency cannot be considered normal; the modifications required approximately three months to complete. One of these expansion tanks cracked during later operation; because this problem has not been rectified, it is discussed in the next subsection.

Unresolved Problems

Operating experience uncovered some problems that either have no positive means of

correction or whose resulting difficulties have not yet been corrected.

Crack in Sodium Expansion Tank. The shell of one of the three expansion tanks in the secondary systems cracked near a nozzle.[52] The crack was caused by weld-rod coating entrapment at an internal baffle plate (the lesson learned from this is that internal welds require specifications similar to external sodium-containment welds). Analysis of the nature of this sodium-leakage failure indicates the desirability of replacing all three tanks if the plant is to resume operation.[53] Such a change would be a relatively minor task.

Cold Traps for Oxide. Although the initial efficiency of the cold traps, estimated as nearly 100%, shows their ability to keep the oxide content of the sodium low, the operator must either periodically replace the 10 to 12 plugged cold traps or install larger traps. The original traps plugged relatively rapidly because of the oxide that formed in the sodium during the repairs and modifications to the secondary system and the intermediate heat exchanger.

Because of mechanical interference, maintenance men must enter the cell to remove the primary-system cold traps.[54] This is no problem now, but, if a fuel cladding fails and leaks fission products into the sodium, remote methods might have to be devised to replace the traps.

Hot Traps for Carbon. To monitor the carbon content of the primary-system sodium, operators placed type 304 stainless-steel tabs at the sodium inlet of a carbon trap. After being held at 1200°F in the 30 to 40 gal/min sodium flow for 100 hr, the tabs were removed and analyzed chemically and metallurgically. These tabs showed no evidence of carburization.[55] In contrast, when fresh type 304 stainless-steel tabs were exposed statically at 1200°F for 100 hr to a sodium sample withdrawn from the carbon trap, the tabs invariably carburized to a range of 4 to 147 ppm. Obviously, the problem of understanding and measuring the chemical effects of various forms of carbon in sodium is still unsolved.

Freeze Traps for Sodium Vapor. Condensation or freeze traps are installed at high points in the reactor auxiliary sodium systems to remove sodium vapor from the cover gas that is vented or purged when the sodium system is being drained or filled.[56] Each of these traps contains a sodium-level float valve that controls the leakage of cover gas to the vent; the valve opens the gas path to the vent when the rising sodium level raises the float, which engages a cam that operates a shaft running through a sodium "freeze seal." However, the shaft packing that contains and backs up the freeze seal has leaked helium and permitted some liquid sodium to leak through the shaft annulus into the vent, which plugged it. Also, because of the variable resistance of the freeze seal, excessive manual pressure has been applied to this shaft, which broke on several occasions.

Although these problems have not been so severe as to warrant redesign of the Hallam system, a better system for venting and filling inert gas is needed for future sodium plants. (For more information on inert-gas systems and vapor traps, see page 259.)

Fuel-Channel Orifices. Adjusting the coolant flow by means of variable orifices in each fuel channel in the core allowed the operators to hold coolant exit temperature from each channel to within 15°F of the average.[41,57] Flow through the orifice could be adjusted 30 to 100% by moving the orifice plug its full 4-in. stroke; at 100% flow, 4-in. travel changes sodium temperature at the channel exit 90 to 150°F. However, the inability to move some of the plugs, due primarily to sodium oxide, has limited the use of these devices. Twelve orifices became either fully closed (but there is also a bypass), stuck, or broken. In other cases, when the drive cable would remain in tension after turning was difficult, the orifice plug would "creep" so that further adjustment would be necessary.

Although these fuel-channel variable orifices could be improved by replacing the flexible shaft with a rod or by installing a bellows, it was not practical to make changes on the initial core.

Moderator-Element Failure. Leakage of the type 304 stainless-steel cladding on the graphite moderator elements[41,58] was a significant event of major proportion in that it necessitated shutting down the plant for core repairs. By the end of September 1964, the cladding on seven moderator elements had failed and had flooded

the elements with sodium; Fig. VIII-10 shows the core locations of the failed and suspect moderator elements.[34] This flooding reduced core reactivity, tilted the flux, and depressed the power, by which means the failures were detected and the suspect failed elements were identified[59] (see Table VIII-1); these tests indicated that 8 and possibly 9 moderator elements had failed, but subsequent examination with boroscopes and electromagnetic probes showed that only 7 elements had failed. However, this leakage also permitted the sodium to react with the graphite, which swelled the elements and caused 19 fuel elements to become stuck in place (none of the thimble-enclosed control rods stuck.)

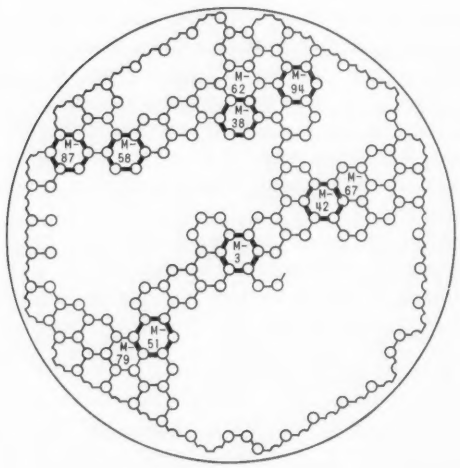

Fig. VIII-10 Locations in the core of the failed and suspect moderator elements.[34] The seven cans that actually failed are shown with heavy borders. Element M-87 was not suspected initially. On the basis of flux patterns, M-62 and M-67 were suspected, and M-79 was regarded as a possible failure, but examination showed that all three were intact.

Subsequent core-repair work removed the 19 stuck fuel elements; the 7 failed moderator elements, together with 3 others that suffered damage in the handling operations, were replaced with 10 new moderator elements by July 12, 1965.

A review of the moderator-element design, material specifications, and inspection and fabrication methods that was made before the failed elements were removed uncovered no obvious reasons for the failures, although it cast suspicion on rewelds that were made on initially defective welds.[60] Although the final report on the detailed examination and analysis of the cans was not available as of this writing, Fig. VIII-11 shows a typical crack,[61] which occurred approximately 3 in. from the top of the element in core position M-42. Six element cans cracked in similar locations; metallographic study of the type 304 stainless steel near the cracks revealed little or no

Table VIII-1 REACTIVITY REDUCTIONS WHEN MODERATOR-ELEMENT CANS CRACKED AND SODIUM ENTERED ELEMENTS[34]

Moderator-element location	Date ruptured	Date of additional disturbance	Reactivity reduction, cents: Actually observed	Corrected for rod-calibration error	Predicted worth*
M-94	2/2/64		3	4	4
M-38 and M-62	2/2/64 and 2/20/64–2/22/64		9 } 25	10.5 } 29	20 (M-38) 11 (M-62) } 31
		3/6/64–3/12/64	9	10.5	
		3/29/64–4/5/64	7	8	
M-3	3/4/64		18	21	21
M-58	5/15/64		16	19	18
M-51	9/9/64		23	23	20
M-42 and M-67	9/26/64		25 } 43	25 } 43	23 (M-42) 20 (M-67) } 43
		9/27/64–9/30/64	18	18	
Total			128	139	137

*Predicted worth is determined by flux weighting to corrected–observed worth of M-3 as base.

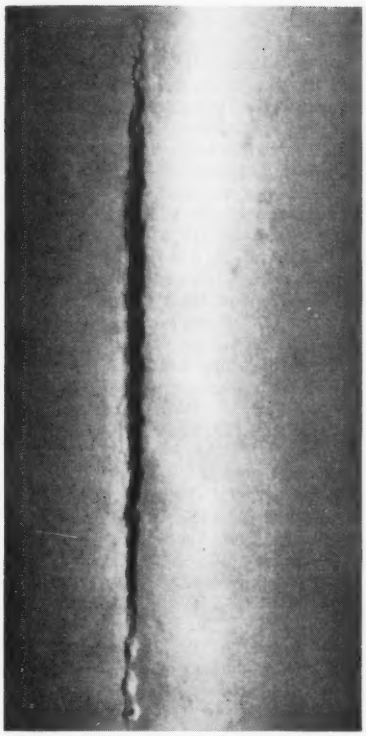

Fig. VIII-11 Crack that occurred near the top of the can on moderator element in core position M-42 is typical of the cracks in six of the seven failed cans.[34]

thinning or grain distortion[62] but found intergranular separation of the type that occurs from long-term stress in the range of creep deformation (below the yield stress). In this area near the top of the cans, which contain a vacuum, the thin type 304 stainless steel is not supported by the graphite. Although a series of "fingers" is intended to support the cladding wall, in six of the failed cans some of the fingers did not give support.[63] (The seventh element failed rapidly when the swelling of the other elements damaged a process tube, which gouged the seventh can.)

The plant designers believe the problem can be solved by eliminating the vacuum in the 141 moderator cans.[63] This could be done within about six months by installing on each moderator element an 11-ft snorkel tube that would vent it to the inert cover gas above the sodium surface in the reactor vessel.

From studies made of the design of the failed moderator elements,[64] it is now clear that the Hallam design does not represent an engineering extrapolation of the moderator elements used in the Sodium Reactor Experiment.[65] Future liquid-metal-cooled reactor designs must be considered carefully to determine precisely which features are truly represented by previous experience and to identify design features that involve advancements in the state of the art and therefore constitute a performance risk.

References

1. J. A. Prestele, Operating Experience at Indian Point, *Trans. Am. Nucl. Soc.*, 8(Suppl.): 30-31 (1965).
2. Robert Campbell and Joseph A. Signorelli, Elk River Reactor Operations, *Trans. Am. Nucl. Soc.*, 8(Suppl.): 31 (1965).
3. Glen A. Reed, Major Operating and Refueling Problems at the Yankee Atomic Electric Company Rowe Power Plant, *Trans. Am. Nucl. Soc.*, 8(Suppl.): 28 (1965).
4. R. E. Heffner, Failure of SPERT III Pressurizer Vessel, *Trans. Am. Nucl. Soc.*, 5(1): (1962); also USAEC Report IDO-16743, Phillips Petroleum Company, January 1962.
5. R. E. Heffner, Six-Years Operating Experience with PWR Plant Components, *Trans. Am. Nucl. Soc.*, 8(Suppl.): 29-30 (1965).
6. J. I. Riesland and E. A. Gustafson, Work Performed on Fuel Channels and the Core Support Plate at Big Rock Point Nuclear Power Plant, *Trans. Am. Nucl. Soc.*, 8(Suppl.): 5-9 (1965).
7. L. M. Hausler, R. L. Haueter, and R. C. Christianson, In-Vessel Modification of Irradiated Reactor Internals at Big Rock Point, *Trans. Am. Nucl. Soc.*, 8(Suppl.): 3-5 (1965).
8. C. Arthur Dalke, Elimination of Hydraulically Induced Core Vibrations in the General Electric Test Reactor, *Trans. Am. Nucl. Soc.*, 8(Suppl.): 2 (1965).
9. Nils Rydell, Some Aspects of Operating Experience at Ågesta Nuclear Power Plant, *Trans. Am. Nucl. Soc.*, 8(Suppl.): 31-32 (1965).
10. R. V. Dulin, Control of Oxygen in PRTR Helium Systems, *Trans. Am. Nucl. Soc.*, 8(Suppl.): 46-47 (1965).
11. Arthur de Saint Maurice and Richard Canfield, Thermal-Column Pneumatic Facility, *Trans. Am. Nucl. Soc.*, 8(Suppl.): 1 (1965).
12. Robert D. Martin, Operating Experience with a Heavy-Water-Reflector Tank, *Trans. Am. Nucl. Soc.*, 8(Suppl.): 46 (1965).
13. Consumers Public Power District, HNPF Monthly Operating Report No. 36, p. 1, July 1965.
14. R. H. Davidson, Moderator Element Failures in the HNPF, *Trans. Am. Nucl. Soc.*, 8(Suppl.): 35 (1965).
15. Consumers Public Power District, HNPF Monthly Operating Reports, A Series, Nos. 1–37.
16. Atomics International–AEC Chicago Operations Office, HNPF Reactor Operating Analysis Reports, USAEC Reports, A Series, Nos. 1–28.
17. R. C. Gerber, Hallam Nuclear Power Facility, in Symposium Proceedings on Sodium Reactors

Technology, Lincoln, Nebraska, May 24–25, 1961, USAEC Report TID-7623, pp. 73-88.
18. W. P. Venable, Integration of Hallam Nuclear Power Facility into Consumers Public Power District of Nebraska System, in Symposium Proceedings on Sodium Reactors Technology, Lincoln, Nebraska, May 24–25, 1961, USAEC Report TID-7623, pp. 89-96.
19. H. O. Monson et al., Components for Sodium Reactors, presented at the Third United Nations International Conference on the Peaceful Uses of Atomic Energy, Geneva, 1964, Paper A/Conf.28/P/228.
20. Atomics International, Final Evaluation Report, Hallam Nuclear Power Facility, USAEC Report NAA-SR-9777(Vols. I–VI), 1964.
21. L. E. Keller and R. H. Davidson, Hallam Operating Experience, *Nucl. Safety*, 7(2): 236-242 (Winter 1965–1966).
22. K. K. Brown, Operating Hallam, *Nucleonics*, 22(9): 41-46 (September 1964).
23. J. D. Cochran, Operating Experience at Hallam Nuclear Power Facility, in *American Power Conference, Chicago, Illinois, March 26–28, 1963*, Vol. XXV, pp. 204-212.
24. J. D. Cochran and J. E. Owens, Initial Operation of the Sodium Graphite Reactor at the HNPF, in *26th Annual American Power Conference, Chicago, Illinois, April 14–16, 1964*, Vol. XXVI, p. 201.
25. Emerson Jones and J. D. Cochran, HNPF Operating Experience and Testing to 250 Mw(t) to November 1, 1963, USAEC Report TID-20396, November 1963.
26. J. E. Price (Comp. and Ed.), Final Evaluation Report, Hallam Nuclear Power Facility, USAEC Report NAA-SR-9777(Vol. I), p. 34, Atomics International, Sept. 29, 1964.
27. J. E. Price and J. W. Rocke (Eds.), Final Evaluation Report, Hallam Nuclear Power Facility, Wet Excess Fuel Loading, AI-PC-710, USAEC Report NAA-SR-9777(Vol. VI), Atomics International, June 12, 1964.
28. *Ibid.*, Zero Power Coefficients of Reactivity, AI-PC-760.
29. *Ibid.*, Xenon Poisoning, AI-PC-840.
30. *Ibid.*, Power Coefficient, AI-PC-770.
31. P. F. Shaw, HNPF Control System Response During Transient Conditions, USAEC Report NAA-SR-9584, Atomics International, June 15, 1964.
32. J. E. Price and J. W. Rocke (Eds.), Final Evaluation Report, Hallam Nuclear Power Facility, Control Rod Drive and Actuator Assemblies, AI-P-1145, USAEC Report NAA-SR-9777(Vol. III), Atomics International, June 12, 1964.
33. J. E. Price and J. W. Rocke (Eds.), Hallam Nuclear Power Facility, Master Schedule Including Rise-to-Power, AI-PC-830, USAEC Report NAA-SR-9777(Vol. VI), Atomics International, June 12, 1964.
34. Ivan O. Sunderman, Consumers Public Power District, personal communication, Sept. 17, 1965.
35. J. E. Price (Comp. and Ed.), Final Evaluation Report, Hallam Nuclear Power Facility, USAEC Report NAA-SR-9777(Vol. I), p. 17, Atomics International, Sept. 29, 1964.
36. *Ibid.*, Sodium Service System, AI-P-1104.
37. J. E. Price and J. W. Rocke (Eds.), Final Evaluation Report, Hallam Nuclear Power Facility, Wash Cells, AI-P-1133, USAEC Report NAA-SR-9777(Vol. III), June 12, 1964.
38. *Ibid.*, Maintenance Cell., AI-P-1139.
39. W. A. Kaspic, Experimental Testing of Core Component Handling Equipment and Handling Techniques for Hallam Nuclear Power Facility, USAEC Report NAA-SR-7785, Atomics International, Sept. 15, 1964.
40. J. E. Price (Comp. and Ed.), Final Evaluation Report, Hallam Nuclear Power Facility, USAEC Report NAA-SR-9777(Vol. I), p. 69, Atomics International, Sept. 29, 1964.
41. Atomics International, Final Summary Safeguards Report for the Hallam Nuclear Power Facility, USAEC Report NAA-SR-5700, pp. 257-269, Apr. 15, 1961.
42. J. E. Price (Comp. and Ed.), Final Evaluation Report, Hallam Nuclear Power Facility, USAEC Report NAA-SR-9777(Vol. I), p. 60, Atomics International, Sept. 29, 1964.
43. *Ibid.*, p. 63.
44. R. K. Wagner and S. L. Essglebert, Results of HNPF Control Rod Thimble Examinations, USAEC Report NAA-SR-TDR-9142, Atomics International, October 1963.
45. J. E. Price (Comp. and Ed.), Final Evaluation Report, Hallam Nuclear Power Facility, USAEC Report NAA-SR-9777(Vol. I), pp. 13-17, Atomics International, Sept. 29, 1964.
46. R. E. Durand, Operating Experience with Intermediate Heat Exchangers at HNPF, USAEC Report NAA-SR-9718, Atomics International, June 15, 1964.
47. Robert W. Dickinson and John B. Williams, Trends in Sodium Equipment, *Nucleonics*, 19(1): 65-70 (January 1961).
48. Frank Boni and Philip S. Otten, Fermi and Hallam Steam Generators, *Nucleonics*, 19(6): 58-61 (June 1961).
49. Consumers Public Power District, HNPF Operating Report for December 1963.
50. Atomics International, HNPF Reactor Operations Analysis Program, Semiannual Progress Report No. 2, March 1–August 31, 1963, USAEC Report NAA-SR-9265, pp. 105-111, Mar. 1, 1964.
51. J. E. Price (Comp. and Ed.), Final Evaluation Report, Hallam Nuclear Power Facility, Main Heat Transfer System, AI-P-1103, pp. 12-29, USAEC Report NAA-SR-9777(Vol. I), Atomics International, Sept. 29, 1964.
52. Consumers Public Power District, HNPF Monthly Operating Report No. 26, October 1964.
53. Consumers Public Power District, HNPF Monthly Operating Report No. 28, December 1964.
54. J. E. Price (Comp. and Ed.), Final Evaluation Report, Hallam Nuclear Power Facility, USAEC Report NAA-SR-9777(Vol. I), p. 52, Atomics International, Sept. 29, 1964.
55. Atomics International, HNPF Reactor Operations Analysis Program, Semiannual Progress Report No. 1, September 1, 1962, to February 28, 1963, USAEC Report NAA-SR-8401, July 1, 1963.
56. J. E. Price (Comp. and Ed.), Final Evaluation Report, Hallam Nuclear Power Facility, USAEC Report NAA-SR-9777(Vol. I), p. 54, Atomics International, Sept. 29, 1964.
57. J. E. Price and J. W. Rocke (Eds.), Final Evaluation Report, Hallam Nuclear Power Facility, Radial Power Distribution and Fuel Channel

Orifice Adjustment, AI-PC-800, USAEC Report NAA-SR-9777(Vol. VI), Atomics International, June 12, 1964.
58. *Power Reactor Technol.*, 5(3): 39-51 (June 1962).
59. Atomics International, HNPF Reactor Operations Analysis Program, Semiannual Progress Report No. 4, February 29–September 30, 1964, USAEC Report NAA-SR-10743, May 15, 1965.
60. *Ibid.*, pp. 61-69.
61. Consumers Public Power District, HNPF Monthly Operating Report No. 35, June 1965.
62. John J. Purcell, AEC Chicago Operations Office, Sodium Components Development Program, Project Coordination Report, Hallam Nuclear Power Facility, p. 12, August 1965.
63. *Nucl. Ind.*, 12(9): 11 (September 1965).
64. *Reactor Handbook*, 2nd ed., Vol. IV, Engineering, p. 677, edited by Stuart McLain and J. H. Martens, John Wiley & Sons, Inc., New York, 1964.
65. *Reactor Handbook*, 2nd ed., Vol. IV, Engineering, p. 665, edited by Stuart McLain and J. H. Martens, John Wiley & Sons, Inc., New York, 1964.

Section

IX

Power Reactor Technology

Systems Technology

Advancements in Organic Coolants

By J. E. Sawyers, Combustion Engineering, Inc.

The investigations in organic-coolant technology have involved seven general aspects: (1) decomposition by radiolysis and pyrolysis, (2) additives to improve resistance to decomposition, (3) reclamation methods for used coolant, (4) fouling-film formation, (5) corrosion properties, (6) heat-transfer properties, and (7) possible new coolant materials. Although biphenyl and other organics have been studied, the major work has concentrated on the terphenyls, especially Santowaxes OMP and R. Much of the work summarized here is discussed[1] in detail in a comprehensive analysis of the status of organic-coolant technology through mid-1964.

Decomposition

Experiments on pyrolysis of biphenyl, orthoterphenyl, and metaterphenyl included limited investigations of gamma radiolysis.[2]

The pyrolytic exposures involved various durations at 750 to 825°F in an autoclave controlled within 5°F. After pyrolysis products were analyzed and molecular-weight distributions were measured, rate constants and heats of reaction were calculated. Orthoterphenyl pyrolyzes about five times faster than biphenyl and metaterphenyl. The data indicate that pyrolysis is a first-order reaction. Rate constants for all three materials increase with temperature and fit reasonably well to an Arrhenius plot. Calculated heats of reaction are 93 kcal/mole for biphenyl, 89 kcal/mole for orthoterphenyl, and 83 kcal/mole for metaterphenyl.

Probable mechanisms are discussed on the basis of reaction-product analyses. Calculations of entropies of activation (at 800°F) suggest formation of a high-entropy complex that subsequently reacts or decomposes to give the products observed.

The radiolysis experiments were conducted by surrounding the autoclave with spent reactor fuel elements. Low-temperature (below 500°F) experiments, where pyrolysis is not significant, indicate that radiolysis depends on temperature—but there were insufficient data to determine this effect quantitatively. In a 775°F radiolysis experiment, exposure to 2.5 Mr/hr for 840 hr (2.1×10^9 r total dose) decomposed approximately twice as much organic as did pyrolysis alone in a control sample. Analysis of the radiolytic decomposition products suggests that the reaction mechanisms change as temperature increases. Gases produced by gamma irradiation in the absence of air include acetylene, ethylene, propylene, and propane. The observations that radiolysis rate and reaction mechanisms depend on temperature agree with work summarized earlier.[3]

The dose-rate effect on the radiolysis of paraterphenyl was investigated by exposing samples at approximately 660°F to electrons from a Van de Graaff generator.[4] Values of $G_{polymer}$, defined as the number of molecules of paraterphenyl converted to less-volatile material per 100 ev absorbed, were 0.17 to 0.26; G_{gas} values, defined analogously for conversion to gaseous products, were 0.017 to 0.037. Dose rates between 0.24 and 10 watts/g did not affect either $G_{polymer}$ or G_{gas}.

Reactor irradiations of Santowax OMP at 600°F in a loop in the MIT reactor have been reported.[5] After initial buildup of high boilers, unirradiated organic was added to maintain

their content at approximately 33 wt.%. Total irradiation time was approximately seven months (equivalent energy dose to the coolant was not reported); specimens were taken throughout this time. Coolant viscosity, density, and average molecular weight remained essentially constant because of the coolant replacement. The Santowax OMP degraded to higher boiler at the rate of 0.15 molecule per 100 ev absorbed.

Seventeen organic compounds, including 12 condensed-ring polyaromatics, biphenyl, orthoterphenyl, metaterphenyl, and paraterphenyl, and bibenzyl, were studied in pyrolytic and radiolytic experiments.[6] The objectives were to determine their general decomposition behavior and parameters that correlate with it. All experiments were performed in vacuum and in the range 375 to 840°F. A ^{60}Co gamma facility and the Brookhaven Graphite Research Reactor (BGRR) were used for the irradiations. Gamma-irradiated samples were exposed to 7×10^8 rads over 7 days; reactor-irradiated samples were exposed to 2.1×10^9 rads over 19 days.

Gas production increases with temperature in gamma radiolysis and in pyrolysis (no provision was made for measuring gas from the BGRR samples). For many compounds, pyrolysis and gamma radiolysis produced markedly different concentrations of hydrogen and methane. In general, the most common gases produced were ethylene and propane, with less consistent or smaller amounts of ethane, acetylene, and about eight other gases.

The decomposition rate usually increases with temperature, and the amount of decomposition in the radiolytic experiment always exceeded that from the control samples, in which only pyrolysis occurred. Data for decomposition rate as a function of temperature reveal the same general relation for all compounds—there is a temperature "breakpoint," below which the increase in decomposition rate with temperature is not very substantial and above which the increase becomes very marked. For a given compound this apparent breakpoint occurs at about the same temperature during radiolysis as in pyrolysis, but it occurred at lower temperatures for the reactor-radiolyzed samples than for the gamma-radiolyzed samples. This difference is attributed to the threefold difference in irradiation times.

Experiments showed that, in general, aromatic carbon–carbon bonds are more stable against both radiolysis and pyrolysis than are aliphatic carbon–carbon bonds. The control pyrolysis experiments show that pyrolytic decomposition rate increases with time, that is, pyrolysis products form increasingly quickly as pyrolysis products build up. Thus the investigators concluded that the results of short-term pyrolysis studies cannot be extrapolated meaningfully to long exposures. On the basis of breakpoint observations, they recommend that the maximum operating temperature for these organic materials be in the neighborhood of 750°F to avoid extensive decomposition.

Several attempts were made to obtain a correlation between radiolytic stability and other compound parameters. Two of these parameters, singlet–triplet excitation energy and electron affinity, were reported to indicate some reasonable degree of correlation with radiolytic decomposition rate.

Six-Mev electrons have been used[7] to irradiate biphenyl, the three terphenyl isomers, and Santowax OMP at approximately 600°F to decompositions of approximately 40%. Five specific conclusions are reported: (1) second-order kinetics best describe the radiolysis reaction; (2) paraterphenyl is more stable than metaterphenyl, which is more stable than orthoterphenyl; (3) rate constants increase for successive steps in biphenyl radiolysis reactions; (4) concentration of molecular-weight multiples of the starting material (biphenyl or terphenyl) rises rapidly in the radiolysis-product fraction; and (5) there is a linear relation between total dose and molecular weight (up to $\sim 1.5 \times 10^{10}$ rads). Nuclear magnetic-resonance measurements were interpreted to suggest that part of the hydrogen generated during radiolysis might react with the polymeric products.

Additives

Irradiations with 6-Mev electrons were performed to determine the effects of selected additives on the radiolytic stability of terphenyl.[7] Total dose was 0.5 to 1.0×10^{10} rads at approximately 650°F. Additives that contribute substantial stability against electron radiolysis can be broadly described in three general groups: (1) elemental sulfur and compounds containing divalent or tetravalent sulfur; (2) fused-ring

compounds structurally related to anthracene, in which either none of the rings, the end rings only, or the center ring only is hydrogenated and in which 9 and 10 positions of the center ring are occupied by sulfur, nitrogen, and carbon (or, in a few cases, oxygen) atoms; and (3) hydrogenated or partially hydrogenated fused-ring compounds not necessarily related to anthracene. They reduce electron radiolysis by approximately 10 to 25% when added to terphenyls in concentrations of 3 mole % or less. Compounds of the second group depend only slightly on concentration, but those of the first and third groups depend greatly on concentration — elemental sulfur is most effective at 0.7 mole %. Effectiveness of none of the better additives appears to depend much on temperature.

Electron and reactor irradiations have been used to measure how various additives affect the decomposition of biphenyl, Santowax R, and paraterphenyl.[8] The addition of small (10 to 20%) portions of paraquaterphenyl to biphenyl slows the decrease in biphenyl degradation by electrons slightly (≤20%) but does not significantly affect the reactor-irradiation results. In reactor irradiation of paraterphenyl, gas and high-boiler formation was slowed 10 to 20% by the addition of approximately 0.5% of any of various additives, including ferrocene, phthalocyanine, iron, copper, and cobalt phthalocyanines.

Coolant Reclamation

Catalytic hydrocracking has been studied as a means to reclaim used organic coolant.[9–11] In catalyst-screening experiments, cobalt molybdate, nickel oxide, platinum, and cobalt oxide plus vanadia (all on low-surface alumina, 50 to 80 m^2/g) proved to be efficient catalysts for terphenyls at 600 to 900°F and 500 to 1000 psig. Catalytic efficiency increased with phenyl chain length; nickel oxide on alumina was the most selective to chain length. Further experiments were performed with the cobalt molybdate and nickel oxide using coolant from core 2 of the Organic Moderated Reactor Experiment (OMRE) and several other synthetic terphenyl mixtures. Continuous-flow hydrocracking of OMRE core 2 coolant (23% high boilers) at 900°F and 1000 psig removed 90 to 100% of the high boilers and recovered 85 to 95 wt.%. of the feed as usable product (some material was lost as light ends and some deposited on the catalyst). The average molecular weight of the product was 205 to 225, compared to 270 for uncracked core 2 coolant.

Radiolytic stability of the cracking products was investigated by use of a linear accelerator for irradiations of 0.48 to 1.3×10^{10} rads at 650°F. The selectively hydrocracked material was slightly more stable than Santowax OMP. Although the hydrocracked material released up to four times as much gas as did Santowax OMP, the gas amounted to only approximately 0.3 wt.% of the sample, and total radiolytic decomposition was significantly less for the hydrocracked material. Pyrolytic stability of the reclaimed coolant also was studied in 48-hr experiments. No thermal high boiler was measured up to 650°F; results are interpreted to suggest a "threshold" for pyrolysis at 750 to 825°F.

Cost estimates were performed for a 1000-Mw [300 Mw(e)] organic-moderated and -cooled reactor that produces high boilers at either 25,000 or 50,000 lb/day. On the basis of equipment amortization within seven years, total cost for manufacturing hydrocracked usable coolant would be $0.083/lb (later revised to $0.07/lb) for the 25,000 lb/day case and $0.053/lb for the 50,000 lb/day case, compared to fresh terphenyl coolant costing $0.17/lb. Advantages of the hydrocracking reclamation process would be (1) reductions in coolant-makeup and waste-disposal requirements and (2) removal of film-forming material that would foul the fuel elements; these improvements would reduce overall operating costs. A disadvantage would be the possible net buildup in the coolant of biphenyl, whose high vapor pressure might cause reactor operating difficulties.

Economics estimates have been performed for catalytic hydrocracking processes to reclaim damaged coolants from the 11.4-Mw(e) Piqua Nuclear Power Facility.[12] Three hydrocracker feed schemes were considered: feed supplied from the bottoms of a flash tank, from the bottoms of the presently installed distilling column, and directly from the main coolant stream. Selective hydrocracking of either concentrated high boilers or total coolant would be efficient and economical, but flash-tank feed is recommended as the most economical. The plant for the flash-tank-fed hydrocracker recommended for Piqua would cost $300,000. It could maintain high-boiler concentration in the coolant below 10% and ash concentration at 0.3

ppm. Without interest or taxes, payout time would be approximately 4.6 years, with a subsequent power-cost saving of 1.08 mills/kw-hr before taxes (0.52 mill/kw-hr after taxes), assuming full-power reactor operation 60% of the time.

Also studied briefly were the economics of a flash-tank-fed hydrocracker for a 500-Mw(e) organic-cooled D_2O-moderated reactor that operates at full power 60% of the time. If a hydrocracker is used instead of a distillation system to maintain coolant quality, the estimated saving is $205,400/year, and the payout time is 1.0 year if there are no taxes on the saving (or 1.9 years with taxes) and if the unit is amortized over 7.5 years.

The study also evaluated whether hydrogen could be recovered from radiolytic gases to reduce hydrocracker operating costs. Although technically feasible, such a process would be economically advantageous only with plants larger than Piqua.

Film Formation

Pyrolytic capsules were used for fouling tests performed to evaluate the film-forming tendencies of OMRE core 2 coolant.[13-14] These tests consisted essentially of maintaining coolant samples at 600°F for 24 hr under a nitrogen blanket while a stainless-steel tube held at 1050°F was immersed in the coolant, after which the amount of film deposited on the tube was measured. Results indicated that some coking did take place on the heaters and that ^{60}Co and ^{54}Mn concentrated on the heater surface to approximately 500 times their concentration in the coolant. Preliminary screening of adsorbents that might be useful in removing ^{35}S and ^{32}P from organic coolants indicated that metals and reduced oxides might be useful, and, in particular, a reduced nickel oxide hydrogenation catalyst showed good removal efficiencies for the concentrations used.

Engineering-scale equipment and static capsules were used for fouling studies and iron and water solubility studies.[6] In the static-capsule fouling tests, no fouling-film deposits nor detectable traces of alpha iron were found on the type 304 stainless-steel heater test specimens exposed to individual terphenyl isomers at 500 to 800°F. No correlation was apparent between the test conditions and the presence or absence of small amounts of alpha iron. Terphenyl generally absorbed or reacted with 1 vol.% oxygen placed in the cover gas. In the iron and water solubility studies, purified orthoterphenyl and paraterphenyl were covered with argon containing up to 6.5 vol.% water. No iron was found in the coolant. Water added to the coolant to a maximum concentration of 68 ppm did not noticeably affect iron solubility. Although water was slightly soluble in orthoterphenyl, no water was found in paraterphenyl.

Mechanisms of fouling-film formation were studied by testing Santowax OMP and coolant fluid from core 2 of the OMRE in pyrolytic capsules or in a circulating loop in which the organic was irradiated with 6-Mev electrons.[7] Also studied were the effects of temperature, flow, pressure, cover gas, and various preventive additives.

In regard to mechanisms, the study indicated that film formation on hot surfaces comes from (1) mass transfer of iron from the container and pipes and (2) deposition of a composite material that forms when high-molecular-weight polymers adhere to either soluble or insoluble iron in the coolant—and that "to a limited degree, certain higher molecular weight high boilers were more effective in fouling."

The pyrolytic capsule tests showed that film formation increases exponentially with surface temperature, but bulk temperature is also important and is greatly speeded by temperature "spikes" of less than 1-min duration.

In the electron-irradiation loop, film formation was (1) not affected greatly by blanket-gas pressures over the range 400 to 700 psig, (2) inversely proportional to coolant velocity, (3) enhanced by surface roughness or projections into the coolant stream, and (4) affected by the radiation intensity. When the blanket over the fluid was hydrogen, rather than nitrogen, the film was heavier and had greater thermal conductivity.

Corrosion Properties

Out-of-pile tests in a tilting-furnace apparatus were used to test the corrosion properties of type 304 stainless steel, A-285C mild steel, 1100 aluminum, Al-288, and SAP M-257 in 500 to 800°F paraterphenyl and 500 to 710°F orthoterphenyl.[6] On the basis of rather sketchy data, it was concluded that these materials are highly resistant to corrosive and mass-transfer attack by the terphenyls.

The combined effects of exposure to both an organic moderator–coolant and reactor radiation were measured on specimens of various materials that had been placed in the core of the OMRE for 26 months.[15] Specimens included SAE 1020 carbon steel, SAE 4130 low-alloy steel, types 410 and 304 stainless steels, aluminum, and magnesium. High-boiling-point impurities in the organic were allowed to rise to nearly 30%, at which level they were held during most of the last half of the exposure. The SAE 1020 and 4130 steels corroded at the rate of approximately 0.0001 in./year. Aluminum and types 410 and 304 stainless steels were quite resistant to corrosion. Magnesium was the only metal that corroded appreciably; these measurements seemed to confirm that magnesium, whether anodized or not, is unsuitable for organic-reactor service. It was concluded that measurements of corrosion rates in an out-of-pile laboratory can predict in-pile corrosion rates with sufficient accuracy for design purposes.

Corrosion of iron by terphenyl was investigated with a variety of organic mixtures and reagent-quality iron wire.[7] Clean terphenyl, either irradiated (by 6-Mev electrons) or unirradiated, does not corrode iron, but it becomes corrosive upon oxidation by air. Two commercial automotive motor-oil detergents were tested for preventive effects, but first indications were unfavorable.

Autoclave and loop tests have been used to determine the corrosion rates of structural materials exposed to commercially available terphenyls (Santowax mixtures); potential corrosion inhibitors also were evaluated.[16] Santowax R was used in agitated autoclave tests, and Santowax OMP was used in the loop tests. Corrosion rates usually decrease with exposure and depend on fluid velocity and temperature. Although the corrosion rates of the various alloys seem relatively insensitive to water additions, water did seem to promote a more adherent oxide scale in the autoclave tests.

Steel corrosion rates were insensitive to water content up to 2000 ppm, which contrasts to the OMRE experience in which particulate-formation rates depended directly on water or air contamination. Corrosion rates that can be expected for carbon or SAE 4130 steels as a function of organic bulk temperature are reported as 0.05 to 0.06 mg/(cm^2)(month) at 600°F, 0.10 mg/(cm^2)(month) at 650°F, and 0.20 to 0.25 mg/(cm^2)(month) at 750°F. Of the three steels tested, annealed, or sensitized, type 304 stainless steel is the most corrosion resistant (it shows negligible corrosion in both the autoclaves and the loop), and carbon steel is less resistant than ferritic type 410 stainless steel. Limited tests with type 406 stainless steel (13% chromium–4% aluminum) indicate a corrosion rate as low as that for type 304 stainless steel. One advantage of type 406 stainless steel is that it absorbs approximately 25% fewer thermal neutrons than type 304.

Aluminum and specimens made from sintered aluminum powder (called SAP or APM) were almost inert to terphenyls with normal water content. Type 1100 aluminum oxidized only when water content exceeded 1000 ppm. Although the tests indicated that magnesium and its alloys might be attractive as water-removal agents, they are unsuitable for use in organic reactors because they are readily corroded by organic coolants.

Protective coatings were evaluated in autoclave tests. None of a wide variety of coatings on zirconium alloys was able to prevent hydriding of the zirconium. Copper and brass corrodes faster than carbon steel, but beryllium appears to be quite inert. Although niobium apparently corrodes more than carbon steel, it might be an effective diffusion barrier between aluminum cladding and metallic-uranium fuel.

Contaminants. The results of these tests and other considerations show that, in general, the presence of water, hydrogen, air (oxygen), or sulfur in terphenyl enhances corrosion and film formation. Although the effects of minor air contamination were negligible in the laboratory experiments, experience at the OMRE indicates that air contamination of irradiated coolant tends to increase fouling. The fouling tendency of coolants can be reduced if (1) the water or oxygen content is minimized, (2) the access of air and water to the coolant system is strictly controlled, and (3) larger and more effective particulate-removal systems are used.

Sampling. For these experiments the workers developed a significantly improved technique for sampling Santowax to determine its water content. The difficulty had been caused by the ability of water to flash off from the Santowax at 750°F when the pressure was reduced. A

sampler that simulated a flow sample from the autoclave was developed to avoid this problem.

Heat-Transfer Properties

Forced-circulation heat transfer in organic systems has been studied extensively.[17] Boiling heat transfer with forced-circulation Santowax R and isopropyl diphenyl has been measured in an out-of-pile test loop having an electrically heated vertical test section;[18] Table IX-1 shows

Table IX-1 CONDITIONS IN BOILING HEAT-TRANSFER EXPERIMENTS[18]

Conditions	Isopropyl diphenyl	Santowax R
Heat flux, Btu/(hr)(sq ft)	40,000–100,000	27,000–110,000
Mass velocity, lb/(sec)(sq ft)	325–630	280–750
System pressure, psia	21–33	15–28
Flow direction	Up only	Up and down
Subcooling, °F	0–17	0–57

the range of variables investigated. Data for Santowax R heat transfer correlated best with Levy's equation;[19] Rohsenow[20] and Forster–Greif[21] equations were less successful. The correlation was insensitive to flow direction. Data for isopropyl diphenyl correlated within 10% using Levy's equation; the Rohsenow and Forster–Greif relations were not tried because of uncertainty concerning the surface tension of isopropyl diphenyl.

Void fraction was measured in the Santowax R experiments by an X-ray transmission technique. With greater than 8°F subcooling, these data were correlated using a modified form of Maurer's equation.[22] An expression was developed and used with moderate success to correlate void-fraction data near equilibrium bulk boiling. For equilibrium boiling the experimental results were consistent with predictions from a modified Martinelli model.[23]

Possible New Coolants

Attempts have been made to find an inexpensive organic coolant with properties similar to the terphenyls.[7,24] A large group of high-boiling distillates from the petroleum industry which were studied included recycled oils from some catalytic-cracking operations, highly aromatic fractions used as feed for producing carbon black in furnaces, and coal-tar distillates. Irradiation with 6-Mev electrons usually liberated more gas from these oils than from Santowax OMP. Radiation resistance of these oils ranged from somewhat lower to somewhat greater than Santowax OMP. In general, their thermal stabilities were unsatisfactory above 650°F.

When these petroleum-base stocks had been hydrodealkylated and the coal-tar stocks hydrodesulfurized, they had pyrolytic thresholds approximately 50°F less than terphenyl. Radiolysis of coolants prepared in this manner formed polymer only 50 to 75% as fast as did terphenyl but liberated gases several times faster than terphenyl. Viscosities, vapor pressures, densities, and hydrogen densities were very similar to terphenyl. The film-forming tendency of these materials has not been tested, but no coking was observed up to 750°F. Although estimates based on these data indicate that these coolants could be produced cheaply enough that inventory and makeup costs would be somewhat less than for terphenyl in a conventional steam plant where bulk temperatures do not exceed 700°F, these experiments did not include in-pile or neutron irradiations. Thus the results are only indicative.

Acknowledgments

The author gratefully acknowledges the assistance of reviewers at Atomics International for their help with, and further organization of, this article.

References

1. R. F. Makens (Ed.), Organic Coolant Summary Report, USAEC Report IDO-11401, Idaho Operations Office, December 1964.
2. D. G. Kuper, Organic Coolant Degradation Studies, USAEC Report IDO-16851, Phillips Petroleum Company, Mar. 25, 1963.
3. *Power Reactor Technol.*, 6(3): 71 (June 1963).
4. A. W. Boyd, The Radiation and Thermal Stability of Some Potential Organic Moderator-Coolants, Part VII. The Effect of Radiation Intensity on the Decomposition of Paraterphenyl by Fast Electrons, British Report AERE-R-4048, August 1963.
5. E. A. Mason and C. D. Sawyer, Irradiation Loop Studies of Organic Reactor Coolants, Progress Report, January 1–September 30, 1962, USAEC Report MITNE-29(IDO-11106), Massachusetts Institute of Technology, Feb. 15, 1963.
6. H. Susskind et al., Organic Reactor Coolant Studies, USAEC Report BNL-7650, Brookhaven National Laboratory, June 30, 1963.
7. J. C. Hillyer, Organic Coolant Research Summary

Report, July 1, 1960–March 31, 1963, USAEC Report IDO-16911, Phillips Petroleum Company, Oct. 1, 1963.
8. W. G. Burns, C. R. V. Reed, and J. A. Winter, The Radiation and Thermal Stability of Some Potential Organic Moderator-Coolants. Part VIII. Pile and Electron Irradiation of Various Polyphenyl Mixtures and Work with Additives, British Report AERE-R-4072, November 1963.
9. L. E. Gardner, Reclamation of Damaged Nuclear Reactor Coolant by Catalytic Hydrocracking, USAEC Report IDO-16853, Phillips Petroleum Company, Mar. 29, 1963.
10. L. E. Gardner, Evaluation of Catalysts for Selective Hydrocracking of Polyphenyls, USAEC Report IDO-16858, Phillips Petroleum Company, Apr. 25, 1963.
11. L. E. Gardner, Catalytic Hydrocracking of High Boiler in Nuclear Reactor Coolant, USAEC Report IDO-16877, Phillips Petroleum Company, May 20, 1963.
12. J. L. Griffith and G. J. Russell, Economics of Hydrocracking Damaged Coolant from Organic Reactors, USAEC Report IDO-11400, Idaho Operations Office, November 1963.
13. J. F. Black, M. E. Conn, and P. R. Geissler, First Semi-Annual Progress Report on Organic Coolant Technology During May Through October 1962, USAEC Report IDO-11221, Esso Research and Engineering Company, Dec. 14, 1962.
14. P. R. Benson, Development of the Pyrolytic Fouling Test for Organic Reactor Coolants, USAEC Report NAA-SR-7362, Atomics International, Nov. 30, 1962.
15. R. S. Neymark, Performance of Structural Materials Exposed to the Coolant in the OMRE, USAEC Report NAA-SR-9796, Atomics International, Aug. 1, 1964.
16. R. S. Neymark, Corrosion of Structural Materials in Impure Santowax, USAEC Report NAA-SR-7755, Atomics International, May 15, 1963.
17. Atomics International, Organic Reactor Heat Transfer Manual, USAEC Report NAA-SR-Memo-7343, Dec. 1, 1962.
18. F. Bergonzoli and F. J. Halfen, Heat Transfer and Void Formation During Forced Circulation Boiling of Organic Coolants, USAEC Report NAA-SR-8906, Atomics International, June 15, 1964.
19. S. Levy, Generalized Correlation of Boiling Heat Transfer, ASME Paper 58-HT-8, *J. Heat Transfer*, 81: 37-42 (1959).
20. W. M. Rohsenow, A Method of Correlating Heat Transfer Data for Surface Boiling Liquids, *Trans. Am. Soc. Mech. Engrs.*, 74: 969-976 (1952).
21. H. K. Forster and R. Greif, Heat Transfer to a Boiling Liquid: Mechanism and Correlations, ASME Paper 58-HT-11, *J. Heat Transfer*, 81: 43-53 (1959).
22. G. W. Maurer, A Method of Predicting Steady-State Boiling Vapor Fraction in Reactor Coolant Channels, in Bettis Technical Review—Reactor Technology, USAEC Report WAPD-BT-19, Westinghouse Electric Corp., Bettis Atomic Power Laboratory, June 1960.
23. R. W. Lockhart and R. C. Martinelli, Proposed Correlation of Data for Isothermal Two-Phase, Two-Component Flow in Pipes, *Chem. Eng. Progr.*, 45(1): 39-48 (January 1949).
24. L. E. Gardner, W. M. Hutchinson, and J. C. Hillyer, Low Cost Organic Moderator-Coolants for Nuclear Reactors, USAEC Report IDO-16907, Phillips Petroleum Company, Dec. 23, 1963.

Index

Power Reactor Technology

Volume 8

Note: The page range for each of the four issues of Vol. 8 is as follows: No. 1, pages 1 to 108; No. 2, pages 109 to 156; No. 3, pages 157 to 198; and No. 4, pages 199 to 296.

A

Accidents
  frequency, 221-22
  loss-of-coolant, 240-41
Aerosols
  formation in NaK systems, 260
  traps for, 259-70
Air
  effects on corrosion by polyphenyls, 294
  reactivity effects, 109
Air-water systems
  flow, techniques for observing, 165
Aluminum
  corrosion by polyphenyls, 293-94
Aluminum alloys
  (see also SAP)
Aluminum alloys (Al-Pu)
  criticality, 210, 212
Aluminum oxide systems (Al_2O_3-UO_2)
  radiation effects, 8
Analog computers
  use for reactor control, 227
Annuli
  heat transfer in, 121-22
Argonne National Laboratory
  liquid-metal magnetohydrodynamic research, 207-8
ARGOSY code
  for graphite-moderated reactor core design, 160-61
ARGUS code
  thermal conductivity calculations, 118
Atomics International
  liquid-metal magnetohydrodynamic system research, 207

B

Bellows
  failures in Hallam Power Reactor, 282-83
Beryllium
  corrosion by polyphenyls, 294
Beryllium-9
  integral cross section, 115
Beryllium oxide systems (BeO-UO_2)
  radiation effects, 8
Beryllium oxide systems (BeO-UO_2) (Hastelloy-X-clad)
  fuel elements, evaluation, 173
Bibliographies
  two-phase flow, 164
Biphenyl
  heat transfer properties, 295
  pyrolysis, 290
  radiolysis, 290-92
Boiling, 14-17
  bubble growth and control, 256
  burnout in Freon, 166
  burnout in Na, 164
  burnout in steam-water systems, 166-70
  heat transfer, 235
  heat transfer from K, 163-64
  phase velocity in two-phase flow, 235
  stability in two-phase flow, 228
  subcooled, burnout heat flux in, 122-23
Boiling (film)
  heat transfer coefficients, 231
  theoretical studies, 232
Boiling (nucleate)
  bubble phenomena, 232
  convection effects, 235
  effects on frictional pressure drop, 253
  heat flux effects on, 229
  heat transfer in brines, 238
  liquid metal instability, 231
Boiling (pool)
  effects of heat flux, 229-30
  heat transfer, 253
Boric acid
  use as chemical shim, 272
  use as soluble poison, 214
  use of solution for reactor shutdown, 225
Boron
  use as soluble poison, 10-12
Brass
  corrosion by polyphenyls, 294
Breeding blankets
  design for large fast breeder reactors, 147-52
Brines
  deposit formation in boiling, 238
Brookhaven National Laboratory
  liquid-metal magnetohydrodynamic system research, 208
Bubbles
  effects on heat transfer, 253
  effects on thermal stresses, 255
  formation and control in boiling, 256
  formation rate during boiling, 235
  phenomena in nucleate boiling, 232
  in turbulent flow, 234-35
Buckling
  experiments, 109-10
  fuel elements, UC, 111
  materials, in light-water reactors, 214-15
Burnable poisons
  (see Poisons)
Burnout, 14-17
  in boiling Na, 164
  in fog-cooled reactors, 228-29
  in Freon, 166
  safety margin computation, 227
  in steam-water systems, 166-70
  in water, 121-23
Burnup
  fuel elements, Magnox-clad, 62
  measurements, 216-17

C

Cadmium sulfates
  solution, use as poison, 214
Calcium sulfates
  deposits in boiling solutions, 238
Catalytic hydrocracking
  reclaiming of organic coolants, 292
Ceramics
  (see Fuel elements (ceramic))
Cermets
  (see Fuel elements (cermet))
Cesium (liquid)
  thermal, thermodynamic, and flow properties, 164
Channels
  burnout of water in vertical, 121
  fluid flow stability in heated, 231
Chloride ions
  corrosive effects on stainless steels, 254
Coatings
  corrosion by polyphenyls, 294
Cold traps
  for oxides in Hallam Power Reactor, 285
Components
  reliability, 221
Computer codes
  ARGOSY, 160-1
  ARGUS, 118
  GAM-I, 210, 212
  HEAT-1, 118
  HFN, 212
  HRG, 212
  MARC-2B, 215
  MOCA-2, 215
  REX, 210
  ROB, 118
  SOFOCATE, 210
  STOKE, for heavy water reactor simula-

tion, 35
TEMPEST, 212
THERMOS, 212, 215
TYCHE, 113
Computers
use for reactor control, 226-27
Condensation
dropwise, of ethylene glycol, 233
dropwise, of water, 233
of laminar films, 232
of liquid metals, 232-33
vapor traps utilizing, 259-60
Conductivity
(see Thermal conductivity)
Control, 221-27
calibration for EBR-I, with Pu core, 158
calibration for SRE, second core, 157
computer use for, 226-27
critical assemblies using moderator level, 223-24
gas-cooled reactors, 68-69
poisons, 10-12, 214, 217, 225-26
Control rods
drive mechanisms for EBR-II, 133-34
gravity independent, 223
operation in Hallam Power Reactor, 282
radiation effects, 271
reliability, 221-22
thimble failure in Hallam Power Reactor, 283-84
Control systems, 272-75
ASTR, 223
development, 18
Elk River Power Reactor, 271-72
Hallam Power Reactor, 280, 282
Indian Point Power Reactor, 271
large pressurized-water reactors, 144-46
Yankee Power Reactor, 271-72
Convection (forced)
in boiling K, 163-64
burnout heat flux in subcooled boiling water, 122
effects in boiling, 235
fluid flow stability, 231-32
two-phase flow, 228
Convection (free)
burnout of water in vertical channel, 121
coolant loop transient behavior, 122
effects on film condensation, 232
heat transfer coefficients for ice-water systems, 239-40
heat transfer at cryogenic temperatures, 239
heat transfer to finned tubes, 236-37
liquid metal boiling in, 231
Coolant loops
fluid flow stability, 122
transient behavior under free convection, 122
Coolants
(see also Potassium alloys (K-Na) (liquid))
contamination in Dounreay Fast Reactor, 75
flow oscillations in Elk River Power Reactor, 273
loss accidents, 240-41
Na, 75-96
Coolants (organic)
corrosive effects, 293-94
film formation by, 293-94
heat transfer properties, 123-24, 295
pyrolysis, 290-91
radiolysis, 290-94
reactivity effects of Dowtherm A, 109
reclamation, 292-93
Cooling systems
Hallam Power Reactor, 282
Copper
corrosion by polyphenyls, 294
Cores
radiation effects on lifetime, 216
Cores (graphite moderated)
physics calculations, 160-61
Corrosion
by nitrogen, 173-74
by organic coolants, 44-45, 293-94
in Agesta Reactor, 275
of ceramic fuel elements (Zircaloy-2-clad), 177-82
of Hastelloys, 23, 173-74
of Incoloy-X, 23
of Nb alloys, 42-45
of stainless steels, 254-55, 293-94
of steels, 9-10, 293-94
of Yankee Power Reactor control rods, 271-72
Corrosion products
deposition in reactors, 252, 256
Cracks
propagation in boiling water reactor fuel elements, 254
Critical assemblies
control by moderator level, 223-24
perturbations in graphite-moderated, 115
Critical assemblies (Anna)
design, 111-12
Critical assemblies (Helena)
design, 111
Critical assemblies (OCF)
pulsed neutrons in, 112
Critical assemblies (ROSPO)
design, 112
Critical assemblies (Scorpio I)
criticality measurements in, 212
Critical assemblies (Scorpio II)
criticality measurements in, 212
Critical assemblies (TCA)
pulsed neutrons in, 112
Critical experiments, 109-13, 210-14
Critical facilities (Alize-II)
use of soluble poisons in, 214
Cross sections, 114-15
absorption, thermal neutrons in graphite, 114-15
calculations, 210, 212
fission, of ^{241}Pu, 115
fission spectrum, of ^{235}U, 115
integral, of ^{9}Be, 115
neutron capture, of Pu isotopes, 211
Crud
analysis from VBWR, 254, 256
Cryogenics
heat transfer, 232-33

D

Decontamination
sodium reactor coolants, 75-77
Delayed neutrons
calculations, 161-62
Departure from nucleate boiling
effects of nonuniform heat flux on, 229
Desalination
deposits during boiling and heat transfer through films, 238
Diffusion length
thermal neutrons in graphite, 114-15
Digital computers
use for reactor control, 226
Diphenyl
(see Biphenyl)
Direct power conversion
plants, 105-6
"Dowtherm A" coolant
reactivity effects, 109

E

Economics
of catalytic hydrocrackers for organic coolant reclamation, 292-93
fast breeder reactors, 85
radiation effects on core lifetime, 216
sodium graphite reactors, 185
Electrical circuits
SPERT-3, failure, 272-73
Electrons
radiation effects on polyphenyls, 291-92
Electrostatic precipitations
use with NaK vapors, 260
Energy conversion (direct)
plants, 105-6
Ethylene glycol
condensation, dropwise, 233
Excursions, 221-22
Exponential experiments, 109-13, 211-14

F

Fission parameters
calculations, 161-62
Fission products
contamination at Dounreay Fast Reactor coolant, 75
gases, monitor for, 263
Fluid flow, 14-17, 118-25, 163-71, 228-44
effects on boiling, 253
large pressurized water reactors, 142-44
oscillations in Elk River Power Reactor, 273
Fluid flow (annular)
transition to two-phase, 234
Fluid flow (froth)
occurrence and characterization, 123
Fluid flow (turbulent)
bubble studies, 234-35
heat transfer in annuli, 122
Flowsheets
Halden Reactor, 50
soluble poison control systems, 11
Forced convection
(see Convection (forced))
Free convection
(see Convection (free))
Freeze traps
for Na in Hallam Power Reactor, 285
Freon systems
boiling burnout in, 166
Froth flow
(see Fluid flow (froth))
Fuel assemblies
design for large pressurized-water reactors, 139-41
Fuel cycles
evaluation for large fast breeder reactors, 154-55
Fuel elements
Agesta Reactor, 51-52
burnout of rods, 167
criticality of pins, 210
design, 3, 6-9
design for AGR Reactor, 62
design for Anna Critical Assembly, 112
design for BONUS Reactor, 27
design for NORA Reactor, 112
design for RB Reactor, 112
development for fast breeder reactors, 86-91
development of SAP, 37, 39
fabrication, 126-31
failures in boiling water reactors, 254-56

failure due to internal pressure, 252
failure in VBWR, 252-54, 256
Marviken Reactor, 51-52
radiation effects, 7-8, 62, 82, 255-56
thermal conductivity, 118-21, 129
Fuel elements (Al-Pu)
criticality in graphite lattices, 212
Fuel elements (BeO-UO_2)(Hastelloy-X-clad)
evaluation, 173
Fuel elements (ceramic)
design, 3, 6-9, 147-52
evaluation, 172-74
Fuel elements (ceramic)(Zircaloy-2-clad)
fretting corrosion, 177-82
Fuel element (cermet)
development, 89, 126-28
fabrication, 129
thermal conductivity, 129
Fuel elements (enriched U)
criticality in D_2O lattices, 213
Fuel elements (Incoloy-800-clad)
evaluation for superheating reactors, 174-75
Fuel elements (Magnox-clad)
burnup, 62
design, 63-66
radiation effects, 62
Fuel elements (Mo-UO_2 cermet)
fabrication and thermal conductivity, 129
Fuel elements (Mo-W-UO_2 cermet)
development, 128
Fuel elements (Nb-ThO_2-UO_2 cermet)
thermal conductivity, 129
Fuel elements (Pu)
criticality in graphite lattices, 212
Fuel elements (Pu-U)
criticality in graphite lattices, 212-13
Fuel elements (PuC-UC)
design for large fast breeder reactors, 147-49, 151-52
Fuel elements (PuO_2-UO_2)
criticality in water, 212
design for large fast breeder reactors, 149-52
specifications, 129
Fuel elements (PuO_2-UO_2)(Zircaloy-2-clad)
fretting corrosion, 177-82
Fuel elements (PuO_2-UO_2)(Zr-clad)
criticality, 210
fretting corrosion, 177-82
Fuel elements (stainless steel-clad)
design, 3, 6-9
Fuel elements (stainless steel-UO_2 cermet)
development, 126-27
Fuel elements (Th-U)
development for fast breeder reactors, 89
Fuel elements (Th-U-Zr)(Zircaloy-2-clad)
fabrication, 130
Fuel elements (ThO_2-UO_2)
design, 3, 6-9
Fuel elements (W-UO_2 cermet)
development, 127-28
Fuel elements (U)
criticality in graphite lattices, 212-13
Fuel elements (UC)
buckling studies, 111
development for sodium graphite reactors, 81-83
radiation effects, 82
Fuel elements (UC)(stainless steel-clad)
evaluation, 174
fabrication of Na-bonded, 129-30
Fuel elements (UO_2)
design, 3, 6-9
fabrication, 129
thermal conductivity, 119-21
Fuel elements (UO_2)(enriched)
pulsed neutron studies, 112
Fuel elements (UO_2)(stainless steel-clad)
evaluation, 172
fabrication, 128-29
Fuel elements (UO_2)(Zircaloy-2-clad)
evaluation, 172-74
fretting corrosion, 177-82
Fuel elements (Zircaloy-clad)
design, 3, 6-9
evaluation, 18
Fueling machines
Bradwell Reactor, operation, 68
EBR-2, vapor traps for, 262-63
design, 68, 141-42

G

Gadolinium nitrates
use of solutions for reactor shutdown, 226
GAM-I code
criticality and cross section calculations, 210, 212
Gases
entrainment in Hallam Power Reactor, 284
fission product monitoring, 263
thermodynamic properties, 121, 239
Graphite
criticality of Pu alloys in lattices of, 212-13
moderator, pulsed neutron studies in, 112-13
thermal neutron absorption cross section and diffusion length in, 114-15
Gravity
control rod independence from, 223

H

Hastelloy-C alloy
corrosion in superheating reactors, 23
Hastelloy-X alloy
corrosion by N_2, 173-74
HEAT-1 code
thermal conductivity calculations, 118
Heat exchangers
concentric tube, dynamic analysis of, 237
design, 236-37
efficiency, 236
failures in Hallam Power Reactor, 284
finned tube, 236-37
heat transfer coefficients for NaK, 235-36
Heat transfer, 14-17, 118-25, 163-71, 228-44, 253
large pressurized-water reactors, 142-44
organic coolants, 123-24, 295
Heavy water
chemistry of, 39-40
control of oxygen in, 277
criticality studies in lattices of, 213
moderator, pulsed neutron studies in, 113
reactivity effects, 109
reflector, in University of Michigan Reactor, 277, 279
Heavy Water Lattice Project
buckling experiments, 109-10
Helium
thermodynamic properties, 121
HFN code
cross section calculations, 212
Hot traps
for carbon in Hallam Power Reactor, 285
HRG code
cross section calculations, 212
Hydriding
Zr alloys, 9, 246-51
Hydrogen
effects on corrosion by polyphenyls, 294
reactions with Zircaloys, 245-46
thermal conductivity at high temperatures, 239

I

Ice-water systems
free convection melting, heat transfer calculations, 239-40
Impingement
vapor traps utilizing, 260
Incoloy-800 alloy
testing for fuel element cladding, 174-75
Inconel-X alloy
corrosion in superheating reactors, 23
Indium resonance energy
flux age, 113-14
TYCHE code, determination by, 113
Instrumentation
gas-cooled reactors, 68-69
Hallam Power Reactor, 283, 285
large pressurized water reactors, 145-47
level controllers, failure, 272
liquid metal level indicators, 176-77
neutron detectors, 224-25
pressure switches, failure, 272
temperature sensors, failure, 272
Integral cross sections
^9Be, 115
Iron
corrosion by polyphenyls, 294

J

Jet Propulsion Laboratory
liquid-metal magnetohydrodynamic system research, 207

L

Leaks
Hallam Power Reactor, 282
pressure vessels, 3
SPERT-3, 275-76
Yankee Power Reactor, 275-76
Level controllers
SPERT-3, failure, 272
Level indicators
for liquid metals, 176-77
Light water
(see Water)
Liquid metals
(see Metals (liquid))
Lithium (liquid)
thermal, thermodynamic, and flow properties, 163-64
Loss-of-coolant
accident analysis, 240-41

M

Magnesium
corrosion by polyphenyls, 294
Magnesium alloys
corrosion by polyphenyls, 294
Magnesium oxide systems (MgO-PuO_2)
radiation effects, 8

Magnetohydrodynamic systems, 199-209
Maintenance
  handling of Hallam Power Reactor core components, 283
MARC-2B code
  thermal neutron distribution calculation, 215
Massachusetts Institute of Technology
  liquid-metal magnetohydrodynamic system research, 208
Melt Refining Process
  vapor traps, 266
Mercury
  condensation in Ni surfaces, 232-33
  thermal, thermodynamic, and flow properties, 163-64
Metals (gaseous)
  film condensation, 232-33
Metals (liquid)
  boiling behavior, 231
  level indicators, 176-77
  pumps for, 282
  thermal, thermodynamic, and flow properties, 163-64
  use in magnetohydrodynamic systems, 199 209
  vapor traps for use with, 259-70
Meters
  plugging in Hallam Power Reactor, 283
MHD system
  (see Magnetohydrodynamic systems)
MOCA-2 code
  criticality calculation, 215
Moderators
  criticality control with, 223-24
  element failure in Hallam Power Reactor, 285-87
Molybdenum systems (Mo-W-UO_2 cermets)
  development for fuel elements, 128
Molybdenum systems (Mo-UO_2 cermets)
  fabrication into fuel elements and thermal conductivity, 129
Multiplication factors
  for EBR-I, with Pu core, 158-59

N

NaK
  (see Potassium alloys (K-Na)(liquid))
Natural convection
  (see Convection (free))
Neutrons
  age determination, 113-15
  delayed, 161-62
  detector design, 224-25
  flux measurements, 157-58
  pulsed, 112-13
  scattering, 116
  thermal, 114-15, 215
  thermalization, 115-16
Nimbus Satellite
  thermal design calculations, 240
Niobium
  corrosion by polyphenyls, 294
Niobium alloys (Nb-Zr)
  corrosion, 42-45
  hydriding stress allowance, 9
  use in pressure tubes, 41
Niobium systems (Nb-ThO_2-UO_2 cermets)
  thermal conductivity, 129
Nitrogen
  corrosive effects, 173-74
Noble gases
  thermal conductivity at high temperature, 239
NPY Project, 111-12

O

Organic coolants
  (see Coolants (organic))
Orifices
  operating problems in Hallam Power Reactor, 288
Oxide films
  effects on hydriding of Zr alloys, 246-48
Oxygen
  control of concentration in D_2O, 277
  effects on corrosion by polyphenyls, 294

P

Packed beds
  heat transfer, 237-38
Petroleum distillates
  development for reactor use, 295
Physics, 109-17, 154-55, 157-62, 210-20
Plates
  evaporation rates from hot, 240
  heat transfer from at cryogenic temperatures, 239
Plutonium
  critical experiments, 211-14
  neutron capture cross sections, 211
Plutonium-239
  neutron capture cross sections, 211
Plutonium-240
  neutron capture cross sections, 211
Plutonium-241
  fission cross sections, 115
  neutron capture cross sections, 211
Plutonium alloys
  criticality in D_2O lattices, 213
Plutonium alloys (Al-Pu)
  criticality, 210, 212
Plutonium alloys (Pu-U)
  criticality in lattices, 212-13
Plutonium carbide systems (PuC-UC)
  design of fuel elements for large fast breeder reactors, 147-49, 151-52
  radiation effects, 8
Plutonium carbides (PuC)
  radiation effects, 8
Plutonium nitrates
  criticality of solution, 213-14
Plutonium oxide systems
  critical experiments in water lattices, 210
Plutonium oxide systems (MgO-PuO_2)
  radiation effects, 8
Plutonium oxide systems (PuO_2-UO_2)
  critical experiments in water lattices, 210, 212
  design of fuel elements for large fast breeder reactors, 149-52
  fuel elements, fretting corrosion of Zircaloy-2 cladding, 177-82
  fuel elements, specifications, 129
  radiation effects, 8
Plutonium oxide systems (PuO_2-ZrO_2)
  radiation effects, 8
Plutonium oxides
  criticality in polystyrene, 214
Pneumatic systems
  use in control systems, 223
Poisons, 10-12
  boric acid, 214, 225
  $CdSO_4$ solution use, 214
  $Gd(NO_3)_3$, 226
  use in water-moderated reactors, 217
Polyethylene
  reactivity effects, 109
Polyphenyls, 123-24, 290-95
Polystyrene
  moderating effects on PuO_2, 214
Potassium (liquid)
  thermal, thermodynamic, and flow properties, 163-64
Potassium alloys (K-Na)(liquid)
  aerosol formation in, 260
  heat transfer coefficients, 235-36
  thermal, thermodynamic, and flow properties, 163
Power conversion (direct)
  plants, 105-6
Pressure
  effects on boiling superheat, 253
Pressure drop
  of air in finned-tube heat exchangers, 236-37
  turbulent flow through wire-wrapped, seven-rod fuel assemblies, 123
  two-phase, 166, 233-35
Pressure switches
  Elk River Power Reactor, failure, 272
Pressure tubes
  design, 40-41
  fretting corrosion, 177-82
Pressure vessels, 12-14
  design for large pressurized water reactors, 138-39
  design for Magnox reactors, 66-68
  KRB Reactor, 12-13
  leaks, 3
  SENA Reactor, 12-13
SENN Reactor, 12-13
SEP Reactor, 12
WWER-1 Reactor, 9-10, 12-14
Pressurized water
  burnout calculations, 121-23
Pumps
  development for reactors, 18
  liquid metal, for Hallam Power Reactor, 282
  Hallam Power Reactor, 282
Pyrolysis
  organic coolants, 290-91

R

Rabbit facility
  design and fabrication, 277
Radiation (thermal)
  heat transfer calculations, 238-39
Radiation effects
  biphenyl, 290
  control rods, 271
  core lifetime, 216
  fuel elements, 7-8, 62, 82, 255-56
  hydriding of Zr alloys, 246-48
  polyphenyls, 290-91, 293-94
  reactivity, 217
  SAP, 38
  Zircaloy-2, 38, 41
Radiolysis
  organic coolants, 290-94
Reactivity
  calculations, 217
  changes with irradiation, 216
  effects on, 109-10
  measurements in reactors, 157-59
Reactors
  (see also Critical...)
  corrosion product deposition in, 252
  future development, 17-20
  reactivity, 216-17
  subcriticality measurement during shutdown, 224-25
Reactors (Advanced Gas Cooled)(AGR)
  design, 58
  fuel element design, 62
  operation, 60
Reactors (Advanced Sodium Graphite)
  buckling studies, 111

Reactors (Aerospace Shield Test)(ASTR)
control system, 223
Reactors (Agesta)
corrosion in, 275
design, 47-48, 52-53
repair procedures, 276
Reactors (AKB)
design, 36
Reactors (Aquilon-II)
criticality measurements in, 213
Reactors (ARBUS)
design and operation, 103-4
Reactors (AVR)
design, 73-74
Reactors (Bashful-600)
design, 53, 55-56
Reactors (Beloyarsk-1)
design, 28-34
Reactors (Beloyarsk-2)
design, 28-34
Reactors (Big Rock Point Power), 6
design, 4, 7
flow-induced vibrations, failures from, 273
operating experience, 3
pumps, 18
Reactors (BN-350)
design, 94
status, 92
Reactors (Bodega Bay Power)
design, 4
Reactors (Boiling, Experiments-5) (BORAX-5)
design, 23
Reactors (Boiling heavy-water)
design, 55
Reactors (boiling-water), 3-29
corrosion product deposition in, 256
fuel element failure, 254-56
radiation effects on fuel elements, 255
water quality control, 254
Reactors (BONUS)
design, 23, 25, 27
Reactors (BR-3)
design, 5
use of soluble poison control, 10, 12
Reactors (BR-5)
coolant contamination, 75-76
status, 95
Reactors (Berkeley)
design, 58
performance, 60
Reactors (Bradwell)
design, 58
performance, 60
refueling machine operation, 68
Reactors (Calder Hall)
design, 58
Reactors (CANDU), 37-44
physics, 217
Reactors (Chapelcross)
design, 58
Reactors (Connecticut Yankee Power)
design, 5
Reactors (Czechoslovakian Heavy Water)
design, 56
Reactors (DON)
design, 36
Reactors (DOR)
design, 36
Reactors (Dounreay Fast)
fission product contamination of coolant, 75
status, 92
Reactors (Dragon)
design, 72-73
Reactors (Dresden Power), 6
design, 4, 7
operating experience, 3
pumps, 18
Reactors (Dungeness)
design, 58
Reactors (EDF-1)
criticality studies in, 213
design, 58
Reactors (EDF-2)
design, 58
Reactors (EDF-3)
design, 58
pressure vessel, 67
Reactors (EDF-4)
design, 58
pressure vessel, 67
Reactors (EL-4)
design, 36
Reactor (Elk River Power)
control system, 271-72
coolant flow oscillations, 273
design, 4
instrument failure, 272
Reactors (Enrico Fermi Fast Breeder)
auxiliary systems, 77-78
coolant decontamination, 77
design, 78-80
operation, 78
status, 92
vapor traps, 261
Reactors (Experimental Beryllium Oxide) (EBOR)
development, 106
Reactors (Experimental Boiling Water) (EBWR)
operation, 147
scaling, 252
Reactors (Experimental Breeder-I) (EBR-I)
nuclear parameters for Pu core, 158-9
vapor traps, 260-61
Reactors (Experimental Breeder-2) (EBR-2)
control rod drive mechanisms, 133-34
design, 78-80
coolant decontamination, 77
status, 92
vapor traps, 261-63
Reactors (fast breeder), 84-95
criticality studies, 110
design of large, 147-55
gas coolant, 95
Reactors (Fast Supercritical Pressure Power)(FSPPR)
design, 186-93
Reactors (Fast, Test)(FARET)
vapor traps, 264-65
Reactors (First Atomic Power Station)
design, 28-29
Reactors (fog-cooled)
heat transfer, 228-29
Reactors (G2)
design, 58
pressure vessel, 67
Reactors (G3)
design, 58
pressure vessel, 67
Reactors (gas-cooled), 56, 58-74
design of fast breeders, 95
operating experience, 216
physics, 216
Reactors (General Electric Test)(GETR)
flow-induced vibrations, failures from, 273-74
Reactors (graphite-moderated), 28-34
core physics calculations, 160-61
Reactors (Halden)
flowsheets, 50
operation, 50-51
water chemistry, 52
Reactors (Hallam Power)
coolant decontamination, 77
design, 78-80
operation, 81, 279-80, 282-88
vapor traps, 264
Reactors (Hanford Graphite Superheat) (HGSR)
design, 193-98
Reactors (heavy-water), 35-37
oxygen concentration control in coolant, 277
physics, 217
Reactors (Heavy Water Components Test) (HWCTR)
control rod-guide-tube rupture, 222-23
shutdown with boric acid, 225
Reactors (Hector)
criticality measurements in, 212
Reactors (Hinkley Point)
design, 58
Reactors (Humboldt Bay Power), 6
design, 4, 7
operating experience, 3
Reactors (Hunterston)
design, 58
Reactors (Indian Point Power) (CETR), 6
control system, 271
operating experience, 3
repair procedures, 276-77
Reactors (Industrial Reactor Laboratories)
rabbit facility design and fabrication, 277
Reactors (JPDR)
design, 4
Reactors (Kahl Superheating)
design, 22, 24
Reactors (KBWP)
design, 5
Reactors (KRB)
design, 4
pressure vessel, 12-13
Reactors (La Crosse Boiling Water) (LACBWR)
design, 4
Reactors (Large Closed Cycle Water)
fuel element evaluation, 172
Reactors (Latina)
design, 58
Reactors (Lenin)
design and operation, 97-98
Reactors (liquid metal-cooled), 75-96
Reactors (Lithium Cooled, Experiment) (LCRE)
vapor traps, 266-67
Reactors (Los Alamos Fast, Core Test Facility)(FRCTF)
vapor traps, 265
Reactors (Los Alamos Molten Plutonium, Experiments)(LAMPRE)
vapor traps, 265
Reactors (Loss-of-Flow Test)(LOFT)
program analysis, 240-41
Reactors (Lucens)
design, 36
Reactors (Magnox), 58-71
Reactors (Malibu-1 Power)
design, 5
Reactors (marine), 97-102
Reactors (Marius)
criticality measurements in, 213
Reactors (Maryla)
design, 111
Reactors (Marviken)
design, 47, 49, 52-55
Reactors (Minerve)
criticality measurements in, 213
Reactors (ML-1)
fuel element evaluation, 173-74
Reactors (Molten Salt, Experiment) (MSRE)

development, 106
Reactors (NERO)
design, 100-1
Reactors (New Production)(NPR)
tubes and fittings, 134-36
Reactors (Nine Mile Point Power)
design, 4
Reactors (NORA)
fuel element design, 112
Reactors (Novo-Veronezh)(WWER)
burnup, 217
Reactors (NPD), 35-44
Reactors (NRX)
testing of reactor materials in, 38
Reactors (Oldbury)
design, 58
pressure vessel, 67
Reactors (Organic Cooled, Heavy Water Moderated Power)
design, 36
Reactors (Otto Hahn)
design, 98-99
Reactors (Oyster Creek Power)
design, 4
Reactors (Parr Shoals Power)
design, 36
Reactors (Pathfinder Power)
design, 23
Reactors (Peachbottom Power)
design, 72-73
Reactors (pebble bed)
design, 73-74
Reactors (Plutonium Recycle Test) (PRTR)
control of oxygen in D_2O system, 277
nuclear parameters, 158
pressure-tube fretting corrosion, 177-82
Reactors (PM-1)
status, 103
Reactors (PM-2A)
status, 103
Reactors (PM-3A)
status, 103
Reactors (portable power), 103-4
Reactors (pressure-tube), 35-45
Reactors (Pressurized Heavy Water)
design, 51-53, 55
Reactors (pressurized-water), 3-29
development and design of large, 137-47
use of soluble poisons for control, 10-12
Reactors (Puerto Rico Power)(BONUS)
design, 23, 25, 27
Reactors (R-1)
design, 36
Reactors (R-2)
design, 36
Reactors (R3/Adam)
(see Reactors (Agesta))
Reactors (Rapsodie)
status, 92
Reactors (RB)
fuel element design, 112
Reactors (Romaska)
design, 105-6
Reactors (RWE)
design, 4
Reactors (San Onofre Power)
design, 5
pumps, 18
Reactors (Savannah River)
burnout computation, 227
Reactors (Saxton Power)
design, 5, 7
operating experience, 3
use of soluble poison control, 12
Reactors (SELNI)
design, 5
Reactors (SENA)
design, 5
pressure vessel, 12-13
Reactors (SENN)
design, 4
pressure vessel, 12-13
Reactors (SEP)
design, 4
pressure vessel, 12
Reactors (Shippingport Pressurized Water) (PWR), 6
design, 5
fuel element performance, 172, 252
operating experience, 3
use of burnable poison, 12
Reactors (Sizewell)
design, 58
Reactors (SM-1)
status, 103
Reactors (SM-1A)
status, 103
Reactors (SNAP-10A)
design, 105
Reactor (Sodium, Experiment)(SRE)
nuclear parameters of second core, 157-58
operation, 80-81
vapor traps, 264
Reactors (sodium graphite), 80-84
steam cycles, 183-85
Reactors (Southwest Experimental Fast Oxide)(SEFOR)
vapor traps, 265
Reactors (Special Excursion, Tests-2) (SPERT-2)
critical experiments with, 109
Reactors (Special Power Excursion, Tests-3) (SPERT-3)
electrical circuits, failure, 272-73
flow-induced vibrations, failures from, 273-75
leaks, 275-76
level controller failure, 272
Reactors (Steam Generating Heavy Water)
design, 36
Reactors (superheating), 22-34
design of HGSR, 193-98
fuel element development, 174-75
Reactors (Tarapur)
design, 4
Reactors (TES-3)
operation, 104
Reactors (Tokai Mura)
design, 58
Reactors (Transient, Test Facility) (TREAT)
vapor traps, 265-66
Reactors (Trawsfynydd)
design, 58
Reactors (UEM)
design, 5
Reactors (Ultra High Temperature, Experiment) (UHTREX)
development, 106
Reactors (Ulyanovsk)
design, 25-26
Reactors (University of Michigan)
D_2O reflectors, 277, 279
Reactors (University of Missouri at Rolla) (UMRR)
control rod swelling, 222
Reactors (Vallecitos Boiling Water) (VBWR)
fuel element failure in, 252-54, 256
Reactors (Vallecitos Superheat)
design, 22, 24
Reactors (VULCAIN)
design, 99-101
Reactors (water-cooled), 3-29
material buckling in, 214-15
physics, 216
Reactors (water-moderated), 3-29
material buckling in, 214-15
physics, 216
use of poisons in, 217
Reactors (WWER)
design, 5
operating experience, 3
Reactors (WWER-1)
design, 19-20
pressure vessel, 9-10, 12-14
Reactors (WWER-2)
design, 19-20
Reactors (Wylfa)
design, 58
pressure vessel, 67
Reactors (Yankee Power), 6
control system, 271-72
critical experiments, 210
design, 5
flow-induced vibrations, failures from, 273-74
leaks, 275-76
operating experience, 3
pumps, 18
use of soluble poison control, 12
Reactors (ZPR-3)
core design, 110-11
Reflectors
D_2O in University of Michigan Reactor, 277, 279
Resonance absorption
mathematical analysis, 159-60
Resonance capture
in U-238, 215
Resonance Integral Theory
calculations, 218
REX code
criticality calculations, 210
ROB code
thermal conductivity calculations, 118
Rubidium (liquid)
thermal, thermodynamic, and flow properties, 163-64

S

Safety
accident frequency, 221-22
burnout computation in Savannah River Reactors, 227
coolant flow oscillations in Elk River Power Reactor, 273
fast breeder reactors, 85-86, 153-54
Hallam Power Reactor, 280
instrument failures, 272-73
leaks, 275-76, 282
loss-of-coolant accidents, 240-41
shutdown, emergency, 225-26
University of Michigan Reactor, 279
University of Missouri at Rolla Reactor, 222
vibrations, flow-induced, 273-75
Salt solutions
heat transfer to, from wire-wrapped, seven-rod fuel element bundles, 123
Santowax
sampling techniques, 294-95
Santowax OMP
corrosive effects, 294
film formation by, 293-94
radiolysis, 290-91
use in ROSPO Critical Assembly, 112
Santowax-R
corrosive effects, 294
heat transfer properties, 123-24, 295
radiolysis, 291-92
SAP

corrosion by polyphenyls, 293-94
development for reactor fuels, 37, 39
radiation effects, 38
Satellites (man-made)
Nimbus, thermal design calculations, 240
Seals
pressure vessel, leaks, 3
use of freeze, in Hallam Power Reactor, 283
Shims (chemical), 10-11
Yankee Power Reactor, 272
Shutdown (emergency)
use of boric acid, 225
use of gadolinium nitrate, 226
Sintered aluminum products
(see SAP)
Sodium (gaseous)
freeze traps for, 285
Sodium (liquid)
heat transfer from boiling, 164
reactor cooling, 75-96
thermal, thermodynamic, and flow properties, 163-64
Sodium alloys (K-Na)(liquid)
aerosol formation in, 260
heat transfer coefficients, 235-36
thermal, thermodynamic, and flow properties, 163
Sodium Components Test Installation
vapor traps, 264
Sodium Test Facility
vapor traps, 265
SOFOCATE code
criticality calculations, 210
Specifications
fuel elements, PuO_2-UO_2, 129
pressure vessels, 13-14
Spiralator
heat exchanger, design, 237
Springs
use in control system, 223
Stagnation
vapor traps utilizing, 260
Stainless steel systems (stainless steel-UO_2 cermets)
development for fuel elements, 126-27
Stainless steels
cladding for fuel elements, 3, 6-9
corrosion of, 254, 293-94
effects of boiling water on, 255
performance in water-cooled reactors, 254, 256
Steam
effects on hydriding of Zr alloys, 246
Steam (superheated)
heat transfer, 40, 121
Steam generators
design for large pressurized water reactors, 138
operating problems in Hallam Power Reactor, 284
Steam-water systems
boiling burnout in, 166-67
flow and heat transfer, 165, 166-70
Steels
corrosion, 9-10, 293-94
STOKE code, 35
for heavy water reactor simulation, 35
Stress corrosion
effects of oxygen concentration, 255
Stresses
(see also Thermal stresses)
effects on cracking, 252, 255
Subcriticality
measurement, 224-25
Sulfur
effects on corrosion by polyphenyls, 294
Superheated steam
(see Steam (superheated))
Superheating
pressure effects on boiling, 253
Surfaces
effects on boiling, 231, 253

T

Tanks
failure of Na expansion, in Hallam Power Reactor, 285
Teflon
flexible tube heat exchangers, 237
Temperature sensors
failure in Elk River Power Reactor, 272
TEMPEST code
cross section calculations, 212
Terphenyl
heat transfer properties of irradiated, 123-24
Thermal conductivity
effects on pool boiling, 230
fuel elements, 118-21, 129
heat transfer calculations, 239
hydrogen at high temperatures, 239
noble gases at high temperature, 239
Thermal neutrons
absorption cross section and diffusion length in graphite, 114-15
distribution in light-water reactors, 215
Thermal radiation
heat transfer calculations, 238-39
Thermal stresses
in fuel elements, 253, 255
Thermometers
failure in Elk River Power Reactor, 272
THERMOS code
cross section calculations, 212
thermal neutron distribution calculations, 215
Thorium alloys (Th-U)
fuel element development for fast breeder reactors, 89
Thorium alloys (Th-U-Zr)(Zircaloy-2-clad)
fabrication of fuel elements, 130
Thorium oxide systems (Nb-ThO_2-UO_2 cermets)
thermal conductivity, 129
Thorium oxide systems (ThO_2-UO_2)
fuel element design, 3, 6-9
radiation effects, 8
Traps
for aerosols, 359-70
for carbon, oxides, and Na in Hallam Power Reactor, 285
for liquid metal systems, 259-70
Tubes
(see also Pressure tubes)
burnout, 16-17
burnout of water in, 121
heat transfer from, at cryogenic temperatures, 239-40
Tubes (finned)
use in heat exchangers, 236-37
Tungsten systems (Mo-W-UO_2 cermets)
development for fuel elements, 128
Tungsten systems (W-UO_2 cermets)
development for fuel elements, 127-28
Turbulent flow
(see Fluid flow (turbulent))
Two-phase flow
(see Fluid flow)

U

Uranium
criticality in D_2O lattices, 213
criticality in graphite lattices, 212-13
radiation effects on reactivity, 217
Uranium-233
radiation effects on reactivity, 217
Uranium-235
fission ratio to U-238, 110
fission spectrum cross section, 115
radiation effects on reactivity, 217
Uranium-238
fission ratio to U-235, 110
resonance capture, 215
Uranium (enriched)
criticality in D_2O lattices, 213
Uranium alloys (Pu-U)
criticality in lattices, 212-13
Uranium alloys (Th-U)
fuel element development for fast breeder reactors, 89
Uranium alloys (Th-U-Zr)(Zircaloy-2-clad)
fabrication of fuel elements, 130
Uranium carbide systems (PuC-UC)
design of fuel elements for large fast breeder reactors, 147-49, 151-52
radiation effects, 8
Uranium carbides (UC)
buckling studies, 111
development for fuel elements for sodium graphite reactors, 81-83
evaluation for fuel elements, 174
fabrication of Na-bonded fuel elements, 129-30
radiation effects, 8, 82
Uranium nitrides (UN)
radiation effects, 8
Uranium oxide systems
critical experiments in water lattices, 210
Uranium oxide systems (Al_2O_3-UO_2)
radiation effects, 8
Uranium oxide systems (BeO-UO_2)
radiation effects, 8
Uranium oxide systems (BeO-UO_2) (Hastelloy-X-clad)
fuel elements, evaluation, 173
Uranium oxide systems (Mo-UO_2 cermets)
fabrication into fuel elements and thermal conductivity, 129
Uranium oxide systems (Mo-W-UO cermets)
development for fuel elements, 128
Uranium oxide systems (Nb-ThO_2-UO_2 cermets)
thermal conductivity, 129
Uranium oxide systems (PuO_2-UO_2)
critical experiments in water lattices, 210, 212
design of fuel elements for large fast breeder reactors, 149-52
fuel elements, fretting corrosion of Zircaloy-2 cladding, 177-82
fuel elements, specifications, 129
radiation effects, 8
Uranium oxide system (stainless steel-UO_2 cermets)
development for fuel elements, 126-27
Uranium oxide systems (ThO_2-UO_2)
fuel element design, 3, 6-9
radiation effects, 8
Uranium oxide systems (W-UO_2 cermets)
development for fuel elements, 127-28
Uranium oxide systems (UO_2-ZrO_2)
radiation effects, 8
Uranium oxides (UO_2)
evaluation, 172-74
fretting corrosion, 177-82
fuel elements, design, 3, 6-9
fuel elements, evaluation, 172-74
fuel elements, fabrication, 128-29
fuel elements, thermal conductivity,

119-21
pulsed neutron studies, 112
radiation effects, 8
Uranium silicides (U_3Si)
radiation effects, 8
Uranium sulfides (US)
radiation effects, 8
Uranium systems
criticality in water lattices, 210-11
Uranyl nitrate
criticality of solutions, 213

V

Valves
performance in Hallam Power Reactor, 282-84
Vapor traps
for liquid metal systems, 259-70
Vaporizers
flow stability in forced convection, 231-32
Vena contracta
mixing during reexpansion, 235
Vertical channels
(see Channels)
Vibrations
flow-induced, failures from, 273-75

W

Water
burnout heat flux under forced convection, 122
condensation, 233
corrosion of steel, 9-10
criticality studies in lattices of, 210-212
dissociation, effects on hydriding of Zr alloys, 248
effects on corrosion by polyphenyls, 294
moderator, pulsed neutron studies in, 113
quality control, 254
reactivity effects, 109-10
Water (pressurized)
burnout calculations, 121-23
Water-air systems
flow, techniques for observing, 165
Water-ice systems
free convection melting, heat transfer calculations, 239-40
Water-steam systems
boiling burnout in, 166-67
flow and heat transfer, 165, 166-70

Z

Zircaloy alloy
cladding for fuel elements, 3, 6-9
effects of hydriding on properties, 245
Zircaloy-2 alloy
corrosion, 42-45
effects of hydriding on properties, 245, 248-49
hydriding, control of, 249-50
hydrogen absorption, 246
radiation effects, 38, 41
use in pressure tubes, 41
Zircaloy-2 alloy (Ni-tree)
hydrogen absorption, 246
Zircaloy-4 alloy
hydriding, control of, 250
hydrogen absorption, 246
Zirconium alloys
hydriding, 246-51
Zirconium alloys (coated)
corrosion by polyphenyls, 294
Zirconium alloys (Nb-Zr)
corrosion, 42-45
hydriding stress allowance, 9
use in pressure tubes, 41
clad)
Zirconium alloys (Th-U-Zr)(Zircaloy-2-clad)
fabrication of fuel elements, 130
Zirconium hydride
formation in Zircaloys, 245-46
orientation, 250-51
Zirconium oxide systems (PuO_2-ZrO_2)
radiation effects, 8
Zirconium oxide systems (UO_2-ZrO_2)
radiation effects, 8

LEGAL NOTICE

This journal was prepared under the sponsorship of the U. S. Atomic Energy Commission. Neither the United States, nor the Commission, nor any person acting on behalf of the Commission:

A. Makes any warranty or representation, expressed or implied, with respect to the accuracy, completeness, or usefulness of the information contained in this journal, or that the use of any information, apparatus, method, or process disclosed in this journal may not infringe privately owned rights; or

B. Assumes any liabilities with respect to the use of, or for damages resulting from the use of any information, apparatus, method, or process disclosed in this journal.

As used in the above, "person acting on behalf of the Commission" includes any employee or contractor of the Commission, or employee of such contractor, to the extent that such employee or contractor of the Commission, or employee of such contractor prepares, disseminates, or provides access to, any information pursuant to his employment or contract with the Commission, or his employment with such contractor.

NUCLEAR SCIENCE ABSTRACTS

The U. S. Atomic Energy Commission, Division of Technical Information, publishes *Nuclear Science Abstracts* (*NSA*), a semimonthly journal containing abstracts of the literature of nuclear science and engineering.

NSA covers (1) research reports of the U. S. Atomic Energy Commission and its contractors; (2) research reports of government agencies, universities, and industrial research organizations on a worldwide basis; and (3) translations, patents, books, and articles appearing in technical and scientific journals.

Complete indexes covering subject, author, source, and report number are included in each issue. These are cumulated quarterly, semiannually, and annually providing a detailed and convenient key to the literature.

Availability of *NSA*

SALE *NSA* is available on subscription from the Superintendent of Documents, U. S. Government Printing Office, Washington, D. C., 20402, at $30.00 per year for the semimonthly abstract issues and $22.00 per year for the four cumulated-index issues. Subscriptions are postpaid within the United States, Canada, Mexico, and all Central and South American countries, except Argentina, Brazil, British and French Guiana, Surinam, and British Honduras. Subscribers in these Central and South American countries, and in all other countries throughout the world, should remit $37.00 per year for subscriptions to semimonthly abstract issues and $25.00 per year for the four cumulated-index issues.

EXCHANGE *NSA* is also available on an exchange basis to universities, research institutions, industrial firms, and publishers of scientific information. Inquiries should be directed to the Division of Technical Information Extension, U. S. Atomic Energy Commission, P. O. Box 62, Oak Ridge, Tennessee, 37830.

TECHNICAL PROGRESS REVIEWS may be purchased from Superintendent of Documents, U. S. Government Printing Office, Washington, D. C., 20402, at $2.50 per year for each journal or $0.70 per issue. The use of the coupon below will facilitate the handling of your order.

POSTAGE AND REMITTANCE: Postpaid within the United States, Canada, Mexico, and all Central and South American countries except Argentina, Brazil, British and French Guiana, Surinam, and British Honduras. For these Central and South American countries and all other countries, add $0.75 for each annual subscription or $0.20 for a single issue. Payment should be by check, money order, or document coupons, and MUST accompany order. Remittances from foreign countries should be made by international money order or draft on an American bank payable to the Superintendent of Documents or by UNESCO book coupons.

order form

SUPERINTENDENT OF DOCUMENTS
U. S. GOVERNMENT PRINTING OFFICE
WASHINGTON, D. C., 20402

Enclosed:
document coupons ☐ check ☐ money order ☐

Charge to Superintendent of Documents No._____

Please send a one-year subscription to

☐ NUCLEAR SAFETY

☐ POWER REACTOR TECHNOLOGY

☐ REACTOR FUEL PROCESSING

☐ REACTOR MATERIALS

☐ ISOTOPES AND RADIATION TECHNOLOGY

(Each subscription $2.50 per year; $0.70 per issue.)

SUPERINTENDENT OF DOCUMENTS
U. S. GOVERNMENT PRINTING OFFICE
WASHINGTON, D. C., 20402

(Print clearly)

_____
Name

_____
Street

_____
City, State, ZIP Code